

SABRE AND MAGNETOMETER STUDIES OF  
SUBSTORM ASSOCIATED PULSATIONS

ERIC GEORGE BRADSHAW

Being a dissertation submitted to the Faculty of Science,  
University of Leicester, in candidature for the degree  
of Philosophiae Doctor

Department of Physics,  
University of Leicester,

August, 1989

UMI Number: U017729

All rights reserved

INFORMATION TO ALL USERS

The quality of this reproduction is dependent upon the quality of the copy submitted.

In the unlikely event that the author did not send a complete manuscript and there are missing pages, these will be noted. Also, if material had to be removed, a note will indicate the deletion.



UMI U017729

Published by ProQuest LLC 2015. Copyright in the Dissertation held by the Author.  
Microform Edition © ProQuest LLC.

All rights reserved. This work is protected against  
unauthorized copying under Title 17, United States Code.



ProQuest LLC  
789 East Eisenhower Parkway  
P.O. Box 1346  
Ann Arbor, MI 48106-1346



3393  
X 751556091

750068499

This thesis is dedicated to

mum, dad and papa

Rachel and Steve

Chris, Wanda, Jackie and Debbie

Dave and Jane

Angie

#### ACKNOWLEDGEMENTS

Sincere thanks to my supervisor Professor Tudor Jones and to Dr. Jeff Waldock and Dr. Mark Lester for their constructive ideas and informative discussions at various times during this study. The thorough reading and constructive criticism of the manuscript was also greatly appreciated.

I would also like to thank the following people:

Dr. Bill Stuart and Dr. Chris Green for helpful discussions and worthwhile ideas for this project during my visits to the British Geological Survey (CASE collaborating institution) in Edinburgh.

Past and present members of the Ionospheric Physics group at Leicester for their company and help during the period of this study.

Dr. Chris Thomas, Chris Stewart and Roderic Maude for the maintenance of the Wick radar and the SABRE analysis computer.

Dr. W.C. Bain for a copy of his Maximum Entropy spectral analysis subroutine.

All members of the Geomagnetism Research Group at the British Geological Survey in Edinburgh for their friendly welcome and help during my visits there.

The Max Planck Institut fur Aeronomie, Lindau, W. Germany in cooperation with the Uppsala Ionospheric Observatory for the operation

of the Swedish radar of the SABRE system.

Dr. H. Luhr of the Technical University of Braunschweig, W. Germany for providing EISCAT cross magnetometer data for selected pulsation intervals.

Professor K.A. Pounds, Professor J.L. Beeby and Professor E.A. Davis for the opportunity to work in the Physics Department at Leicester.

The SERC for financial support, via a CASE award with the BGS (NERC) during the period of this study.

—0—

Special thanks are due to Dr. Angela Wilkinson whose support and encouragement kept me going through the (long) writing-up stage of this thesis.

## CONTENTS

### GLOSSARY

#### CHAPTER 1 INTRODUCTION

1.1 The neutral atmosphere and the ionosphere	1
1.2 The magnetosphere	2
1.3 The auroral oval	4
1.4 The inner magnetosphere	5
1.5 Magnetospheric convection	6
1.6 Field-aligned and ionospheric currents	7
1.7 The present investigation	10

#### CHAPTER 2 MAGNETOSPHERIC SUBSTORMS AND Pi2 PULSATIONS

##### - A BRIEF REVIEW

2.1 Introduction	12
2.2 Observations during substorms	13
2.2.1 Magnetospheric observations	13
2.2.2 Auroral observations	16
2.2.3 Ground-based magnetic observations	17
2.3 Pi2 pulsations	19
2.3.1 General features	19
2.3.2 Pi2 pulsations and the substorm current wedge	20
2.3.3 Pi2 pulsation generation mechanisms (theory)	22
2.3.4 Models of Pi2 pulsation generation	24
from observation	
2.3.5 Pi2 propagation to mid-latitudes (theory)	27
2.3.6 Pi2 propagation to mid-latitudes (observation)	29
2.4 Summary of Pi2 pulsation mechanisms	32

CHAPTER 3	EXPERIMENTAL OBSERVATIONS	
3.1	SABRE and magnetometer systems	33
3.2	Magnetometer data analysis	34
3.3	SABRE data analysis	36
3.3.1	SABRE time series analysis	36
3.3.2	SABRE spectral analysis	38
3.3.3	SABRE polarisation analysis	39
3.4	Summary	40
CHAPTER 4	GENERAL FEATURES OF SABRE Pi2 PULSATIONS	
4.1	Introduction	42
4.2	The SABRE data	42
4.2.1	Occurrence of SABRE Pi2 pulsations	42
4.3	SABRE Pi2 pulsation amplitudes	45
4.4	SABRE Pi2 pulsation dominant periods	46
4.5	Positioning of the SABRE viewing area relative to the substorm current wedge	48
4.6	SABRE observations of Pi2 pulsations	51
4.6.1	Introduction	51
4.6.2	Type 1 SABRE Pi2 pulsation signatures	52
4.6.3	Type 2 SABRE Pi2 pulsation signatures	57
4.6.4	Latitudinal and longitudinal profiles	58
4.7	Polarisation studies of SABRE Pi2 pulsations	61
4.7.1	Introduction	61
4.7.2	Comparison with ground magnetometer polarisation data	63
4.7.3	SABRE polarisation relative to local time and the substorm current wedge	64
4.8	Conclusions	66

CHAPTER 5	SABRE SPATIAL PATTERNS DURING Pi2 PULSATIONS	
5.1	Introduction	70
5.2	Morphology of SABRE spatial patterns during Pi2 pulsations	70
5.2.1	Introduction	70
5.2.2	Type (a) spatial patterns	71
5.2.3	Type (b) spatial patterns	78
5.3	Spatial studies of SABRE wave spectral power	81
5.3.1	Location and localisation of peak wave spectral power in dominant Pi2 pulsation periods	81
5.3.2	Change in position of the cell exhibiting peak wave spectral power over a series of Pi2 pulsations	82
5.4	Summary	86
CHAPTER 6	CASE STUDIES	
6.1	Introduction	89
6.2	Case study 1 : eastward electrojet Pi2 pulsations	89
6.2.1	SABRE and magnetometer pulsation signatures	89
6.2.2	Spectral analysis	91
6.2.3	Spatial velocity studies	92
6.2.4	Polarisation analysis	93
6.2.5	Summary of case study 1	94
6.3	Case study 2 : flow pattern features	96
6.3.1	SABRE and magnetometer pulsation signatures	96
6.3.2	Spectral analysis	97
6.3.3	SABRE flow patterns	98
6.4	Case study 3 : repetition time between Pi2 pulsations and changing position of peak power cell	100

correlates with movement of substorm current wedge	
6.4.1 SABRE, magnetometer Pi2 pulsation data and spectral analysis	100
6.4.2 Substorm current wedge movement from SABRE ME spectral analysis	102
6.4.3 Summary of case study 3	104
6.5 Case study 4 : low magnetic activity	105
6.5.1 Introduction	105
6.5.2 Occurrence of SABRE backscatter	106
6.5.3 SABRE and magnetometer pulsation signatures	106
6.5.4 Spectral analysis and possible pulsation generation mechanisms	107
6.6 Summary and conclusions	109

## CHAPTER 7 CONCLUSIONS

7.1 Introduction	112
7.2 Principal results of the study	112
7.3 Indications of future work	115

## APPENDIX A: MAXIMUM ENTROPY SPECTRAL ANALYSIS

A.1 Introduction	118
A.2 Maximum Entropy Spectral Analysis	118

REFERENCES	122
------------	-----

## GLOSSARY

Definition of symbols and abbreviations which appear most frequently in this thesis.

B	Magnetic field
BGS	British Geological Survey
CW	clockwise
CCW	counter-clockwise
D	East-west component of the geomagnetic field
E	electric field
EISCAT	European Incoherent SCATter radar facility
FFT	Fast Fourier Transform
FTE	Flux transfer event
GG	Geographic
H	North-south component of the geomagnetic field
IGRF	International Geomagnetic Reference Field
IGS	Institute of Geological Sciences (former name of BGS)
IMF	Interplanetary magnetic field
J	Ionospheric current density
K	magnetic activity index from a single station
$K_p$	planetary magnetic activity index
L	Distance in earth radii from the centre of the earth to the equatorial crossing of a geomagnetic field line in a dipole field
LT	local time
m	Pi2 pulsation azimuthal wave number
ME	Maximum Entropy
MLT	Magnetic local time

r	correlation coefficient
$R_e$	radius of the Earth
RTI	Range Time Intensity
RTV	Range Time Velocity
SABRE	Sweden And Britain Radar aurora Experiment
STARE	Scandinavian Twin Auroral Radar Experiment
UT	Universal Time
v	irregularity drift velocity
WTS	westward travelling surge
Z	Vertical component of the geomagnetic field

## CHAPTER 1

### INTRODUCTION

#### 1.1 The neutral atmosphere and the ionosphere

The terrestrial atmosphere surrounds the earth in a relatively thin layer comprising a mixture of gases. The neutral component of the atmosphere may be described by the basic properties pressure, density, mean molecular weight and temperature. Both pressure and density decrease rapidly with altitude, with the particle number density falling from a value of about  $10^{25} \text{ m}^{-3}$  at sea level to  $10^{19} \text{ m}^{-3}$  at 100km. The temperature profile is rather more complicated however due to absorption of different wavelengths of the incident solar radiation at different heights. The presence or absence of turbulence is the over-riding factor in the relative composition of the constituent gases in the ionosphere. In the lower atmosphere turbulence is present, the gases are therefore mixed and their relative proportions remain constant. The increase in temperature with heights above 100km means that the atmosphere is stable to vertical motion and no turbulence is present in this region. The composition therefore changes with altitude, the mean molecular weight decreases with increasing height. The lighter atomic species dominate at higher altitudes due to diffusive separation.

In the upper atmosphere oxygen and nitrogen are ionised by solar radiation in the x-ray and extreme ultra-violet wavelength bands. As

the ions and electrons formed then tend to re-combine with other gases to form new ions, the concentration of free electrons depends on the balance between the rates of electron-ion production and loss through recombination. Above about 60km the concentration of free electrons is sufficient to influence the propagation of radio waves. The idea of such an ionised layer was first suggested independently by Kennelly and Heaviside following the radio transmission experiments of Marconi in 1901. This region is known as the ionosphere and was first named as such by Watson-Watt in 1926. The principal electron (ion) density layers have been named, with increasing altitude, the D (60-90 km), E (90-120 km) and F (above 150 km) regions. During the daytime the F-region is often divided into two parts, the F1 and F2 layers. Typical electron density profiles are presented in Figure 1.1. The D and F1 regions vanish at night and the E region becomes much weaker. The F2 region, however, tends to persist although at reduced intensity. The reason for the disappearance of these layers is that the source of the ionising radiation (the sun) is removed and the electron density decays away.

At heights of about 1000km the ionosphere is normally taken to end and the magnetosphere to begin, however there is no physical separation between the two regions. The magnetosphere has a relatively complex structure and its interaction with the solar wind and the ionosphere will be described in the following sections.

## 1.2 The magnetosphere

Figure (1.2) depicts a north-south meridional view in the noon-midnight plane of the magnetosphere surrounding the earth and some of the many regions that make up its complex structure. The magnetosphere is formed by the interaction of the interplanetary

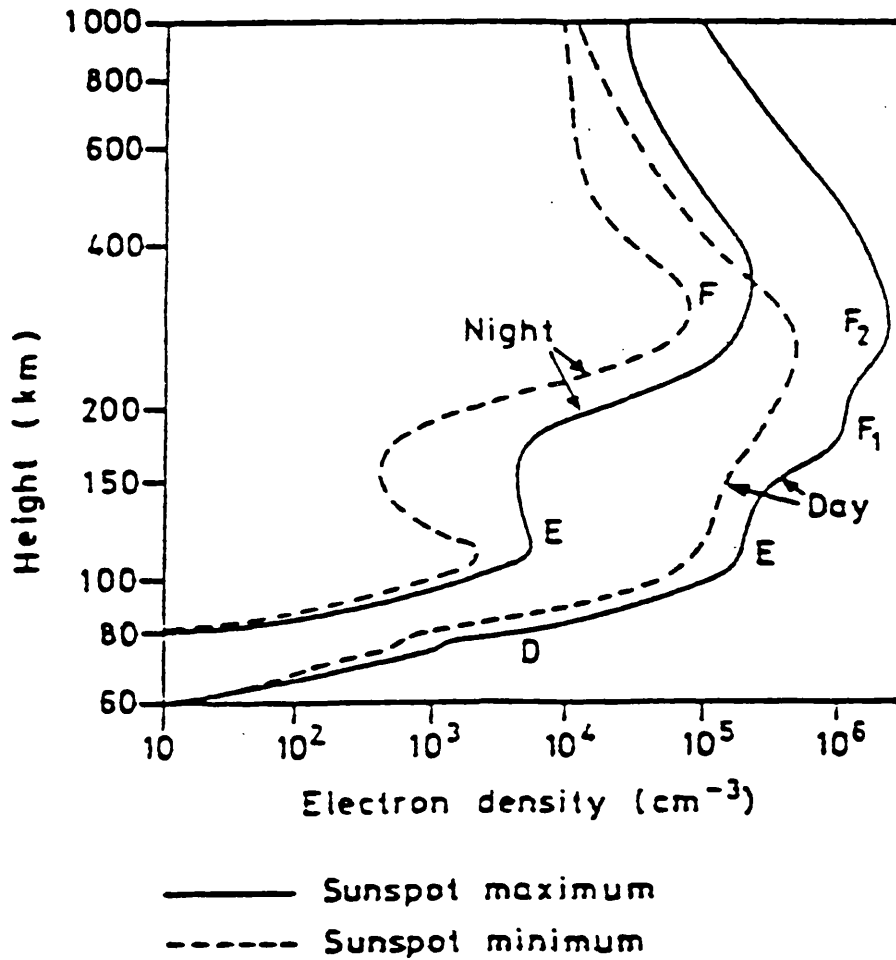


**Figure 1.1**

Typical vertical profiles of electron density in the mid-latitude ionosphere (from wallchart, "Aerospace Environment", W. Swider, Air Force Geophysics Laboratory, Hanscom Air Force Base, Massachusetts).

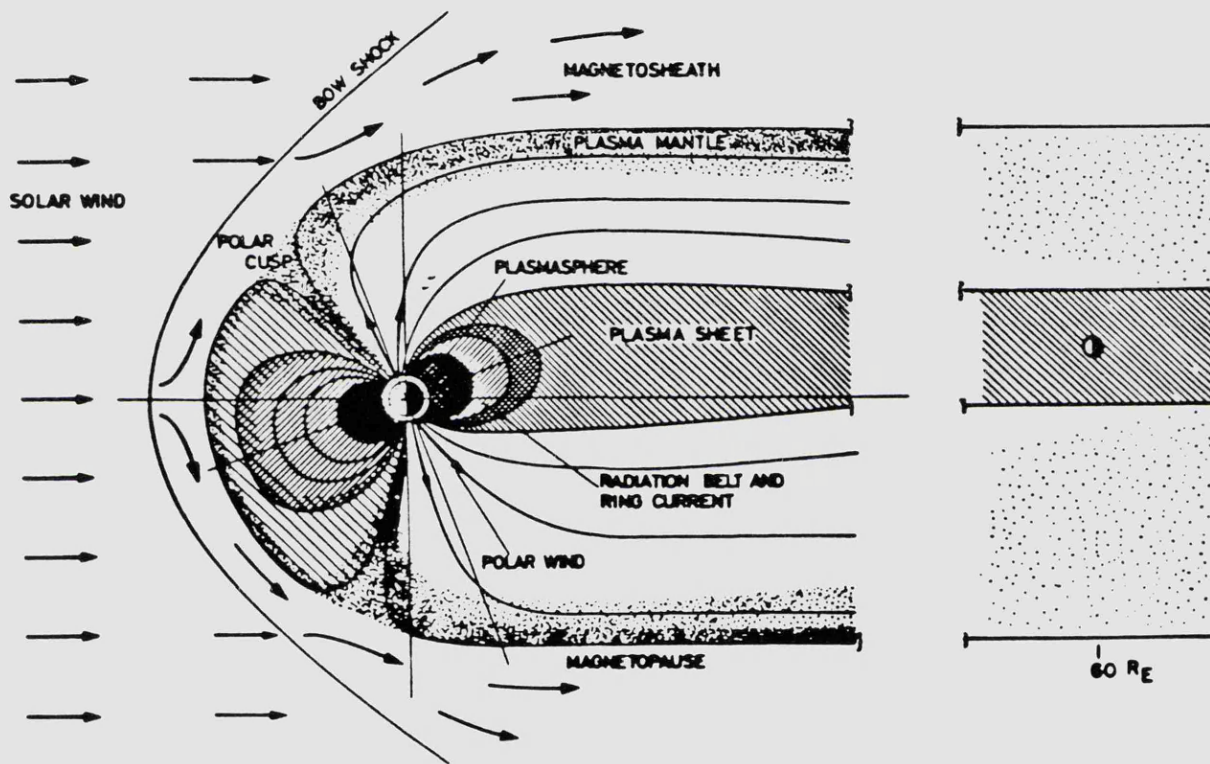


Figure 1.2

A north-south meridional view of the magnetosphere surrounding the earth depicting the many regions that make up its complex structure (Akasofu, S.-I., 1977).

magnetic field (IMF) with the earth's magnetic field. The IMF is carried by the bulk motion of the solar wind, a continuous stream of plasma flowing radially outwards from active regions on the sun's surface. The IMF is said to be 'frozen-in' to the solar wind as the magnetic energy density of the IMF is less than the particle kinetic energy density of the solar wind.

As the solar wind is travelling supersonically when it reaches earth orbit, a shock wave, the bow shock, forms ahead of the solar wind. The solar wind is slowed and heated by the more dense, subsonic and hotter plasma in the shock region and deflected to flow round the boundary of the magnetic cavity, the so called magnetosphere, containing the geomagnetic field. The boundary, named the magnetopause, is a surface where solar wind pressure outside is balanced by the pressure of the confined geomagnetic field inside. This interaction distorts the geomagnetic field away from a simple magnetic dipole, compressing it on the sunward side and stretching it out into a long tail on the dark side of the Earth. The magnetopause is approximately spherical on the sunward side, lying typically at a distance of ten Earth radii in front of the Earth. This distance varies with changes in the structure of the solar wind which arise from activity fluctuations on the Sun's surface. On arrival at the earth the solar wind variations affect the pressure balance at the magnetopause thus changing the radius of the dayside magnetosphere.

On the nightside of the earth, the region known as the magnetotail forms. The geomagnetic field lines are highly distended and stretch great distances in the anti-sunward direction. Observations in the magnetotail have been reported far beyond the moon's orbit at 60 earth radii as far as 1000 earth radii (Villante, 1975). The magnetotail

itself is roughly cylindrical and is bisected into two tail lobes by the plasma sheet. The geomagnetic field points earthward in the northern lobe but tailward in the southern lobe. This implies that a current flows across the tail and this current closes on the magnetotail boundary. The plasma sheet is a very dynamic region and plays an important role in the triggering of substorms as discussed later.

Geomagnetic field lines in the tail lobes are 'open', i.e. one end of the field line is connected to, and moves with, the IMF, while the other is connected to the earth in the polar cap. Field lines in the plasma sheet are 'closed', i.e. both ends are connected to the earth in the nightside auroral ovals in the northern and southern hemispheres.

### 1.3 The auroral oval

The auroral oval, as described from the statistics of the position of occurrence of visible aurora (Figure 1.3) by Feldstein (1963), is that region which maps along closed field lines into the plasma sheet. Energetic particles can precipitate down the highly conducting geomagnetic field lines to the ionosphere to produce the visual aurora by colliding with and exciting oxygen and nitrogen ions in the high latitude upper atmosphere. In addition, roughly co-located with the visual auroral oval, are locations of E-region plasma irregularity generation which can backscatter radio waves and be observed as the radar aurora. Figure 1.3 demonstrates that the auroral oval is asymmetric relative to the geomagnetic pole and increases in width and moves equatorward at times of enhanced magnetic activity. (The statistical maximum is situated around a magnetic latitude near 67 degrees north at local midnight but about 77 degrees north at local

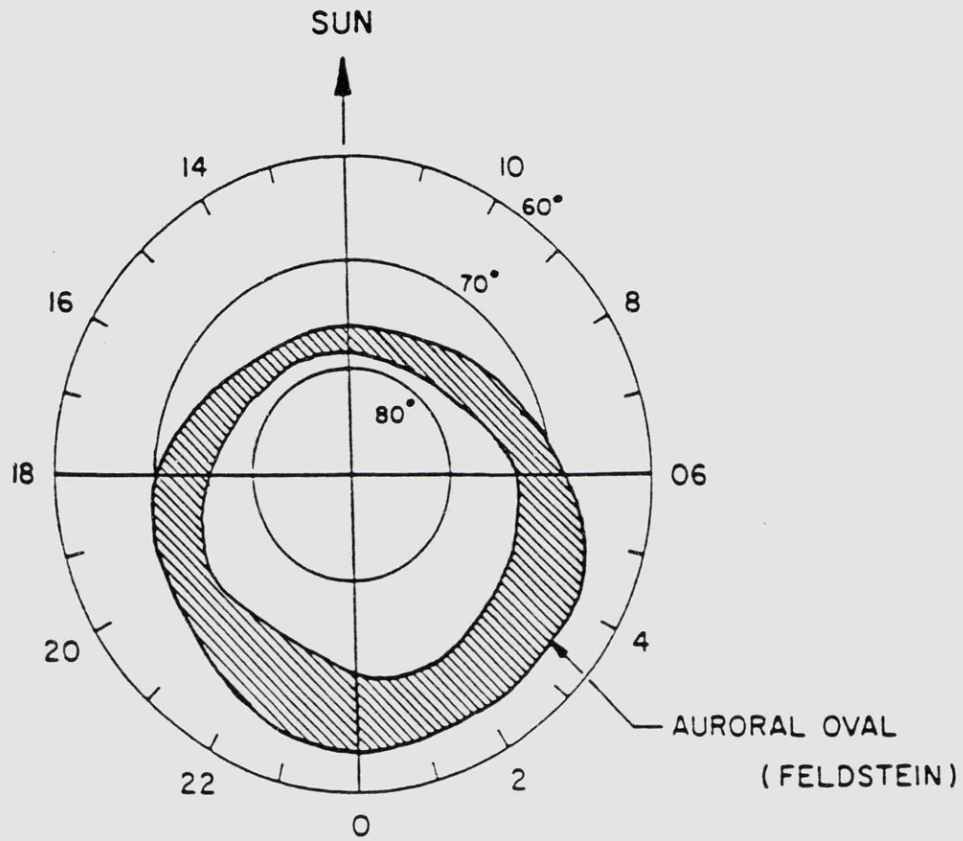


Figure 1.3

The auroral oval (shaded) as determined from the statistics of the position of occurrence of visible aurora (Feldstein, 1963).

noon. On the dayside, the boundary between field lines closing through the equator and open field lines swept back over the pole into the tail lobe is called the polar cusp. These occur at the two points on the magnetopause, one in the northern and southern hemispheres, where the total magnetic field is zero. Direct entry of solar wind particles in the magnetosheath down into the ionosphere along field lines which connect to about 68 degrees geomagnetic latitude on the earth's surface can occur in these regions. The projection of the polar cusp down to the dayside ionosphere produces the dayside auroral oval.

#### 1.4 The inner magnetosphere

The surface between open and closed field lines is called the boundary of the plasma sheet and field lines in this region pass through a distant neutral line at which the magnitude of the field approaches zero. In this region there exists a thin (1000km) region, the neutral sheet, across which the direction of the magnetic field reverses. This neutral sheet is thought to play an important part in the physical processes that lead to the geomagnetic substorms which are described later.

In the interior of the magnetosphere, close to the earth, there is a field-aligned 'doughnut' of high density, low energy plasma of ionospheric nature called the plasmasphere. The plasmasphere co-rotates with the earth and its boundary, the plasmopause, is important because it separates the inner magnetosphere, dominated by co-rotation, from the outer magnetosphere which is dominated by magnetospheric convection. It is especially important however because a very sharp density gradient exists at the plasmopause. Measurements of the electron density indicate a reduction by a factor of ten or more in a distance of about 0.5 earth radii (Carpenter, 1963). This

gradient is important in determining the propagation and structure of the substorm associated geomagnetic pulsations from their source regions in the auroral zone to mid-latitudes where they are most easily and clearly observed.

### 1.5 Magnetospheric convection

Although it was initially stated that the structure of the magnetosphere is determined by pressure balance considerations it should also be borne in mind that when a fluid flows past a solid object there should be some frictional interaction between the two. In that case it might be expected that the friction at the boundary is a mechanism for the transfer of energy from the solar wind to the magnetosphere. This concept was suggested by Axford and Hines (1961) as a viscous interaction which could give rise to the anti-sunward flow over the polar cap with subsequent return flows at lower latitudes at the dawn and dusk sides. A problem with this concept is that friction implies collisions and as the solar wind is so tenuous these are few and far between.

A second method of driving the observed magnetospheric convection was introduced by Dungey (1961) in his now widely accepted re-connection, or 'open', model of the magnetosphere. This model entails the transport of plasma from the dayside to the tail on 'open' polar cap field lines following re-connection between geomagnetic and IMF lines at the sub-solar point on the dayside magnetopause (Figure 1.4). As the IMF is 'frozen-in' to the solar wind bulk flow, the geomagnetic field lines now connected to the IMF field lines are dragged over the pole and therefore plasma is transferred from the day to the night side of the earth. This connection and transfer of plasma to the tail is thought to occur both as a quasi-continuous process and in discrete

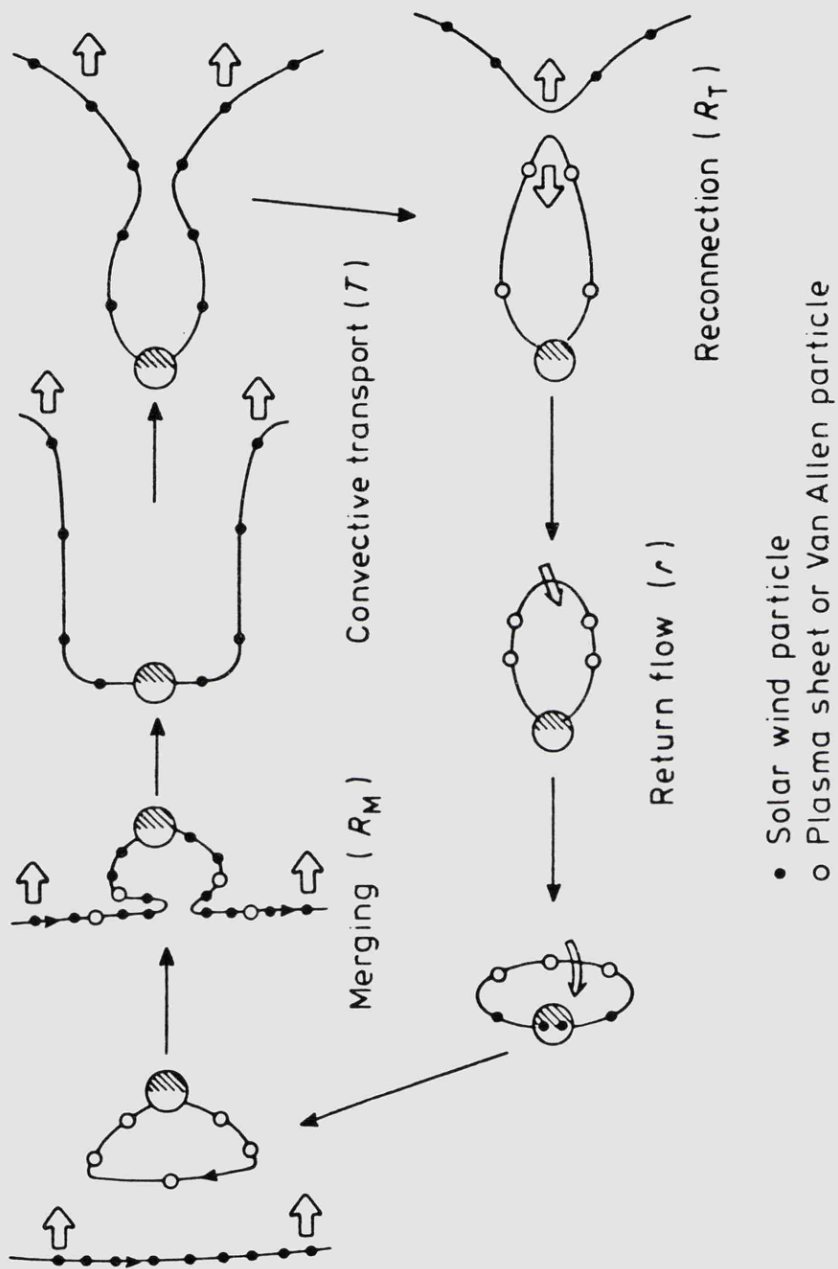


**Figure 1.4**

Time history of a field line taking part in the merging, tailward plasma transport, re-connection in the tail and earthward return flow processes of the magnetospheric convection in Dungey's (1961) 'open' model of the magnetosphere (after Akasofu, S.-I., 1973).

events. The discrete events are known as flux-transfer-events (FTEs) (Rijnbeek et al. 1984) and have a characteristic magnetic signature as observed by spacecraft borne magnetometers, occur quite frequently (1-2/hr), are of limited duration (about 5 mins.) and are relatively small in spatial extent. The field lines then re-connect after the formation of an X-type neutral line in the plasma sheet region of the tail and plasma flows back towards the earth on 'closed' field lines at lower, sub-auroral latitudes.

Although both mechanisms are thought to drive the convection of plasma, re-connection is probably dominant except perhaps at times of little solar activity when the magnetospheric configuration described previously is thought to approach a ground state. This is probably the case when the IMF is pointing northward and the magnetosphere is effectively 'closed' to re-connection. It is then more difficult for the oppositely directed field line geometry required for re-connection to occur.

Associated with the convecting plasma is an electrostatic field which is projected along the magnetic field into the earth's atmosphere as an ionospheric electric field. The electric field pattern here in the oval is poleward directed in the 14-21 MLT sector, equatorward directed in the 00-10 MLT sector and rotates from pointing northward, through west, to pointing southward in the pre-midnight sector. This electric field coincidence thus causes the ionospheric plasma to convect in the same sense as the magnetospheric plasma producing the well-known two-cell convection pattern illustrated in Figure 1.5.

#### 1.6 Field aligned and ionospheric currents

As the ionosphere is an electrical conductor, the magnetospheric

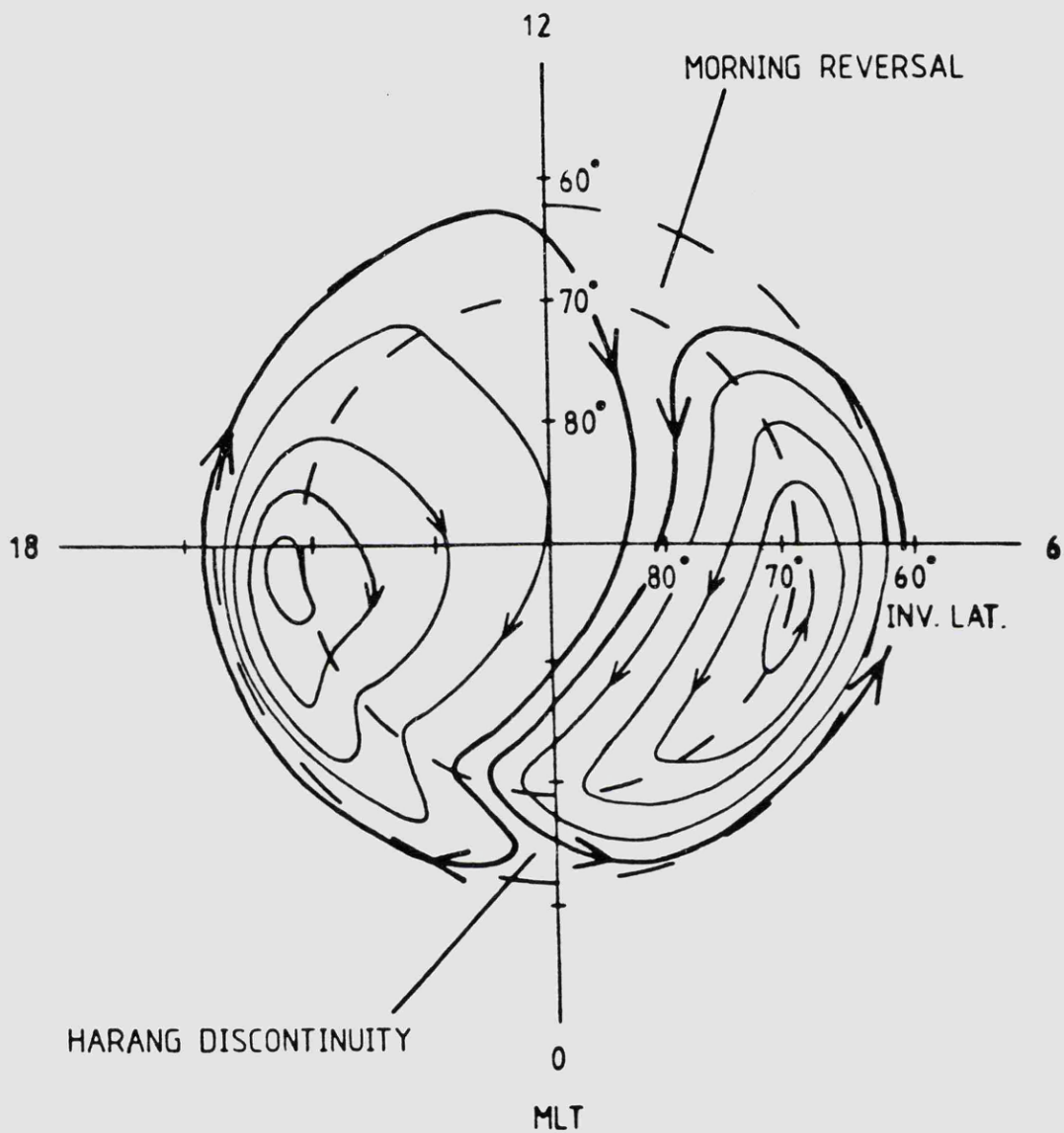


**Figure 1.5**  
 Idealised illustration of the two cell convection pattern in the polar ionosphere which results from the electrical connection with the convecting magnetospheric plasma.

electric field mentioned above is projected down to the ionosphere by the formation of a three dimensional system of field-aligned currents. This current system is closed by Hall currents flowing in the ionosphere which form the eastward (pre-magnetic midnight) and westward (post-magnetic midnight) electrojets. Both westward and eastward electrojet currents originate near noon and are fed by 'net' downward field-aligned currents (they are not balanced along a meridian). The current densities in the electrojets increase toward midnight due to a similar increase toward midnight of the ionospheric Hall conductivity. The conductivity increases here due to enhanced precipitation of electrons energised in the magnetosphere into the midnight sector. The eastward electrojet terminates in the Harang discontinuity where it partially flows up the geomagnetic field as net field-aligned current and partially diverges northward in the region of westward electric field and joins the westward electrojet. The westward electrojet extends into the evening sector along the poleward border of the auroral oval where it also diverges as net upward field-aligned current.

In addition, data obtained from satellite borne magnetometer experiments indicate the presence of twin sheets of oppositely flowing field-aligned currents encircling the geomagnetic pole as depicted in Figure 1.6a left (Iijima and Potemra, 1976a,b; Potemra et al., 1980 and references therein). Pedersen currents flow northward in the eastward electrojet and southward in the westward electrojet to provide current continuity for these sheets of balanced field-aligned current. It is important to note the difference between the balanced and net field-aligned currents present in the ionosphere. The circuit involving Pedersen currents dissipates energy in the ionosphere via Joule heating ( $\underline{E} \cdot \underline{J} > 0$ ) and must be driven by a magnetospheric generator

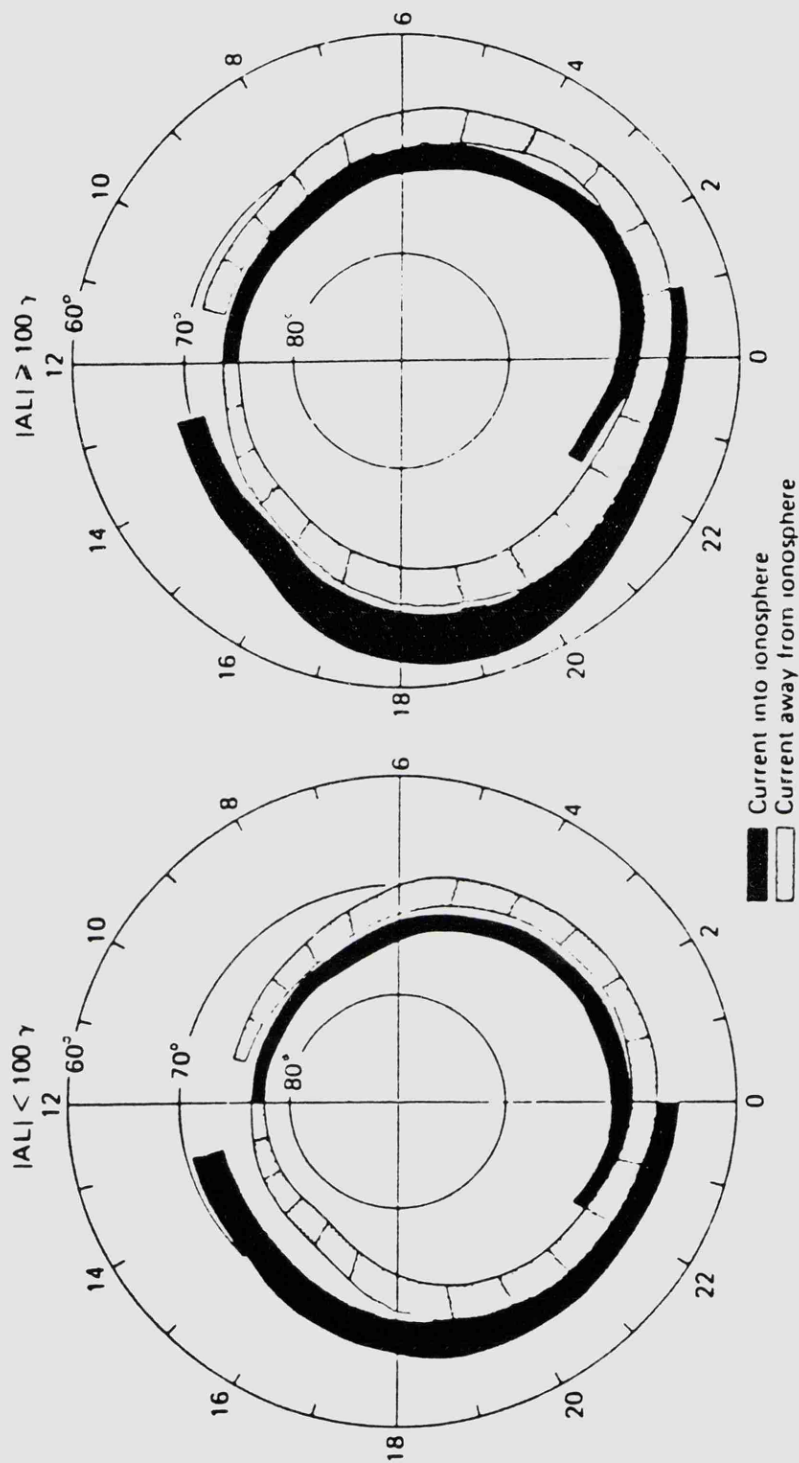


**Figure 1.6**

A summary of the distribution of flow directions of large scale field aligned currents during (left) weakly disturbed conditions and (right) active periods (Iijima and Potemra, 1978).

while the Hall current circuit is load free ( $\underline{E} \cdot \underline{J} = 0$ ) in the ionosphere.

These field-aligned current systems are known to be important in the transfer of energy and momentum between the magnetosphere and ionosphere and in the substorm processes to be described later (Baumjohann, 1983).

When solar activity increases the rate of re-connection increases on the dayside and this leads to enhanced convection of plasma and magnetic flux to the nightside. Although the basic current system and flow pattern described above remain much the same the two electrojet currents strengthen, they widen by 1.2-1.3 times in area and their centres move equatorward by about two or three degrees during disturbed periods (Figure 1.6, right). This behaviour is, not surprisingly, similar to that found to be the case for the statistical auroral oval described by Feldstein (1963). It results from an imbalance in the rate of connection of field lines at the magnetopause and in the tail.

This marks the beginning of a sequence of events that may lead to the occurrence of a magnetospheric substorm and the various phenomena associated with it. The magnetospheric substorm is the major means of cancelling out the imbalance of magnetic flux which enhanced convection has built-up on the nightside. This is achieved by the explosive return flow of plasma earthward at substorm onset. In particular, the geomagnetic pulsations termed Pi2 occur with the onset and/or intensification of each substorm. It is the investigation of these pulsations employing the ground-based radar (SABRE) in association with the BGS network of magnetometers which forms the basis of this thesis. As Pi2 pulsations and substorm onsets are so

intimately related, the study of the pulsations may also lead to a better understanding of the possible substorm onset processes.

### 1.7 The present investigation

The general features such as pulsation amplitude, dominant period and polarisation of 130 pulsations observed by SABRE have been characterised. These have been related to the nominal substorm current wedge and also compared with corresponding events observed by the BGS network of ground-based magnetometers. The spatial flow patterns observed in the ionosphere by the SABRE radar associated with substorms and Pi2 pulsations have been determined. These provide an insight into the complicated system of field-aligned and ionospheric currents observed at substorm onset and thereafter. By examining the spatial variation of the wave spectral power at the dominant pulsation period across the SABRE viewing area, changes to, and the possible movement and expansion of the substorm enhanced electrojet region are examined in the course of a train of Pi2 pulsations. A detailed study of four selected intervals of Pi2 pulsation activity observed by SABRE and the magnetometers has been undertaken and these are presented as 'case studies'. The intervals were chosen to illustrate the varying signatures observed by SABRE at different levels of magnetic activity and at different positions relative to the substorm generation region. Attempts are made to interpret these observations in terms of the physical concepts introduced in the substorm and Pi2 pulsation generation models.

For the first time it has been possible to study the ionospheric currents and flows associated with Pi2 pulsations and substorms directly in the ionosphere, without the modifications imposed by the ionosphere as in the case of ground-based magnetometer observations.

This has been accomplished with an unprecedented degree of spatial and temporal resolution by the SABRE radar. A clearer picture of the transfer of energy and momentum at substorm onset via the substorm associated field-aligned and ionospheric currents has thus been established. In addition, a better understanding of the Pi2 pulsations themselves, their generation, propagation and morphology, is now possible.

## CHAPTER 2

### MAGNETOSPHERIC SUBSTORMS AND Pi2 PULSATIONS - A BRIEF REVIEW

#### 2.1 Introduction

The term substorm was first introduced by Akasofu (1964) to qualitatively describe the sequence of visual auroral displays observed on the ground during magnetic storm activity. Subsequently the concept of the substorm was expanded to include the magnetic variations recorded simultaneously with the visual displays and the events were termed the polar magnetic substorm (Akasofu et al., 1965). Eventually it was recognised that magnetospheric disturbances also occurred at these times and the concept of the magnetospheric substorm was introduced to include the electron precipitation and magnetic pulsation events (McPherron, 1979). It is now agreed that a magnetospheric substorm is a transient process, initiated in the nightside magnetosphere, in which a significant amount of energy derived from the solar wind-magnetosphere interaction is deposited in the auroral ionosphere and in the magnetosphere (Rostoker et al., 1980). These authors reached a consensus of opinion on what constitutes a magnetospheric substorm as follows:

"The term magnetospheric substorm describes an interval of increased energy dissipation confined, in the most part, to the region of the auroral oval. The onset of this process is signalled by explosive increases in auroral luminosity in the midnight sector, and the entire process encompasses an interval during which the strength of the

current in the auroral electrojets increases from and returns to the background level from which the substorm arose. During this interval there may be a sequence of intensifications of the westward electrojet, each associated with a Pi2 micropulsation burst and a westward travelling surge (WTS). As the substorm develops, the region of discrete auroras in the midnight sector expands poleward and westward (the poleward bulge). Eventually, the region of disturbed aurora reaches a maximum latitude and begins to recover toward its pre-substorm location. The interval of time between the first Pi2 pulsation burst and the time the aurora reaches a maximum latitude has been called the expansive phase. The interval during which the aurora in the midnight sector returns to lower latitudes is called the recovery phase".

This differs from Akasofu's original description in that no time scales for an auroral substorm are now specified and that multiple onsets/surges are allowed within a single magnetospheric substorm. The location of the original arc brightening near the equatorward boundary of the oval of discrete aurora suggested that substorm onset may occur near the equatorward edge of the boundary plasma sheet (Fukunishi, 1975; Akasofu, 1977).

## 2.2 Observations during substorms

### 2.2.1 Magnetospheric observations

There are times when the magnetosphere appears to exist in a 'ground state' and during these periods the probability of a substorm occurring is very low, although magnetospheric convection and energetic particle precipitation into the auroral ionosphere both continue at a low level. The magnetotail always continues to exist through such periods. The 'ground state' configuration occurs when the

IMF has had a large northward component for an interval of time corresponding to several substorm time scales (1 to 3 hours, Rostoker et al., 1980).

The magnetosphere changes from the 'ground state' during a substorm although the manner in which it does so has been the subject of much controversy over the past twenty years. It is not clear whether the substorm can be interpreted in terms of a directly driven dynamo process (Akasofu, 1979, 1981), or as the more usually accepted loading-unloading of energy (McPherron, 1979; Hones, 1979a, 1979b).

The merits of these two possible components of substorm activity have been discussed recently by Rostoker et al. (1987a).

Briefly, the driven process involves a direct relationship between magnetospheric and solar-wind phenomena and is controlled by changes in the solar wind. The energy output from the magnetosphere into the ionosphere and neutral atmosphere closely follows, perhaps with a slight delay, the solar wind energy input to the magnetosphere, there being no role for storage of energy in the geomagnetic tail. Alternatively, the loading-unloading process involves the accumulation of magnetic energy in the tail lobes, an interval known as the growth phase, followed by the expansive phase. The substorm is thought to be triggered by an instability process converting the stored magnetic energy into 'substorm' energy. Finally the recovery phase completes the process when the magnetosphere returns to pre-substorm levels of activity. The two models for the substorm process are illustrated schematically in Figure 2.1.

Baker et al. (1985) suggest that neither of these extreme models is totally correct, since there is evidence that both are probably in

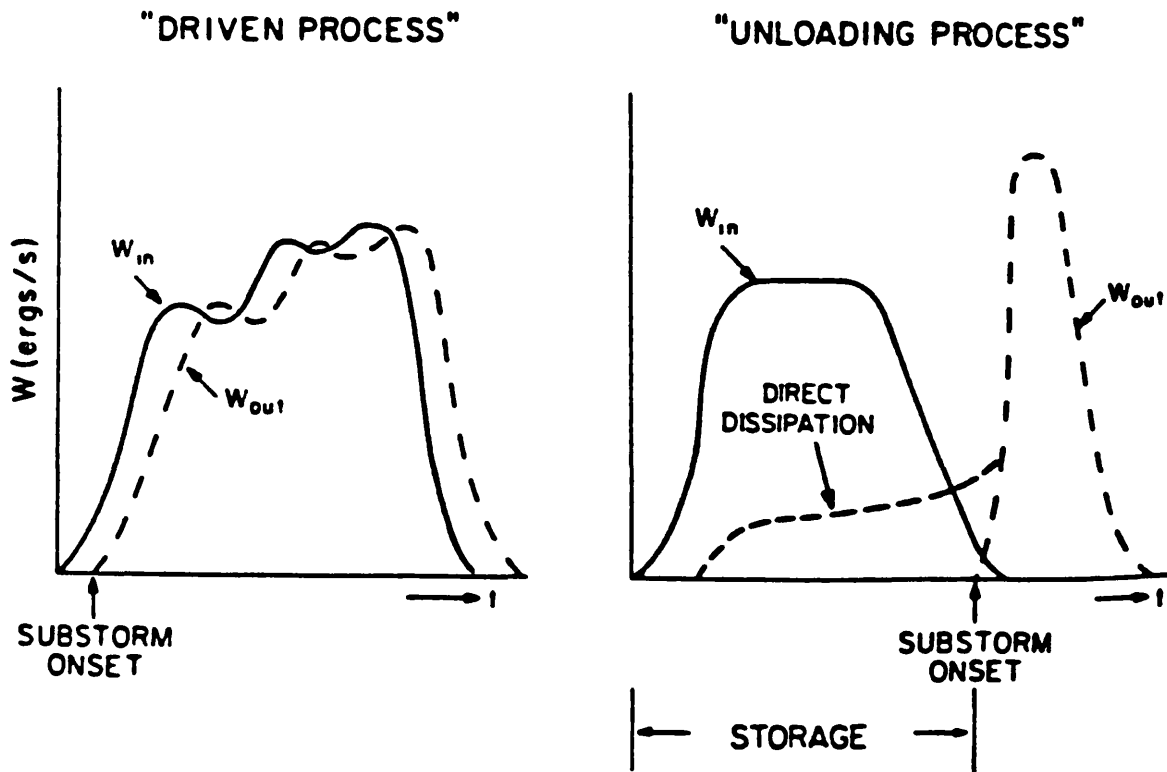


Figure 2.1  
 An idealised illustration of the directly driven (left) and unloading (right) models of the relationship between magnetospheric energy input  $W_{in}$  and energy output  $W_{out}$ .

operation during different phases of the substorm. During the growth phase there is a steady and significant energy dissipation (driven) accompanying the accumulation of energy into the magnetotail lobes (loading), while the onset of the expansive phase corresponds to the unloading of energy from the tail. Baker et al. (1985) also state that both processes can, and have been observed to occur at the same time. This is thought to be the case during the longer intervals of enhanced magnetic activity associated with multiple onset substorms or substorms that have many intensifications (Clauer and McPherron, 1974; Wiens and Rostoker, 1975; Pytte et al., 1976). Rostoker et al. (1988) suggest that the pre-existing level of activity in the system prior to substorm onset determines the ratio of directly-driven to unloading energy input through the level of conductivity in the ionosphere. The higher the conductivity, the easier it would be for directly-driven currents to grow.

Recently a new model incorporating both of the above substorm processes has been presented by Rostoker and Eastman (1987). In this model the substorm expansive phase is represented by a perturbation of an already existing directly-driven system. Time-limited bursts of reconnection near  $100R_E$  in the magnetotail lead to the non-linear growth of the Kelvin-Helmholtz instability in an azimuthally limited portion of the dusk sector boundary between the central plasma sheet and the low latitude boundary layer (equivalent to closed and open field lines respectively). This leads, at the onset of the expansive phase, to enhancements in the generation of parallel electric fields and therefore particle acceleration on the field lines threading the boundary (Thompson, 1983). The substorm current wedge and the westward travelling surge are a direct result of the non-linear growth of these field aligned currents which map to the region in the tail which is

experiencing the non-linear growth of the Kelvin-Helmholtz instability. The Kelvin-Helmholtz waves generated lead, when mapped down to the ionosphere, to a poleward motion of the equatorward boundary of the boundary plasma sheet and, therefore, to the observed poleward motion of the visual aurora associated with substorm expansion. The observed westward motion of the disturbed region is then dependent on the relative magnitudes of the momenta densities in the two interacting regions. More work is needed however before this model is placed on a firm theoretical footing. Recent satellite observations (Nishida et al., 1988) in the magnetotail have also cast some doubt on this substorm mechanism.

### 2.2.2 Auroral observations

The visual onset of a substorm is signalled in the auroral zone ionosphere by the sudden brightening of an auroral arc near the equatorward boundary of the discrete aurora in the midnight sector. This is accompanied by the intensification of the ionospheric current flowing westward around the arc and by bursts of Pi2 pulsations. As the expansion continues, a westward travelling surge (WTS) develops. The WTS has the shape of a bright fold or vortex and travels westward along a well established, east-west extended arc. The WTS carries the leading edge of the westward electrojet along the poleward boundary of the eastward electrojet. Intense, energetic precipitation into the WTS carries the westward electrojet back into the magnetosphere via a field aligned current. Behind (east of) the WTS, auroral activity expands poleward leading to a bulge in the aurora inside which the irregular geomagnetic pulsations are observed through their magnetic signatures on ground based magnetometers.

In addition to producing the initial arc brightening at substorm

onset, the beams of high energy precipitating electrons (energy of 20keV and more) also lead (Samson, 1982) to bursts of bremsstrahlung X-rays (Akasofu, 1968; Pytte and Trefall, 1972) and to the increased absorption of cosmic radio noise as observed by riometers (Pytte and Trefall, 1972; Pytte et al., 1976; Hargreaves et al., 1979; Opgenoorth et al., 1983). Modulation of the precipitation is closely connected to the substorm associated Pi2 pulsations (Stuart et al., 1977) to be described later.

### 2.2.3 Ground-based magnetic observations

In addition to the visual auroral features, variations in the magnetic field components at the earth's surface also indicate the occurrence of substorms. A spatially distributed array of magnetometers on the earth's surface can establish the approximate position of the current systems overhead. Detailed information concerning the spatial distribution of the current flow over a limited area can be obtained from coherent and incoherent radar observations.

The classic magnetic signature of substorm onset at an auroral zone observatory (Figure 2.2) is a sudden negative perturbation in the north-south (H) component of the earth's magnetic field due to a sudden enhancement of the electrojet current flowing overhead. Simultaneous changes in the east-west (D) and vertically downward (Z) components position the substorm enhanced westward electrojet relative to the auroral zone station (Rostoker et al., 1980).

In the initial studies of magnetic bay signatures at mid-latitudes it was realised by Stuart (1972a,b) that the region of generation of the substorm in the magnetosphere must be of limited azimuthal extent. This conclusion was based upon observations of the special type of Pi2

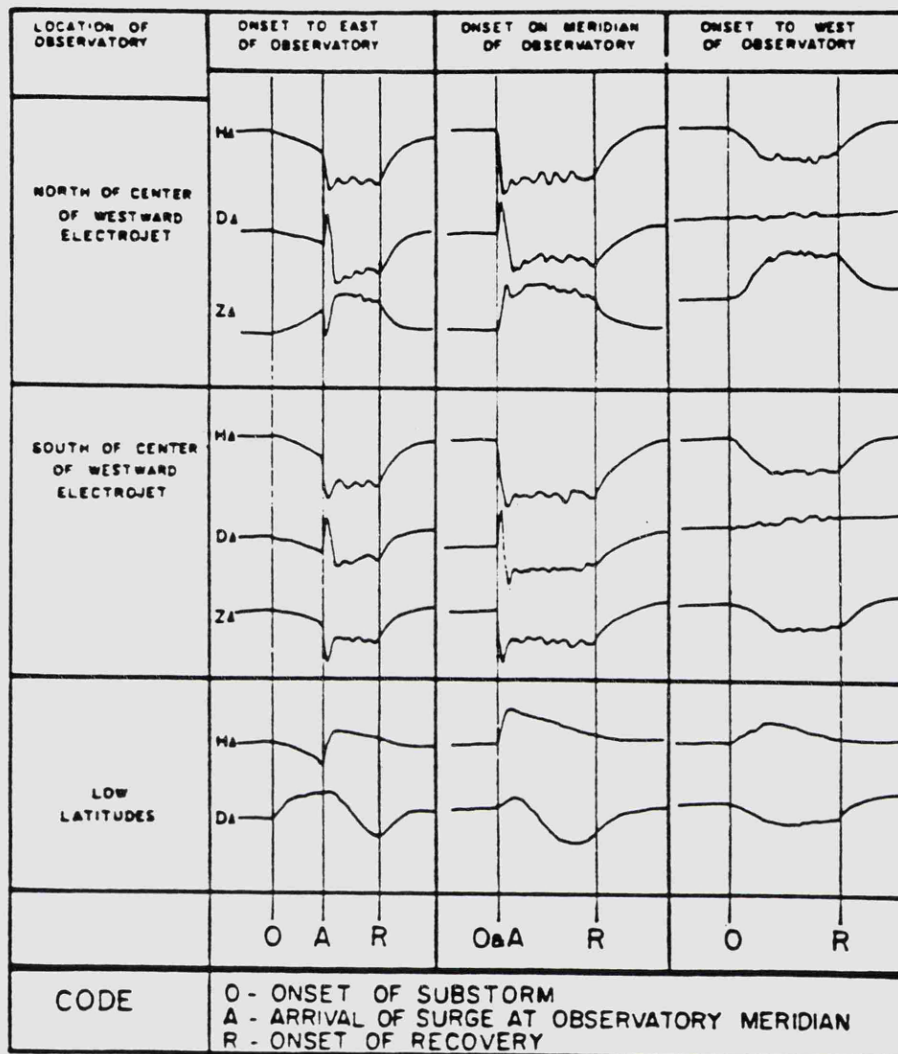


Figure 2.2

Schematic representation of magnetograms from various sites placed at different positions relative to the high latitude current systems. These schematic figures may be compared with real data to determine the position and time sequence of events for an interval of substorm activity (after Rostoker et al. 1980).

pulsations observed (termed dPi) which are only observed in a limited meridional sector near the time of the maximum bay occurrence. In addition, Stuart also supported the theory of an impulsive earthward movement of plasma occurring at substorm onset in this limited longitudinal area. This in some ways pre-empted the introduction of the substorm current wedge, perhaps the most successful method of ordering magnetic observations which arose from the work of McPherron et al., (1973) and Clauer and McPherron, (1974). These authors introduced the concept of the substorm current wedge for the system of field-aligned and ionospheric currents present at substorm onset (Figure 2.3). This model, although almost certainly an oversimplification of the true currents present, involves the diversion of a part of the current which normally flows westward through the plasma sheet down field lines to the auroral ionosphere where the current flows as the substorm enhanced westward electrojet before returning to the magnetosphere via a field-aligned current in the west which completes the wedge. As illustrated in Figure 2.4 this substorm current wedge produces, at mid-latitudes on the ground, a positive perturbation in the H component which is symmetrical about the centre of the wedge when inside the wedge, the perturbation being negative outside. The perturbation in the D component is asymmetrical about the centre of the wedge and reaches a maximum (minimum) at the location of the upward (downward) field aligned currents located at the west (east) of the wedge. The centre of the wedge occurs where the D component perturbation is equal to zero, the H-component perturbation having its maximum extent at this position also.

The concept of the substorm current wedge is very important in ordering various parameters of the Pi2 pulsations observed at mid-latitudes on the ground and will be returned to shortly.

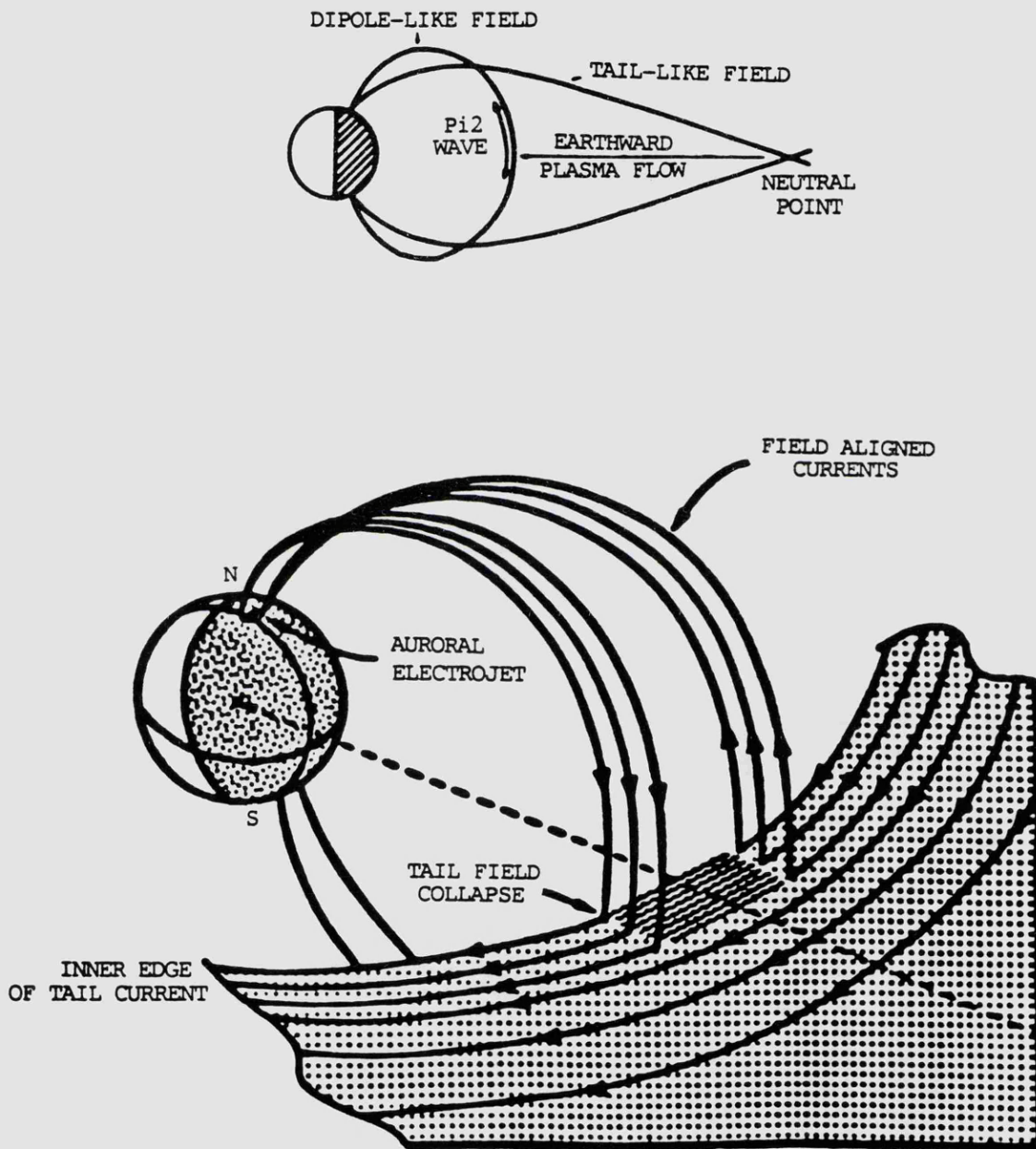
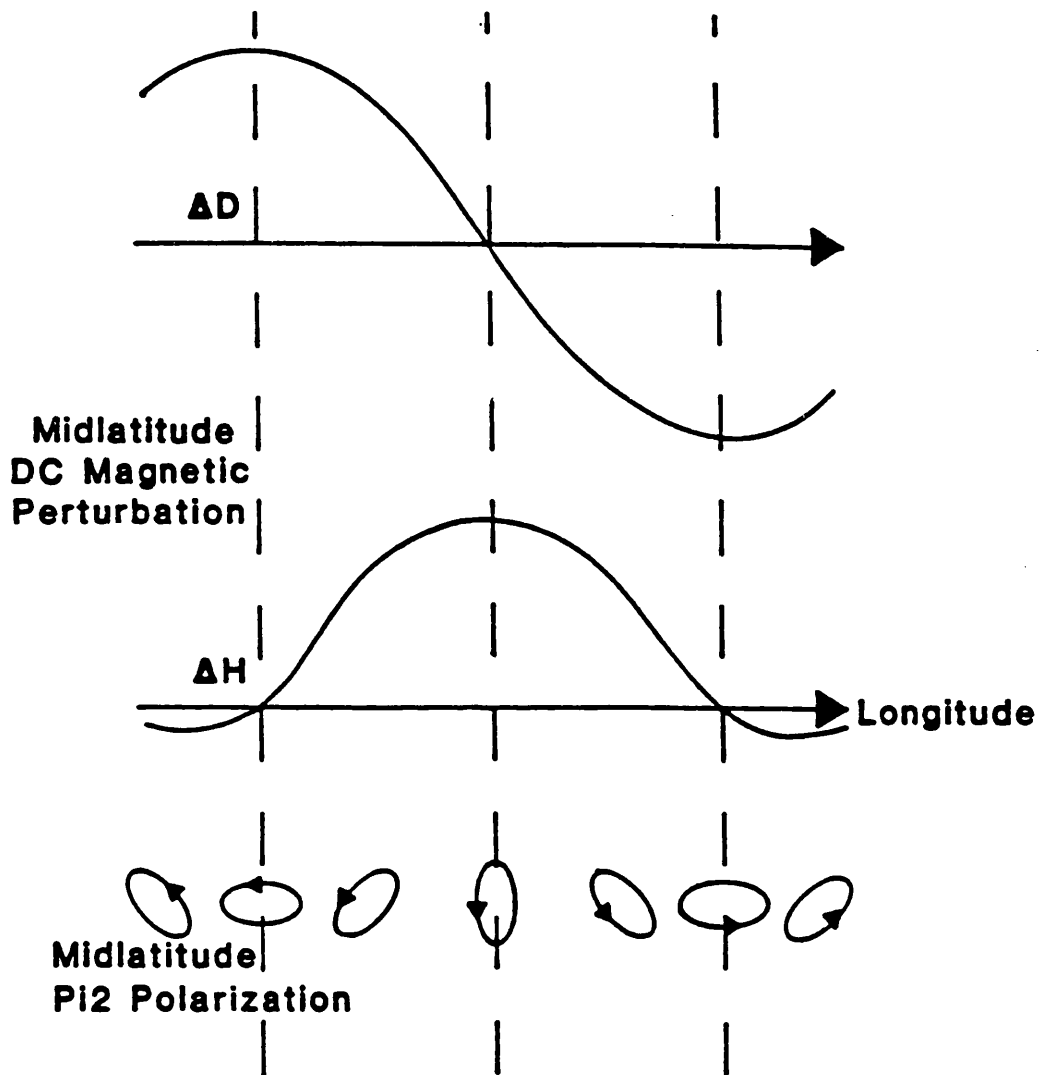


Figure 2.3

top: Diagram representing the reconfiguration of the nightside magnetospheric field associated with the disruption of the cross-tail current at substorm onset.

bottom: Schematic representation of the substorm current system introduced by McPherron et al. (1973). Part of the cross-tail current is diverted down field lines and closes via a westward electrojet in the auroral ionosphere.



**Figure 2.4**

The mid-latitude magnetic perturbations caused by the substorm current wedge current system illustrated in Figure 2.3 with the associated Pi2 pulsation polarisation pattern predicted for a chain of mid-latitude ground magnetometers by Lester et al. (1983,1984).

## 2.3 Pi2 pulsations

### 2.3.1 General Features

The irregular pulsations associated with substorm onsets are designated Pi2 (Jacobs et al., 1964) because they are pulsations, are irregular and lie in a second, probably arbitrarily prescribed, period range (40s-150s). It is important to note that Pi2 pulsations occur at each substorm onset or intensification and are generated on field lines that thread the auroral zone break-up region. Being so closely associated with substorms, Pi2 pulsations are in general a nighttime phenomenon with a peak occurrence around 23:00 local time and a peak in amplitude at auroral zone latitudes (Rostoker, 1967). The Pi2 pulsation energy maximises in the centre of the substorm enhanced electrojet (Olson and Rostoker, 1975), but the peak in the polarised part of the Pi2 pulsation signal is found at the equatorward border of the substorm enhanced electrojets (Rostoker and Samson, 1981).

Although the Pi2 pulsation amplitude peak lies in or at the equatorward boundary of the auroral zone, the signals are very noisy due to the presence of Pi1/Pi2 band electrojet noise (Samson, 1982). Several features separate Pi2 pulsations from the electrojet noise: Pi2 pulsation onset occurs simultaneously with substorm onset with a minimal time delay at all observing sites; Pi2 pulsations are damped, quasi-sinusoidal oscillations which seldom last for more than 10-15 minutes with narrow band spectra; Pi2 pulsation spectra are typical of pure states of polarised waves in contrast to the Pi2 band noise spectrum which is broad band, unpolarised and can last for as long as the substorm enhanced electrojet. These features of Pi2 pulsations should also be observed at mid-latitude stations to confirm the presence of the corresponding high-latitude Pi2 pulsation. The one

dominant mid-latitude frequency should also be among those present at high latitudes. Previous to this, Stuart and Booth (1974) had found that as magnetic activity increased and the generation region therefore moved to lower latitudes and nearer their observatory, so the number of frequency components increased away from the single frequency observed at low activity. This may have been a result of the increase in Pi2 band noise (Samson, 1982).

The absence of Pi2 band noise at mid-latitudes means that a much clearer signal is observed in these regions although the manner in which it propagates from the auroral zone source region to mid-latitudes is a matter of some debate at the present time and will be returned to shortly.

### 2.3.2 Pi2 pulsations and the substorm current wedge

It has long been known that the initial impulsive onset of the mid-latitude positive bays and Pi2 pulsations are closely connected and are a signature of substorm onset (Rostoker, 1967; Stuart, 1972). Initially in the study of Pi2 pulsations at mid-latitudes the various parameters i.e., occurrence, polarisation etc, were usually ordered in terms of local or geomagnetic time and/or geographic(geomagnetic) longitude and latitude (e.g. Sherwood et al., 1973; Bjornsson et al., 1971; Fukunishi, 1975; Stuart and Macintosh, 1974; Mier-Jedrzejowicz and Southwood, 1979; Baransky et al., 1980). The introduction of the substorm current wedge lead researchers to order their observations relative to a substorm centred system of coordinates.

Perhaps the most successful in this respect were Lester et al. (1983, 1984) who were able to order the Pi2 pulsation parameters observed on an array of five magnetometers situated across the United States at a

geomagnetic latitude of 55 degrees north with the substorm current wedge. They demonstrated that the orientation of the horizontal (H-D) polarisation ellipse (azimuth) changes as depicted in Figure 2.4 (bottom), rotating from pointing to the east at the western field-aligned current associated with the wedge to north-east, north, north-west and finally west as we proceed through the centre of the wedge to the eastern field-aligned current. They also demonstrated that the bay perturbations followed those suggested by McPherron et al. (1973) and could also be utilised to position their stations relative to the substorm current wedge. The perturbations in the horizontal components were obtained by subtracting the H,D values at the start of the Pi2 pulsation from those obtained when wave activity had ceased. Lester et al. (1984) found that for isolated clear onsets, or for the first in a series of onsets, the two methods of positioning their stations relative to the wedge (Pi2 polarisation azimuth and perturbations in the H,D components) gave consistent results. A similar study (Hughes and Singer, 1985) employing 80 magnetometers worldwide to uniquely determine the ionospheric and field-aligned currents confirmed the results of Lester et al. (1983, 1984).

In addition Lester et al. (1983, 1984) noted that westward phase propagation was predominant especially to the west and in the centre of the wedge while the sense of rotation of the horizontal polarisation ellipse was counter-clockwise throughout the wedge. Gelpi et al. (1985b) confirmed the mainly westward phase propagation but also noted that the cases of eastward phase propagation observed were associated with clockwise rotation of the polarisation ellipse.

Samson and Harrold (1983) and Samson (1985) also employed substorm centred coordinates in ordering the ellipticity and azimuth of the

horizontal polarisation ellipse of Pi2 pulsations (see later).

Furthermore, the substorm current wedge provided a co-ordinate system for ground-satellite investigations in which the position of the satellite in space relative to the wedge could be determined from the Pi2 pulsations observed on the ground (Singer et al., 1983, 1985; Gelpi et al., 1985a, 1987; Smits et al., 1986; Nagai, 1987; Nagai et al., 1987). This facilitated the study of the field-aligned current systems associated with substorm onset and indicated that the wedge is azimuthally localised in space and does expand to the west and east during the substorm. The wedge is also asymmetric, being wider to the east of centre of the wedge. The centre of the wedge also separates regions of dipolar magnetic field to the west, incorporating the particle injection at substorm onset, from tail-like magnetic field to the east.

### 2.3.3 Pi2 pulsation generation mechanisms (theory)

Pi2 pulsations are believed to be Alfvén wave transients set up at substorm onset and associated with sudden changes in the state of the magnetosphere. These changes at substorm onset may be due to the short-circuiting of a section of the cross-tail current into the auroral oval by the field-aligned currents forming the substorm current wedge described previously. Although the exact mechanism for substorm onset is unclear, it certainly involves a rapid impulsive change in the field-aligned current systems that link the ionosphere to the magnetosphere. A reconfiguration of the ionospheric electric fields and currents results and initially the excess current is carried off up the field line as an Alfvén wave. Hydromagnetic theory in a cold uniform plasma (Southwood and Hughes, 1983) indicates that this transverse mode wave is the only one that can carry field

parallel currents as the energy in the wave is guided by the magnetic field. This wave mode is analagous to a wave on a stretched string with the magnetic field line as the string and the force being the electromagnetic tension on the string due to the finite conductivity in the ionosphere. The conductivity causes ionospheric Pedersen currents to flow which produce a drag on the convective flow of plasma over the ionosphere. This leads to the reconfiguration of ionospheric electric fields and currents mentioned above and the launching of an Alfven wave up the field line. The theory of the generation of such a wave following a change in the ionospheric conductivity distribution was presented by Maltsev et al. (1974) and further developed by Mallinckrodt and Carlson (1978) who included a source in the magnetosphere. The initial wave generated will be subsequently reflected at the conjugate ionosphere and will bounce back and forth reducing in amplitude at each reflection due to ionospheric absorption. The transient hydromagnetic signal set up in this way is observed on the ground as the classic damped Pi2 pulsation signature.

Recently, work has been undertaken on the effect of non-uniform ionospheric conductivities on the reflection of these waves (Ellis and Southwood, 1983; Glassmeier, 1984; Kan et al., 1982; Yarker and Southwood, 1986). Ellis and Southwood (1983) demonstrated that if the electric field of the initial shear Alfven wave pulse, localised to field lines that thread an ionospheric conductivity gradient, has the correct orientation relative to the gradient, then on reflection from the ionosphere, additional field-aligned current sheets are produced which lead to the generation of subsidiary surface waves centred on the magnetic flux tubes connected to the ionospheric discontinuity. Yarker and Southwood (1986) expanded this work to the temporal development of standing hydromagnetic waves between non-uniform

ionospheres and discovered that the additional field-aligned currents and subsidiary surface waves are still generated. This was considered important in establishing a mechanism for the generation of the mid-latitude Pi2 pulsation signal (Southwood and Hughes, 1985).

In reality the magnetosphere is neither cold nor uniform and as a result it is possible for this transient signal to couple to the fast or isotropic mode, so-called because magnetic pressure dominates and the energy in the wave travels in the direction of propagation of the wave. At substorm onset therefore both the transverse and fast modes might be excited as changes in the field-aligned current configuration would be accompanied by particle pressure changes which would become apparent through the fast mode signals (synchronous spacecraft observations of Pi2 pulsations indicate a significant compressional component in the wave (Lin and Cahill, 1975; Sakurai and McPherron, 1983)). As the fast mode propagates isotropically this would lead to the propagation of the signal throughout the magnetosphere.

#### 2.3.4 Models of Pi2 pulsation generation from observation

In the past decade the auroral zone characteristics of substorms have been extensively studied in Scandinavia by means of an array of magnetometers, the STARE coherent radar system (Baumjohann et al., 1981; Opgenoorth et al., 1983) and with optical auroral imaging (Inhester et al., 1981; Pashin et al., 1982). These observations and the resultant modelling of conductivities, electric fields and field-aligned currents in the auroral region led Baumjohann and Glassmeier (1984) to present a transient response model for the generation of Pi2 pulsations.

This model incorporated a voltage generator in the magnetotail to

produce the initial signal, the substorm current wedge and a shear Alfvén wave to carry the upward field-aligned current co-located with the region of enhanced ionospheric conductivity in the auroral break-up region (Baumjohann et al., 1981). This region arose due to the imperfect coupling that exists between the magnetosphere and ionosphere, leading to the generation of a southward polarisation electric field. In turn, the polarisation electric field drives a strong westward ionospheric current which closes by the strong and highly localised upward field-aligned currents at the western edge of the break-up region, Figure 2.5, (Baumjohann et al., 1981). This 'current wedge' expanded as the substorm progressed, following or perhaps even driving the WTS, an eastward expansion also being observed. This region is allowed to move westward and possibly change its shape to account for the observed polarisation characteristics. The shear Alfvén wave also produced the changing equivalent current vortex pattern observed by Pashin et al. (1982). Westward and eastward currents that were observed to the north and south of the active region (Oppenorth et al., 1983) form part of the substorm enhanced electrojet flow in the region of the Harang discontinuity along which the surge is believed to travel.

Similar models for the generation of Pi2 pulsations involving multiple reflections from auroral ionospheres or other magnetospheric boundaries have been presented on a theoretical basis by Nishida (1979), Kan et al. (1982), Sun and Kan (1985) and Rothwell et al. (1986, 1988). These models however are not yet able to predict the polarisation and apparent group and phase velocities observed for the Pi2 pulsations.

Samson (1985) has recently presented an alternative model for the

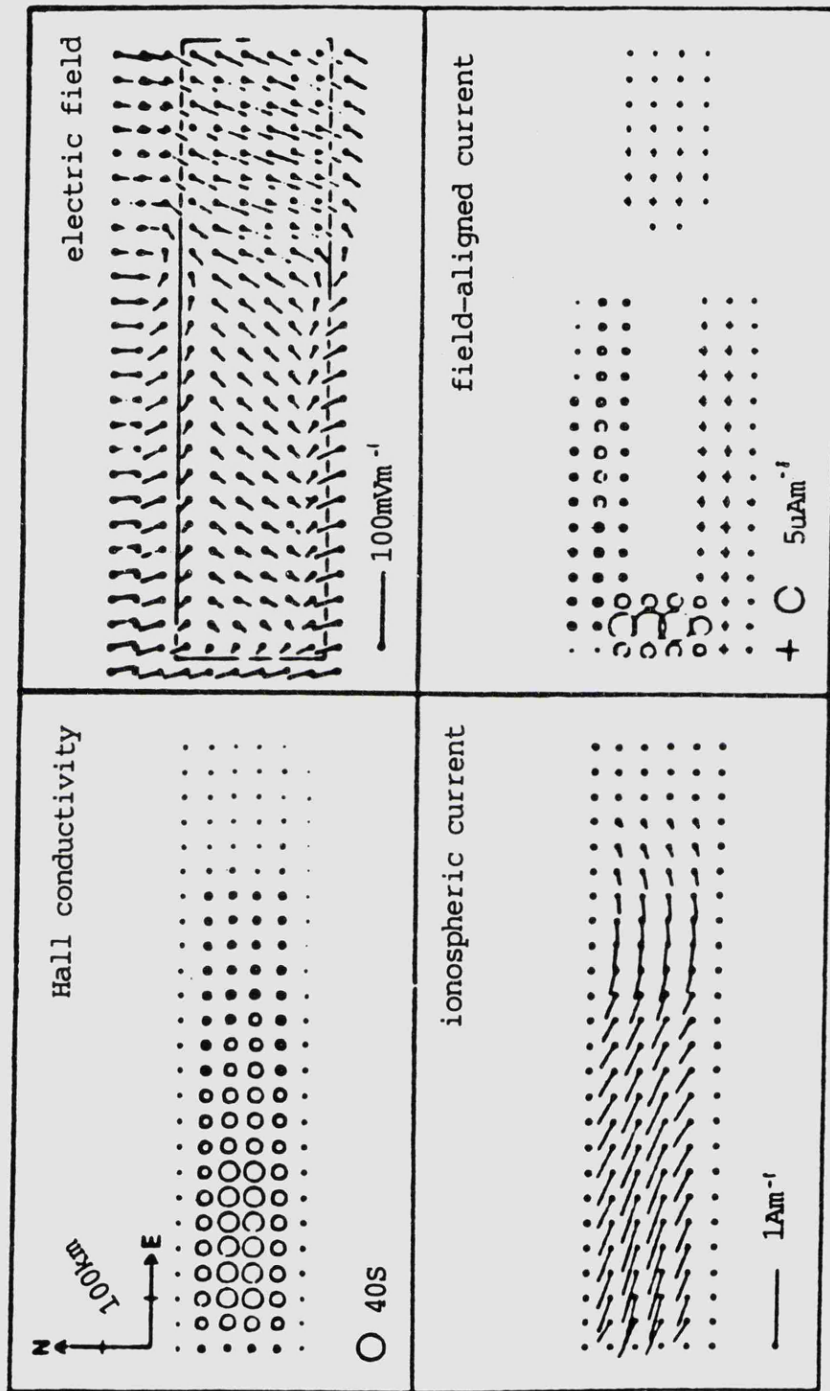


Figure 2.5

The spatial distribution of Hall conductivity, horizontal electric field vectors and ionospheric and field-aligned current in the region of active break-up aurora around local magnetic midnight. The rectangle in the electric field panel approximately frames the region of active aurora. Circles and crosses in the field-aligned current panel denote upward and downward direction of field-aligned current flow (after Baumjohann et al., 1981).

generation of Pi2 pulsations. This model retains the initial propagation of the shear Alfvén waves described previously leading to the enhanced field-aligned currents associated with the substorm expansive phase. The geometry of this system of currents is illustrated schematically in Figure 2.6 (Samson and Rostoker, 1983). They envisaged a current system in which an initially upward directed, oscillating field-aligned current associated with the arc which brightens at substorm onset expands to the east and west feeding south-westward and north-eastward ionospheric currents. These ionospheric currents are then closed by field-aligned current sheets at the northern and southern boundaries of the conducting region, have the same temporal and spatial structure as the original sheet, but are shifted longitudinally due to the southwest-northeast orientation of the ionospheric currents. This system of field-aligned currents is then thought to move westward at a constant velocity but with diminishing strength. Although the current system itself does not oscillate in the moving frame of reference, observers on the ground would see the normal oscillating Pi2 pulsation magnetic fields.

Studies of the characteristic growth and decay time constants and velocities of high and mid-latitude Pi2 pulsations (Samson and Harrold, 1985; Samson et al., 1985) suggest that the Pi2 pulsations observed could not be due to hydromagnetic resonance or multiple reflection type theories because the times involved were shorter than the one-way travel time for Alfvén propagation between auroral ionospheres. Instead they suggest that the Pi2 pulsations are associated with the azimuthal expansion of the substorm current system in conjunction with two longitudinally (east-west) propagating Alfvén waves in the magnetosphere which carry the enhanced field-aligned and ionospheric currents of the substorm expansive phase. Of the two, the

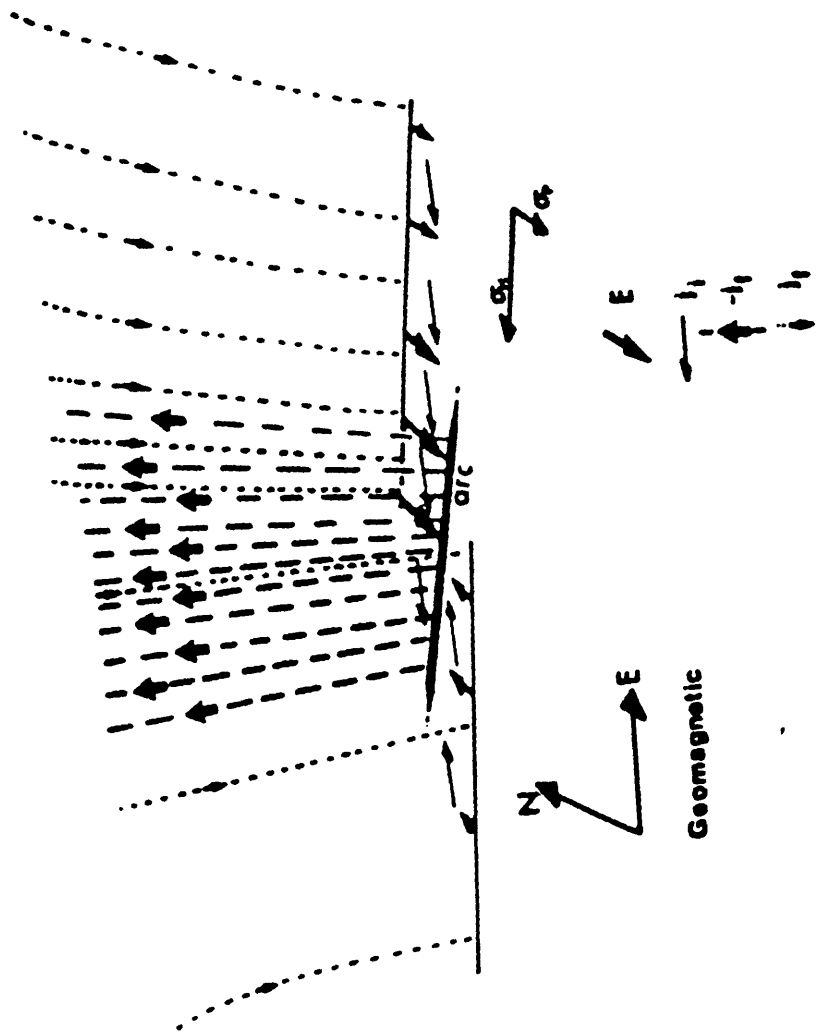


Figure 2.6  
 A model for the field-aligned and ionospheric currents associated with the onset of a substorm (after Samson and Rostoker, 1983).

westward propagating wave probably has the stronger field-aligned current, leading to the westward apparent phase velocities observed at mid-latitudes near the centre of the substorm current wedge (Lester et al., 1983, 1984; Samson et al., 1985).

This model current system also predicts the polarisation reversals and structure across the auroral oval in the region of the WTS as observed by Samson and Harrold (1983) in a statistical study of many Pi2 pulsations. This involved two reversals in polarisation sense when crossing the surge region latitudinally although there was only one reversal observed to the east and west of the surge (Figure 2.7). The change in polarisation sense near the latitudinal maximum is caused by the field-aligned currents associated with the highly conducting strip similar to the surface wave theory of Southwood and Hughes (1985).

Whatever the fine detail of the generation mechanism for the Pi2 pulsations, Samson (1985) states that it seems unlikely that it can be separated from the mechanism leading to the field-aligned currents and arc brightening during the substorm expansive phase, these being so closely connected observationally to Pi2 pulsations.

Although the above models are somewhat different they both include the westward movement and/or expansion of ionospheric and field-aligned current systems after the initial auroral break-up thus explaining some of the observed substorm current wedge type polarisation characteristics and the fact that westward phase velocity for the Pi2 pulsations is nearly always observed.

#### 2.3.5 Pi2 propagation to mid-latitudes (theory)

The initial generation mechanisms for the Pi2 pulsations on field

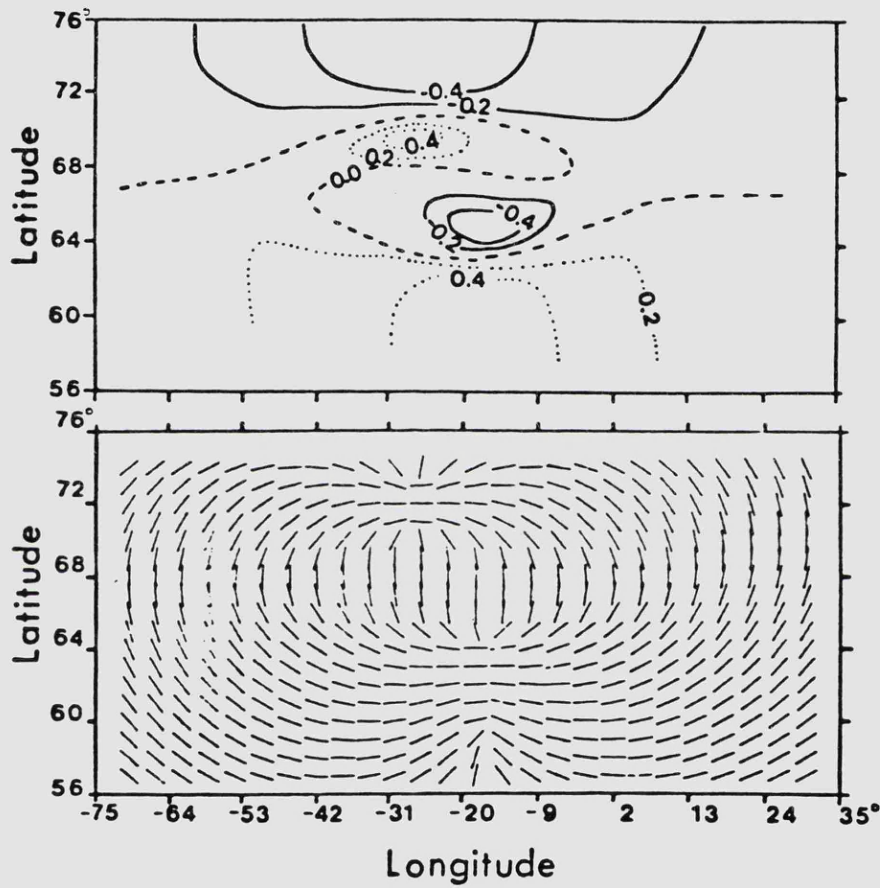


Figure 2.7

Polarisations for the Pi2 pulsation model (Samson and Harrold, 1983).  
 Top: ellipticity (ratio of minor to major axis). Positive and negative  
 ellipticities denote counter-clockwise and clockwise polarisation  
 respectively.

Bottom: Orientations of the major axes of the polarisation ellipses.

lines threading the auroral zone have been described. It is now necessary to discuss the propagation of the disturbances to mid-latitudes, where, as stated previously, the signatures are much clearer. Southwood and Hughes (1983), Southwood (1974) and Chen and Hasegawa (1974a) suggest that spatial plasma non-uniformities in the magnetosphere can lead to the coupling of the fast mode waves to the transverse mode wave which sets-up field line resonances on isolated magnetic shells where the fast mode signal frequency is equal to the local transverse Alfvén mode eigenfrequency. This theory predicts an amplitude peak at the resonance location and a reversal in polarisation sense across it latitudinally.

Equally important, Chen and Hasegawa (1974b) demonstrate that surface waves can be excited by the same broad band sources on sharp plasma boundaries such as the plasmapause. The response of the magnetosphere to a source which generates fast mode waves has been modelled by Orr and Hanson (1981); Gough and Orr (1984) and reviewed by Orr (1984). Southwood (1974) and Orr (1975), in addition to the above authors, have investigated the amplitude and phase variation on the ground of geomagnetic signals and discovered three regions where a resonance may occur. These are the plasmasphere, at the plasmapause and in the plasmatrough, and a phase change of 180 degrees in the H (north-south) magnetic component is produced at each boundary (Figure 2.8). In addition, Southwood indicated that polarisation reversals would be associated with these resonance locations.

Theoretical studies by Southwood and Hughes (1985) indicated that the subsidiary surface waves generated at a conductivity gradient (see above) could, under certain circumstances, combine to reproduce the well-known mid-latitude substorm current wedge pattern of polarisation

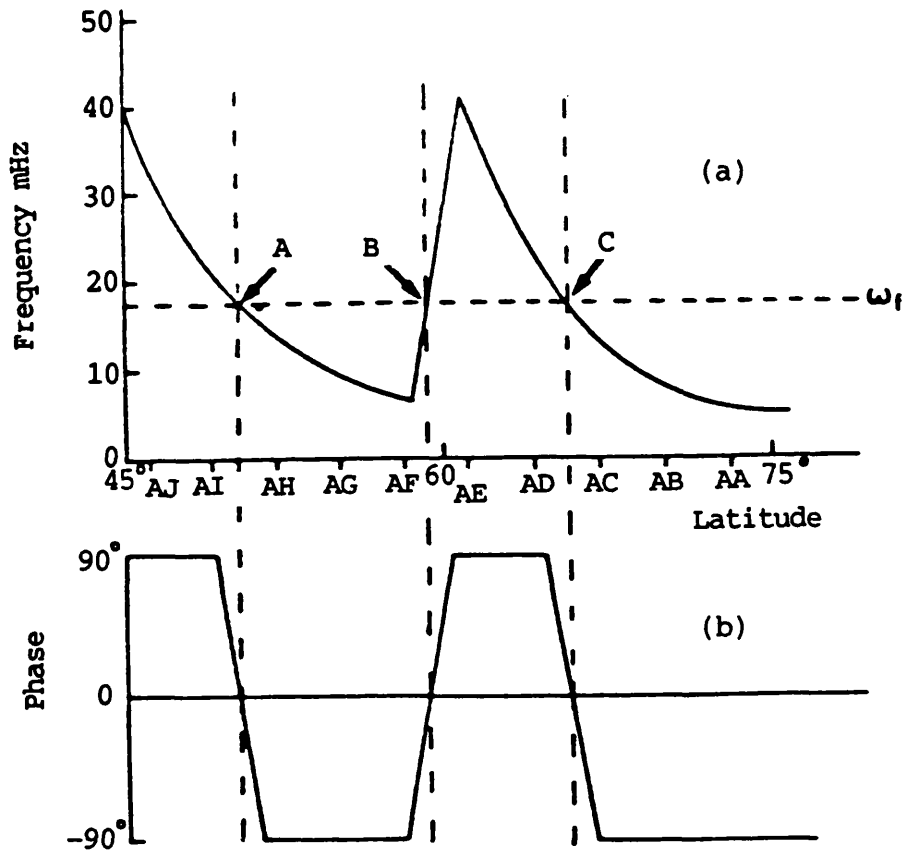


Figure 2.8

- a) A schematic representation of the variation of geomagnetic pulsation eigenfrequencies with latitude.
- b) The idealised predicted phase variation with latitude for a forcing wave corresponding to  $\omega_f$  in a) when steady state conditions have been achieved (Orr and Hanson, 1981).

azimuths observed by Lester et al. (1983). To do this, the waves would have to be of opposite circular polarisation, of equal wavelength but different amplitude and be travelling in opposite directions (Figure 2.9). The observed pattern in the polarisation azimuth was predicted but the longitudinal variation in ellipticity was not, the model giving constant ellipticity with longitude.

From these theoretical studies the following mechanisms have been suggested to account for the propagation of the Pi2 pulsation to mid-latitudes:

- a) a surface wave on the plasmopause (Fukunishi,1975; Sutcliffe,1975; Lester and Orr,1983)
  - b) a mid-latitude field line resonance (Stuart et al.,1979)
  - c) a cavity resonance of the plasmasphere (Doobov and Mainstone, 1973; Stuart, 1974; Lester and Orr, 1981)
- and
- d) a combination of the effects of both high-latitude field-aligned and electrojet currents (Samson 1982, 1985).

#### 2.3.6 Pi2 propagation to mid-latitudes (observation)

Southwood and Stuart (1980) reviewed the observational results and suggested that the following features are consistent with a forced Alfvén wave field line resonance with the resonant shell near the amplitude peak:

- a) predominantly westward propagation, (Mier-Jedrzejowicz and Southwood, 1979; Lester et al., 1984; Samson et al.,1985; Samson and Harrold, 1985; Gelpi et al., 1985b).
- b) polarisation structure changing from clockwise to counter-clockwise when moving equatorward across the

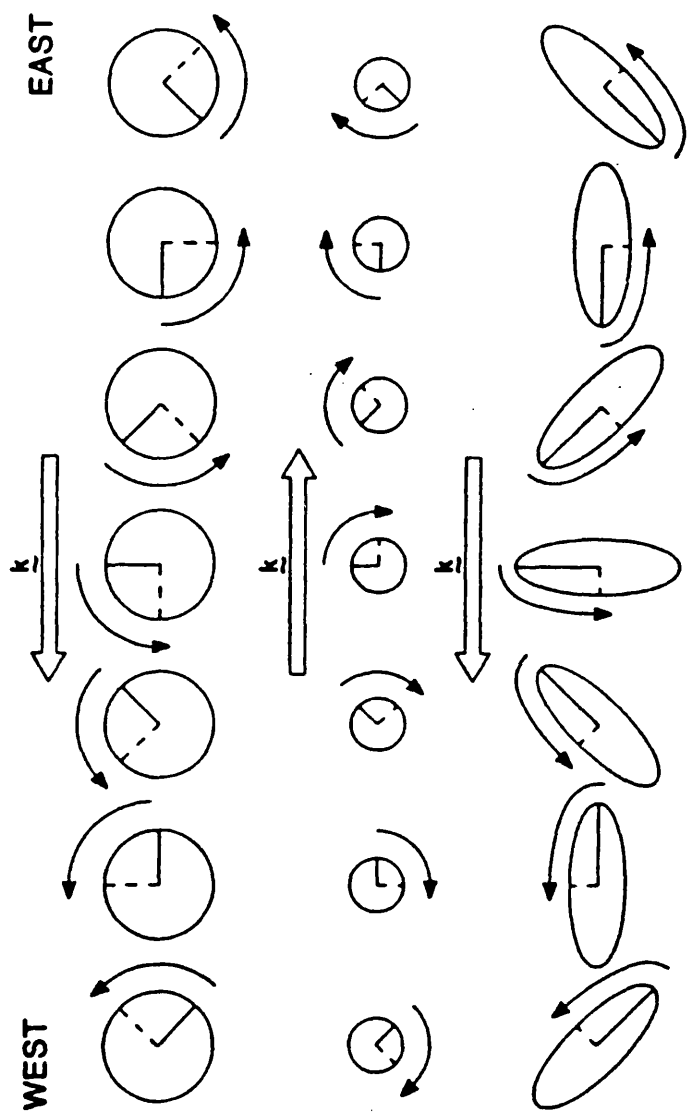


**Figure 2.9**  
 Illustration that interference between two waves of equal east-west wavelength but travelling in opposite directions and of different amplitudes produces the observed mid-latitude Pi2 polarisation pattern (after Southwood and Hughes, 1985).

mid-latitude amplitude peak (Fukunishi, 1975; Bjornsson et al., 1971; Saito et al., 1976; Lester and Orr, 1981).

c) at the location of this amplitude peak, there is a north-south phase variation in the H component rather than the D component (Bjornsson et al., 1971; Lester and Orr, 1981).

d) constant frequency observed with latitude (Fukunishi, 1975; Stuart, 1972b).

In a case study of two Pi2 pulsations observed at high latitudes in the eastward electrojet (Lester et al., 1985), the Pi2 pulsation parameters were consistent with those predicted by the field line resonance mechanism.

Southwood and Stuart's premise is true allowing for the 90 degree rotation of the horizontal wave polarisation by the ionosphere (Inoue, 1973; Hughes, 1974). However, Pi2 pulsations have the characteristics of an impulse response and an Alfvén wave impulse response should have a latitude dependent frequency. This led Southwood and Stuart to suggest that the observations mentioned above are consistent with a surface wave travelling along the plasmopause. Pi2 pulsation periods inferred from satellite plasma density measurements obtained simultaneously with Pi2 pulsations on the ground (Lester and Orr, 1983) were consistent with those for surface waves travelling along the plasmopause and the measured Pi2 pulsation period. In addition, Lester and Orr (1983) did not find a strong enough secondary amplitude peak or an ellipticity reversal at this peak, providing further evidence against the field line resonance model. They did however find occasions when the surface wave mechanism was not in operation, the horizontal magnetic components appearing to be decoupled and to have different dominant periods at different latitudes at these times.

The reason for the Pi2 pulsation signal being so clear at latitudes below the auroral zone (Southwood and Stuart, 1980) is that the plasmopause determines the one dominant wave frequency normally observed at mid-latitudes. This frequency is related to the length of the field line involved in the resonance through the Alfvén travel time of the wave between conjugate ionospheres. The period is given by twice the Alfvén travel time (Orr, 1984) and is therefore also dependent on the magnetic field strength and plasma density present on the appropriate flux tube. This may explain the observed increase in the Pi2 pulsation period as the latitude of the break-up region increases (Saito et al., 1976; Kuwashima and Saito, 1981). If the Pi2 pulsations are generated on field lines that thread the break-up region, the field line length increases as the region moves poleward. This would be true for field lines that are dipolar after substorm onset has occurred. An investigation by Hughes and Singer (1985) also found this trend although the periods of the two events did not fit the relationship of Kuwashima and Saito (1981).

Similar arguments apply to the relationship between Pi2 pulsation period and geomagnetic activity; as activity increases the low latitude boundary of the auroral oval moves equatorward, the period decreasing as a result of the field line length at onset also decreasing (Troitskaya, 1967; Troitskaya and Gul'elmi, 1967; Stuart and Booth, 1974). The screening and smoothing effect of the ionosphere on pulsation signals (Hughes, 1974; Hughes and Southwood, 1976a,b; Southwood and Hughes, 1983) may explain why on occasions the positions of a) the secondary amplitude peak, b) the plasmopause, c) the polarisation reversal and d) the secondary amplitude peak are not coincident.

#### 2.4 Summary of Pi2 pulsation mechanisms

There remains considerable debate over the generation mechanisms for Pi2 pulsations and the source of the mid-latitude signature of the Pi2 pulsations which are observed over a large azimuthal range, (Hughes, 1982; Singer et al., 1983). A possible mechanism is the generation of a surface wave at the plasmapause. This is initially excited by fast mode compressional waves created by the tail field collapse at substorm onset or by mode coupling with the shear Alfvén wave (Baumjohann and Glassmeier, 1984). However, there is clear evidence that the current wedge and the subsidiary wave generation from strong conductivity gradients at the equatorward edge of the auroral oval play an important role in the generation and propagation of the observed Pi2 pulsation signals (Lester et al., 1983, 1984; Southwood and Hughes, 1985; Samson, 1985; Samson and Harrold, 1985; Yarker and Southwood, 1986).

This chapter has reviewed the main features of the coupling between the magnetosphere and ionosphere with special reference to magnetospheric substorms and the geomagnetic Pi2 pulsations associated with substorms that are the topic of this thesis. Models for the generation and propagation of the Pi2 pulsations have been discussed together with the results from experimental studies which utilised mainly ground-based magnetometer and coherent radar techniques. The physical concepts introduced in the models will be applied to the interpretation of the Pi2 pulsation events which have been observed by the SABRE radar and form the major study presented in this thesis.

## CHAPTER 3

### EXPERIMENTAL OBSERVATIONS

#### 3.1 SABRE and magnetometer systems

SABRE (Sweden And Britain Radar aurora Experiment) is a bi-static auroral radar consisting of two multi-beam radars that are sensitive to plasma irregularities in the auroral zone E-layer of the ionosphere. The two radars were constructed and operated jointly by Leicester University, U.K. and the Max Planck Institut fur Aeronomie, Lindau, F.R.G. They are located at Wick in Scotland and Uppsala in Sweden. Figure 3.1 indicates the common viewing area of the two radars in the SABRE system, this extends from about 64 to 68 degrees geographic north and from 0 to 12 degrees geographic east.

The radars measure the backscatter amplitude and line of sight Doppler velocity of the plasma irregularities within this 200,000km viewing area with spatial and temporal resolutions of 20x20km and 20s respectively. The Doppler velocity measurements are combined in order to calculate the drift velocity of the irregularities. This is assumed to be a close approximation to the electron drift velocity in the E-region, hence the electric field vector can be determined from the relationship  $\underline{v} = \underline{E} \times \underline{B} / B^2$ .

The accuracy and validity of this approximation has recently been investigated by Nielsen and Schlegel (1983, 1984) who compared the velocities measured by the SABRE/STARE and EISCAT radars. It appears

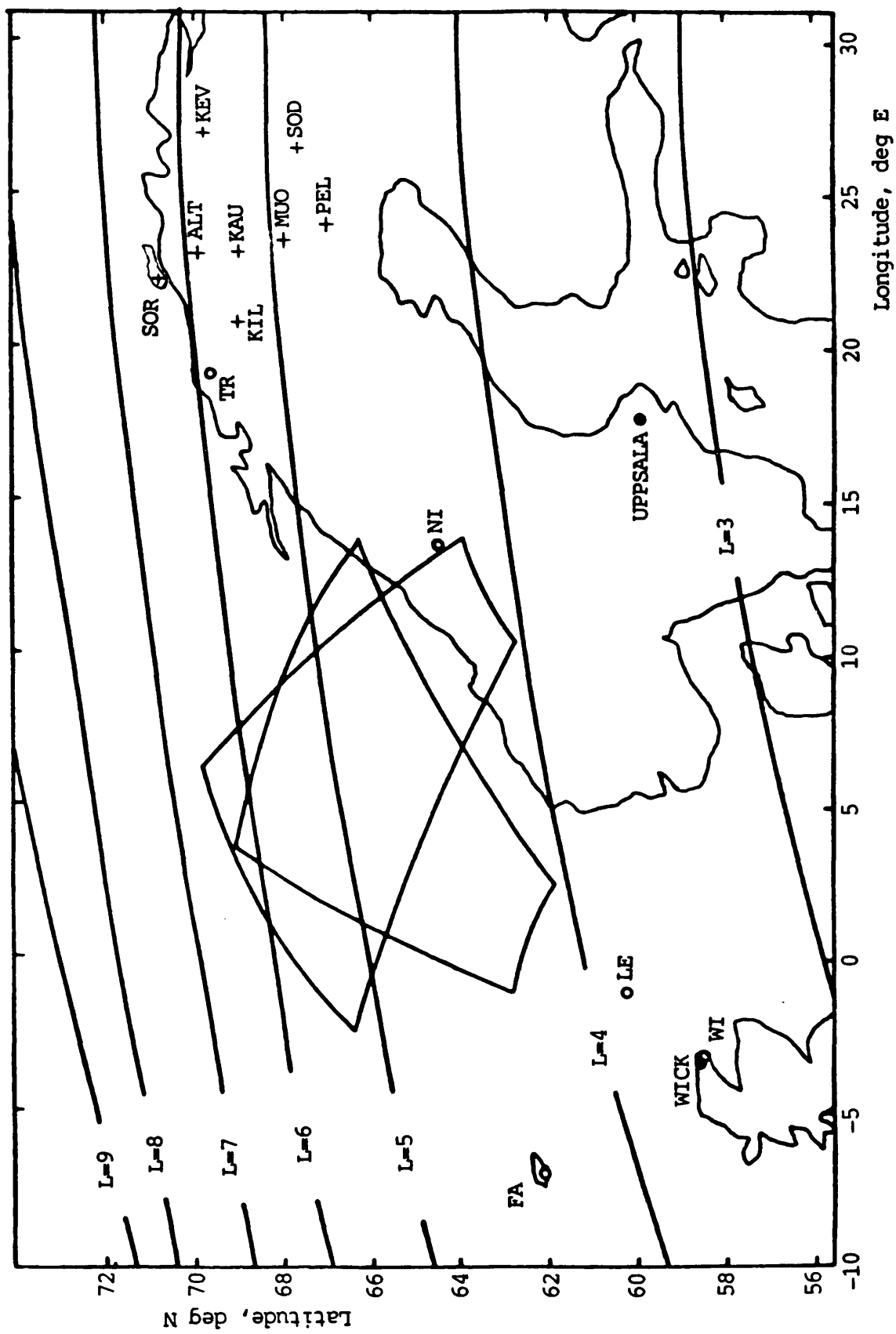


**Figure 3.1**

A diagram to illustrate the SABRE viewing area relative to magnetic L-shells, the positions of the BGS magnetometers (.) and the stations of the EISCAT magnetometer cross (+).

that coherent radars (SABRE/STARE) increasingly underestimate the drift speeds above about 350m/s, however the directions of drift are accurate at all values of velocity. Theoretical studies by Robinson (1986) suggest that the irregularity drift velocity is limited to the ion-acoustic speed by non-linear wave heating effects, the observed variations in the E-region irregularity drift speeds being mainly due to E-region ion temperature variations which change the ion-acoustic speed. When the true E-region electron drift velocity is well in excess of the ion-acoustic velocity, the irregularity drift velocity measured by SABRE is still approximately equal to the ion-acoustic speed, although this will be increased by the increase in temperature. In this study only relative changes in velocity magnitude are important therefore no correction has been applied to the observed speeds.

Figure 3.1 also indicates the positions of the tri-axial fluxgate magnetometers deployed by the Geomagnetism Research Group of the British Geological Survey (BGS) around the SABRE viewing area to study substorms and their related Pi2 pulsations. These are situated at Wick, Faroës, Lerwick, Nordli and Tromsø. Their station codes, geographic and geomagnetic coordinates are given in Table 3.1. The stations of the EISCAT magnetometer cross operated by the Technical University of Braunschweig (Luhr et al., 1984a,b) are also indicated, by a cross, in Figure 3.1 with their coordinates given in Table 3.2. Data were provided from this array for a selection of events (H. Luhr, personal communication 1988).

### 3.2 Magnetometer Data Analysis

The BGS magnetometers measure the fluctuations in the earth's magnetic field in each of three mutually perpendicular directions :

Table 3.1

<u>B.G.S.</u> <u>Magnetometer</u> <u>Station</u>	<u>Geographic</u> <u>Latitude</u> <u>(deg N)</u>	<u>Geographic</u> <u>Longitude</u> <u>(deg E)</u>	<u>Geomagnetic</u> <u>Latitude</u> <u>(deg N)</u>	<u>Geomagnetic</u> <u>Longitude</u> <u>(deg E)</u>
Tromso (TR)	69.6	19.0	66.4	104.2
Nordli (NI)	64.5	13.5	61.6	96.1
Faroes (FA)	62.0	-7.0	61.3	78.9
Lerwick (LE)	60.1	-1.2	58.5	82.2
Wick (WI)	58.4	-3.1	56.9	79.8

Table 3.2

<u>EISCAT Cross</u> <u>Magnetometer</u> <u>Station</u>	<u>Geographic</u> <u>Latitude</u> <u>(deg N)</u>	<u>Geographic</u> <u>Longitude</u> <u>(deg E)</u>	<u>Geomagnetic</u> <u>Latitude</u> <u>(deg N)</u>	<u>Geomagnetic</u> <u>Longitude</u> <u>(deg E)</u>
Soroya (SOR)	70.5	22.2	67.3	107.9
Alta (ALT)	69.9	23.0	66.6	107.8
Kautokeino (KAU)	69.0	23.1	65.8	107.2
Muonio (MUO)	68.0	23.5	64.7	106.7
Pello (PEL)	66.9	24.1	63.6	106.0
Sodankyla (SOD)	67.4	26.6	63.6	108.5
Kilpisjarvi (KIL)	69.1	20.7	66.0	105.5
Kevo (KEV)	69.8	27.0	66.2	110.6

H-component, positive geomagnetic north; D-component, positive geomagnetic east and Z-component which is positive vertically downwards. At each station, the data are recorded digitally in serial form on quarter inch magnetic tape cassettes. When the cassette is full it is returned to the BGS in Edinburgh where the data are transcribed to parallel nine track binary format on half-inch machine readable magnetic tapes. These tapes then constitute master files for each station's data from which selected data events of interest can be retrieved, usually onto floppy disc, for analytical processing. Before this transcription process takes place, an analogue record of the data on the cassette is generated on Z-fold paper via a digital to analogue converter connected to an ink jet pen recorder. This record provides verification of correct operation and as a first means of identifying clear pulsation events for further analysis. Although Pi2 pulsations are distinctive in form, when the level of magnetic activity is high or when they occur with a rapid background field movement representing substorm onset, numerous scale jumps occur in a short time and the observation of Pi2 pulsations at these times is often difficult (Stuart and Green, 1981). For this reason the analogue records from the lowest latitude station (Wick) were employed initially in the selection of Pi2 pulsations for study, although it is possible that some events during high magnetic activity may still have been omitted.

The analysis routines plot either the three magnetic components for each station individually or one component from a range of stations (Figure 3.2 top). The data can be filtered if required and the filter type and parameters may be specified by the user (Figure 3.2 bottom). A range of spectral analysis routines based on the Maximum Entropy (ME) and Fast Fourier Transform (FFT) techniques are available for determining the dominant frequency content of any pulsations present

WICK MAGNETOMETER Day 19, 1984

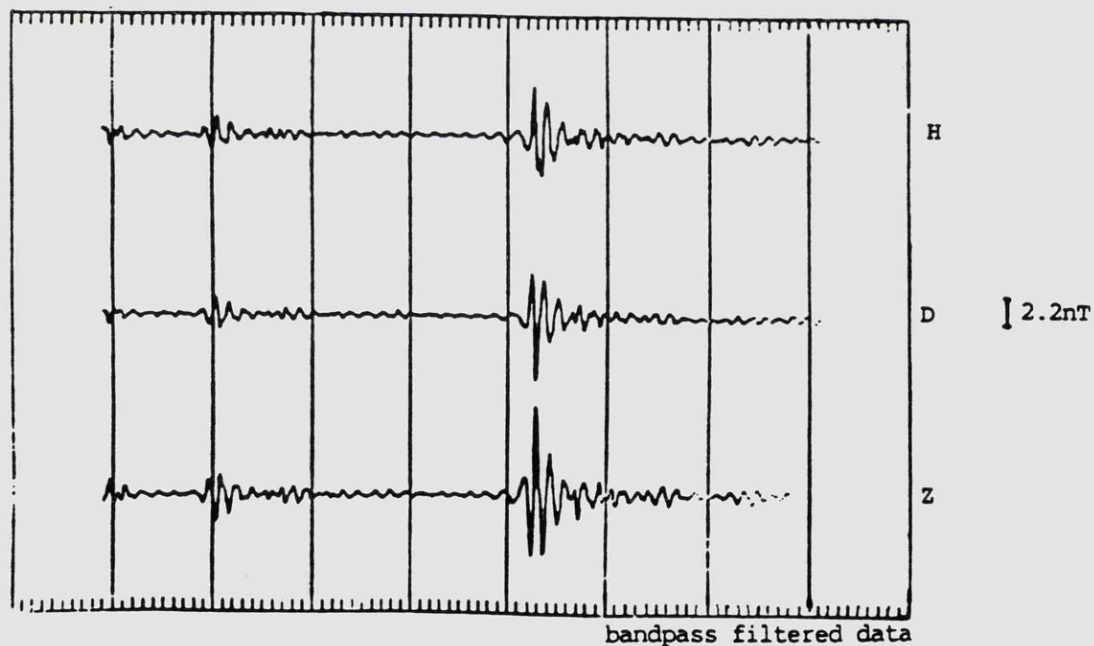
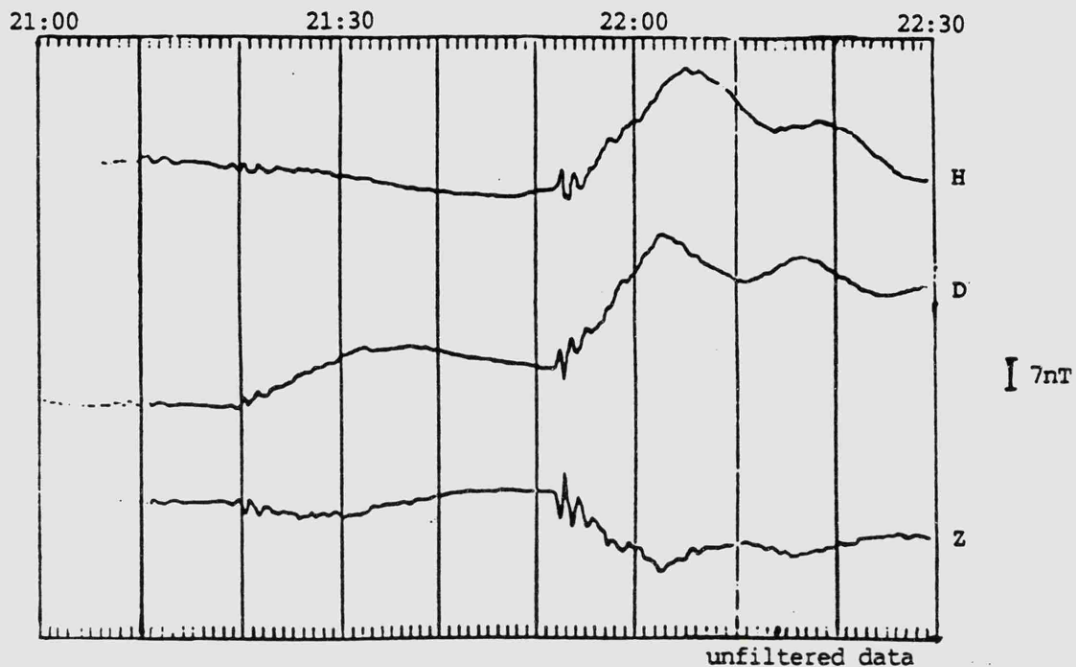


Figure 3.2 (top)

Unfiltered magnetogram from the BGS station at Wick illustrating a Pi2 pulsation occurring at substorm onset (21:52) in the three magnetic components.

Figure 3.2 (bottom)

Same as Figure 3.2 (top) but for bandpass filtered data.

in the data. In the case of FFT spectral analysis, cross polarisation studies between the various components can be undertaken from which the azimuth and ellipticity of the horizontal (H-D) polarisation ellipse of the wave can be obtained. Throughout this thesis the azimuth ranges from -90 degrees through 0 degrees to +90 degrees, corresponding to westward pointing, rotating clockwise through north to eastward pointing. The ellipticity ranges from -1 through 0 to +1 corresponding to circularly polarised in the clockwise sense through linear polarisation to circularly polarised in the counter-clockwise sense when looking down from above the ionosphere in the northern hemisphere.

### 3.3 SABRE Data Analysis

#### 3.3.1 SABRE time series analysis

When the raw SABRE data are returned to Leicester on magnetic tape they are routinely analysed to produce quick-look RTI (Range-Time-Intensity) plots for both Wick and Uppsala. An example of this type of plot for one radar beam is reproduced in Figure 3.3. A black mark is made where the backscatter observed by the radar exceeds the noise level by 3dB or more, the horizontal axis represents time and the vertical axis the range at which backscatter was observed.

From this type of plot long period continuous pulsations have been identified in the SABRE data. For the shorter period pulsations of interest in this study however, the RTI plots could only provide an indication that backscatter was being observed by the radars. When the time of an event is known it is first necessary to combine the single-station data (i.e. Wick and Uppsala) to give merged SABRE data for the event. This then provides a measure of the irregularity drift velocity and backscatter amplitude in each of the 26x26 cells in the

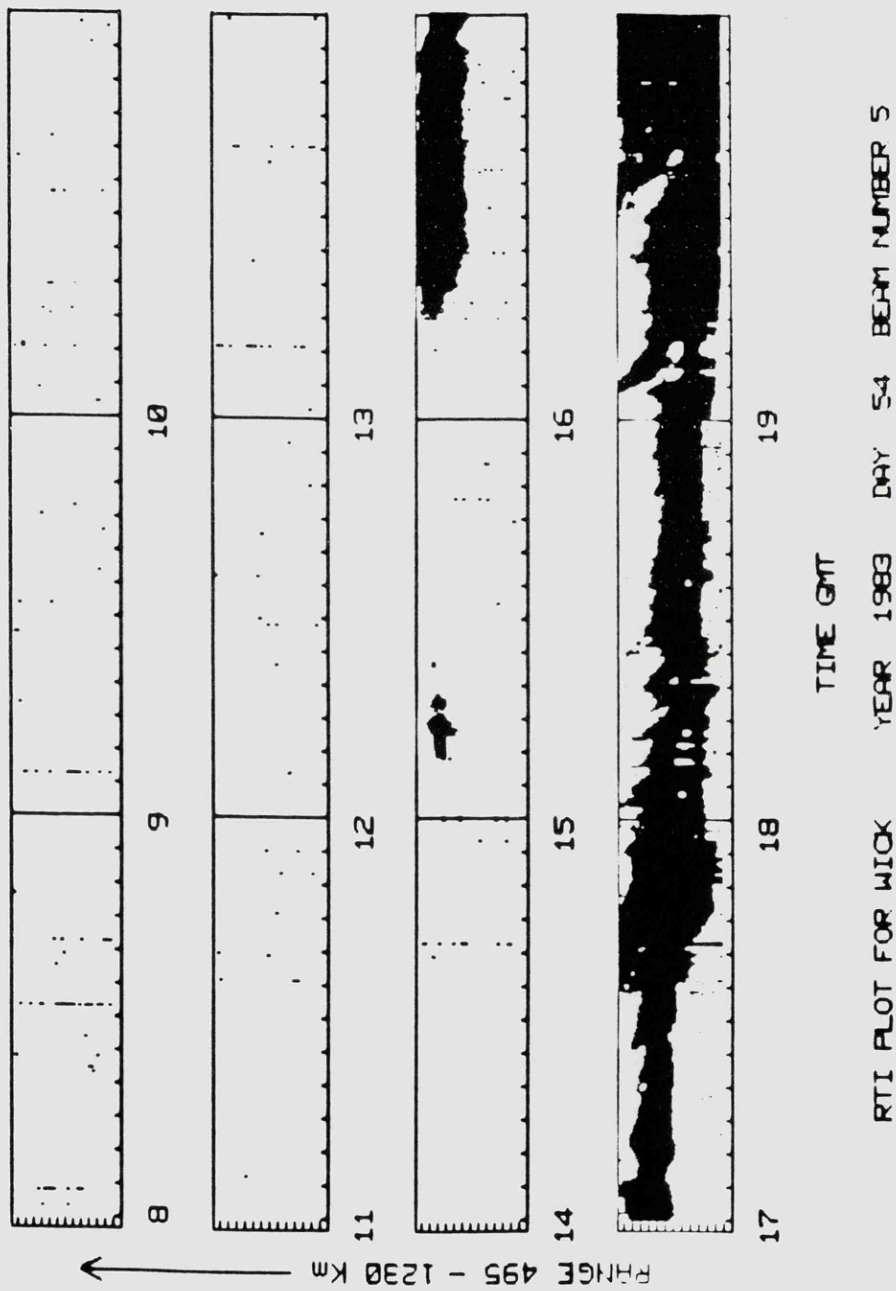


Figure 3.3

Quick-look Range-Time-Intensity (RTI) plot for Wick. A black mark is recorded where the backscatter exceeds 3dB above the noise level.

viewing area as described previously. The usual procedure is then to produce a series of spatial or SABRE plots (Figure 3.4) for the duration of the event. From there the flow patterns present in the ionosphere during the event can be investigated. In these plots the dots represent the 26x26 cells in the viewing area at which the backscatter amplitude and Doppler velocity are measured. The attached line denotes the magnitude and direction of the irregularity drift velocity at that position.

It is then possible to look at time series of the data from any particular cell or from a group of cells as presented in Figure 3.5. This was undertaken separately for east-west and north-south irregularity drift velocities, the vectors displayed in the SABRE plots having been resolved into their mutually perpendicular components. The SABRE data can also be filtered if necessary and the filter type normally adopted was similar to that suggested on a theoretical basis by Behrens and Glassmeier (1986). Their filter technique is optimised to deconvolve the Pi2 pulsation signal from the background bay signal that appears simultaneously with it at substorm onset.

The data may also be displayed as an RTV (Range Time Velocity) plot, an example of which is reproduced in Figure 3.6. In this presentation the horizontal axis is again time while the vertical axis can be either geographic latitude or longitude as required. The magnitude and direction of the SABRE irregularity drift velocity is then displayed at each latitude/time position, the velocity having been averaged over a strip in longitude or latitude as appropriate.

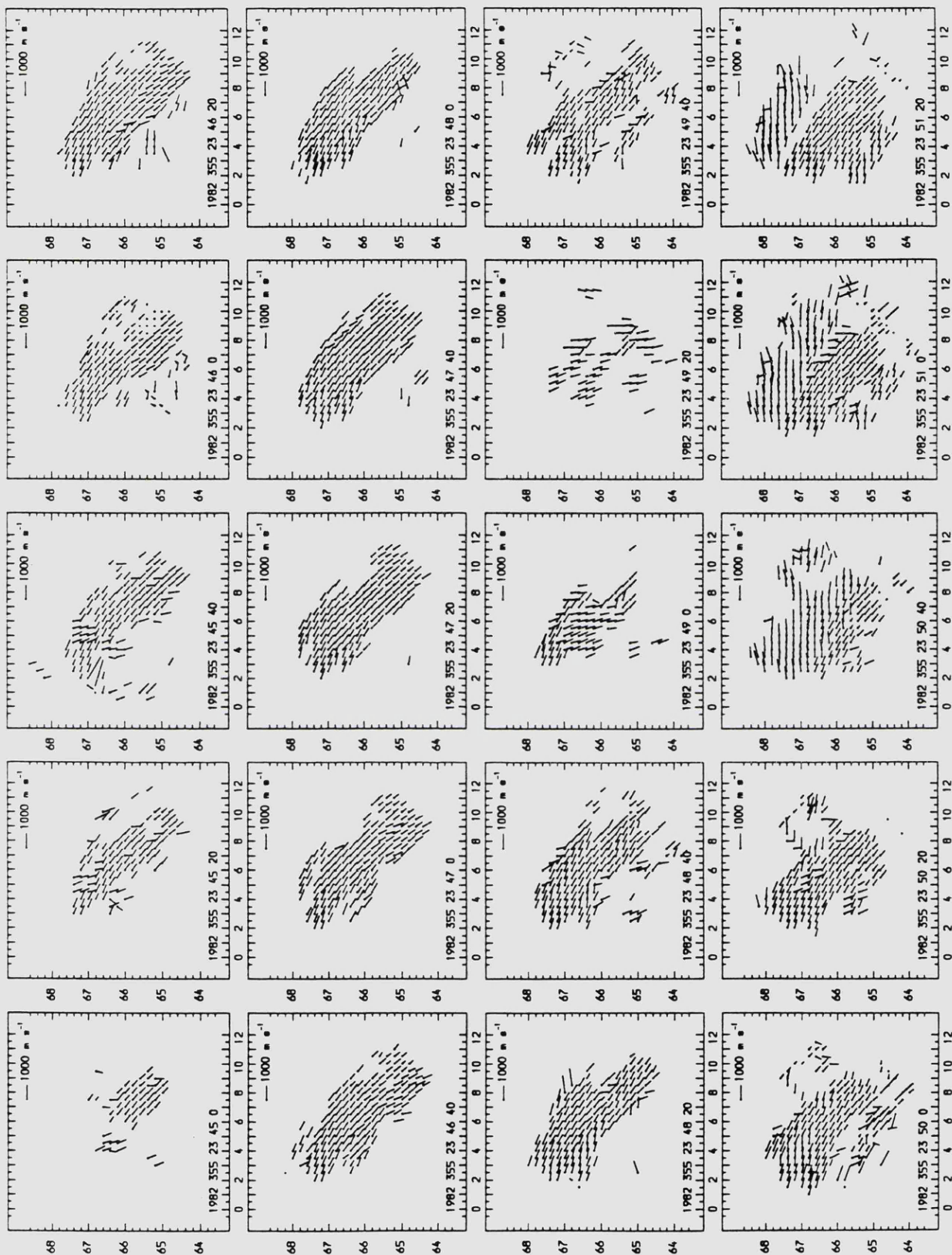
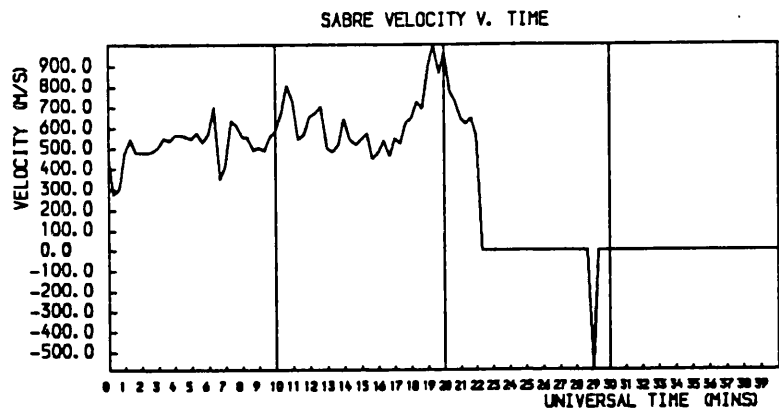


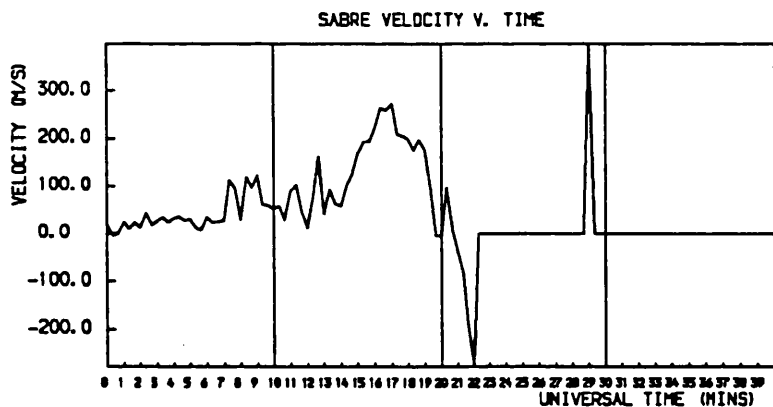
Figure 3.4

A sequence of SABRE spatial plots typically employed in this study to investigate the flow patterns present in the ionosphere at the time of a Pi2 pulsation.



66.2 TO 66.4 DEGREES GG NORTH, 2.0 TO 4.0 DEGREES GG EAST.

1983 110 1 0 0 EAST-WEST COMPONENT



66.2 TO 66.4 DEGREES GG NORTH, 2.0 TO 4.0 DEGREES GG EAST.

1983 110 1 0 0 NORTH-SOUTH COMPONENT

Figure 3.5

The representation of time series data from a group of cells in the SABRE viewing area at the time of a Pi2 pulsation (1:06 and 1:10). East-west velocity component data are presented above north-south velocity component data. The straight line at 0.0m/s (1:23 onwards) corresponds to times when no backscatter was observed by SABRE.

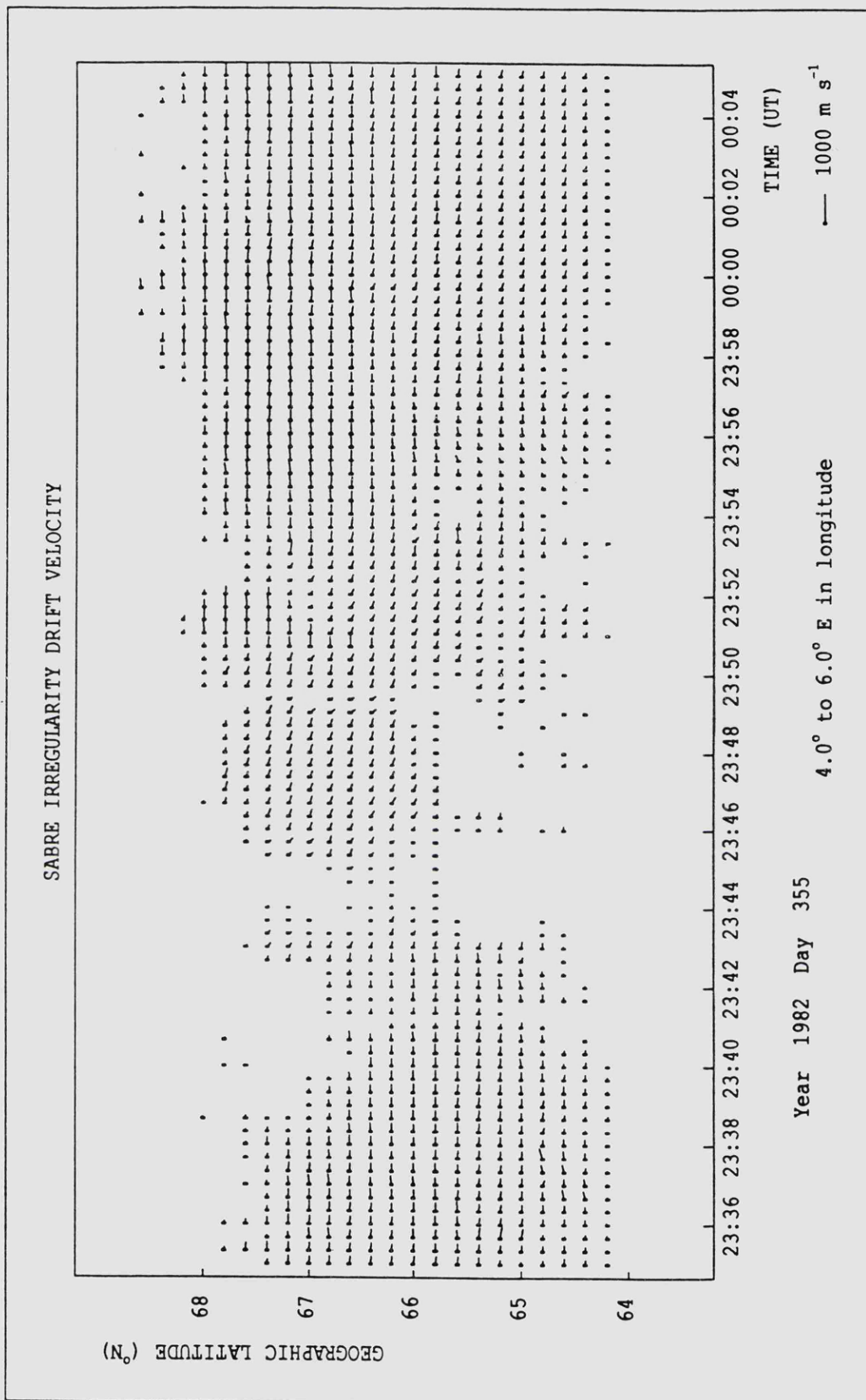


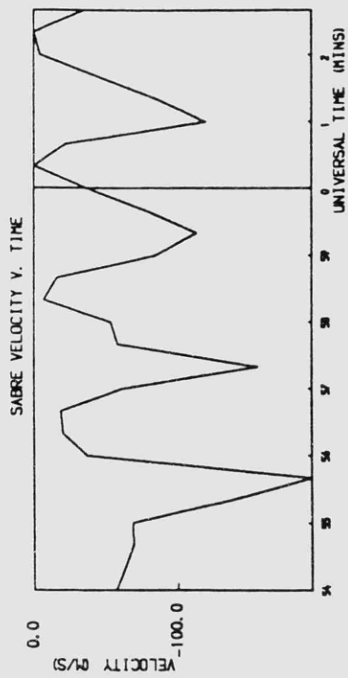
Figure 3.6

An example of a Range-Time-Velocity (RTV) plot also employed in the study of pulsations by SABRE. In this case the data are averaged over a longitudinal strip in the viewing area and plotted as a function of latitude and time.

### 3.3.2 SABRE Spectral Analysis

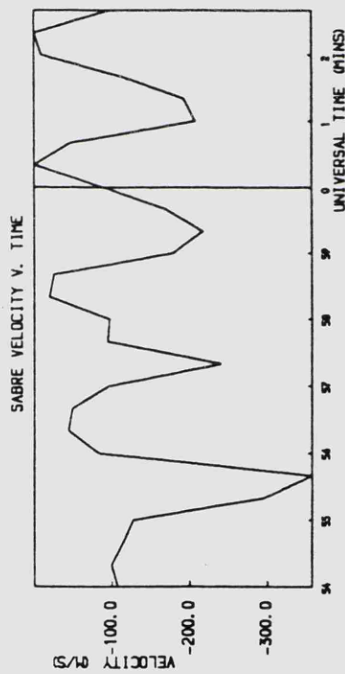
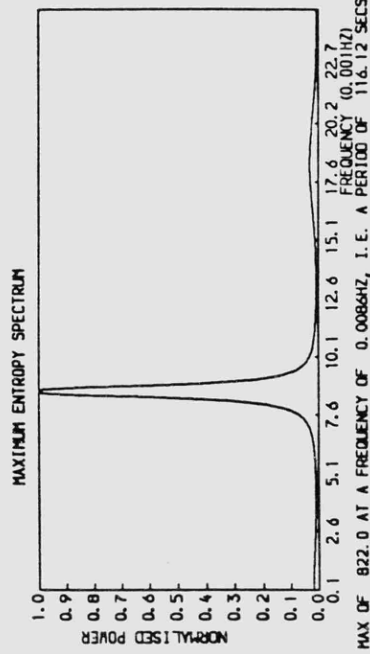
Fast Fourier Transform (FFT) spectral analysis of the SABRE data is difficult to perform due to the short duration of the Pi2 pulsations and the 20s temporal resolution of the SABRE data. Thus there are too few data points available to produce a well resolved spectrum. Maximum Entropy (ME) spectral analysis (Ulrych and Bishop, 1975), was therefore employed although this technique does not yield details of the polarisation or phase. Sharp spectral peaks are obtainable however if the 30% filter criterion suggested by Ulrych and Bishop (1975) and adopted by Stuart et al. (1979) to give the best compromise between spectral resolution and stability is adhered to (see Appendix). It is possible to obtain the ME spectra of the data for both east-west and north-south irregularity drift velocity components separately as indicated in Figure 3.7, which includes the data and their spectral components.

It is also possible to study the variation of the wave spectral power over the entire SABRE viewing area. This was achieved by taking a time series of the Pi2 pulsation in the SABRE data at each of the 26x26 cells in the viewing area and performing ME spectral analysis on each one. In this way a dominant frequency could be obtained for every position in the viewing area. Comparison of the frequencies and relative strengths of the various peaks obtained enabled an overall dominant frequency to be determined for the particular event. The variation in strength of this overall peak was then examined throughout the viewing area. In practice a group of frequencies around the peak (the number of frequencies was determined from a print-out of the spectrum to cover the complete envelope of the peak) was examined to allow for any differences in the shape of the spectral peak i.e. broad or narrow. The area under the peak thus provides a measure of



66.0 TO 67.6 DEGREES GG NORTH, 4.0 TO 6.0 DEGREES GG EAST.

1983 101 20 54 0 NORTH-SOUTH COMPONENT



66.0 TO 67.6 DEGREES GG NORTH, 4.0 TO 6.0 DEGREES GG EAST.

1983 101 20 54 0 EAST-WEST COMPONENT

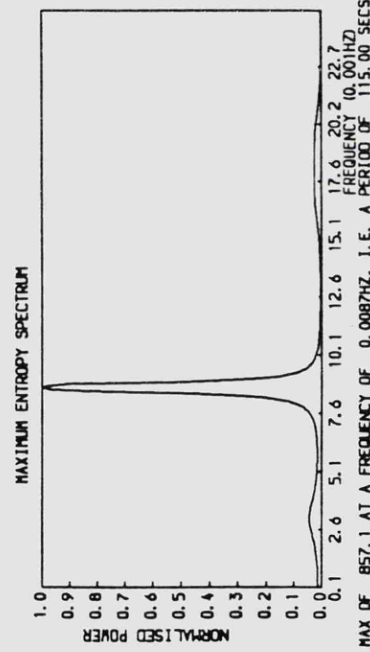


Figure 3.7

Typical output from the SABRE Maximum Entropy spectral analysis routine. The time series data with their associated spectra (below) are presented for east-west (left) and north-south (right) velocity components.

the wave spectral power present at each position in the viewing area.

This analysis may be undertaken for the east-west and north-south irregularity drift velocity components separately. An example of the type of plot produced is presented in Figure 3.8. In this plot the value of the wave spectral power at any particular position in the viewing area has been normalised to the value of the peak wave spectral power obtained as indicated above. The relative powers are represented by the radius of the circle at each position in the viewing area.

### 3.3.3 SABRE Polarisation Analysis

The polarisation of any waves present in the SABRE data is examined by constructing polarisation hodograms from the east-west and north-south irregularity drift velocity components. Usually this procedure gives meaningful results only in regions of the viewing area where the wave spectral power is high (see above). This analysis may be undertaken for both filtered and unfiltered SABRE time series data although the hodograms produced in the unfiltered analysis are not usually ellipses but large open circles. This arises from the presence of background bays in the unfiltered time series data. Consequently, the results from the filtered hodograms have been employed in this investigation, the unfiltered data analysis being mentioned only in specific events where a definite statement can be made on the polarisation. In the analysis of the filtered hodograms, the sense of polarisation is easily obtained by eye but the value of the ellipticity and azimuth, as defined previously, is harder to determine with any accuracy. The reason for this is that the SABRE 20s integration time may often be close to the Pi2 pulsation periods with the result that the polarisation ellipses obtained are often more like triangles or

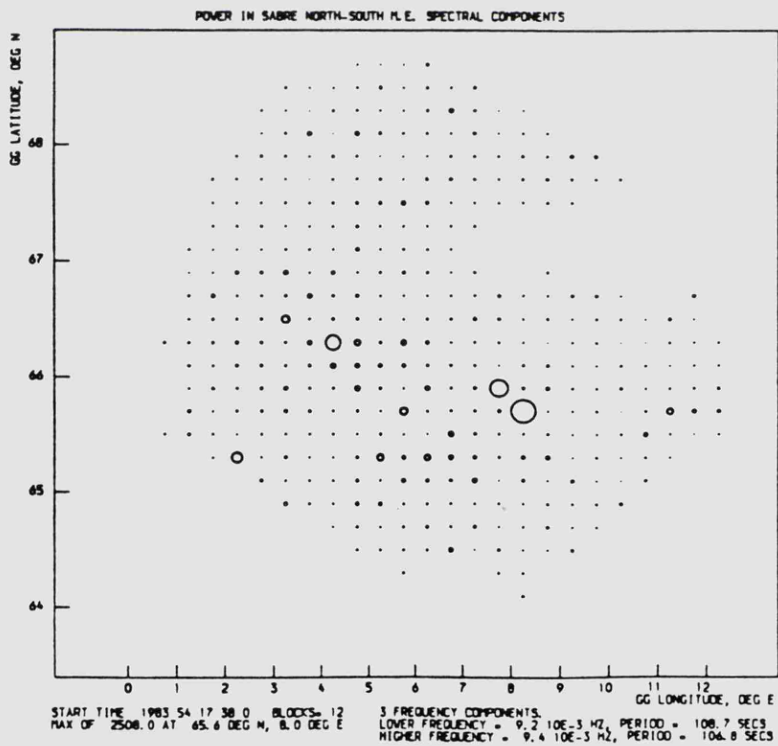
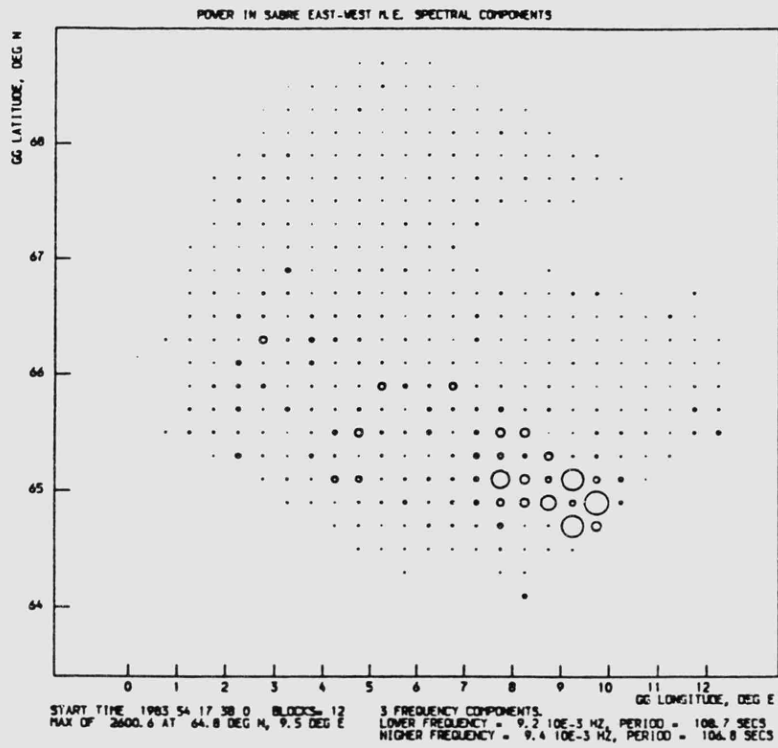


Figure 3.8

Typical output from the investigation of the variation of the wave spectral power across the SABRE viewing area at the dominant Pi2 pulsation period. East-west velocity component data are displayed above north-south velocity component data (see text for details).

squares. When a definite sense of polarisation can be obtained, the variations of the sense of polarisation over the viewing area may also be investigated (Figure 3.9).

### 3.4 Summary

SABRE is uniquely sited for the observation of Pi2 pulsations associated with substorm onset since the SABRE viewing area is located sometimes equatorward of and sometimes within the substorm enhanced auroral electrojet, depending on the level of geomagnetic activity. Statistically, the equatorward edge of the auroral oval moves equatorward during geomagnetically active conditions. Also, since the oval is asymmetric with respect to the geomagnetic pole, in the evening sector the oval is often closer to the viewing area than in the dayside for any particular set of geomagnetic conditions (Figure 3.10). Although the amplitude of the pulsation signal is slightly smaller than in the auroral zone, the events are easier to study because they are free from the Pi2 band noise associated with the substorm enhanced electrojet currents (Samson, 1982).

The locations of the BGS magnetometers are also ideal in that there are two situated at the same geomagnetic latitude (Faroer and Nordli) but on either side of the SABRE viewing area. Thus, from the polarisation characteristics of the Pi2 pulsations from these stations, the position of the SABRE viewing area relative to the substorm current wedge can be determined (Lester et al., 1983). This procedure was originally developed for mid-latitude (55 degrees North) studies and there may be problems in extending the technique in the high latitudes observed by SABRE. The magnetometer at Tromso provides a monitor of the behaviour of the signal in the auroral zone while that at Wick observes the signal at lower latitudes.

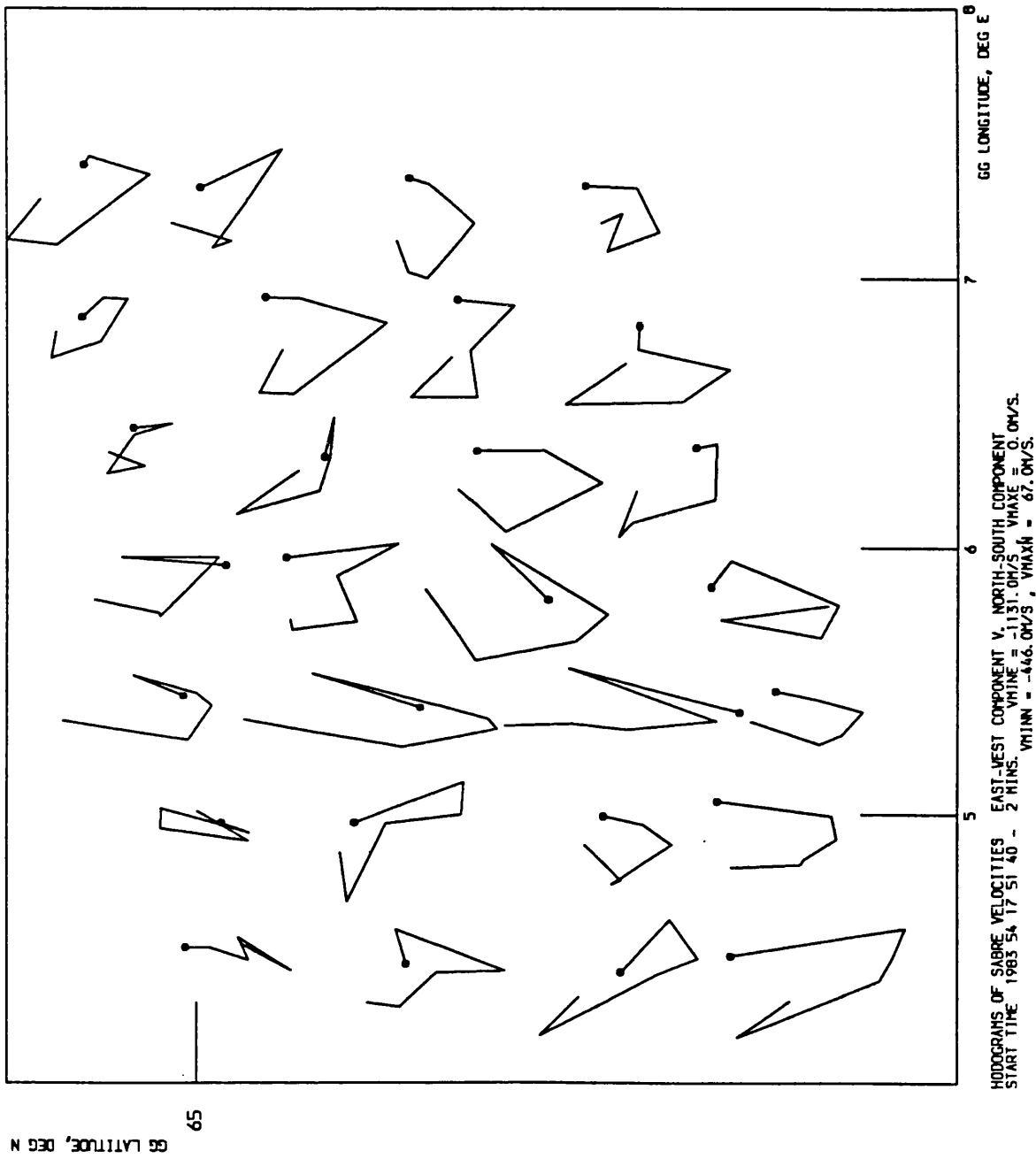


Figure 3.9

SABRE polarisation hodographs constructed from unfiltered east-west and north-south velocity components at positions in the viewing area where the wave spectral power at the dominant pulsation period is high. Similar hodographs may be constructed from the corresponding filtered SABRE data.

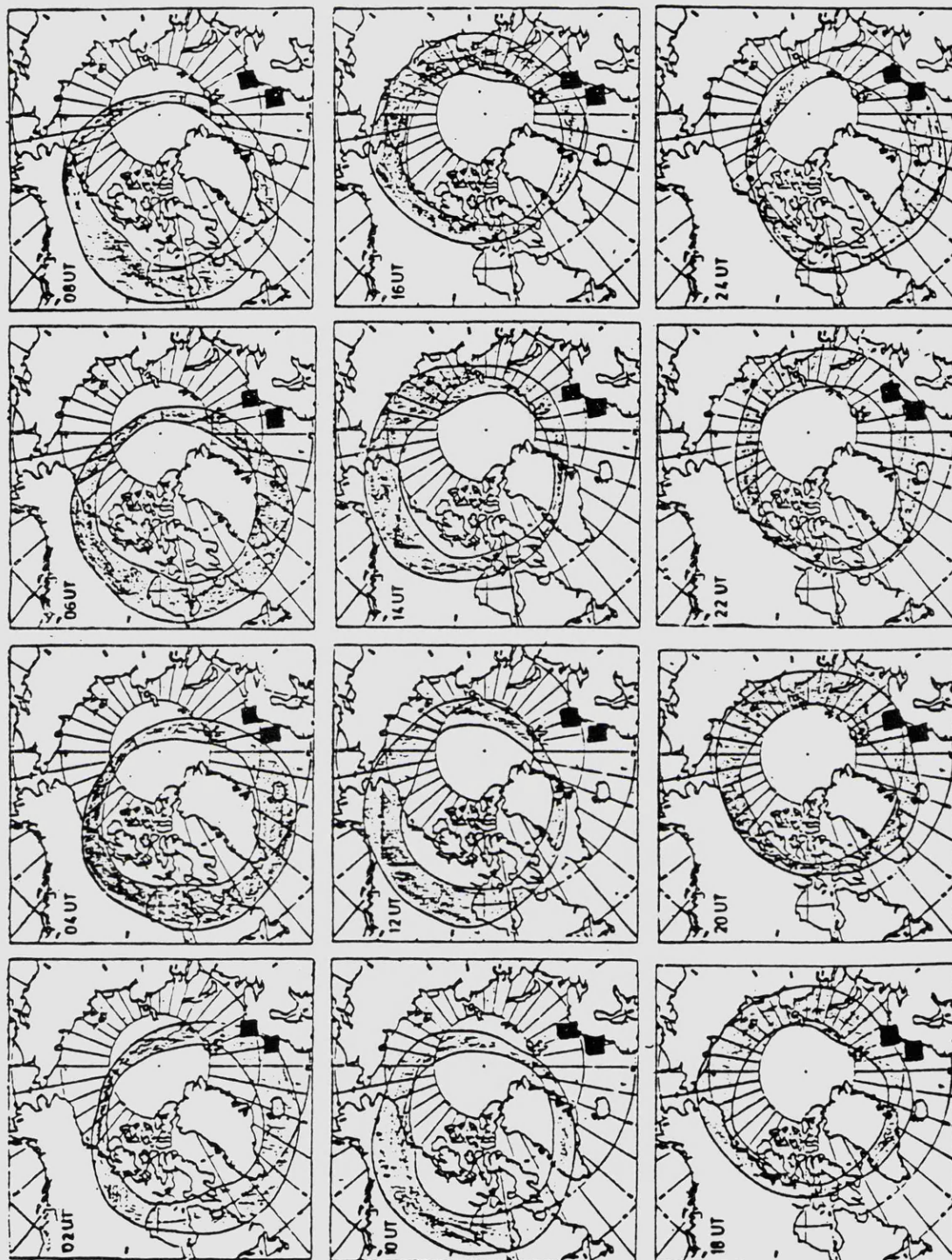


Figure 3.10

Schematic representation of the changing statistical position of the auroral oval relative to the SABRE viewing area during the day. This situation arises as the oval is asymmetric and offset relative to the geographic pole. The SABRE viewing area is, at different times of the day, inside, across and equatorward of the oval as a result. The SABRE viewing area is represented by the lower of the two black squares, the other being the viewing area of the similar STARE radar system.

Other advantages of the viewing arrangement employed include the fact that the two systems compliment each other well in the characteristics of the measurements they make. SABRE has excellent spatial resolution in a relatively small region of the ionosphere which enables the fine detail of the background flow patterns present in the ionosphere at the time of the pulsation to be examined. However, the temporal resolution of 20s is probably at the limit for the observation of the shortest period Pi2 pulsations. The magnetometers on the other hand have improved temporal resolution of 5s and good signal-to-noise capability for identifying the waves. However magnetometers integrate the signal over large areas of the ionosphere and the spatial resolution of the network is poor.

A major advantage of the SABRE system is that the measurements are made in the auroral ionosphere. Ground based magnetometers suffer because the magnetospheric signals are smoothed, and maybe even screened completely, by the ionosphere. In addition, another very important feature of the SABRE system is the division of the viewing area into 26x26 cells in each of which separate measurements of the irregularity drift velocity can be made. On account of this, a time series of any pulsation data can be obtained from any of the individual cells and spectral, polarisation etc analyses of these data can be undertaken. This is equivalent to having a very closely spaced latitudinal and longitudinal array of magnetometers. Thus we are in the unique position of being able to observe the substorm associated waves using a coherent radar for the first time and also having the ability to compare these signals with those observed on the ground by a series of magnetometers surrounding the SABRE viewing area.

## CHAPTER 4

### GENERAL FEATURES OF SABRE Pi2 PULSATIONS

#### 4.1 Introduction

The occurrence statistics and general characteristics of Pi2 pulsations observed by SABRE are considered in this chapter. The techniques employed for their initial identification and subsequent analysis were described in Chapter 3. The statistics characterising the occurrence of the Pi2 pulsations are presented as a function of local time and magnetic activity. The oscillatory nature of the two SABRE irregularity drift velocity components during Pi2 pulsation events are described, together with an investigation of the polarisation characteristics of the SABRE Pi2 pulsations. The features of these events are compared with those observed simultaneously by the BGS ground magnetometer network.

#### 4.2 The SABRE data

##### 4.2.1 Occurrence of SABRE Pi2 pulsations

During the interval December 1982 to December 1984 316 Pi2 pulsations were identified in the BGS ground magnetograms. In this same period 130 of these pulsations were also observed by SABRE, during 49 separate time intervals. The reduction in the number of SABRE events is due to either the lack of backscatter returns or the non-operation of one or both of the two SABRE radars. A threshold electric field of

around 15mV/m (Cahill et al., 1978) is necessary for the excitation of the two stream instability which generates the plasma irregularities which produce the radar backscatter. Also, during a train of Pi2 pulsations, one or more of the train may not be observed by SABRE, perhaps due to an enhancement in conductivity shorting-out the ionospheric electric field. This was the case for 15 pulsations observed by the magnetometers but not by SABRE.

Of the 49 time intervals during which SABRE observed Pi2 pulsations, normal magnetograms from the auroral zone station at Tromso indicate that in 23 cases a substorm onset (a negative H-bay onset in a night-time auroral zone magnetogram) occurred at the time of the first Pi2 pulsation. There are also 23 occasions when substorm activity had begun some time previously, although the Pi2 pulsation concerned is associated with a negative H-bay onset or intensification. The initial Pi2 pulsation was either not identified in the analogue ground magnetic records or is not observed by SABRE. Finally, there are three intervals during which time the H-component is recovering to pre-substorm levels, or is between substorms. The distribution of the number of Pi2 pulsations in each of the 49 intervals is given in Table 4.1.

Table 4.1

<u>No. of Pi2 pulsations in a train</u>	<u>No. of occasions</u>
1	15
2	11
3	11
4	8
6	4

The occurrence of Pi2 pulsations observed by SABRE as a function of

universal time and magnetic activity is illustrated in Figure 4.1. Universal time was adopted as local time varies by just under an hour across the width of the SABRE viewing area. The occurrence frequency maximises in the hour 18:00–19:00 U.T., although there is a relatively broad peak ranging from 17:00 to 00:00 U.T.. When the Pi2 pulsations observed by SABRE are normalised relative to those observed by the magnetometers, a different distribution is indicated. In the early evening sector most of the Pi2 pulsations are observed by SABRE, but the occurrence percentage drops dramatically around magnetic midnight (21:00 to 23:00 U.T.) the time of the Harang discontinuity. There is a small rise in the occurrence percentage for the few Pi2 pulsations in the early morning hours. This distribution is directly attributable to the statistics of occurrence of the radar backscatter (Waldock et al., 1985) where very few irregularities are generated in the Harang discontinuity.

Although SABRE observes Pi2 pulsations over a large range of magnetic activity, the occurrence frequency of Pi2 pulsations maximises for  $K_p=3+$ . When the observation of Pi2 pulsations by SABRE is normalised relative to the occurrence of  $K_p$  over the hours of observation (15–06 U.T.) during the two years of the investigation, a somewhat different distribution is evident. Although there is still a peak around  $K_p=3+$ , it is apparent that if a pulsation occurs during times of high magnetic activity (e.g.  $K_p=6-$ ) then SABRE is very likely to observe it. This is because the observation of pulsations by SABRE depends on the generation of the plasma irregularities that produce the radar backscatter. Therefore, the SABRE distribution of Pi2 pulsations is biased towards events occurring during active conditions and differs from the distribution of Pi2 pulsation occurrence as observed by the ground-based magnetometers. The original choice of pulsations in the

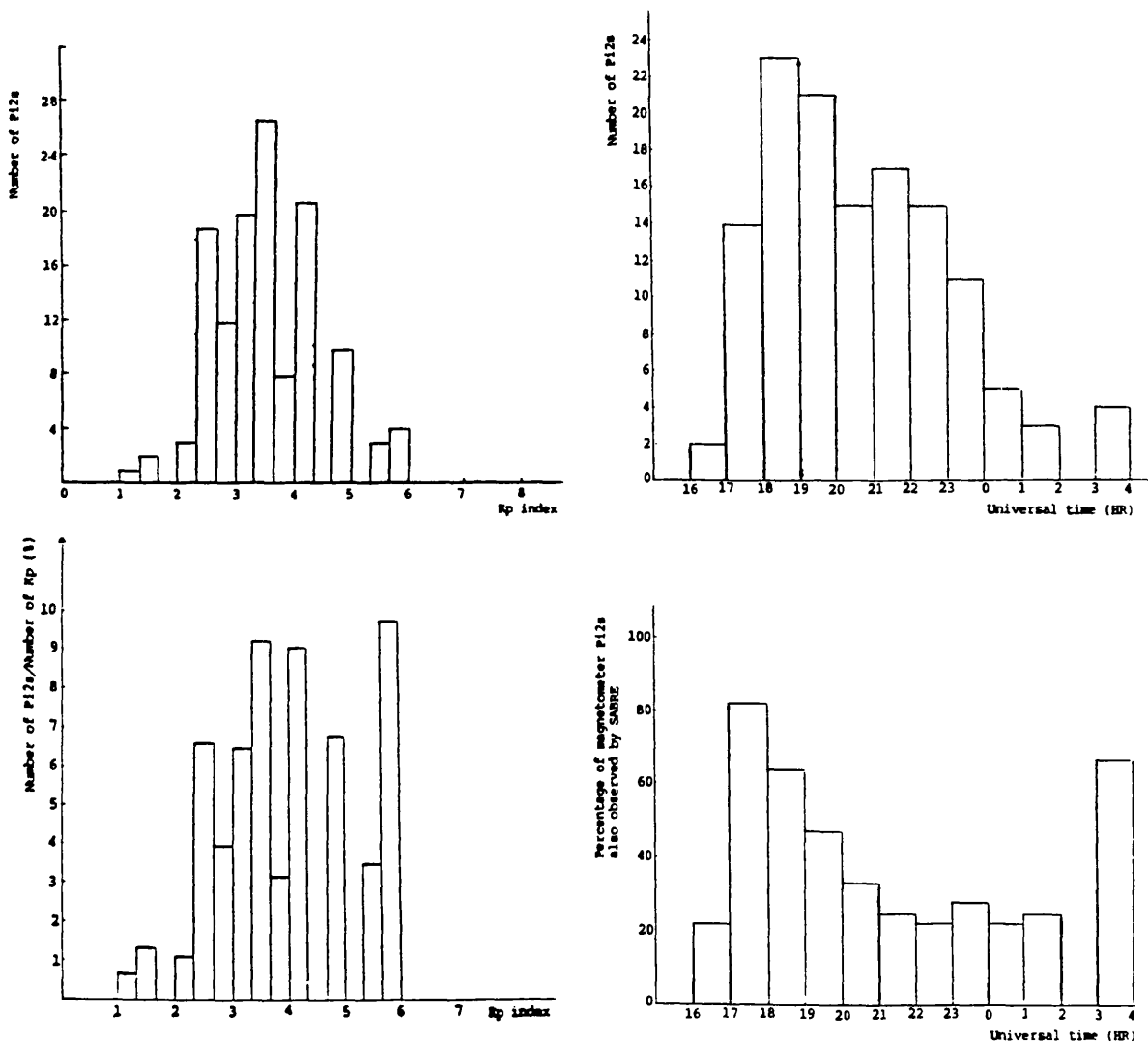


Figure 4.1

Occurrence of Pi2 pulsations observed by SABRE as a function of magnetic activity and universal time. The top two histograms display the mere occurrence statistics whereas the data have been normalised relative to the occurrence of each value of Kp index throughout the two year period of the study (bottom left) and as a function of the events observed by the BGS ground magnetometers which may also be observed by SABRE (bottom right).

ground magnetic records probably introduced a bias to times of lower and moderate activity and away from those events exhibiting large background bay changes at onset for which the pulsation is less clear. This is evident in the fewer number of pulsations observed at higher levels of activity (Figure 4.1 top).

#### 4.3 SABRE Pi2 pulsation amplitudes

The amplitudes of the SABRE Pi2 pulsations were obtained from the cell in the SABRE viewing area with the peak wave spectral power at the dominant pulsation period (see below). Direct comparison (Figure 4.2 top) of the SABRE pulsation amplitudes with those derived from filtered ground H-component magnetometer data from Nordli (Ni) and Wick (Wi) indicate a large scatter in the data. A linear correlation analysis for the radar data and the H-component data at three stations indicates a correlation coefficient ( $r$ ) ranging from 0.20 to 0.25 while the D-component data are even less well correlated, with correlation coefficients ( $r$ ) of less than 0.1. The SABRE Pi2 pulsation amplitudes were then divided into ranges of 100m/s. The mean amplitude in each of these ranges was compared with the mean pulsation amplitude from the corresponding ground magnetic data (Figure 4.2 bottom). There now appears to be a significant trend in the H-component data ( $r > 0.6$ ) from all stations although this is only true for the D-component data from Nordli. Statistically, a 't-test' (Reiff, 1983) implies a 95% confidence that the correlation is non-zero in these four cases. This is only true for the Nordli and Faroes H-components in the unaveraged data.

Another feature of the data is that the ground magnetic pulsation amplitude is larger at higher latitudes, a fact that is well established (Jacobs and Sinno, 1960). Over the five degree latitude

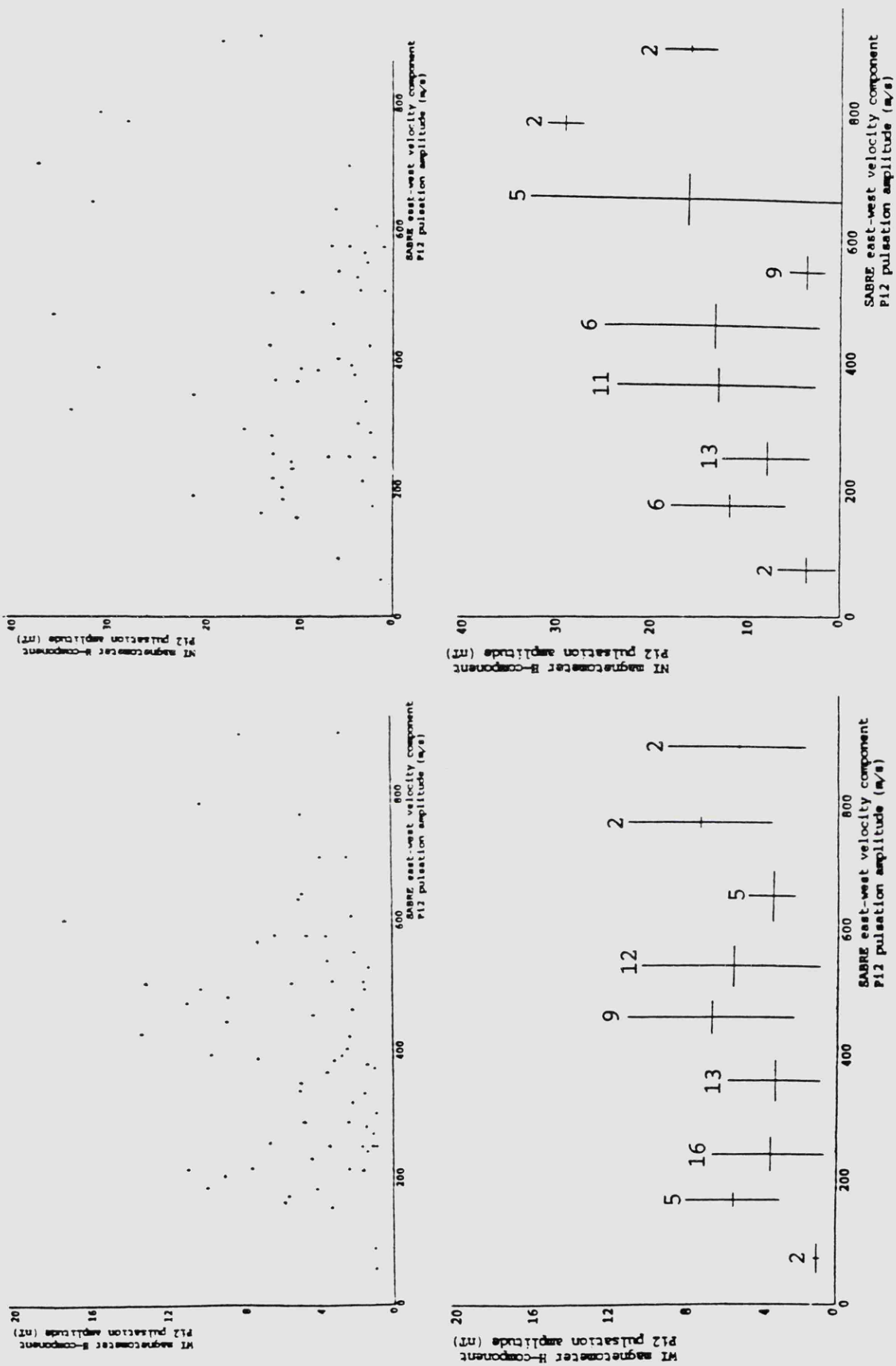


Figure 4.2  
 Comparison of Pi2 pulsation amplitudes derived from the filtered north-south (H) component ground magnetometer data from Wick (left) and Nordli (right) with those from the SABRE east-west velocity component. The bottom two panels display the results of binning the SABRE pulsation amplitudes into 100m/s ranges and plotting the mean and standard deviations of the resultant ground and SABRE amplitude distributions. The number of events in each range is also indicated.

range covered by SABRE there is no such relationship present for either velocity component between the individual SABRE Pi2 pulsation amplitudes and the latitude of the corresponding cell in the viewing area. The same is true for the magnitude of the SABRE vector. On averaging the SABRE pulsation amplitudes which occurred in each one degree of latitude bin across the viewing area, a slight increase (decrease) of mean amplitude with increasing latitude was obtained for east-west (north-south) velocity component data ( $r=0.80$  and  $-0.69$  respectively). The mean vector magnitude also increases slightly with latitude ( $r=0.66$ ). However, because of the few data points available these values of  $r$  are not statistically different from zero at the 95% confidence level. This analysis is limited by the saturation of the velocities to the local ion-acoustic velocity (Robinson, 1986) and the small latitude range over which the pulsations are observed.

#### 4.4 SABRE Pi2 pulsation dominant periods

The mean dominant period for both the east-west and north-south velocity components of the Pi2 pulsations observed by SABRE are presented as a function of magnetic activity in Figure 4.3. Each period was derived from Maximum Entropy (ME) spectral analysis (see section 3.3.2). The range of dominant pulsation periods obtained at each value of magnetic activity is large. No significant trend is present, although the lack of events at higher levels of magnetic activity makes a definitive statement difficult. If the Pi2 pulsation is generated on the last closed field line in the plasma sheet, then, as activity increases and the auroral oval moves to lower latitudes, the length of the field line will decrease producing a similar decrease in the period of the wave (Troitskaya and Gul'elmi, 1967). Such a relation was observed for the mean periods in the ground magnetometer data.

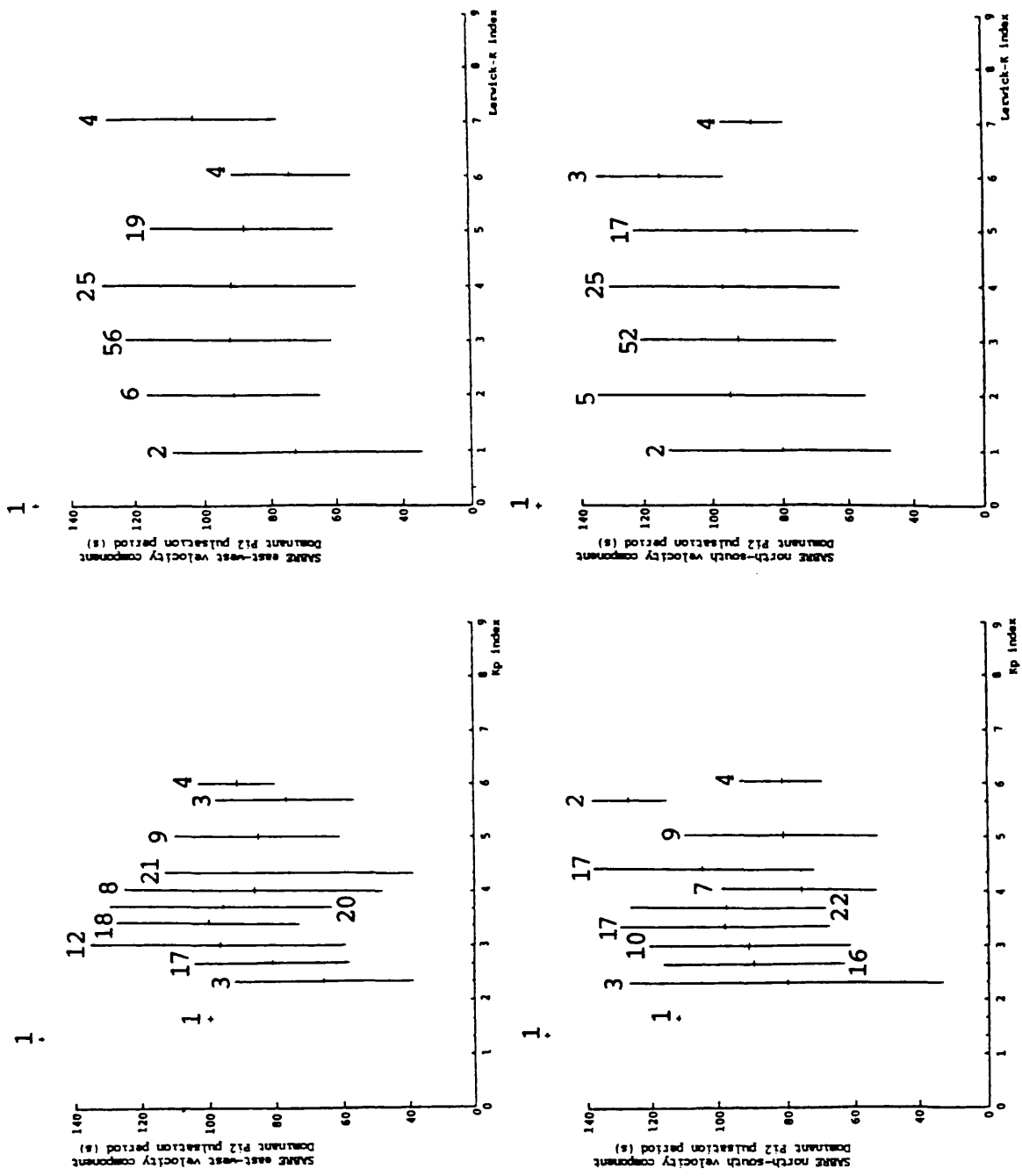


Figure 4.3

The distribution of dominant Pi2 pulsation periods derived from Maximum Entropy spectral analysis of SABRE east-west (top) and north-south velocity components as a function of magnetic activity. The error associated with the mean value at each level of activity is the standard deviation of the particular period distribution. The number of pulsations at each level of activity is also indicated.

A comparison of the periods obtained from ME spectral analysis (H and D components) of the ground magnetometer data with those obtained from SABRE indicated a large degree of scatter around a line with gradient=1. It was therefore decided that further comparison of the periods from the two data sets should be made after sub-dividing the data in the following two ways: (1) those events when the dominant pulsation period is the same at all the available magnetometer stations and those when it is not; (2) those events for which the SABRE viewing area is inside the substorm current wedge and those when the viewing area is outside.

In the first sub-division, the pulsation periods derived from the two data sets give similar values for those pulsations with periods which agree between stations, particularly for the H-component magnetometer (SABRE east-west velocity) data (Figure 4.4 left, from top to bottom,  $r=0.384^*$  ,  $0.409^*$  and  $0.534^*$ ). The pulsation periods are comparatively more widespread when the periods differ between magnetometer stations ( $r=0.002$ ,  $0.310^*$  and  $0.257$ ). Only those values of  $r$  indicated (\*) are statistically different from zero at the 95% confidence level. These results suggest that when the pulsation period is spatially coherent across the longitudinal and latitudinal separation of the BGS magnetometer stations, SABRE observes the same pulsation period. It seems likely that the pulsation is being observed equatorward of the generation region in this case. The presence of field-aligned currents and structure in the ionospheric conductivity would introduce Pi2 band noise to the system, leading to changes in the period, or to the introduction of more than one period, being present over this spatial range.

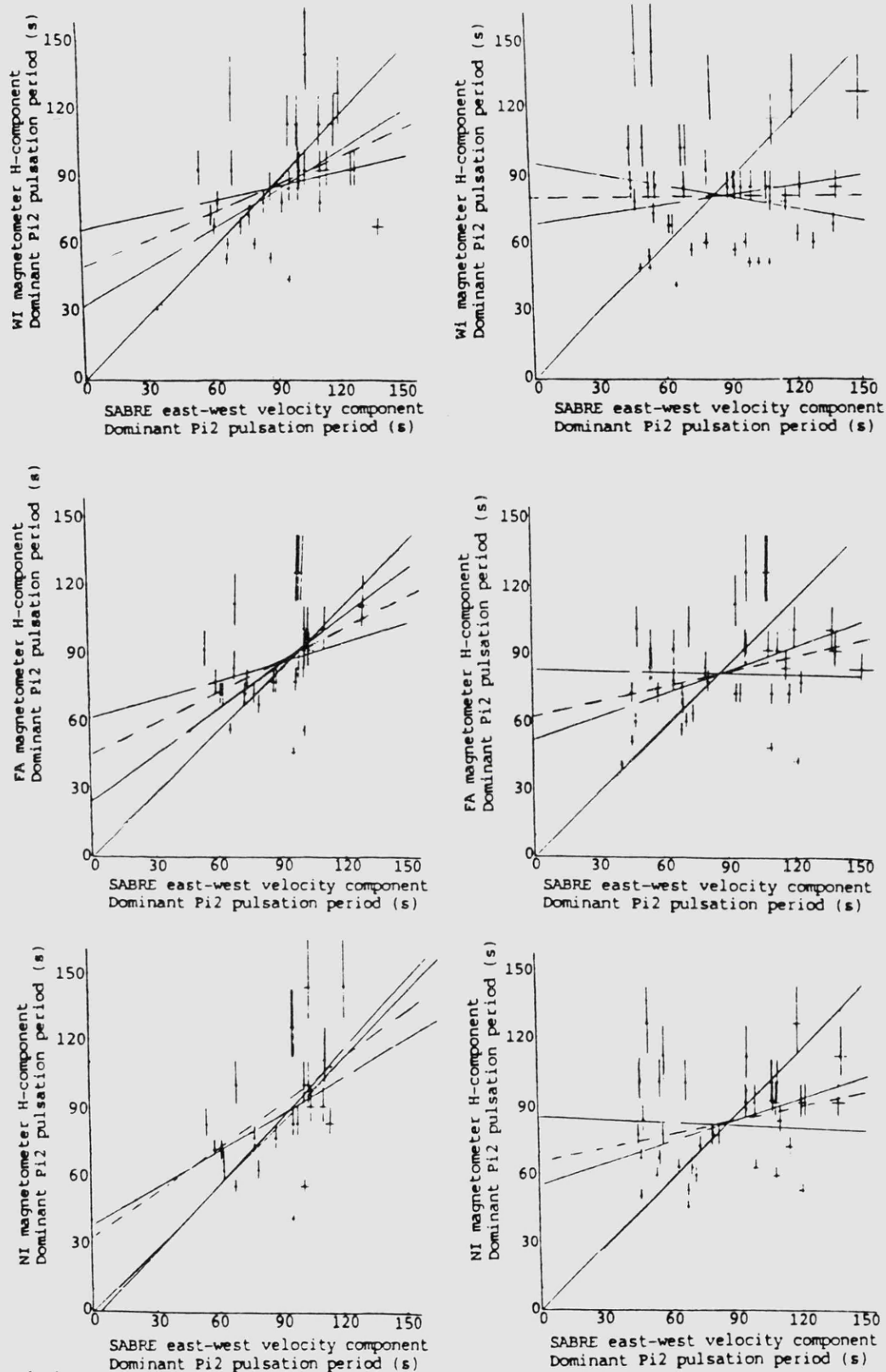


Figure 4.4

Comparison of dominant Pi2 pulsation periods derived from ME spectral analysis of north-south (H) component ground magnetometer data from Wick (top), Faroes (middle) and Nordli (bottom) with those from SABRE east-west velocity component. Data to the left are for pulsation periods which agree at all magnetometer stations while those to the right do not. The error bars represent the resolution of the spectral analysis. The dashed line is the best-fit straight line derived from least squares analysis of the data. The broken lines result from the standard error in the gradient and intercept of the best-fit line. A line with gradient=1 was also constructed on the diagrams to aid in the interpretation of the data.

In the second sub-division of the data, the distinction between the SABRE viewing area being inside or outside the substorm current wedge appears to have little effect on the Pi2 pulsation period distributions obtained (Figure 4.5). However, the periods obtained have a higher correlation when the SABRE viewing area is within the substorm current wedge at all three magnetometer sites. In Figure 4.5, from top to bottom,  $r=0.191$ ,  $0.415^*$  and  $0.516^*$  inside the wedge (left) and  $r=0.083$ ,  $0.170$  and  $0.170$  outside the wedge (right). The asterisk again indicates values of  $r$  that are significantly different from zero at the 95% confidence level.

It is interesting to note that the highest values of  $r$  are normally obtained from Nordli, the station closest to the SABRE viewing area. This appears to be the case for both the pulsation amplitude and period.

In the above analysis no account is taken of the position of maximum wave spectral power in the dominant pulsation period within the SABRE viewing area. To investigate if this has any significance, the latitude of the SABRE cell exhibiting maximum wave spectral power was plotted against the corresponding dominant Pi2 pulsation period for east-west and north-south velocity components. There is no apparent relation in either velocity component even after binning the data by value of magnetic index ( $K_p$  and Lerwick- $K$ ) at the time of the pulsation. All values of dominant Pi2 pulsation period are observed at a wide range of cell latitudes for each level of magnetic activity.

#### 4.5 Positioning of the SABRE viewing area relative to the substorm current wedge

Before describing the signatures of the Pi2 pulsations in the SABRE

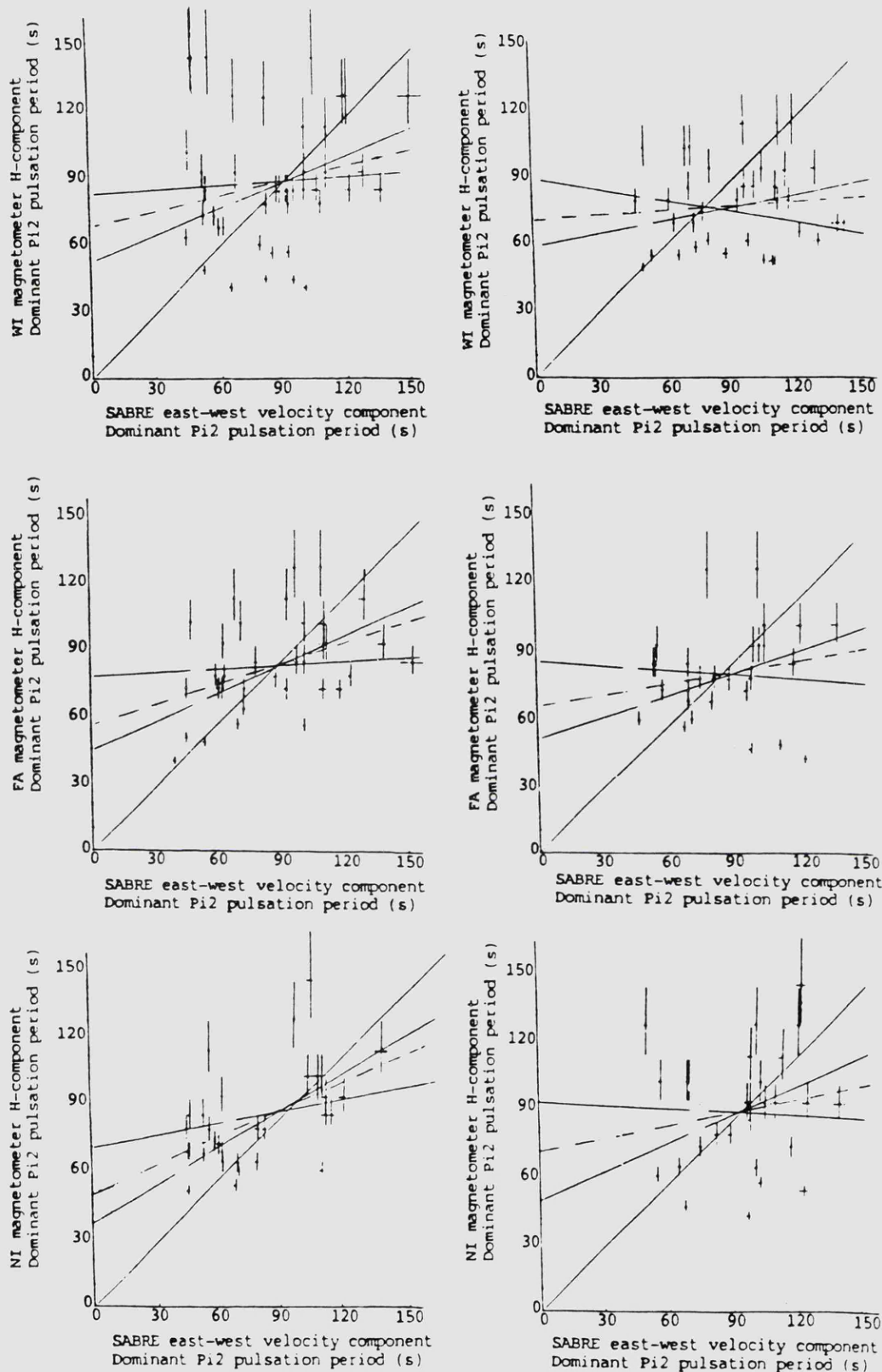


Figure 4.5

Comparison of dominant Pi2 pulsation periods derived from ME spectral analysis of north-south (H) component ground magnetometer data from Wick (top), Faroes (middle) and Nordli (bottom) with those from SABRE east-west velocity component. Data to the left occur when the SABRE viewing area is inside the substorm current wedge, those to the right when it is outside the substorm current wedge. The error bars represent the resolution of the spectral analysis. The dashed line is the best-fit straight line derived from least squares analysis of the data. The broken lines result from the standard error in the gradient and intercept of the best-fit line. A line with gradient=1 was also constructed on the diagrams to aid in the interpretation of the data.

data the position of the SABRE viewing area relative to the substorm current wedge is considered. The BGS magnetometer stations at Faroos and Nordli are both situated at 61 degrees north geomagnetic latitude but are separated by 21 degrees in longitude (Table 3.1). The two stations are positioned on either side of the SABRE viewing area and, at times of lower magnetic activity, are able to indicate the position the SABRE viewing area relative to the substorm current wedge (Lester et al., 1983). During high magnetic activity, however, the auroral electrojets are closer to the stations and the assumption that the magnetic bays are due solely to the substorm field aligned currents is invalid. This appeared to be the case in the majority of events studied (see below). The Wick magnetometer, at a geomagnetic latitude of 58 degrees north, is, therefore, also utilised in this study.

Results for the location of the SABRE viewing area relative to the substorm current wedge, for the 130 Pi2 pulsations observed simultaneously by SABRE and the magnetometers, are summarised in Table 4.2. Both positioning techniques to give an estimate of the position, the H-D component bay perturbations and the orientation of the horizontal (H-D) polarisation ellipse (azimuth derived from FFT polarisation analysis) were employed (see section 2.3.2).

Table 4.2

ground magnetometer data available	number of Pi2 pulsations	consistent result from the two positioning techniques
Nordli and Faroos	86	22 (7)*
One of Ni or Fa	33	16
Neither of Ni/Fa	11	0
Wick	117	75
no Wick	13	0

\* Seven of the 22 pulsations were the first in a series or single

pulsations. Lester et al. (1984) found these to be the best for positioning their array of stations relative to the wedge.

Analysis of the 22 pulsations where the two techniques produce a consistent location of the substorm current wedge indicates a range of possible locations (Figure 4.6). The SABRE viewing area is situated between Faroës and Nordli and the two vectors represent the horizontal polarisation azimuth of the Pi2 pulsation at the two stations. From the changing relative orientations of the two vectors, the apparent width of the substorm current wedge differs from event to event independently of magnetic activity or local time. When the azimuths from the second pulsation in a train are examined (e.g. 1983 341-1,2 and 1984 41-1,2), the wedge appears to widen, the azimuths at the two stations are now almost identical. The relative azimuths suggest that the wedge has moved and expanded to the west, with the same spatial separation between the two stations now occupying less of the total wedge width. A further consideration is that the wedge may have moved latitudinally relative to the SABRE viewing area. In both the above cases the Z-component variations at Ni and Fa suggest the electrojet has moved latitudinally to higher latitudes during the interval covering the two pulsations. The change in the Z-component becomes more positive in the eastward electrojet case (1983 341) and more negative in the westward electrojet case (1984 41). Similar changes would follow from a simple intensification of the substorm current. However, observations of Pi2 pulsations on two widely spaced meridians spanning mid and low latitudes, together with results from a model substorm current wedge, indicate that the wedge is wider at lower latitudes (Lester et al., 1989).

This apparent change in wedge width was also observed in the H,D-bay



perturbation changes at the lower latitude station of Wick during 11 time intervals containing 31 Pi2 pulsations. The position of the magnetometer station relative to the wedge centre changed to one further east. It is not possible, however, to quantify this movement as the polarisation derived magnetometer azimuths were not consistent over the series of Pi2 pulsations. In seven of these eleven intervals, the change in the WI Z-component suggests that the electrojet has moved to higher latitudes during the course of the pulsations. On one occasion, when the wedge appeared to expand to the east, the electrojet moved to lower latitudes over a sequence of five pulsations. The remaining three intervals occurred during highly structured flows around the time of the Harang discontinuity when it was impossible to position the SABRE viewing area relative to the electrojet. However, the width of the wedge varies from event to event due to the combined spatial and temporal changes in apparent station position.

#### 4.6 SABRE observations of Pi2 pulsations

##### 4.6.1 Introduction

Pi2 pulsations are identified in SABRE data from the time series of (i) the east-west and north-south irregularity drift velocity components and (ii) the backscatter intensity from the individual radars at Wick and Uppsala (Figure 4.7). Although it is known that Pi2 pulsations are related to changes in precipitation into the E-region (Stuart et al., 1977) and that this will change the electron density and hence possibly modulate the backscatter intensity observed by SABRE, the interpretation of the data is more difficult due to geometrical effects of the radar system and the ionospheric conductivities (Wilkinson et al. 1986). Therefore, only the signatures obtained from the irregularity drift velocity components are discussed

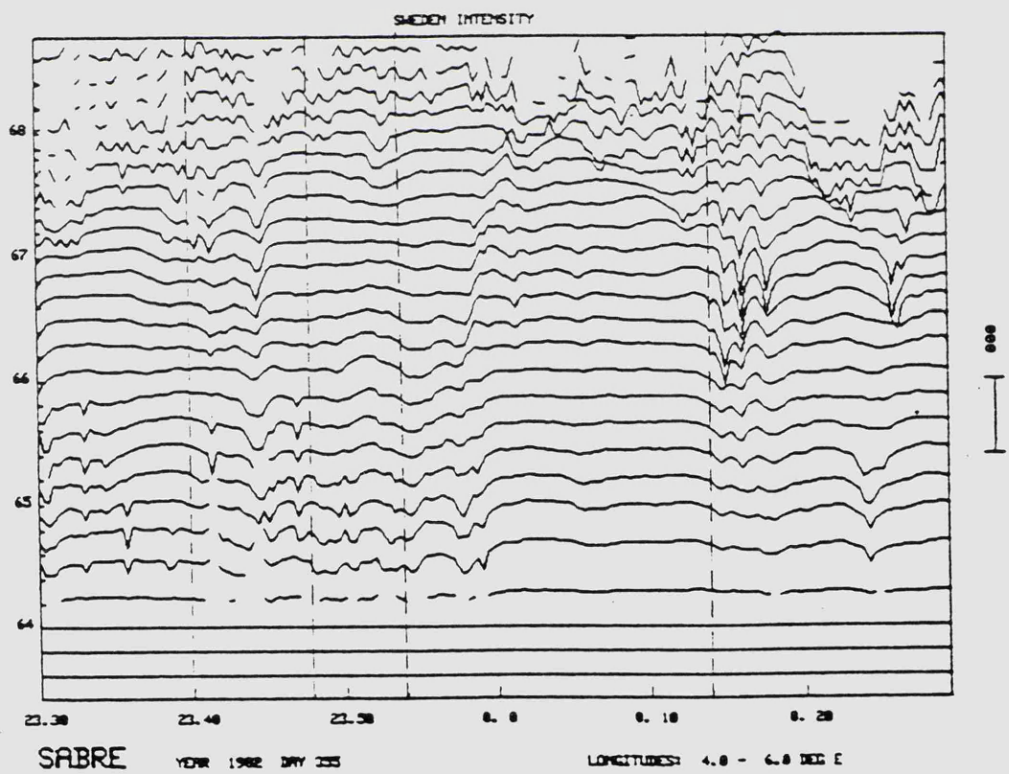
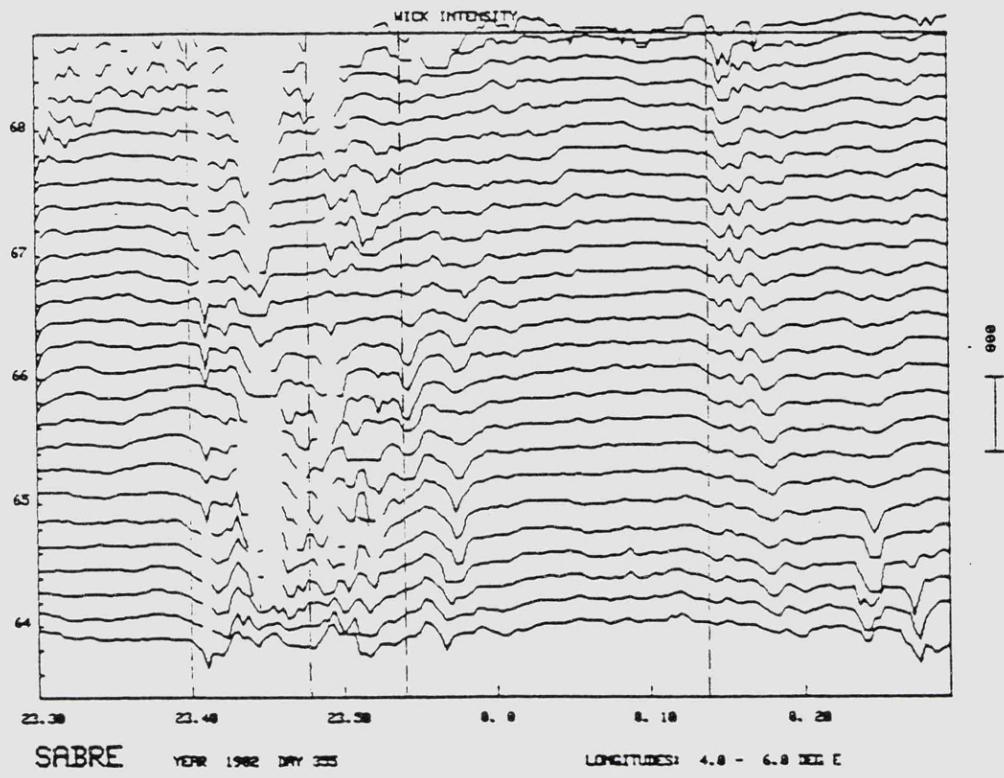


Figure 4.7

An example (Wick above, Uppsala below) of Pi2 pulsations observed in time series constructed from backscatter intensity data from the individual SABRE radars at Wick and Uppsala. Dashed vertical lines indicate the time of Pi2 pulsation onset in ground magnetometer records.

in this study. These SABRE velocity signatures are divided into Types 1 and 2.

#### 4.6.2 Type 1 SABRE Pi2 pulsation signatures

The first type of Pi2 pulsation signature in the time series of the SABRE irregularity drift velocity components is characterised by the oscillatory nature of the Pi2 pulsation, with the same number of wave cycles observed in both radar and magnetometer data. In addition, the pulsations are normally situated on the back of a bay-like dc signature which signifies a change of magnitude in the background velocity. This bay can represent a switching-on of backscatter returns observed by SABRE, the irregularity drift velocity therefore starting from zero velocity, or a change in the existing velocities. In the latter case, the background velocity flow direction remains the same.

When the irregularity drift velocity starts from zero the shape of the bay in the east-west velocity component is characterised by a positive or negative initial change. This change is dependent on the time of occurrence of the Pi2 pulsation, before or after magnetic midnight i.e. in the eastward or westward electrojet, and is in the same direction as the expected background flow. The initial change in the north-south velocity can be positive or negative at different locations in the viewing area for a single positive or negative east-west velocity change. This may result from the presence of a vortex or shear in the flow at the time of the Pi2 pulsation as discussed in the following chapter.

When the initial irregularity drift velocity is non-zero, the slope of the initial change in the east-west velocity component can be positive or negative. The Pi2 pulsation normally occurs at the start of the

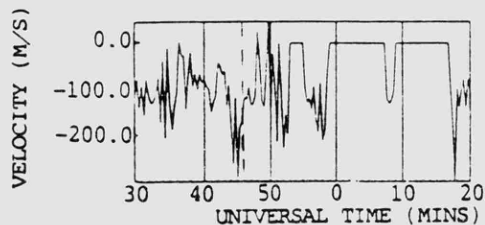
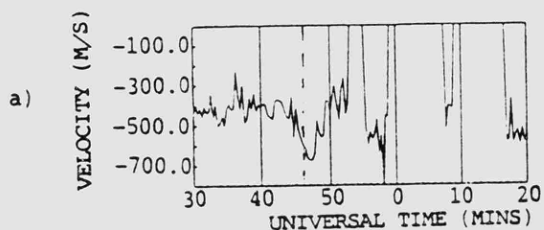
enhancement in a manner similar to that observed in ground magnetic data. Throughout Figure 4.8, the Pi2 onset time in ground magnetic data of the Pi2 pulsation under investigation is indicated by a dashed vertical line. East-west velocity component data are to the left while north-south velocity component data are to the right of Figure 4.8. The SABRE viewing area is inside the substorm current wedge for these events.

For Pi2 pulsations occurring in the eastward electrojet (westward background flow), the velocity can exhibit either positive or negative slopes at the time of the Pi2 pulsation. When the slope in the background flow is positive, the velocity reaches a maximum value of westward velocity just after the ground onset time of the Pi2 pulsation then turns, or recovers, to a lesser value of westward velocity as the event progresses (Figure 4.8a left). The corresponding north-south velocity components at these times (Figure 4.8a right) exhibit an enhancement in background southerly velocity or oscillate around a constant value of velocity. When the slope in the background westward flow is negative (Figure 4.8b left), the Pi2 initiates an enhancement in the westward flow to a maximum value before a subsequent recovery eastward. The north-south velocity component normally has a positive slope and is recovering from a maximum value of southerly velocity (Figure 4.8b right).

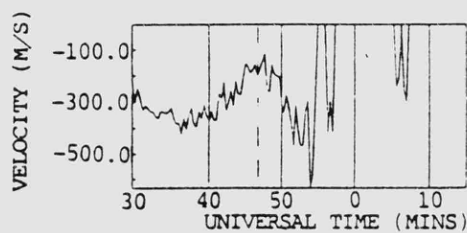
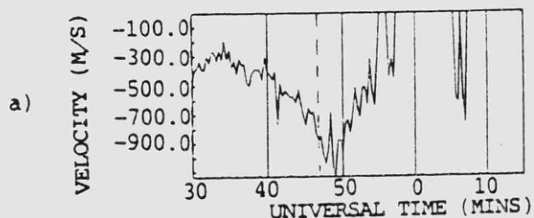
For pulsations occurring in the westward electrojet (eastward background flow), the background velocity can again exhibit positive or negative slopes at the time of a Pi2 pulsation. The positive slope here represents an enhancement of the existing eastward flow (Figure 4.8c left). The corresponding north-south velocity component (Figure 4.8c right) exhibits an enhancement then reduction in background

SABRE east-west velocity component

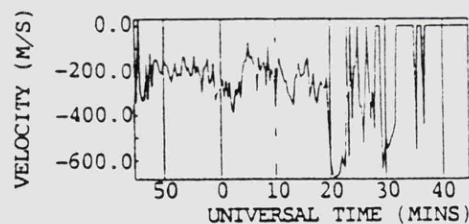
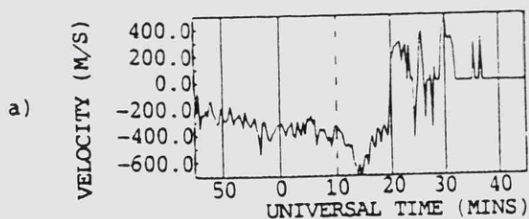
SABRE north-south velocity component



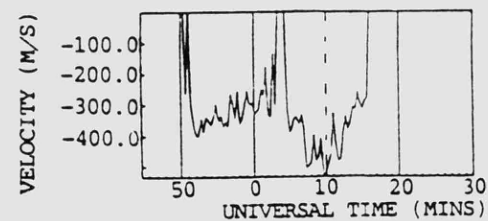
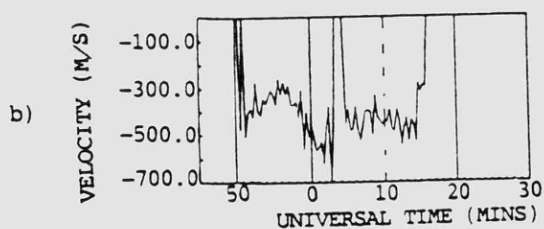
START TIME : 1984 102 18 30 0



START TIME : 1984 356 19 30 0



START TIME : 1984 356 21 45 0



START TIME : 1984 356 21 45 0

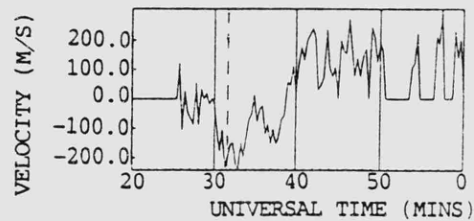
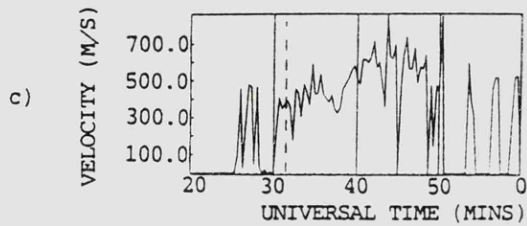
Figure 4.8

Type 1 SABRE Pi2 pulsation signatures as observed in time series data constructed from east-west (left) and north-south (right) velocity components when the SABRE viewing area is inside the current wedge. Dashed vertical lines indicate the time of Pi2 pulsation onset in ground magnetometer data.

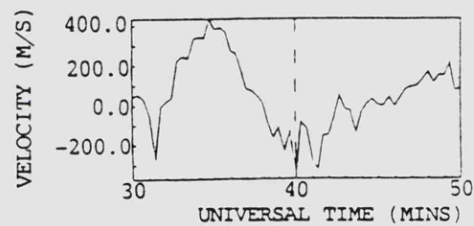
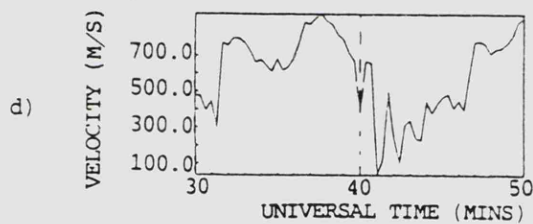
a) positive slope in E-W velocity when background flow is westward.  
b) negative slope in E-W velocity when background flow is westward.

SABRE east-west velocity component

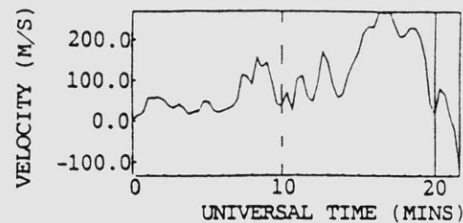
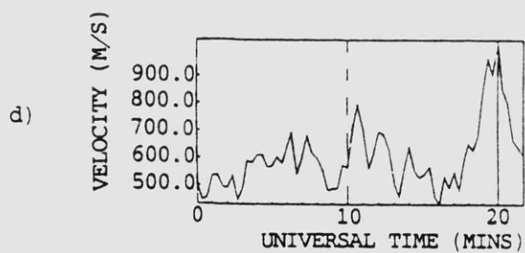
SABRE north-south velocity component



START TIME : 1984 326 21 20 0



START TIME : 1983 59 23 30 0



START TIME : 1983 110 1 0 0

Figure 4.8 continued

Type 1 SABRE Pi2 pulsation signatures as observed in time series data constructed from east-west(left) and north-south (right) velocity components when the SABRE viewing area is inside the current wedge. Dashed vertical lines indicate the time of Pi2 pulsation onset in ground magnetometer data.

c) positive slope in E-W velocity when background flow is eastward.

d) negative slope in E-W velocity when background flow is eastward.

southerly velocity. When the slope in the background eastward flow is negative (Figure 4.8d left) the velocity has just risen to a maximum value of eastward velocity and, at Pi2 pulsation onset, turns westwards to a lesser value of eastward velocity. The north-south velocity component oscillates around a constant value of velocity (Figure 4.8d right).

These observations can be explained with reference to the two electrojets, the Harang discontinuity and the westward travelling surge (WTS) which travels along the poleward border of the eastward electrojet after substorm onset (Figure 4.9). The positions a-d roughly correspond to possible positions of the SABRE viewing area at the time of the respective time series data a-d in Figure 4.8. For the time series labelled a in Figure 4.8, the SABRE viewing area may be positioned at increasingly eastern longitudes (Figure 4.9 position a). The positive background slopes during these time series represent the signature in the SABRE data of the arrival at and passage across the longitudinal width of the viewing area of the enhanced eastward flows due to the substorm enhanced westward electrojet. In the first two examples (position a) the background westward flow diminishes as a result of the intrusion of the enhanced westward electrojet along the poleward border of the eastward electrojet thereby forcing the eastward electrojet equatorward and leaving SABRE to observe diminished flows in the poleward region of the eastward electrojet. Rostoker and Samson (1981) found that the peak power and amplitude of eastward electrojet Pi2 pulsations was localised to a narrow latitudinal region. The SABRE velocity subsequently dropped to zero as the Harang discontinuity arrives at the location of the SABRE viewing area. The third example of 4.8a has SABRE initially in the eastward electrojet before the Harang discontinuity passes over (flows become

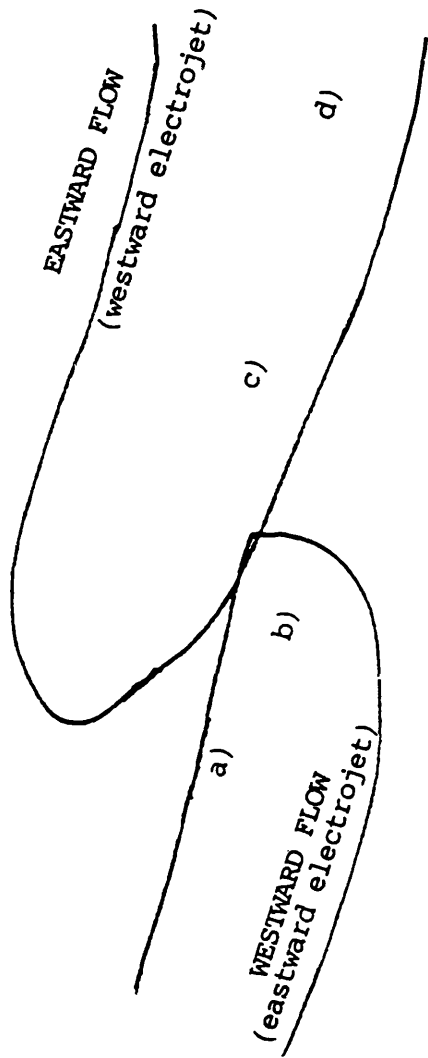


Figure 4.9

Schematic diagram to illustrate the positions of the SABRE viewing area relative to the substorm enhanced westward electrojet at the time of observation of the time series data presented in Figure 4.8.

eastward) and SABRE moves into the westward electrojet. The fact that no backscatter is then observed may be due to SABRE being in a region of sub-threshold electric field to the east of the head of the WTS (Baumjohann et al., 1981). The event in Figure 4.8b is similar in some respects to that in Figure 4.8a. The difference in this case is that the background westward flow velocity is increasing at the time of the Pi2 pulsation (22:10 U.T.). The subsequent rapid and complete drop-out of backscatter at 22:17 U.T. implies the rapid appearance of the Harang discontinuity in the SABRE viewing area. This feature is observed in all examples of type b signatures in time series data across all parts of the viewing area. As a result, position b in Figure 4.9 is closer to the Harang discontinuity and in a region of stronger flow than position a. It may be that the substorm expansion was more rapid in this case leaving no time for reaction in the eastward electrojet flows.

For position c in Figure 4.9, the SABRE viewing area is now in the westward electrojet and the enhancement in background eastward flow is due to the substorm enhanced westward electrojet passing over SABRE.

Finally, for the time series data of Figure 4.8d the SABRE viewing area may be located to the east of the substorm enhanced electrojet flow (Figure 4.9d) and therefore observes only a diminishing eastward flow as the substorm region moves further to the west. In the first of the two Figure 4.8d events, the change from large north-eastward velocities before to small south-eastward velocities at the time of the Pi2 pulsation (23:40 U.T.) suggests that the WTS is close to this position at onset. A region of southward flow (westward electric field) is often observed behind the WTS and is thought to be a sub-threshold field for the radar. This might explain the southward

turning of the flow and the change to small amplitudes at this time. After the pulsation, the SABRE viewing area is again situated in the westward electrojet proper. The second example of Figure 4.8d simply has the SABRE viewing area situated in the westward electrojet.

An interesting feature was observed in a study of the amplitudes of these type 1 SABRE pulsations. In the data from a single cell, the peak to peak amplitude of the SABRE pulsation increased with the amplitude of the maximum change observed in the background bay at the time of the pulsation (Figure 4.10). This feature is particularly apparent for the east-west velocity component and is similar to that observed in the H-component ground magnetic data. The H-component Pi2 pulsation amplitude increases as the change in the H-component perturbation increases towards the centre of the substorm current wedge giving the associated pattern in azimuth orientation. The increase in westward flowing current during substorms increases the ionospheric electric field and is observed as an enhanced irregularity drift velocity by SABRE.

At other times no bay is present and the Pi2 pulsation is only represented by oscillatory changes in the SABRE velocity components. The oscillations can be centred around either zero or a constant value of positive or negative velocity. This type of signature affords the best opportunity for observing the impulsive, damped nature of the Pi2 pulsations in the SABRE data (Figure 4.11). At these times the SABRE viewing area is presumably located in the centre of the respective electrojets as no gradient in flow is observed. Alternatively, the viewing area may be situated well equatorward of the Pi2 pulsation generation region so that the wave alone and not the substorm current systems is observed.

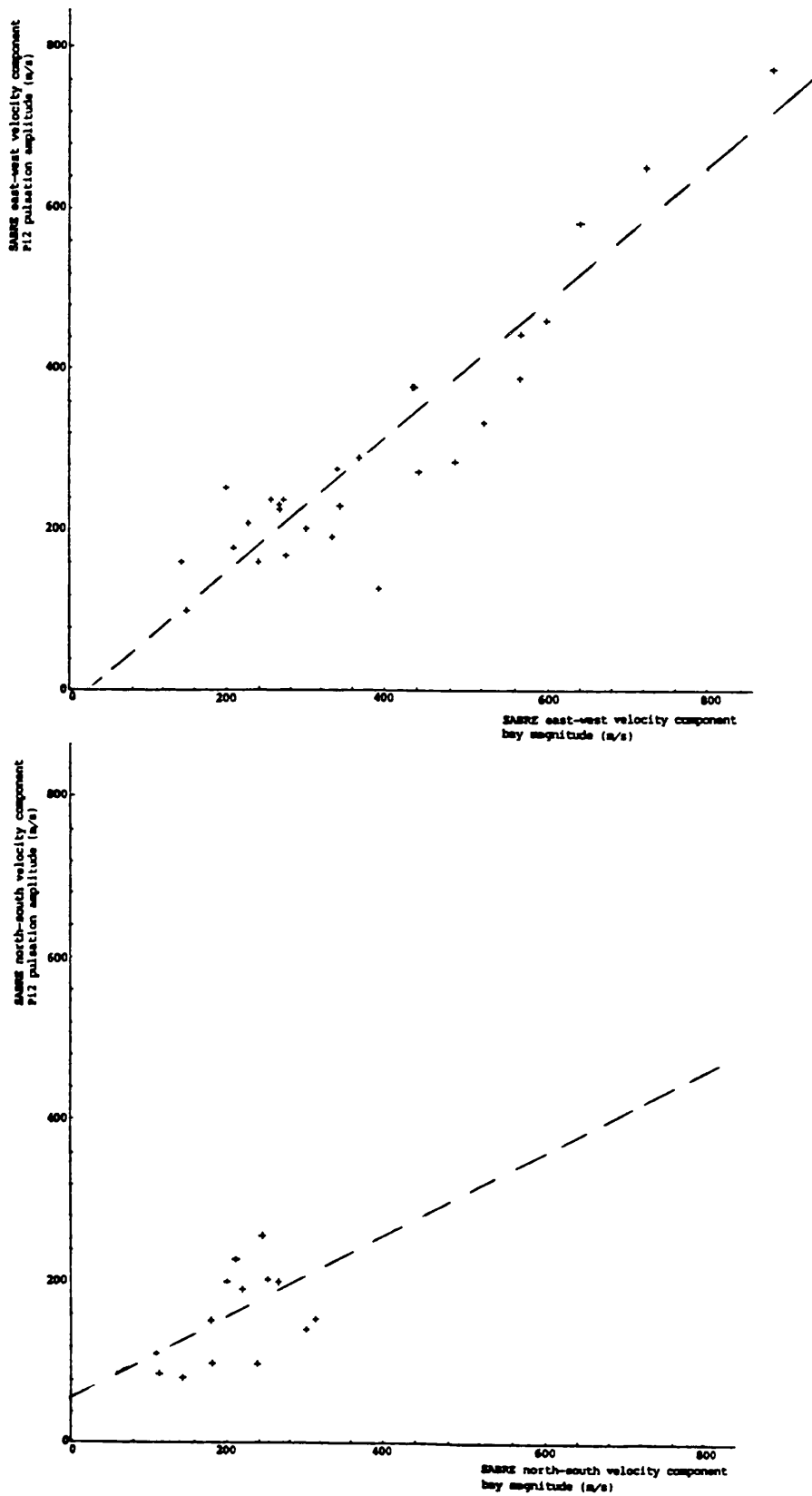
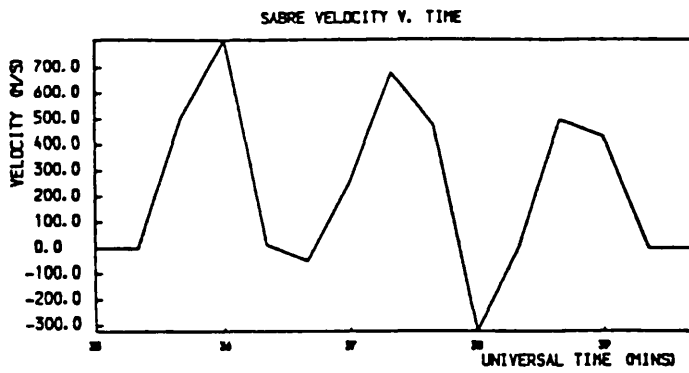
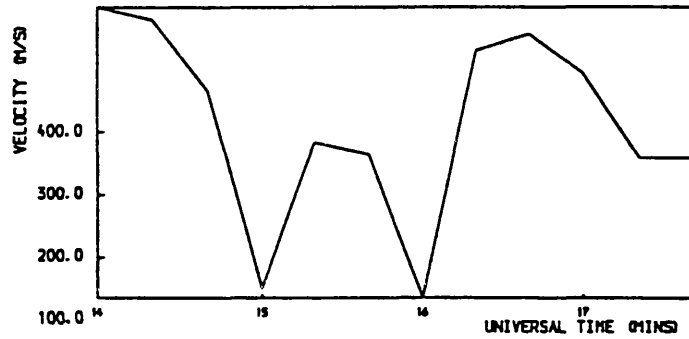


**Figure 4.10**

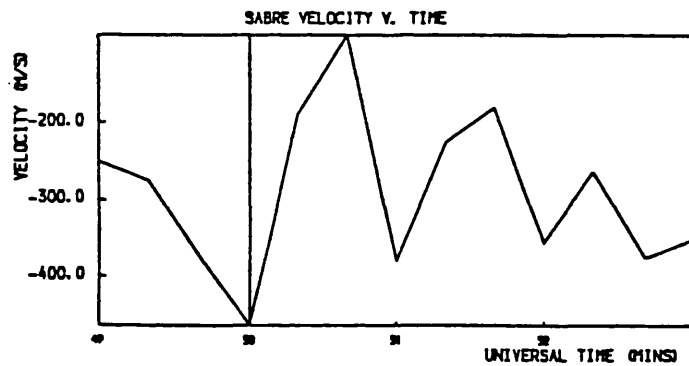
The distribution of the peak to peak amplitude of Type 1 SABRE Pi2 pulsations with the maximum change observed in the SABRE background bay magnitude at the time of the pulsation. East-west velocity data ( $r=0.92$ ) are presented above north-south velocity data ( $r=0.48$ ). The dashed lines are the best-fit straight lines derived from least squares analysis of the data. Both values of  $r$  are significantly different from zero at the 95% confidence level.



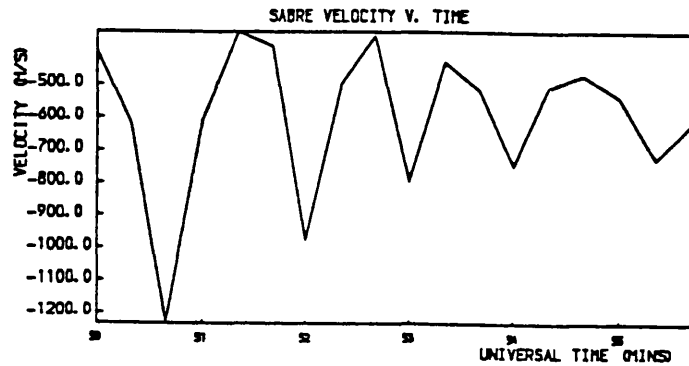
65.8 TO 66.0 DEGREES GG NORTH, 9.0 TO 9.5 DEGREES GG EAST.  
 1983 316 19 35 0 EAST-WEST COMPONENT  
 SABRE VELOCITY V. TIME



66.0 TO 67.2 DEGREES GG NORTH, 5.0 TO 6.0 DEGREES GG EAST.  
 1982 356 0 14 0 EAST-WEST COMPONENT  
 SABRE VELOCITY V. TIME



66.4 TO 66.6 DEGREES GG NORTH, 5.5 TO 6.0 DEGREES GG EAST.  
 1984 34 18 49 0 EAST-WEST COMPONENT  
 SABRE VELOCITY V. TIME



67.0 TO 67.2 DEGREES GG NORTH, 4.0 TO 4.5 DEGREES GG EAST.  
 1984 57 17 50 0 EAST-WEST COMPONENT  
 SABRE VELOCITY V. TIME

Figure 4.11  
 Type 1 SABRE Pi2 pulsation signatures in which no background bay is present at the time of the pulsation, the velocity oscillating about zero or a constant value of positive or negative velocity.

#### 4.6.3 Type 2 SABRE Pi2 pulsation signatures

The second type of Pi2 pulsation observed by SABRE involves rapid and very large changes in the irregularity drift velocities. These fluctuations are apparently switched on and off by the electric field associated with the pulsation itself (Figure 4.12a). If the Pi2 pulsation can be represented by a standing wave then each time the Alfvén wave bouncing between conjugate ionospheres returns to the northern auroral ionosphere, a reconfiguration of the ionospheric electric fields and currents occurs to compensate for the change in the finite ionospheric conductivities produced by the wave. The ionospheric electric field rises above the threshold for the generation of the irregularities observed by SABRE. The impulsive on-off type of Pi2 pulsation signature is then observed in the SABRE time series data. This type of signature is observed nearer the edges of the backscatter returns obtained, often in conjunction with the on-off switching of a small region of backscatter located equatorward of the main region of backscatter in the viewing area (Chapter 5). If a time series is constructed for the event covering all of the backscatter present, a background bay signature is observed with the pulsation superimposed. Such an event is presented as a case study in Chapter 6 and evidence suggests that it is generated by the field line resonance mechanism. Unfortunately, the FFT spectral analysis of the SABRE data which produced this hypothesis can not be applied to the other examples of Type 2 signatures due to the short duration of the events resulting in a poorly resolved spectrum.

On considering the amplitude and dominant ME period of the nine examples of Type 2 pulsations separately from the overall discussion in Sections 4.3 and 4.6, no relationships are present between the

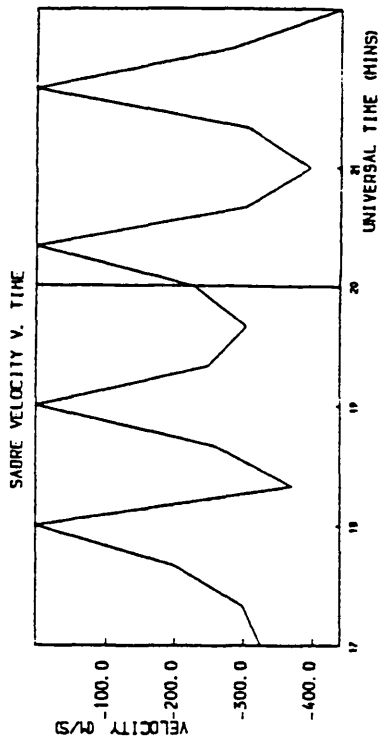
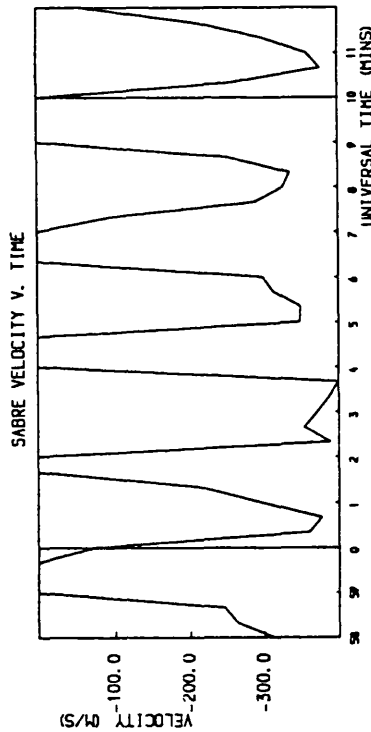
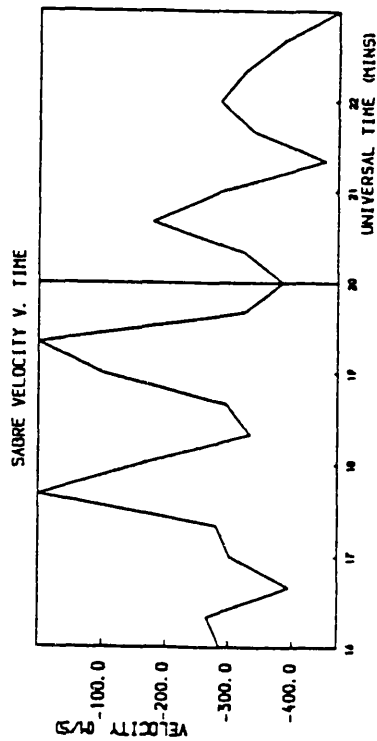
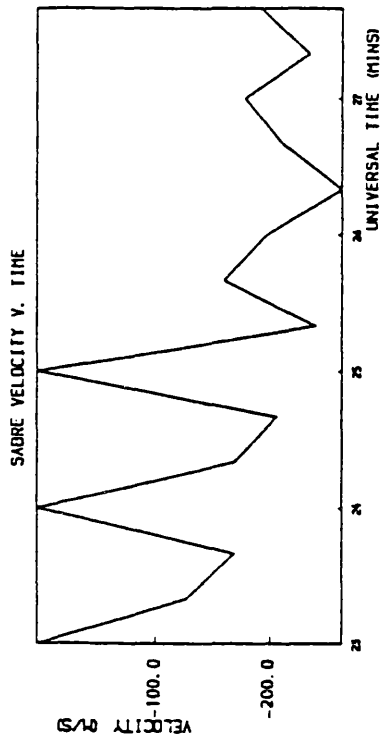


Figure 4.12a (left)

Type 2 SABRE Pi2 pulsations signatures with large changes in the drift velocity apparently switched on and off by the electric field associated with the wave itself.

Figure 4.12b (right)

Examples of events displaying features of both Type 1 and 2 SABRE Pi2 pulsation signatures.

ground and ionospheric measured quantities. For five of the nine events where a determination is possible, the SABRE polarisation is always linear in agreement with those derived from ground magnetic records. Fukunishi (1975) observed linear polarisation at the resonance region of Pi2 pulsations generated by field line resonances. These limited results are included in the discussion of polarisation presented in Section 4.7.

At other times the on-off switching is present at the edges of the backscatter simultaneously with the (Type 1) signatures described previously in the bulk of the backscatter (Figure 4.12b). This is more often the case when the viewing area is full of backscatter, the on-off signature appearing in time series from the nearest or farthest ranges or from the cells at the longitudinal extremes of the viewing area. In these cases the on-off signature is more likely a feature of the radar technique than of the physics of the wave present.

#### 4.6.4 Latitudinal and Longitudinal Profiles

An interesting feature of the SABRE data appears when stacked latitudinal and longitudinal profiles of irregularity drift velocity time series data are examined over a single longitudinal and latitudinal cell respectively. A progressive delay in the switch-on of the backscatter returns is observed by SABRE at lower latitudes for the same longitude range (Figure 4.13a). No backscatter was observed at latitudes above 66 degrees in the example presented in Figure 4.13a and the cell exhibiting peak wave spectral power at the dominant Pi2 pulsation period lies between 65.2-65.4 degrees north. In two other instances, the backscatter switch-on occurs earlier at lower latitudes and on one occasion the time became later then earlier again as data from lower latitudes were examined (Figure 4.13b). These features only

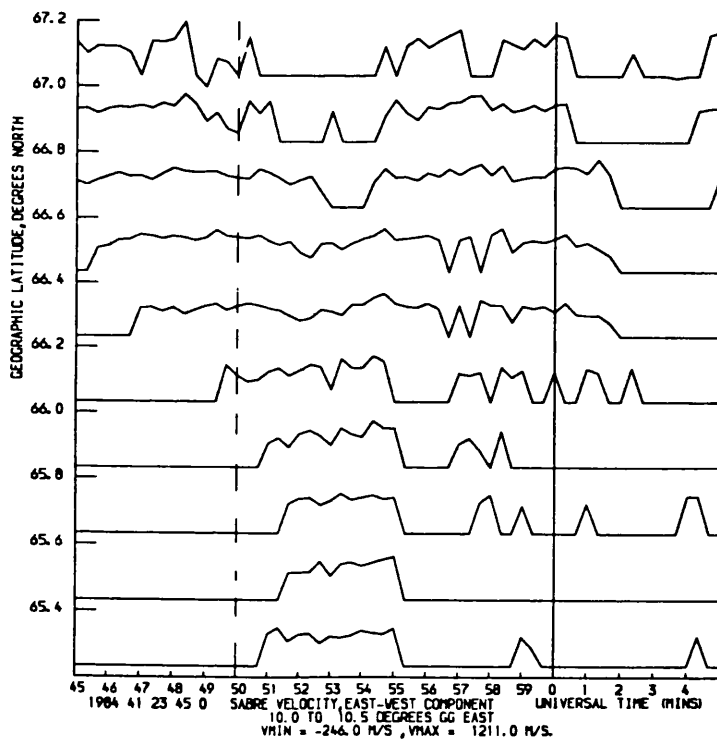
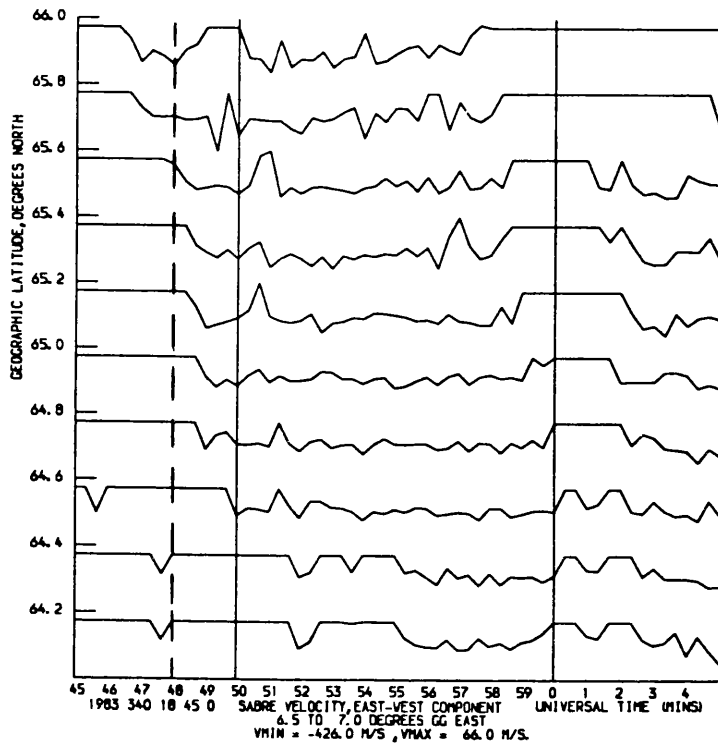


**Figure 4.13a**

A latitudinal stackplot of SABRE irregularity drift velocity time series data taken from a single longitudinal cell in the viewing area. The switch-on of backscatter associated with the Pi2 pulsation (ground onset time delineated by the dashed vertical line) is later at lower latitudes.

**Figure 4.13b**

Same as Figure 4.13a except that the backscatter switch-on occurs later then earlier again as data from lower latitudes are examined.

occur with the Type 1 SABRE Pi2 pulsation in which the 'bay' in the irregularity drift velocity starts from zero velocity. The onset of SABRE Pi2 pulsation signatures is simultaneous at all latitudes when backscatter is already present before the time of pulsation onset.

As the SABRE backscatter is switched-on by the onset of the pulsation these features are simultaneously present in both velocity components. Over the 18 events studied, the latitude range over which the delay is observed tends to increase with the magnitude of the delay present ( $r=0.454$ , and is significantly different from zero at the 95% confidence level). The latitude range and delay were calculated relative to the initial switch-on of backscatter at the highest observable latitude. The average delay in backscatter onset per degree of latitude is 100s with a standard deviation of 60s. The 20s SABRE integration time limits the accuracy of this study. If the progressive delay at lower latitudes is converted into an equatorward propagation velocity of this onset (assuming the SABRE cells are 20km apart, corresponding to 0.2 degrees of latitude), then a wide range of velocities (0.4-7km/s) is obtained. The mean and standard deviation of the equatorward propagation velocities are  $1.69 \pm 1.44$  km/s. This is an order of magnitude greater than the velocities quoted for the initial southward movement of the equatorward boundary of the auroral oval at substorm onset by Craven and Frank (1987).

Large changes in the phase of the pulsation have been reported in a latitude range which could at times include part of the SABRE viewing area (Stuart, 1974; Lester and Orr, 1981). These should theoretically be observable with the high spatial resolution (20km) of the SABRE system. Of the 18 examples presented here however, magnetometer data imply a change in sense of polarisation only once between Faroes and

Wick which latitudinally span the SABRE field of view. This is accompanied by an approximately 180 degree phase change in the H-component between Faroes and Wick with no change in the D-component phase. Of the remaining 17 events, the polarisation remains the same at the two latitudes and there is little (no) change in phase of the H(D) component magnetometer data between Faroes and Wick.

This implies that the delays in the features observed by the radar are not related to the pulsation itself. Also, the initial switch on of backscatter, at the highest latitude, occurs after the time of pulsation onset in the ground magnetic records implying the electric field does not immediately exceed the threshold of around 15mV/m necessary for the generation of the irregularities observed by SABRE. Thus, the generation of the plasma irregularities producing the backscatter, and their growth and propagation, seem to be the significant factors influencing these observations.

In the few isolated events which exhibit a possible longitudinal delay in the onset of backscatter returns (four compared with 18 latitudinal delays) there is no conclusive evidence of a delay occurring. At most, a 20s delay over a range of longitudes is observed and as this is only one SABRE integration time it is unlikely that there is any delay present.

For a typical Pi2 pulsation period of 120s, the 20s integration time of SABRE is equivalent to a phase difference of 60 degrees. This determines the lower limit for the phase difference observable with the SABRE system. The 60 degree phase difference across the width of the SABRE viewing area (12 degrees) is equivalent to an azimuthal wave number ( $m = \text{phase difference} / \text{station separation}$ ) of around five which is

consistent with previous results of  $m < 6$  (Mier-Jedrzejowicz and Southwood, 1979, 1981) and  $m < 5$  (Lester et al., 1984; Gelpi et al., 1985b) for Pi2 pulsations. It is therefore unlikely that SABRE would observe such phase differences in the localised region over which the Pi2 pulsations are normally observed (Section 5.3.1).

#### 4.7 Polarisation studies of SABRE Pi2 pulsations

##### 4.7.1 Introduction

The polarisation of the Pi2 pulsations in the SABRE data was investigated by the construction of hodograms from the filtered and unfiltered east-west and north-south irregularity drift velocity components as described previously in chapter 3. For the reasons outlined there, only the results obtained from the statistical analysis of the filtered data will be presented in this thesis.

The results indicate that a dominant sense of polarisation can often be determined (Figure 4.14) although in many cases the polarisation sense and ellipse orientation from a single cell in the SABRE viewing area change during a single Pi2 pulsation (Figure 4.15). In these latter cases no overall comment is usually possible on the azimuth or ellipticity as defined earlier. However, if each cycle of the Pi2 pulsation is considered to constitute a separate event (Samson, 1985), then an azimuth and/or ellipticity may be derived from the largest amplitude cycle present. Even in the best examples, however, the 20s integration time of SABRE produces hodograms which resemble triangles rather than ellipses. A greater time resolution is required to derive an azimuth with any certainty. This might also enable the ellipticity to be evaluated.

Similar changes in the polarisation sense of Pi2 pulsations from cycle

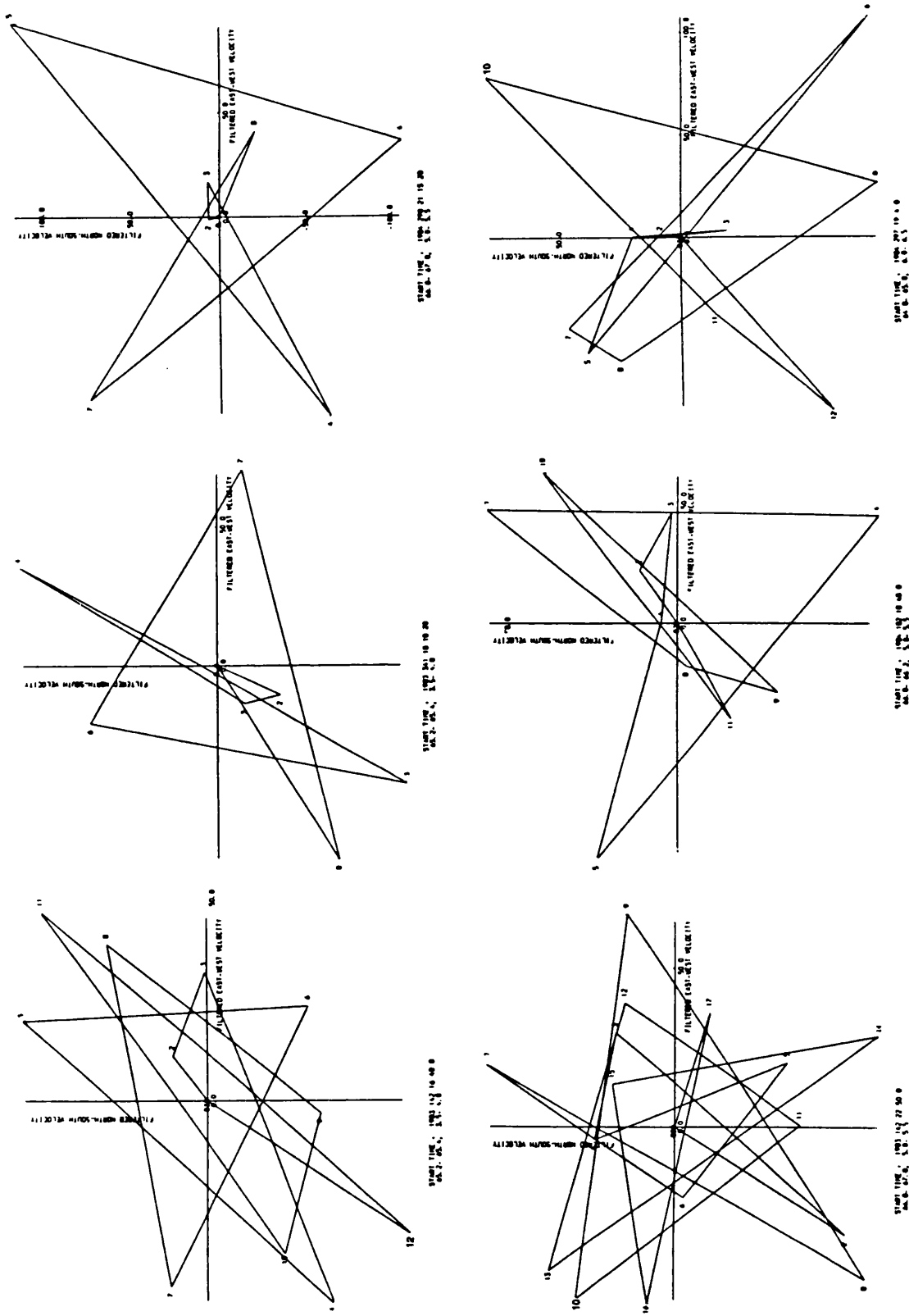


**Figure 4.14**  
Polarisation hodograms constructed from SABRE east-west and north-south velocity components which exhibit a definite sense of polarisation (clockwise top row, counter-clockwise bottom row).

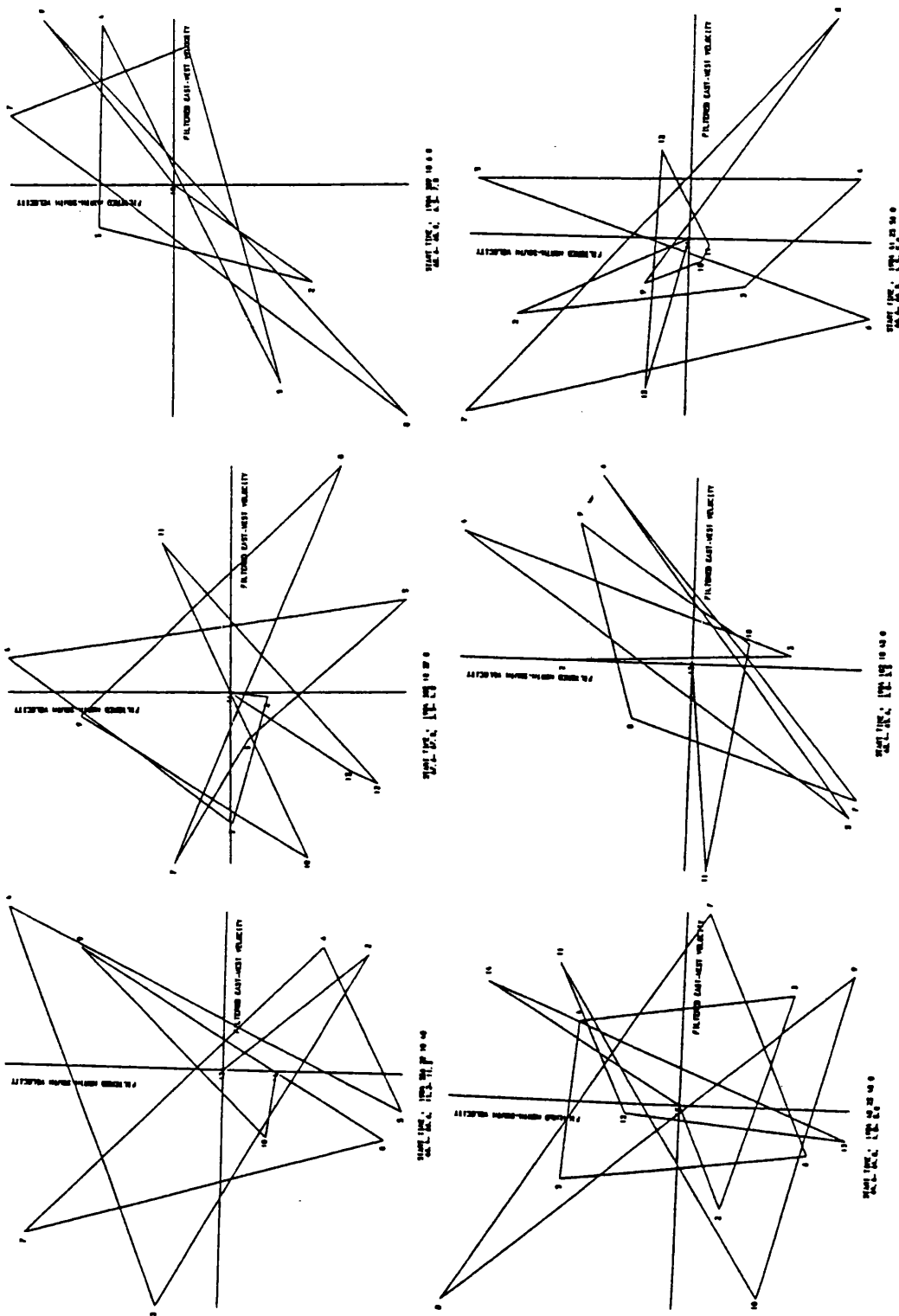
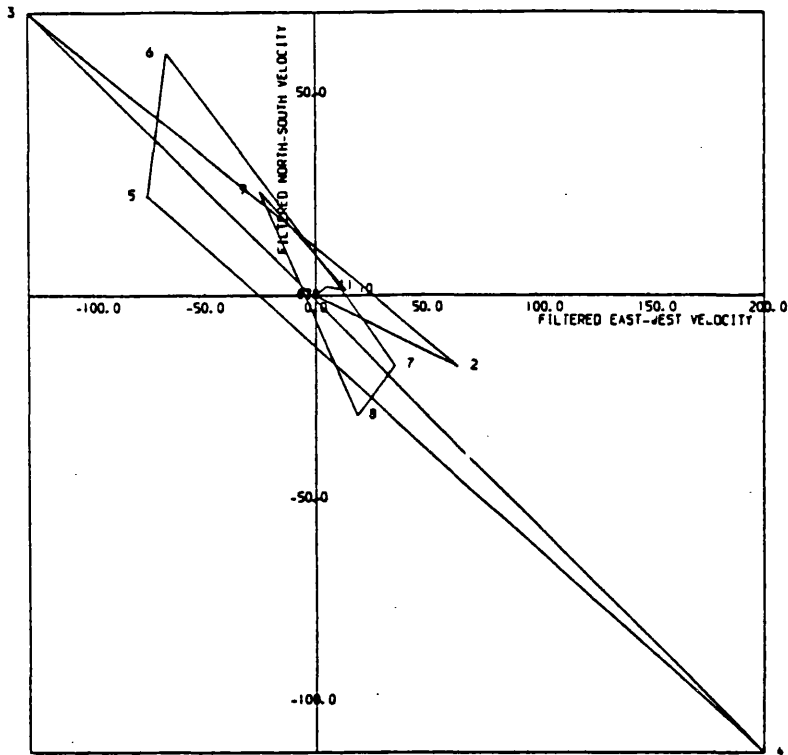


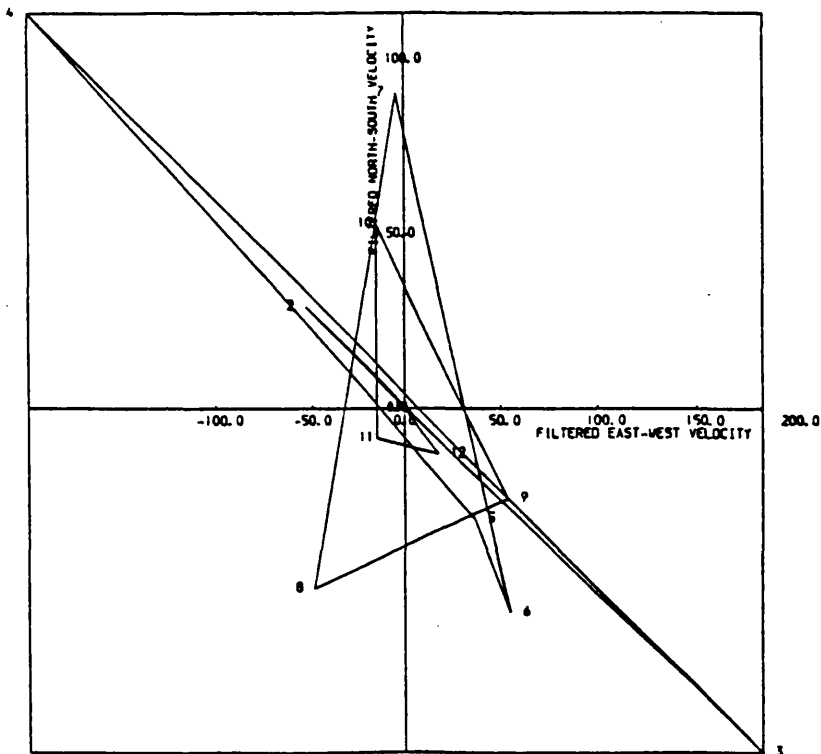
**Figure 4.15**  
 Polarisation hodograms constructed from SABRE east-west and north-south velocity components which exhibit a changing sense of polarisation as the Pi2 pulsation progresses.

to cycle have been observed by Pashin et al. (1982) and Samson and Rostoker (1983) at high latitudes. They attributed this change to the rapid movement of the source region, with its associated field-aligned currents, over the ground based magnetometer from which the data were obtained. Similarly, a changeable sense of polarisation was observed by Lester et al. (1985) in the data from certain stations when examining events which occurred in the eastward electrojet far from the auroral break-up region. This change appears to occur at the polarisation reversal associated with the field line resonance theory of Pi2 pulsation generation.

Another common feature in the SABRE data is the prevalence (53%) of linear polarisation. In such cases it is easier to determine a value for the azimuth of the ellipse (Figure 4.16 top). The orientation of the linear polarisation is often observed to change very quickly (Figure 4.16 bottom), implying the rapid movement of the substorm current wedge longitudinally across the SABRE viewing area during the course of the Pi2 pulsation. The cell in the viewing area from which the data are taken is now at a different position relative to the centre of the wedge. The SABRE viewing area was positioned inside or across one boundary of the wedge during the events exhibiting rapidly changing azimuths. Alternatively, this may reflect the passage of a single field-aligned current sheet across this region of the viewing area as mentioned above. It is of interest to note here that Gelpi and Behring (1984) examined the waves generated at the boundary of an auroral arc employing data recorded by rocket-borne instrumentation that flew across the arc. They discovered that the polarisation sense changed rapidly with each cycle of the wave and explained this as resulting from the addition of two orthogonally polarised waves at nearby frequencies. This may be the origin of the two surface waves



START TIME . 1984 102 18 40 0  
65.6- 65.8, 6.0- 6.5



START TIME . 198 102 18 45 0  
65.8- 66.0, 7.0- 7.5

Figure 4.16

top) SABRE polarisation hodogram which exhibits linear polarisation, a value for the azimuth of the ellipse can be determined in this cases.

bottom) SABRE polarisation hodogram exhibiting linear polarisation the orientation of which changes rapidly during the Pi2 pulsation.

generated at ionospheric conductivity gradients as described in the theory of Pi2 pulsations by Southwood and Hughes (1985).

#### 4.7.2 Comparison with ground magnetometer polarisation data

Comparison of the azimuth determined from ground magnetic records with the azimuth of the SABRE Pi2 pulsation, evaluated from the largest amplitude cycle observed where necessary, indicates that there is no obvious relationship between the two. There is no rotation which, if consistently applied to the SABRE data, would always produce the ground determined value of the azimuth. The distributions of possible values of rotation were investigated by constructing histograms of occurrence of the difference between the SABRE and magnetometer derived polarisation azimuths. This was undertaken for each of the WI, FA and NI magnetometer records (Figure 4.17). There is a large spread in the possible rotation values observed in the data from all three sites. The Wick data are approximately centred about zero while those from Faroes and Nordli appear to be concentrated around large negative values. In the theory of hydromagnetic waves in a cold plasma, the two possible wave modes, the transverse mode and the fast mode, behave differently in travelling through the ionosphere to the ground (Hughes, 1974; Hughes and Southwood, 1976a,b). The polarisation of the Alfvén or transverse mode is rotated CCW through ninety degrees while the fast mode is unaffected. The fact that the SABRE velocity is colinear with the horizontal magnetic perturbation of the Alfvén mode wave in the ionosphere (Figure 4.18 top) suggests that there should be a ninety degree rotation present between the ground magnetometer derived azimuth and that derived from SABRE. This rotation should not be present in the fast mode signal.

The presence of ionospheric conductivity gradients changes the

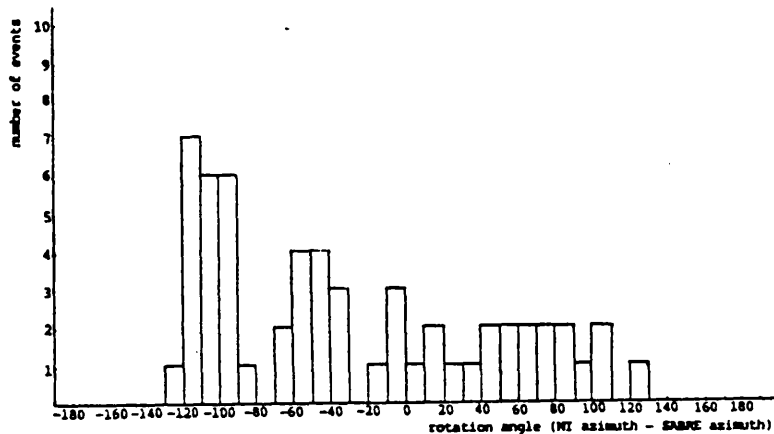
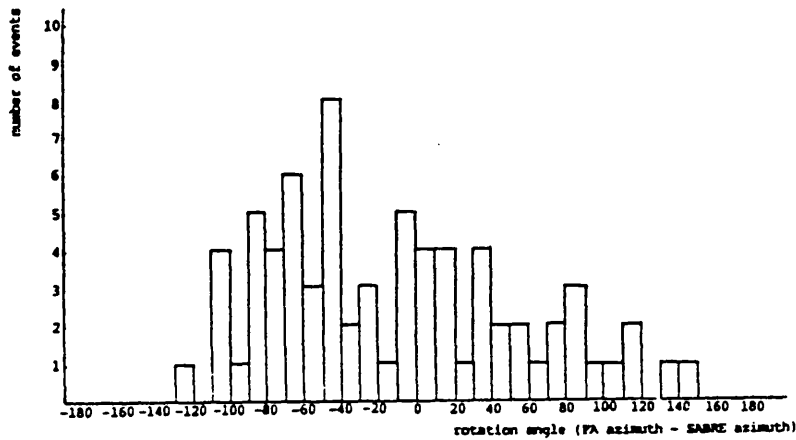
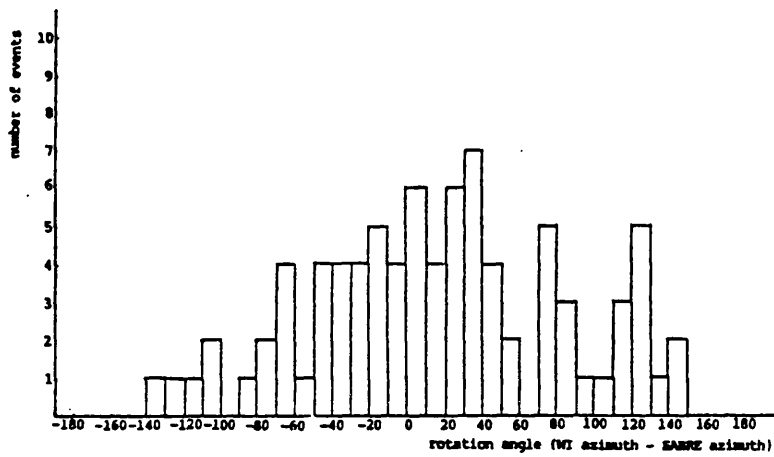


**Figure 4.17**

The occurrence of values for the rotation of the horizontal polarization ellipse on travelling from the magnetosphere, through the ionosphere to the ground. The values are calculated as the difference between the magnetometer and SABRE derived azimuths. Histograms are presented displaying data from the WI(top), FA(middle) and NI(bottom) magnetometer records.

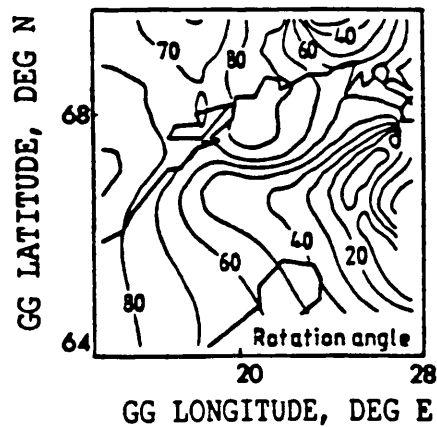
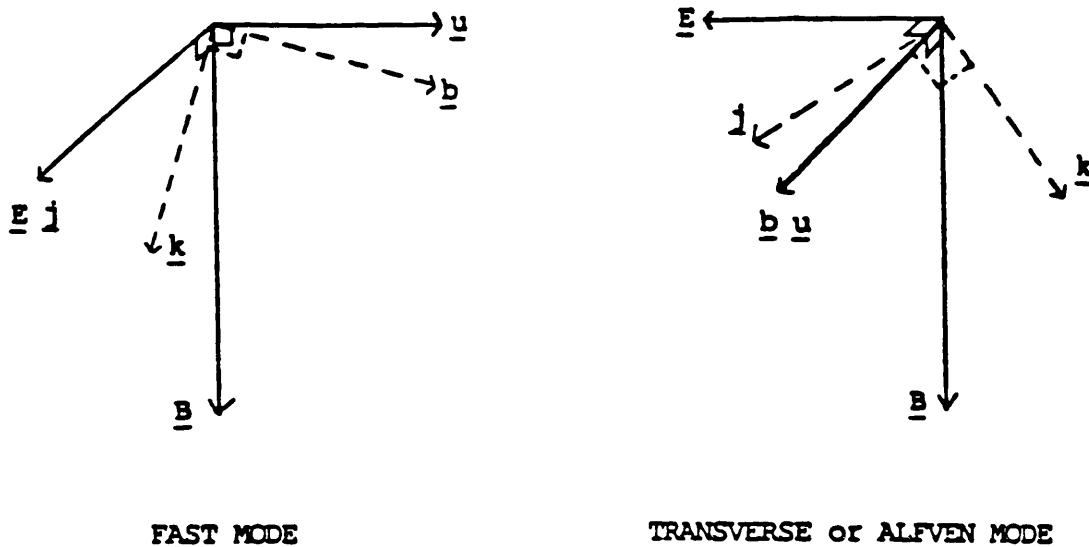


Figure 4.18

top) Schematic representation of the relation between the horizontal wave magnetic perturbation ( $\underline{b}$ ) and the electric field ( $\underline{E}$ ), background magnetic field ( $\underline{B}$ ) and velocity ( $\underline{u}$ ) in the ionosphere for the fast mode wave (left) and the transverse or Alfvén mode wave (right).

bottom) Modelled data from Glassmeier (1988) illustrating that the predicted rotation angle for the horizontal polarisation ellipse may vary greatly over a limited longitudinal extent if there are gradients in ionospheric conductivity present.

magnitude of this rotation for the transverse mode wave (Glassmeier, 1984). The rotation may take different values at different spatial locations relative to the conductivity enhancement during the same event, perhaps as little as ten degrees in regions of greatest inhomogeneity (Figure 4.18 bottom, Glassmeier, 1988). This fact, coupled with the inherent difficulties in calculating a SABRE azimuth helps to explain the spread in rotation values observed in the histograms in Figure 4.17. Another factor is the longitudinal and latitudinal separation of the BGS magnetometer stations relative to the SABRE viewing area. The azimuth on the ground is observed to rotate through 180 degrees across the total wedge width (typically 90 degrees of longitude at lower latitudes than SABRE, Lester et al., 1983) so there may be at least a twenty degree rotation present due to the average ten degree separation between the two observing regimes. Attempts to predict a SABRE azimuth by assuming a linear relationship between the azimuths obtained at FA and NI produced inconclusive results. The difference between the observed and predicted SABRE azimuths took the whole range of possible values. It is therefore not possible to deduce if a rotation is present. The same is true in assuming a linear relation between the azimuths at WI and FA in attempting to predict the SABRE azimuth from the observed latitudinal variation. The longitudinal separation between the WI-FA meridian and the SABRE viewing area also affects the investigation.

#### 4.7.3 SABRE polarisation relative to local time and the substorm current wedge.

To further examine the presence or otherwise of a rotation of the polarisation azimuth, the SABRE and magnetometer derived azimuths were also rationalised by local time and by position relative to the

substorm current wedge. To reduce the problems discovered previously in the positioning of the SABRE viewing area relative to the wedge, the following procedure was adopted: only the Pi2 pulsations which gave consistent results in the positional analysis, together with isolated or the first in a series of Pi2 pulsations, were employed in this section of the study.

The events presented have also been sub-divided by the sense of ellipticity on the ground. The polarisation sense was positive (CCW) for all events examined in the ground data from the lower latitude station of Wick. At the higher latitude stations, when examining mean values of ellipticity, the polarisation changed sense from positive to negative at approximately 00:00 L.T. and 23:00 L.T. at Faroes and Nordli respectively. Relative to the substorm current wedge the ellipticity on the ground at Nordli was mainly positive to the west of centre of the wedge (54 to 19) while negative ellipticity was slightly more prevalent (49 to 33) to the east of centre of the wedge. At Faroes the ellipticity was predominantly positive throughout the wedge although more so to the west of centre (79 to 15) than to the east of centre (35 to 22).

The results obtained concerning the SABRE derived azimuths are summarised schematically in Figure 4.19. The length of the vector roughly indicates the probability of occurrence of the associated azimuth direction. The '+' or '-' sign indicates the predominant sense of polarisation in the ground magnetic data obtained simultaneously, although no relation was found between this and the SABRE derived azimuths. The SABRE data are only divided into cases of positive and negative azimuth for each ground derived orientation, there being no sub-division within these two regimes. The number associated with the



SABRE data indicates the number of events (Nordli above, Faroes below) for which SABRE exhibits that azimuth. No attempt has been made to assign an ellipticity to the SABRE data for the reasons outlined previously.

Only at the earlier local times, and perhaps to the west of centre of the wedge, does SABRE exhibit a consistent direction (NE) of azimuth which agrees with that determined in the ground magnetic data from Wick. The small amount of data from the later local times and to the east of centre of the wedge are mixed with no definite relationship present. In the local time divided data from the two higher latitude stations of Faroes and Nordli the data are also mixed, few in number and inconclusive apart for those events with azimuths on the ground pointing north-west at earlier local times. For the majority of these cases the SABRE derived azimuths point north-east into the opposite quadrant. This implies that a counter-clockwise rotation of the wave azimuth has occurred on travelling from the ionosphere to the ground. The absolute magnitude of this rotation cannot be determined however as the SABRE derived azimuths were only binned by the two possible quadrants. Similar comments are applicable to the comparisons of the substorm current wedge divided data from the two higher latitude stations: when the data are not mixed (in west and out east) there again appears to have been a counter-clockwise rotation of the wave azimuth on travelling to the ground. Overall, the lack of events, especially to the east of the wedge, make definite statements on the SABRE polarisations and the application of an ionospheric rotation to the wave difficult.

#### 4.8 Conclusions

SABRE observes the substorm associated Pi2 pulsations over a wide

range of magnetic activity and over a wide span of local time, from early evening to early morning. The oscillatory, impulsive nature of the pulsations is reproduced in the irregularity drift velocity time series obtained from a single cell or group of cells within the SABRE viewing area. The events observed range from isolated pulsations, at relatively quiet magnetic times, to trains of pulsations during active times. Magnetometer data indicate that the SABRE viewing area is situated both inside and outside the substorm current wedge for different events. SABRE also observes pulsations over the whole Pi2 pulsation period range (40s-150s) although the shortest periods are near to the observation limit imposed by the 20s integration time employed by SABRE. Comparison between SABRE and magnetometer records illustrate a wide spread in the amplitude data, although the dominant pulsation periods are approximately the same.

When the SABRE viewing area is inside the substorm current wedge the signatures obtained in the SABRE time series data exhibit positive or negative changes in the background electric field which are dependent on time of occurrence and position relative to the substorm enhanced westward electrojet. In a similar way to the dPi studies of Stuart (1972) in ground magnetic records, SABRE is here observing the currents involved with the wedge at substorm onset in addition to the oscillatory signature of the Pi2 pulsation itself. The amplitude of the SABRE Pi2 pulsation was observed to increase with an increase in the maximum change of the background bay associated with the pulsation in both velocity components of the SABRE data. At other times only the oscillation is present in the SABRE time series data.

The polarisation of the Pi2 pulsations has been investigated by means of hodograms constructed from filtered SABRE velocity data. A

predominant sense of polarisation is often observed, although changeable polarisation sense within a single Pi2 pulsation, accompanied by changes in the orientation of the polarisation ellipse, has also been noted. Only in the case of linear polarisation is it possible to determine accurately the azimuth of the polarisation ellipse. No relationship was always apparent between this azimuth and that determined for the Pi2 pulsation observed on the ground even after the data were sub-divided by local time and also by position relative to the substorm current wedge. The data were normally inconclusive as to whether a rotation of the wave azimuth had occurred between the ionosphere and the ground. The rotation values displayed a large spread at all three magnetometer sites. At the lower latitude station, WI, there appeared to be a small rotation present while a possible ninety degree CCW rotation was observed in the data from the higher latitude stations. This was only evident at earlier local times and to the west of centre of the substorm current wedge. However, the longitudinal/latitudinal separation of the observing positions together with the possible influence of gradients in ionospheric conductivity make it difficult to be sure of the presence of a rotation. The presence or otherwise of a rotation of the polarisation ellipse is important in theoretical studies of pulsations as it would determine which mode of hydromagnetic wave is present.

The comparative lack of events for which a SABRE derived azimuth could be evaluated was a large factor in this analysis, especially to the east of centre of the substorm current wedge. The principal reason for this is the SABRE 20s integration time as mentioned previously. If the integration time could be reduced, the azimuth may be more often and more easily calculated and an actual value for the ellipticity determined as opposed to only the sense of rotation of the

polarisation ellipse. A shorter integration time would also enable a FFT spectral analysis to be carried-out. One result might be plots of polarisation and phase variation across the viewing area for the Pi2 pulsations as produced for longer period continuous waves (Walker et al., 1979; Waldock et al., 1988). This would help in deciding on a generation mechanism for the pulsations.

## CHAPTER 5

### SABRE SPATIAL PATTERNS DURING Pi2 PULSATIONS

#### 5.1 Introduction

As mentioned in Chapter 3, one of the main reasons for observing Pi2 pulsations with SABRE is the ability to examine a small region of the ionosphere with excellent spatial resolution. Magnetometers, on the other hand, respond to a larger area of the ionosphere, of typically 100km radius. Since the auroral oval, on average, moves to lower latitudes with increasing magnetic activity, SABRE is capable of examining a wide range of possible convection flows associated with Pi2 pulsations. The morphology of the different irregularity drift velocity flow patterns observed under different magnetic conditions and their relationship to the substorm current wedge is discussed. The flows are related to the position and localisation of the cells in the SABRE viewing area which exhibit peak wave spectral power at the dominant Pi2 pulsation frequency.

#### 5.2 Morphology of SABRE spatial patterns during Pi2 pulsations

##### 5.2.1 Introduction

The flow patterns observed by SABRE at the times of Pi2 pulsations can be classified into two main types: (a) occasions when backscatter fills the entire viewing area ; (b) occasions when only a small region of backscatter is present during the time interval of the pulsation. In the case of type (b), the small region is sometimes accompanied by

an additional patch of equatorward backscatter which pulses on and off. Examples of type (a) occur predominantly in the eastward electrojet, pre-magnetic midnight regime whilst examples of type (b) are confined to the Harang discontinuity region or the westward electrojet.

### 5.2.2 Type (a) Spatial Patterns

The first type of spatial patterns regularly observed by SABRE during Pi2 pulsations filled the SABRE viewing area. The Pi2 pulsation was represented by small angular perturbations in the background flow, resulting in changes in the orientation of the mainly east-west directed vectors. Fluctuations in the magnitude of the east-west components are also observed (Figure 5.1). A majority (71%) of the events with this fluctuating signature occur when the SABRE viewing area is positioned inside the substorm current wedge and it is equally likely to be to the west (33%) or east (31%) of the centre of the wedge.

It is often possible to detect a vortex-like flow pattern embedded in the background flow regime. This occurs towards the equatorward edge of the backscatter in the three examples presented in Figure 5.2. In many instances it appears that the vortex structure may not be associated temporally with the Pi2 pulsation observed. In 13 of the 15 examples, the onset of the Pi2 pulsation in the ground magnetometer records occurs before the appearance of the vortical flow patterns in the SABRE data. This suggests that the vortex is more likely to be associated with the substorm current systems. The statistics of occurrence of the vortex-like features are presented in Table 5.1.

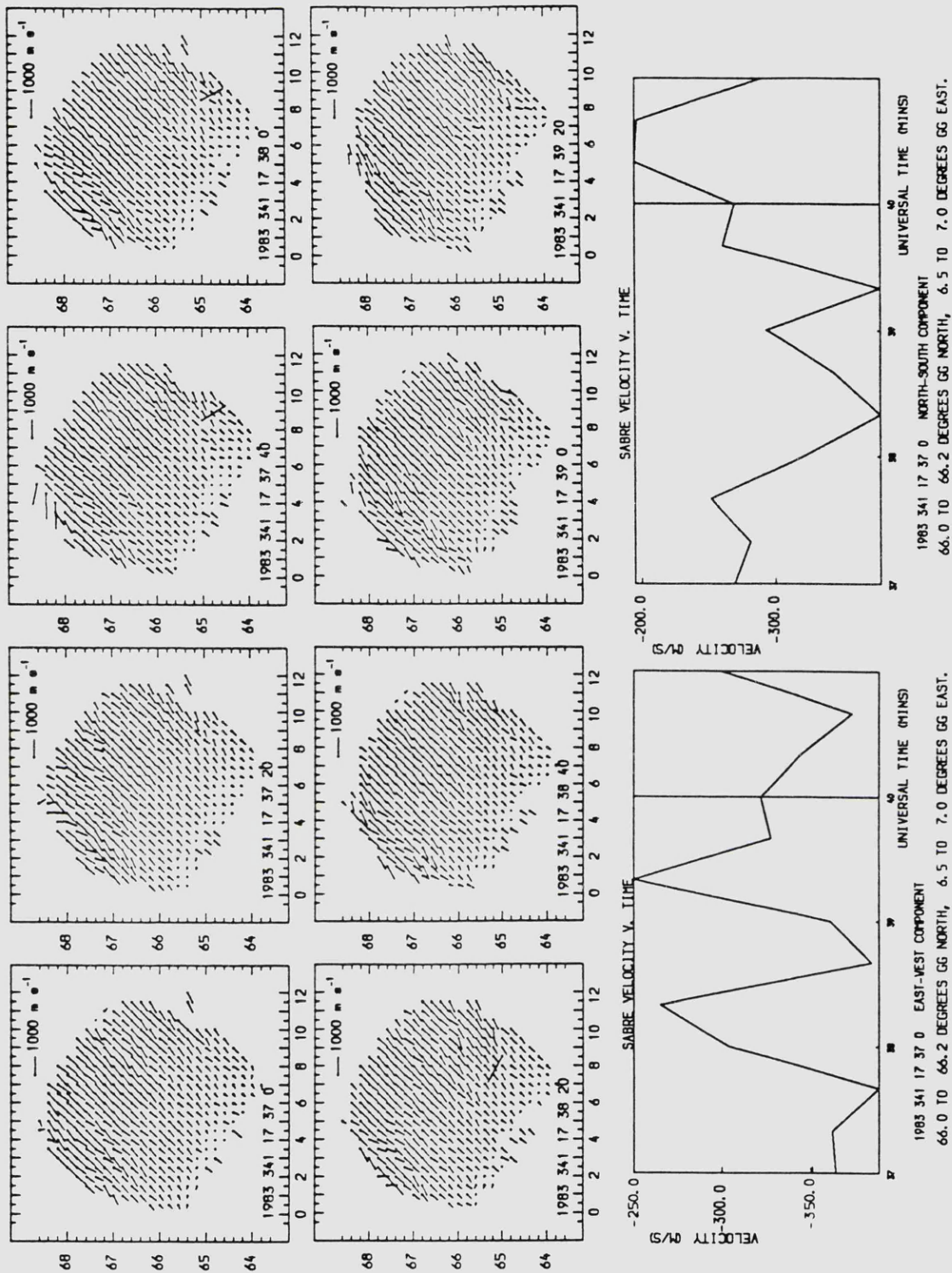


Figure 5.1

A sequence of SABRE spatial velocity plots in which the Pi2 pulsation is represented by small changes in the magnitude and/or orientation of the velocity vectors. The time series data from a single cell in the viewing area are displayed below.

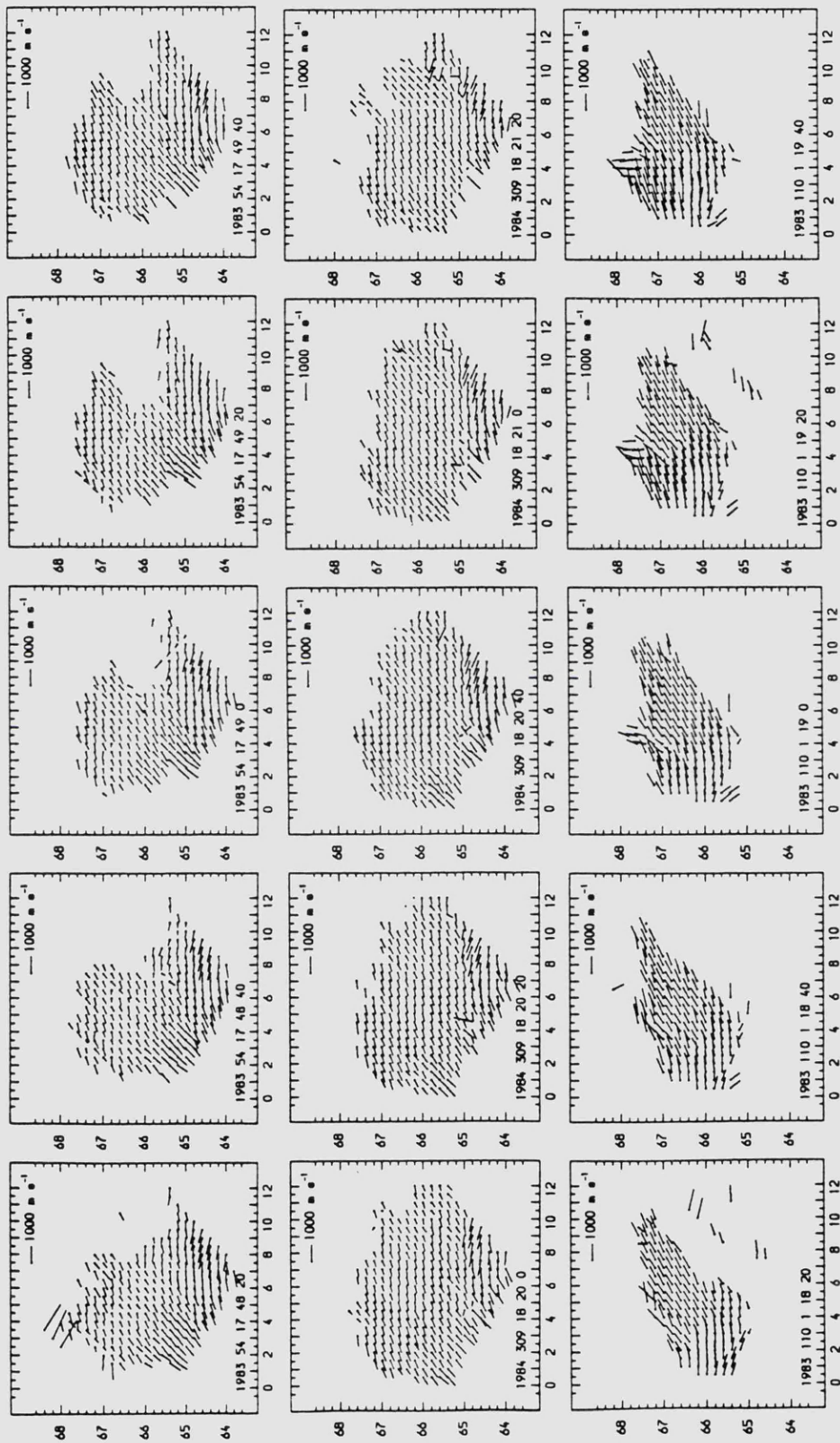


Figure 5.2

Three sequences of SABRE spatial velocity plots in which vortex-like flow patterns are present at the equatorward edge of the returns at the time of the Pi<sub>2</sub> pulsation.

Table 5.1

Occurrence of SABRE vortical flows

number of vortices	pre-magnetic midnight				post-magnetic midnight			
	11				4			
rotation sense	9 ccw		2 cw		2 ccw		2 cw	
position wrt wedge	7 in w	2 in e	2 in w	0 in e	0 in w	2 in e	0 in w	2 in e
Kp range	3-,4+	3+,4-	3-,4+		4-,4+		4,6	

Cases of vortical flow are normally observed at times of moderate to high magnetic activity, as indicated by the range of Kp observed. The SABRE viewing area is therefore more likely to have been close to the generation region for the pulsations when the vortices were observed. There is also some evidence that the dimensions of the vortex structure increase with magnetic activity, although a full vortex was never observed. The vortices keep the same sense of rotation throughout the interval of the Pi2 pulsation associated with it.

On one occasion a double vortex system of flows is observed with a clockwise rotating one in the north-west and a counter-clockwise rotating one in the south-east of the SABRE viewing area (Figure 5.3 top). During this interval the vortices appear and disappear coincidentally with the onset and finish of each of a train of four Pi2 pulsations. On another occasion a similar double vortex system is observed although in this instance the two vortical flows make a figure of eight-like structure with a counter-clockwise vortex situated immediately poleward of a clockwise one (Figure 5.3 bottom). As the flows occur in the north-west of the SABRE viewing area, only the middle third of this system of flows is visible. In this example the vortices appear in the SABRE flow patterns simultaneously with the

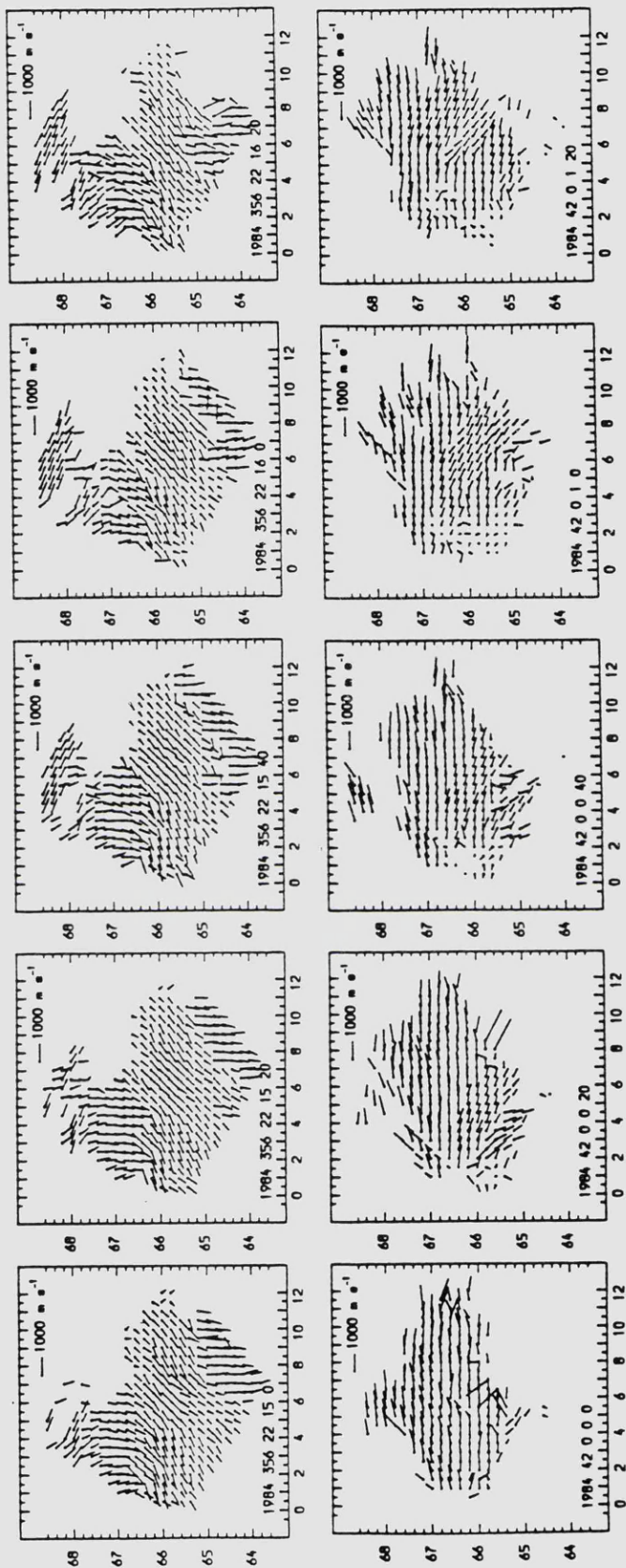


Figure 5.3

Two sequences of SABRE spatial velocity plots in which double vortex-like flows appear and disappear coincidentally with the onset and end of the Pi2 pulsations. The vortices, CW in the north-west and CCW in the south-east, are separated in the first example (top) whereas the two occur in the west of the viewing area but separated only in latitude for the second.

onset of the Pi2 pulsations, but have disappeared before the end of the pulsations on the ground. In both cases the sense of rotation of the twin vortices does not change during the event.

Vortex patterns were observed by Pashin et al. (1982) and Glassmeier et al. (1988) when examining the ground equivalent currents obtained at the time of Pi2 pulsations associated with the auroral break-up at substorm onset. The vortex occurred in the region where a strong, localised upward field-aligned current was thought to flow. This vortex changed its sense of rotation with half of the period of the associated Pi2 pulsation and was a result of periodic modulations in the upward field-aligned currents in the western part of the substorm current wedge. The scale size of these vortices was 1000km and it is therefore not surprising that a complete vortex was not observed in the SABRE viewing area (500x500km). In addition, Baumjohann et al. (1981) and Inhester et al. (1983), in modelling the ionospheric and field-aligned currents associated with auroral break-up and the westward travelling surge (WTS), discovered a vortical flow in the ground equivalent currents close to the foot of the upward field-aligned current associated with the WTS at the western end of the substorm current wedge. Similar vortex-like patterns were also observed in ground equivalent currents by Lester et al. (1985) in a case study of two Pi2 pulsations in the eastward electrojet, far from the auroral break-up region. The sense of rotation of these vortices changed with the observed pulsation period. In addition, for every other quarter period, two oppositely rotating vortices were observed which were latitudinally separated. In the following quarter period only one vortex was observed. This change in the configuration of the equivalent currents continued throughout the period of the pulsation, the vortex system also moving westwards as the pulsation progressed.

The scale size of each vortex was 500km in this case. The observed vortices were reproduced when Lester et al. (1985) modelled the electric field and conductivity in the region assuming a field line resonance mechanism for the generation of the pulsations.

Vortices in the Hall current flow in the ionosphere have also been predicted on a theoretical basis by Southwood and Hughes (1985) in examining the surface waves produced at gradients in ionospheric conductivity. There was usually more than one present and, for the most reasonable ratio of Hall to Pedersen conductivities of 5, they were more elliptical and inclined relative to the enhanced electrojet system. This was an extension of the work of Ellis and Southwood (1982) and illustrated how the predicted ground polarization pattern may be produced from the addition of two oppositely polarised surface waves (see chapter 2). The scale size of these vortices was given relative to the wave-number ( $k$ ) of the surface waves. It appeared that the vortices were of radius equal to a quarter the wavelength of the associated surface waves. For a typical azimuthal wavenumber ( $m$ ) of 5 (Mier-Jedzrejowicz and Southwood, 1979) this implies a scale size, in the ionosphere at 65 degrees north, of around 800km. This is similar to the value suggested by Glassmeier et al. (1988) for vortices observed in ground equivalent currents at the time of Pi2 pulsations. For smaller values of  $m$  (Gelpi et al., 1985b), the scale size of the vortices will increase with the increase in the wavelength of the surface wave. If  $m=2$  the scale size is about 1800 km. This is further evidence that a full vortex is unlikely to be observed in the SABRE viewing area (500kmx500km).

Occasionally, Pi2 pulsations are observed when there are regions of different flow direction embedded in the overall background flows.

These regions appear to move either latitudinally or longitudinally across the SABRE viewing area (Figure 5.4 top or bottom). These flows are observed at times of moderate to high magnetic activity,  $K_p > 3+$ , and when the SABRE viewing area is inside the substorm current wedge. In all but two of these events the start of the movement of this region of flow coincides with the onset, or occurs during the interval, of the associated Pi2 pulsation. Of the five events in which regions of southward flow are observed to move longitudinally across the SABRE viewing area, four occur in the eastward electrojet with westward background flows observed by SABRE. The region of southward flow moves westward, with velocities of 0.7km/s, 1.1km/s, 2.0km/s and 3.3km/s. For one event which occurs in the westward electrojet, the region of southward flow moves eastward with a velocity of 4km/s. The above velocities are, in most cases, larger than the background flow velocity present at the time. The velocities were calculated by first determining the number of cells in the SABRE viewing area across which the feature moved in a specified period of time. This gave a velocity in terms of degrees of longitude per multiple of the 20s integration period in the SABRE data. This was then converted to km/s assuming that the cells in the SABRE viewing area are 20km apart.

The values for the speed of westward propagation of the small region of southward flow across the SABRE viewing area are found to be in agreement with the 'several km/s' (Craven and Frank, 1987) and the 2km/s (Wiens and Rostoker, 1975) quoted for the westward expansion of the region of auroral activity following substorm onset. Craven and Frank (1985) gave an average value for this expansion of around 600m/s, although the initial (<10 minutes) expansion has a velocity of 3km/s and is followed by around 330m/s for the remainder of the substorm. However, it is not certain that the visible and radar aurora

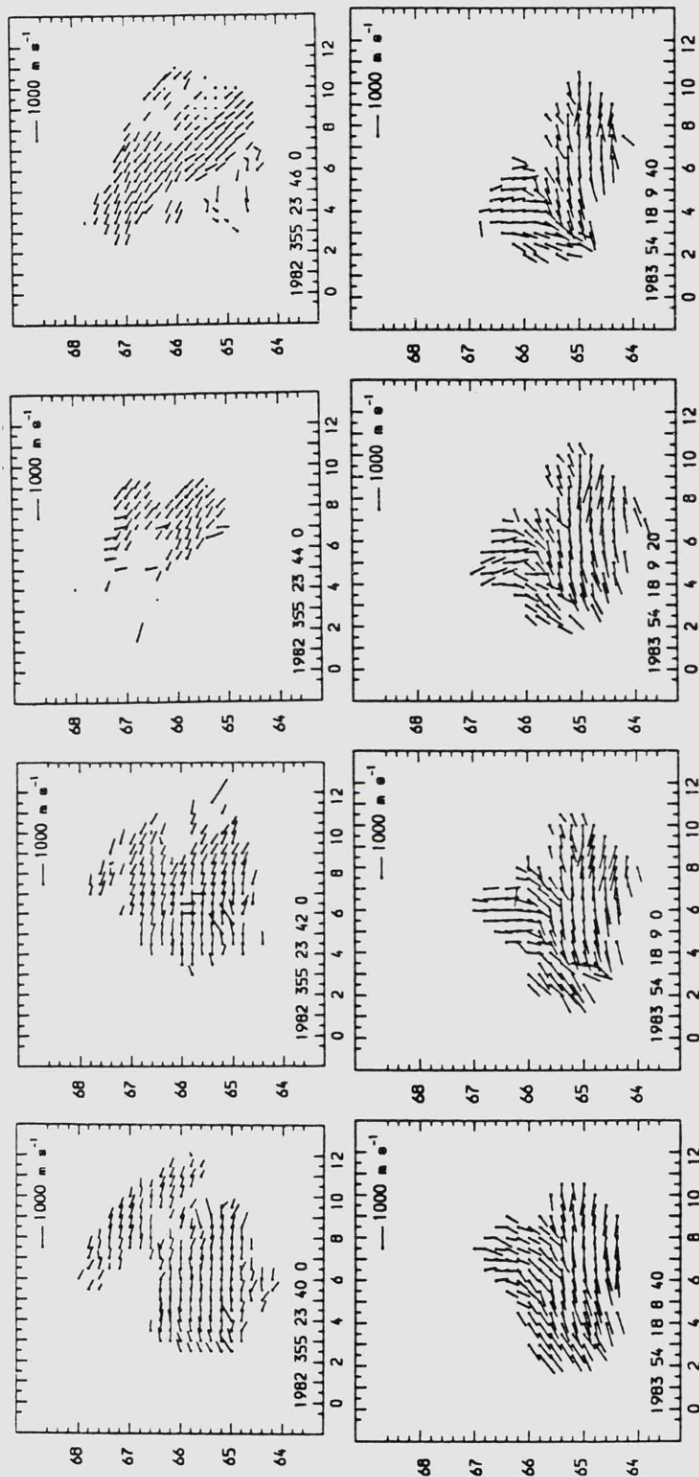


Figure 5.4

A sequence of SABRE spatial velocity plots in which a region of different flow moves latitudinally (top) or longitudinally (bottom) through the SABRE viewing area at the time of a Pi2 pulsation.

are initially coincident and subsequently move together with the same velocity as the event progresses.

Another signature of the Pi2 pulsations in the SABRE spatial data is the switch-on of a region of usually southward flow poleward of the backscatter already present (Figure 5.5). These regions often subsequently move longitudinally across the SABRE viewing area as described previously. If the viewing area is already full of backscatter, this signature manifests itself as a sudden southward or northward turning of the existing vectors at pulsation onset (Figure 5.6). These features occur at times of high magnetic activity, Kp being at least 3+ while Lerwick-K was always 4 or greater. Of eight events, five occur when the SABRE viewing area is inside the substorm current wedge. This southward turning of a region of vectors is temporally coincident, in six of seven events, with the first in a series of Pi2 pulsations, while the remaining event occurs with the second in a series of pulsations. The eighth event involves a northward turning of a region of vectors and coincides with the last in a series of four Pi2 pulsations, the second of which is associated with the southward turning of a region of vectors. This last event is discussed in more detail in a case study in the following chapter.

Since the region of southward flow associated with the Pi2 pulsation moves westward across the viewing area with a velocity similar to that of the westward travelling surge after substorm onset, it is tempting to suggest that the two are closely related. The region of southward flow corresponds to a westward electric field and the modelling work of Baumjohann et al. (1981) place such a field to the east of the head of the WTS. Previously, the electric field in this region was found to be below the 15mV/m threshold for the generation of the irregularities

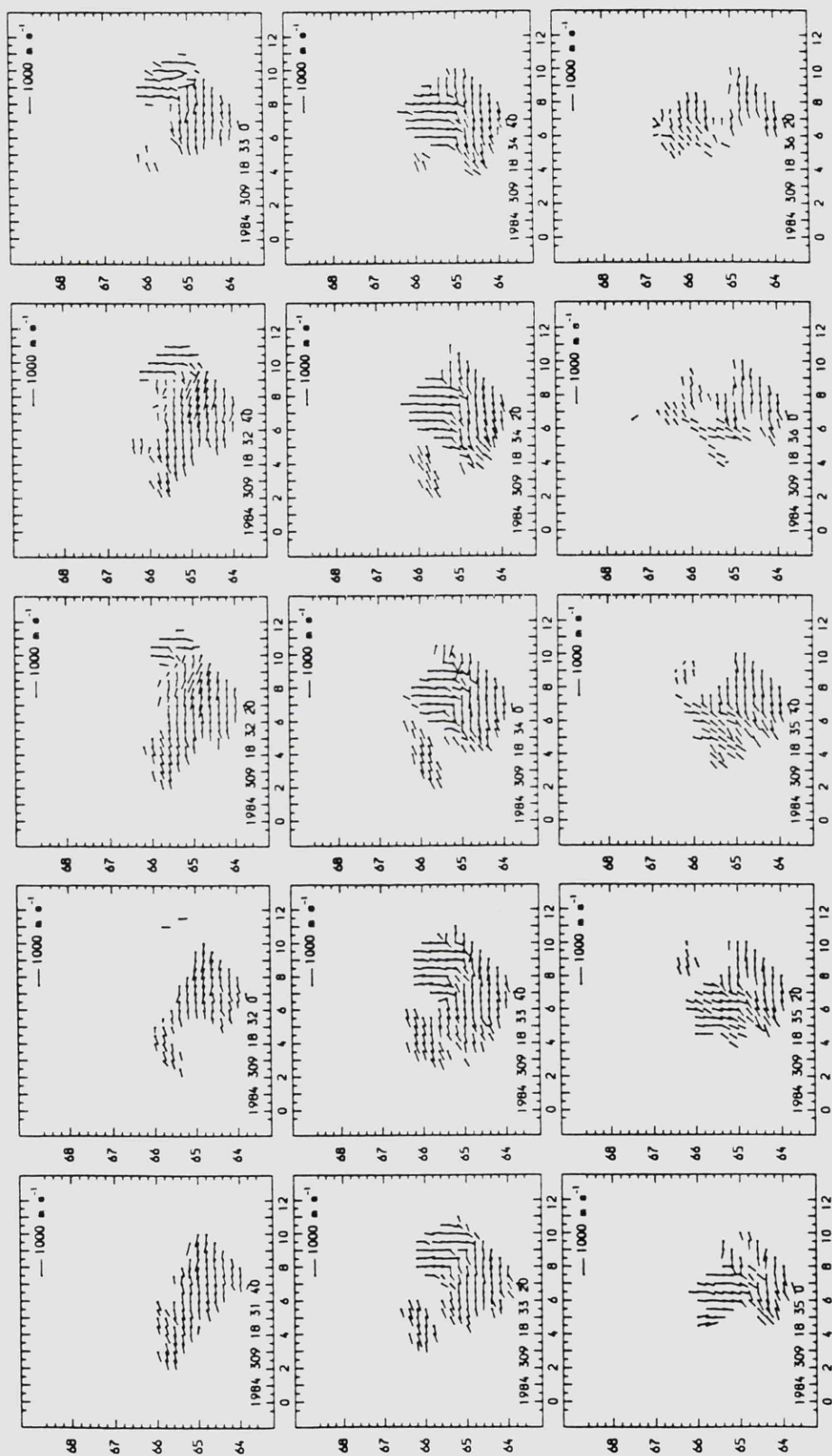


**Figure 5.5**

A sequence of SABRE spatial velocity plots in which a sudden switch-on of southward pointing vectors is observed, at Pi2 pulsation onset (18:32:20 U.T.), at the poleward edge of those that were previously present. This region then moves longitudinally across the viewing area.

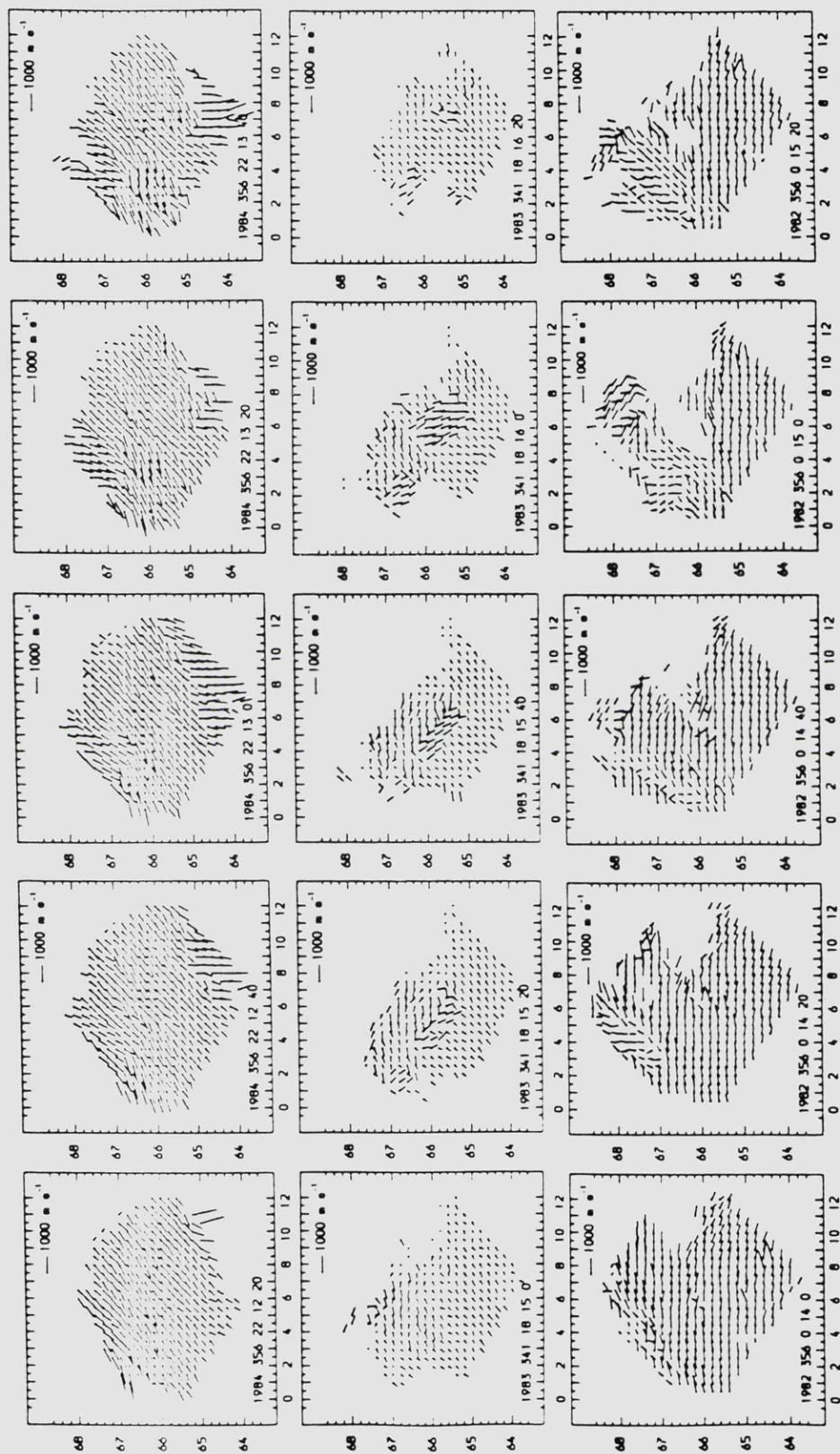


**Figure 5.6**

Three sequences of SABRE spatial velocity plots in which a region of previously uniform flow exhibits a sudden southward (top 22:12:40 U.T. and middle 18:15:20 U.T.) or northward (bottom 0:14:20 U.T.) turning at the time of Pi2 pulsation onset.

observed by the STARE coherent radar system (Opgenoorth et al., 1983). The southward turning of a region of existing vectors may also be a representation of the same phenomenon. Southwood and Hughes (1985) state that the enhancement in earthward flow of plasma at substorm onset should manifest itself as a similar surge in equatorward flow at the poleward edge of the oval. In a similar way, the northward region of flow observed on one occasion may be the signature of the tailward retreat of the new neutral line at the end of a substorm so representing the start of the substorm recovery phase. This feature was observed with the final pulsation in a sequence of four. The Z-component data from the BGS ground magnetometer at Wick suggest that the westward electrojet moves polewards across the SABRE viewing area between the third and fourth pulsations.

An alternative possibility is suggested by the VIKING auroral image data examined by Murphree et al. (1987). These authors observe the westward motion of the connection point of a polar cap arc with the substorm enhanced auroral oval. A similar explanation could apply to the SABRE data in which a new region of southward flow appears poleward of the existing vectors then moves to the west, but only at times of very high magnetic activity.

The fact that the region of southward flow in the SABRE data sometimes does not move may be explained by a similar lack of movement sometimes observed for the WTS (VIKING satellite results, Hultqvist 1987). The occasion on which a region of flow was observed to move eastward may be explained by the lesser known eastward expansion of the substorm current system which is coincident with the westward expansion (Baumjohann and Glassmeier, 1984). This eastward expansion has also been observed in VIKING auroral images (Rostoker et al. 1987b)

concurrent with the westward expansion. The observed expansion was symmetrical about the point of the original intensification. In addition, Shepherd et al. (1987) also observed evening sector auroral intensifications in VIKING auroral data for which only an eastward expansion was present. This occurred at speeds of up to 7.8km/s, the speed being dependent on the position of the onset relative to magnetic midnight. The further from midnight the onset, the more rapid the eastward motion.

On some occasions, the morphology of the flow patterns is very complex particularly if the pulsation occurred around the time of the Harang discontinuity. The viewing area divides into many regions which have different flow directions and magnitudes (three examples in Figure 5.7). This effect becomes even more pronounced as magnetic activity increases. The gaps between the different regions of flow suggest that ionospheric boundaries, perhaps conductivity gradients or the ionospheric location of field-aligned current sheets, may be present at such positions (three examples in Figure 5.8). Although these flow features are normally coincident with the Pi2 pulsations observed, the structure can persist throughout a train of Pi2 pulsations. Thus, they may be related to the complicated substorm current systems suggested by Samson and Rostoker (1983) and Samson (1985).

### 5.2.3 Type (b) spatial patterns

The second type of background flow associated with Pi2 pulsations is a limited area of returns in the SABRE viewing area, although the oscillatory nature of the pulsations in the velocity time series from this small area remain as described previously. The area consisted of a small patch of returns which exhibit greatly varying strengths of flow. In many instances the backscatter present at the time of

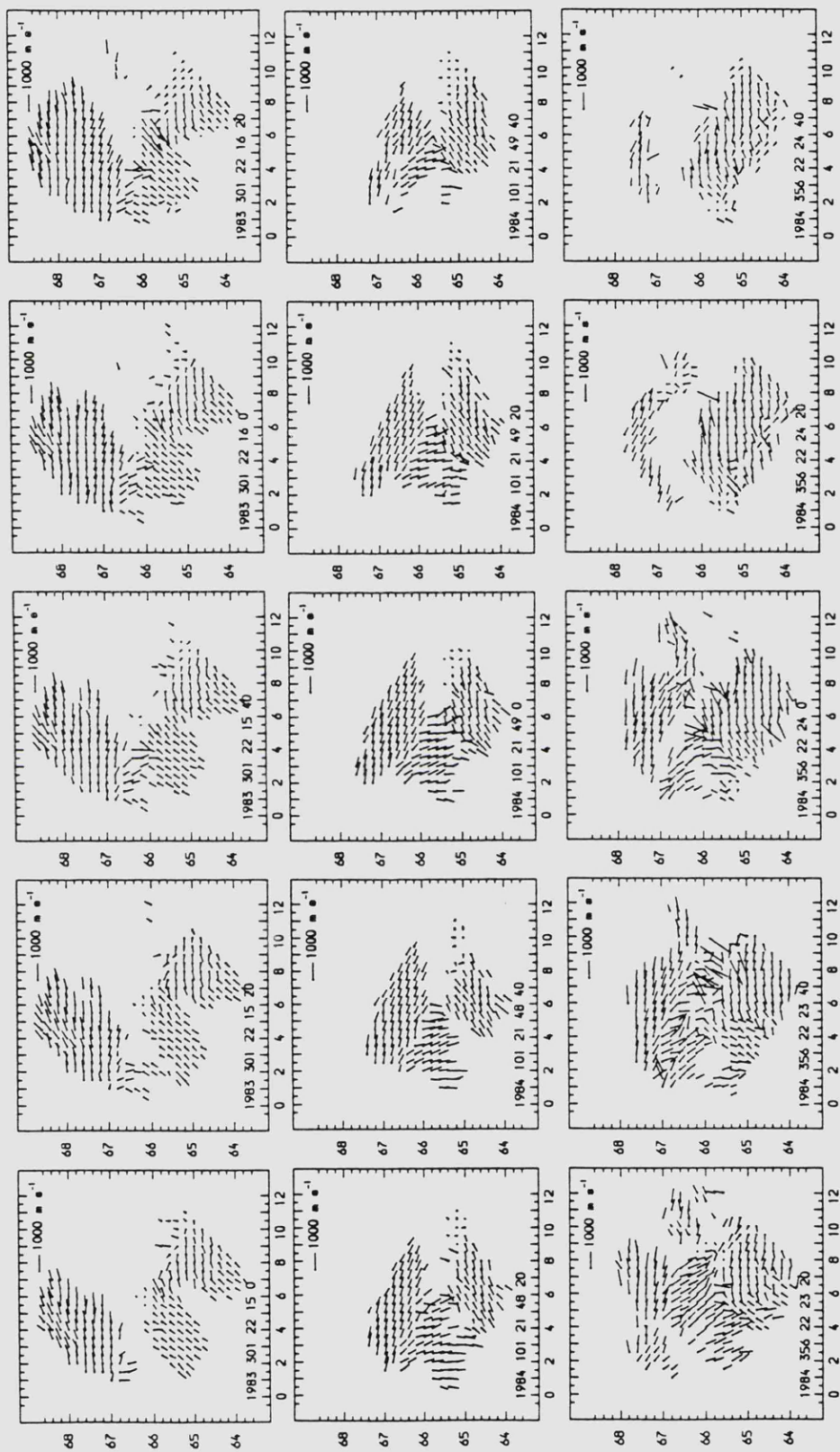


Figure 5.7

Three sequences of SABRE spatial velocity plots in which the flow patterns in the SABRE viewing area become very complicated with regions of differing strength and direction of flow being evident. These examples occur around the time of the Harang discontinuity, the time of the change in background flow direction.

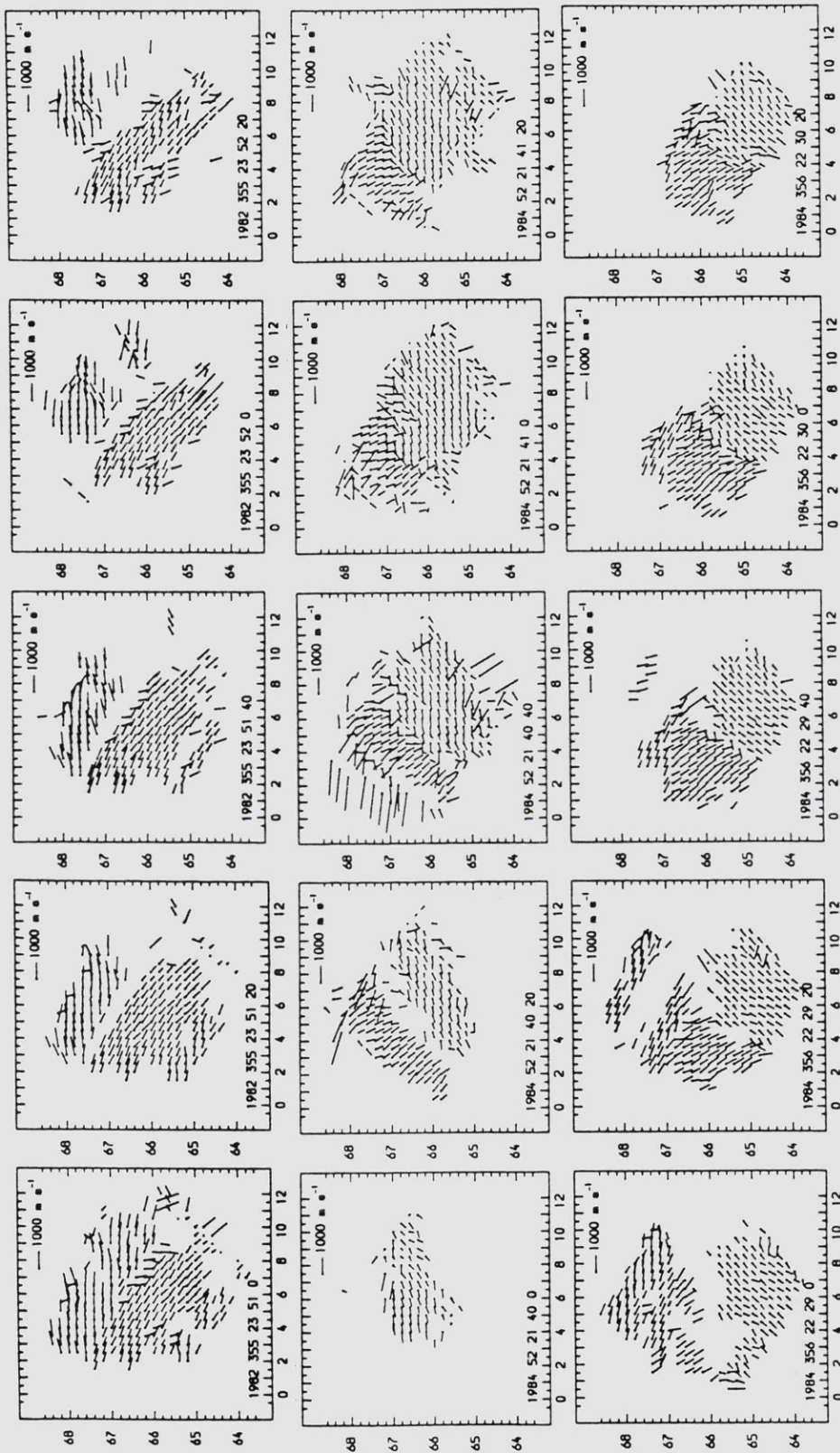


Figure 5.8

Three examples of a sequence of SABRE spatial velocity plots in which shears or gaps in the flow patterns present imply the presence of ionospheric boundaries, perhaps conductivity gradients or the bottom of field-aligned current sheets.

pulsation onset dies-out completely during the interval of the pulsation only to return towards the end of the pulsation. Alternatively, events are observed in which the backscatter dies-out completely before the end of the event. The SABRE viewing area can be positioned anywhere relative to the wedge for such events.

On three occasions, however, a variation on the theme of this small region of backscatter is observed. The small region now consists of a diagonal strip of returns occurring in the westward electrojet regime. The backscatter is coincident with the substorm recovery phase as determined from the H-component of the Tromso normal magnetograms. The SABRE viewing area is outside the substorm current wedge for these events. The three examples are illustrated in Figure 5.9. Also illustrated on the first SABREplot of each sequence are the L=5 and L=5.8 shells derived from the IGRF magnetic field model at an ionospheric height of 120km (C.A. Green, personal communication 1986). The strips of backscatter are roughly field-aligned while the overall flow observed appears to be strongly field-aligned. Another method of investigating the strips is to examine the backscatter intensity obtained by each radar individually. Latitude profiles from a single latitudinal cell and contours of backscatter intensity throughout the viewing area (not shown) demonstrate that the strip is the result of there being far fewer returns observed at Uppsala. There is a cut-off in range apparent below which the Uppsala radar observed no backscatter. This cut-off effect is not observed in the Wick data. In the last of the four SABRE plots of each sequence a line has been constructed at a constant range from the Uppsala radar. As the beams are designed to be roughly perpendicular to the magnetic field, this also implies that the strips are roughly field-aligned.

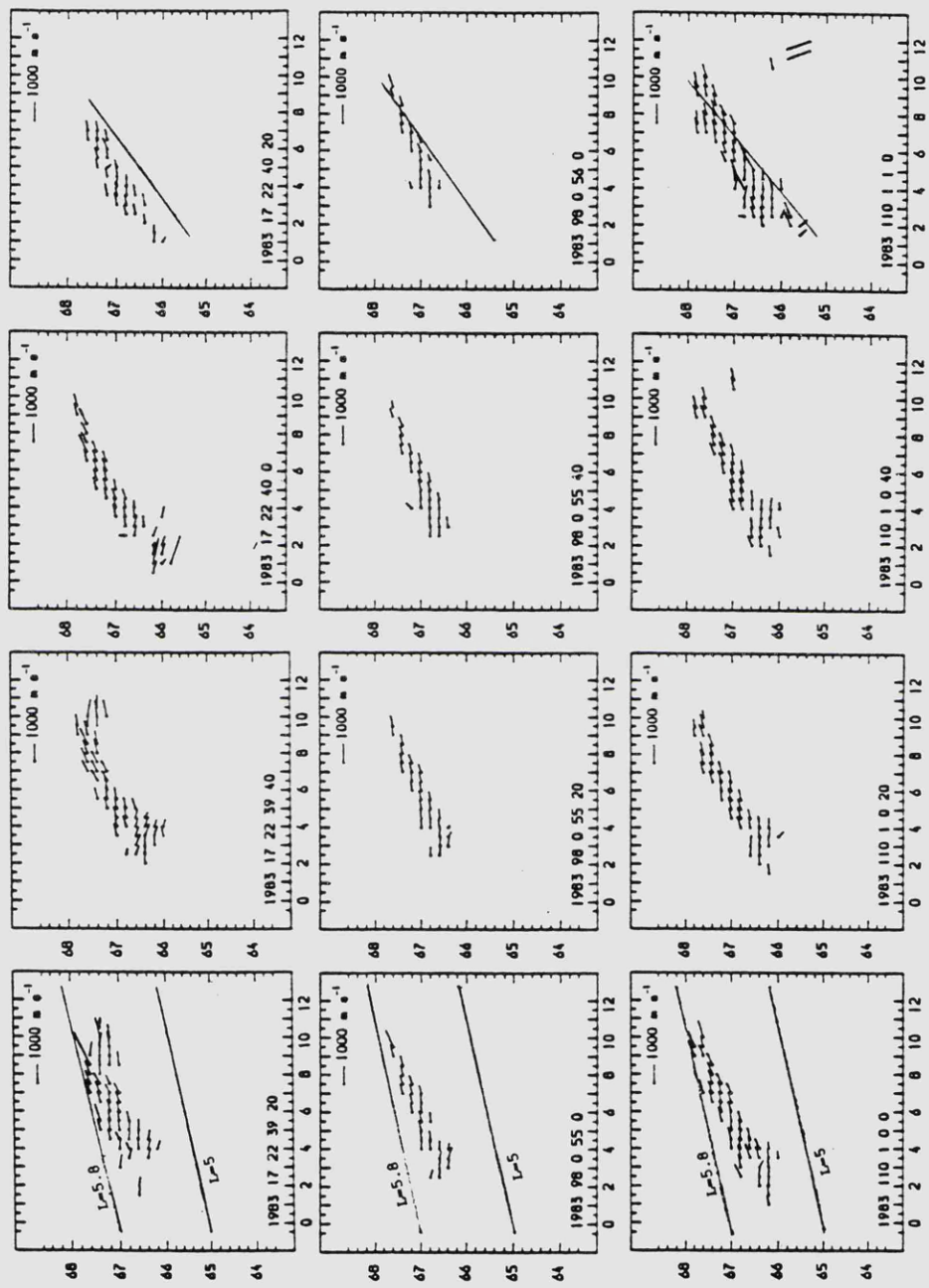


Figure 5.9

The three examples of a sequence of SABRE spatial velocity plots in which only a thin strip of returns is present at the time of the Pi2 pulsation. The  $L=5$  and  $L=5.8$  shells derived from the IGRF magnetic field model for epoch 1984.0 and a height of 120km are also depicted on the first plot of each sequence. A line at constant range from the Uppsala radar has been drawn on the last plot of each sequence. The strip is roughly field-aligned and occurs at a constant range from the Uppsala radar.

The switching on and off of a small patch of irregularities situated below the small permanent region of steady flow (Figure 5.10) was common during times of low magnetic activity. The effect is well illustrated in the RTV type of plot displayed in Figure 5.11. It appears that the ionospheric electric field in this region is changing from above to below the threshold required for the generation of the irregularities. It is possible to relate this situation to a hydromagnetic standing structure between the northern and southern auroral ionospheres in which an Alfvén wave, bouncing between the two, raises the electric field above the threshold value each time it arrives at the northern hemisphere ionosphere.

During times of increased magnetic activity the original small region was often surrounded, to the north-west and south-east, by very strong returns representing very large velocity amplitudes. A whole series of such vectors all pointing in the one direction and aligned along a common L-shell or at a common radar range are present (Figure 5.12). The direction changes rapidly through 180 degrees over one 20s integration time. At other times more than one set of such vectors are present with opposite pointing directions. Initially, the magnitude and common direction of all the vectors, indicated a probable instrumental effect from the Uppsala radar especially since these features are normally observed at positions in the SABRE viewing area corresponding to the nearest and furthest ranges of the Uppsala radar. On examining the SABRE time series data from the region however, the apparent temporal relation to the Pi2 pulsations present in the ground magnetometer data at the time suggested that these are true geophysical features (Figure 5.13). It is possible that these commonly directed vectors may represent the ionospheric signature of sheets of field-aligned current associated with the Pi2 pulsations. This may be

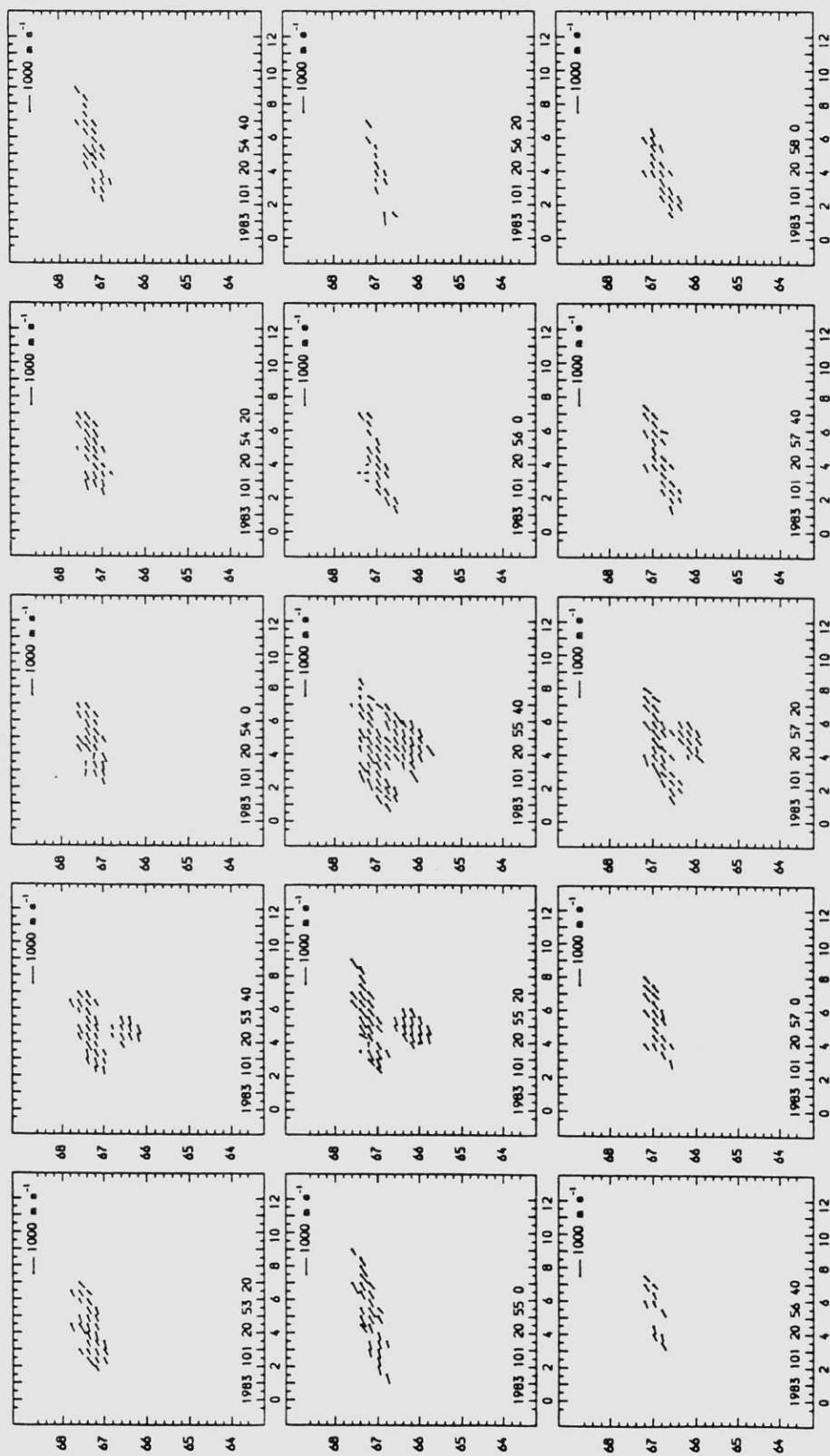


Figure 5.10

A sequence of SABRE spatial velocity plots, often observed at times of low magnetic activity, in which a small region of returns switches on and off below a permanent region of steady flow: i.e. at 20:53:40, 20:55:20 and 20:57:20.

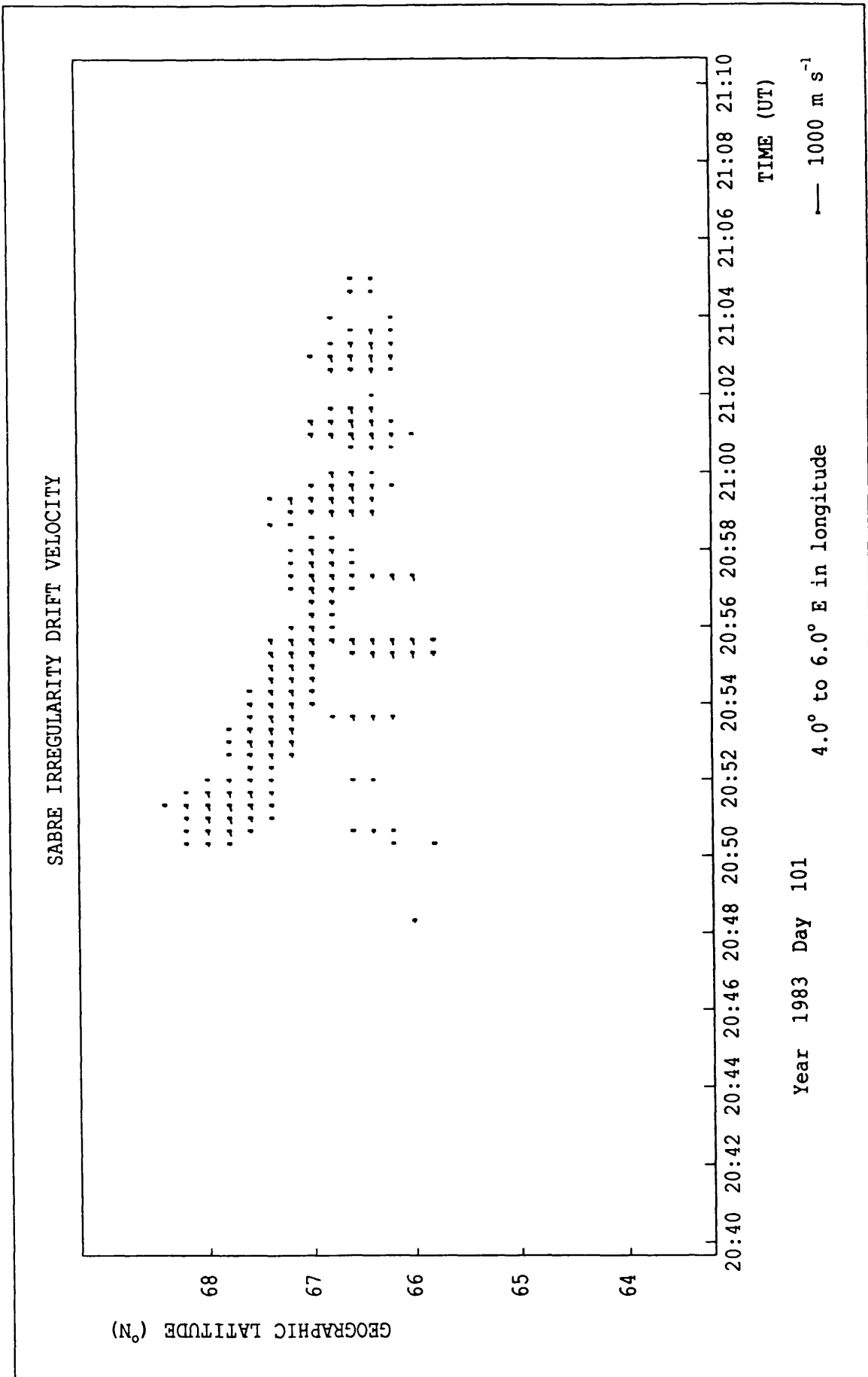


Figure 5.11  
 A SABRE RTV type plot illustrating the on/off switching of a small patch of returns below a permanent region as presented in Figure 5.10.

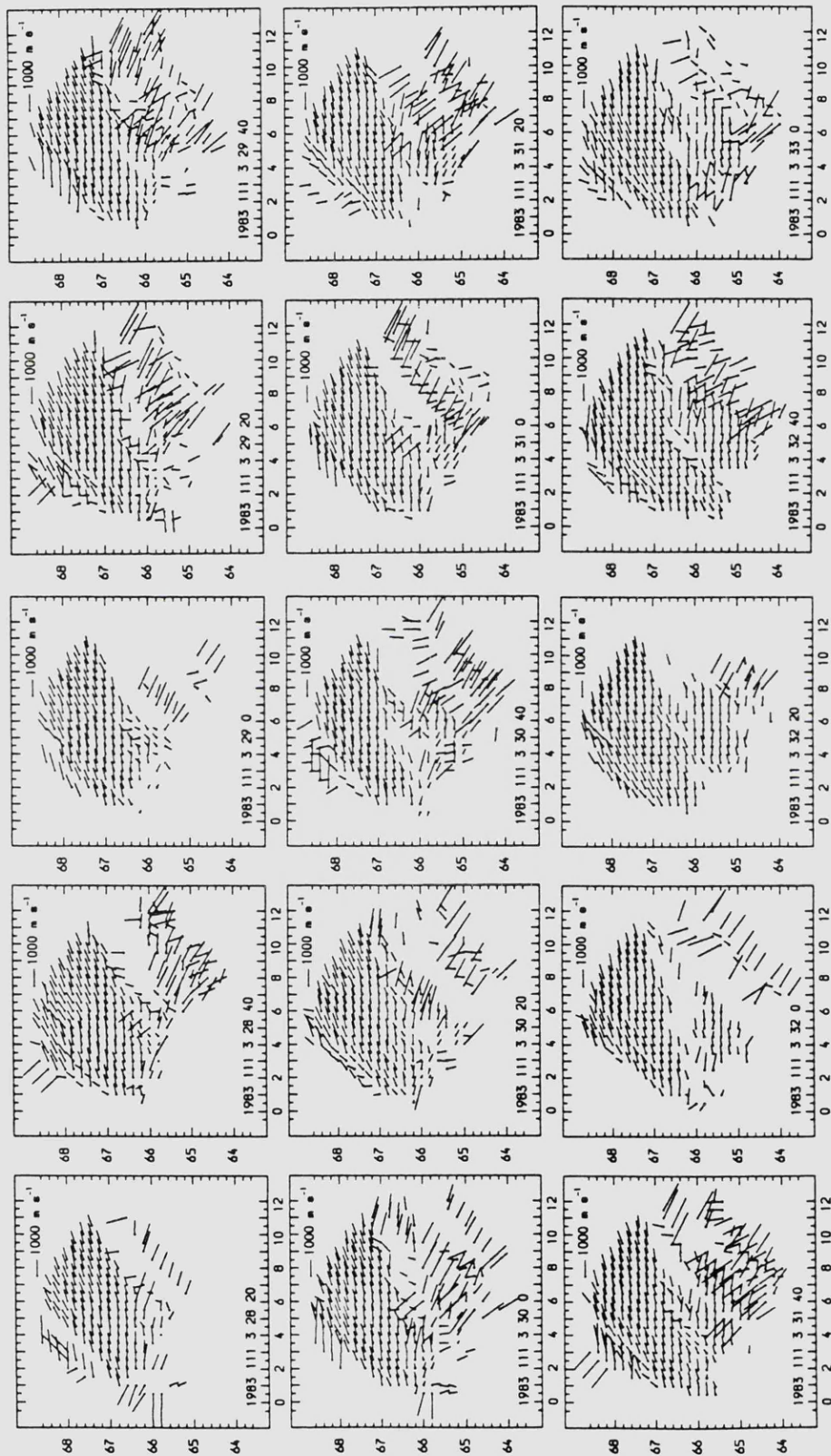
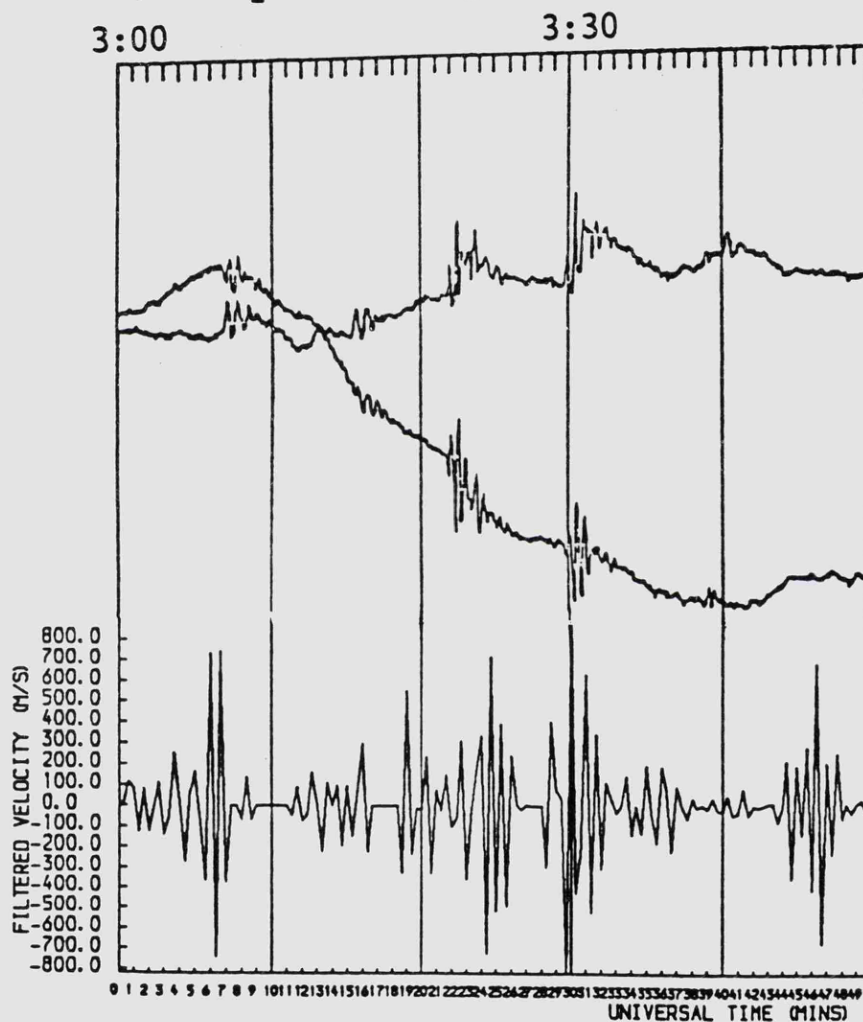


Figure 5.12

A sequence of SABRE spatial velocity plots in which a whole series of vectors appear at a common radar range, exhibit a common pointing direction and are of very large magnitude.

WICK MAGNETOMETER

1983 Day 111 H-component  
1983 Day 111 D-component



65.8 TO 66.0 DEGREES GG NORTH, 7.5 TO 8.0 DEGREES GG EAST.

FILTERED SABRE VELOCITY V. TIME

1983 111 3 0 0 EAST-WEST COMPONENT

Figure 5.13

Unfiltered ground magnetometer data from Wick, the Pi2 pulsations present occur at the same time as the very large and co-aligned vectors presented in Figure 5.12. The SABRE east-west velocity component time series data presented are from a cell in the viewing area containing these vectors.

the signature, in the SABRE data, of the complicated field-aligned and ionospheric currents associated with substorm onset as envisaged by Samson and Rostoker (1983). There is no common time of occurrence or level of magnetic activity for these time intervals. The signal-to-noise ratio initially employed in examining these data may have been too small to remove the noisy vectors. This parameter was however the same as in all cases when no such vectors were observed by SABRE.

### 5.3 Spatial studies of SABRE wave spectral power

#### 5.3.1 Location and localisation of peak wave spectral power in dominant SABRE Pi2 pulsation periods

The location and localisation of wave spectral power in the dominant period for the Pi2 pulsations observed in the SABRE data were investigated in the manner described in Chapter 3. In general the peak wave spectral power in the dominant pulsation period observed by SABRE is localised to a small region in the viewing area, for both velocity components. There is normally more spectral wave power present in the east-west velocity component than in the north-south component.

In about two thirds of the events examined one or two cells in the viewing area exhibit a dominance over the rest in containing most of the wave spectral power associated with the dominant Pi2 pulsation period (Figure 5.14), although on occasion, a group of four or five cells has equal power distributions (Figure 5.15). These cells are often arranged in a circular configuration and, on five occasions, are associated spatially with the vortex-like flows described above. There are however ten cases of vortex-like flows which do not have the circular grouping of cells associated with them. There is no correlation between the value of the dominant period obtained, the

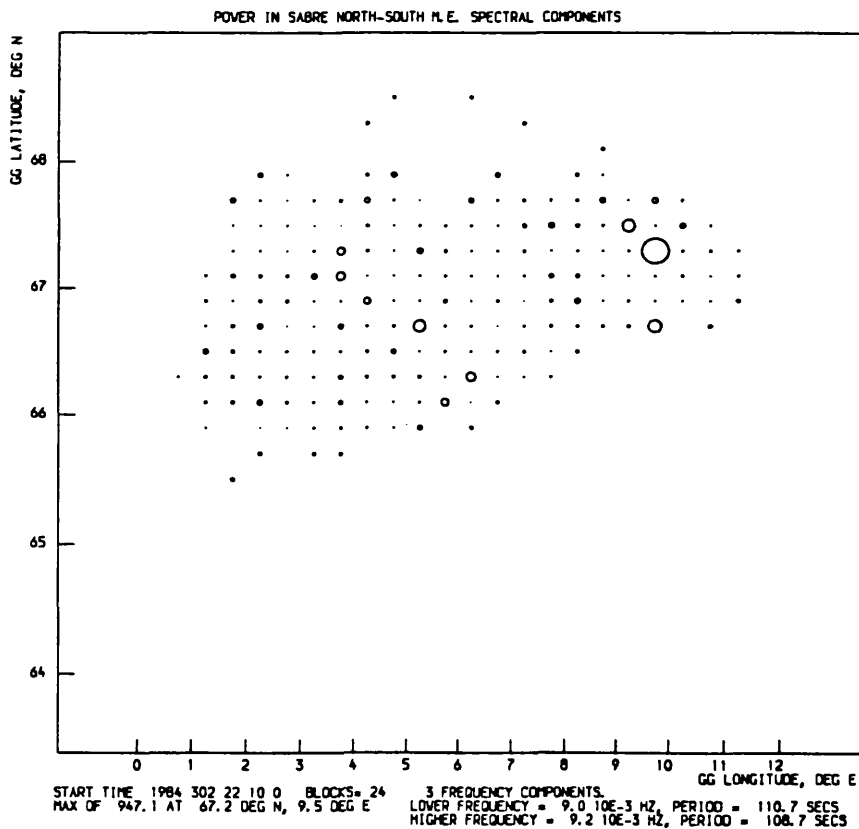
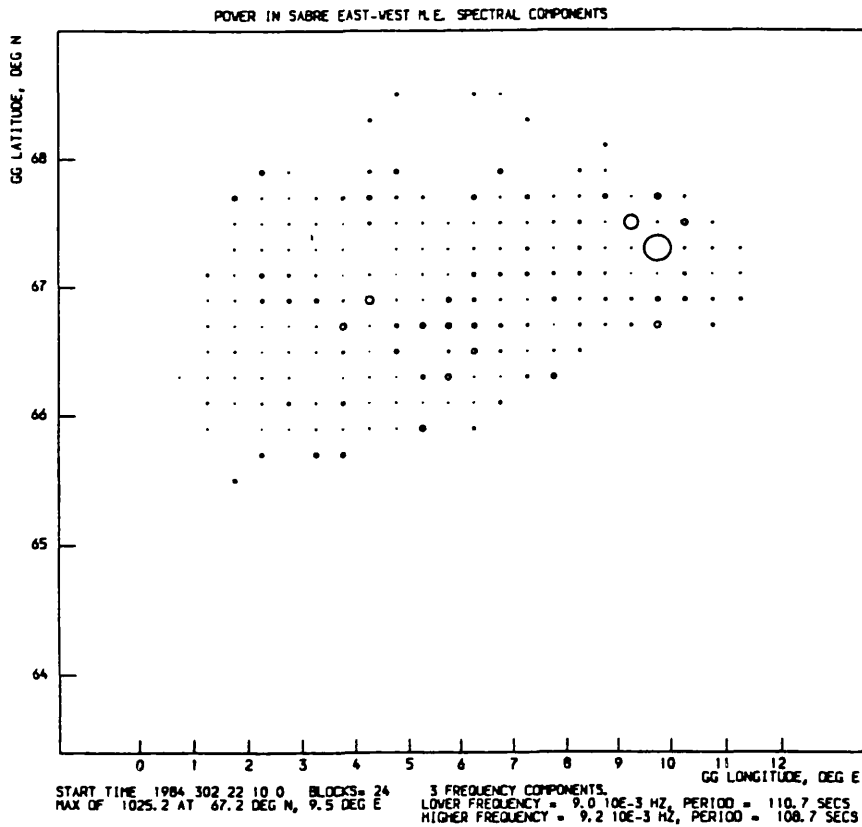


**Figure 5.14**

The typical latitudinal and longitudinal variation across the SABRE viewing area of the wave spectral power at the dominant Pi2 pulsation period in which one or two cells in the viewing area exhibit a dominance over the rest. East-west velocity component data are presented above north-south velocity component data.

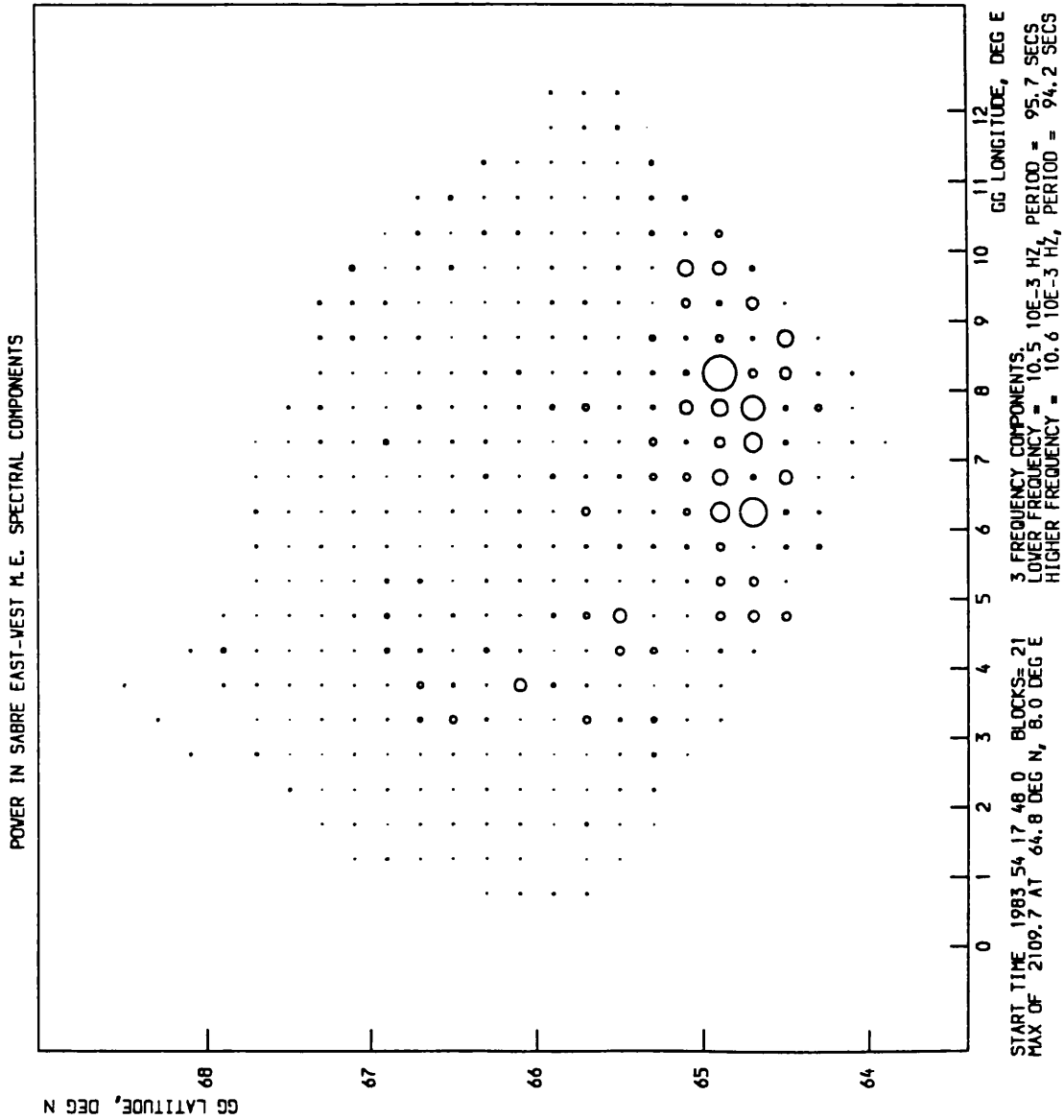


Figure 5.15

The latitudinal and longitudinal variation across the SABRE viewing area of the wave spectral power at the dominant Pi2 pulsation period in which a circular grouping of four or five cells contain most of the wave spectral power. This area is often coincident with a vortex in the flow pattern described previously.

position in the viewing area of the cell exhibiting peak spectral wave power and the level of geomagnetic activity (see the previous discussion on SABRE Pi2 pulsation periods).

Only at times of low magnetic activity when the switching on-off electric fields are observed is there any real deviation from this situation. A broad band of strong power returns in many cells is then observed (Figure 5.16). This indicates that a different generation mechanism is in operation or that the viewing area is now situated at a different location relative to the generation region of the Pi2 pulsations. The low magnetic activity suggests that the auroral zone has retreated poleward and, therefore, the SABRE viewing area is positioned equatorward of the complex current systems associated with substorm onset.

### 5.3.2 Change in position of the cell exhibiting peak wave spectral power over a series of Pi2 pulsations

The change, over a series of Pi2 pulsations, in the position of the SABRE cell containing the maximum wave spectral power in the dominant period of the Pi2 pulsation was then investigated. The variation in the east-west and north-south spectral components was examined and was restricted to examining the longitudinal changes as the latitudinal changes were found to be small in all events examined. Only the changes involved between the first two pulsations in a train were considered initially to avoid any possible changes in later events due to variations in the background current systems.

The results obtained from spectra derived from the two velocity components are similar in the direction of movement if not in the magnitude of the change. The position of the cell exhibiting peak wave

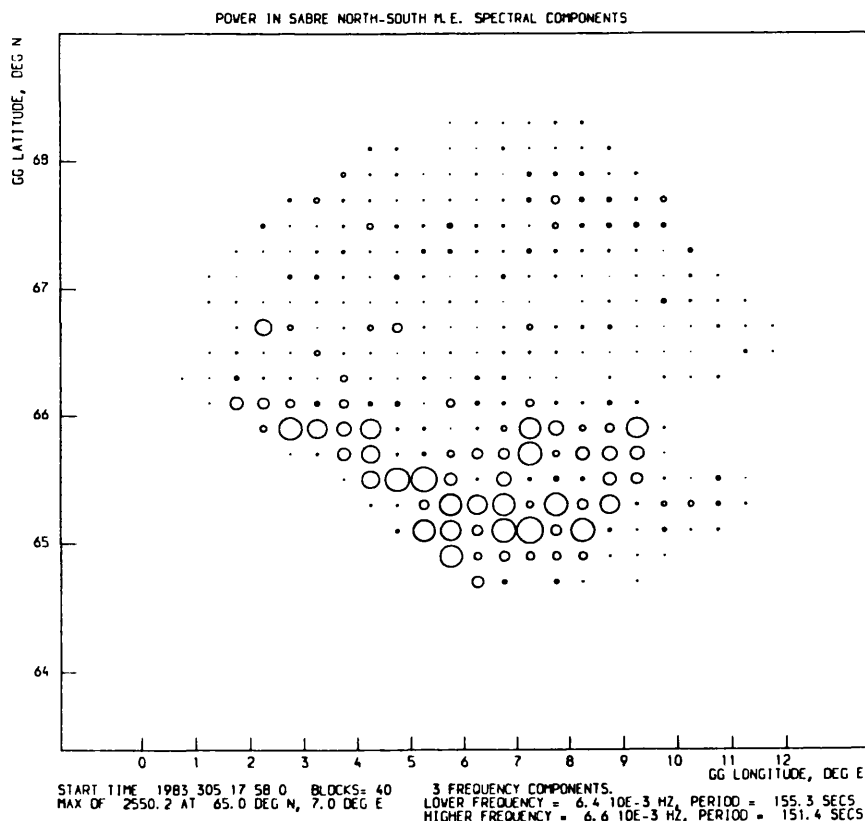
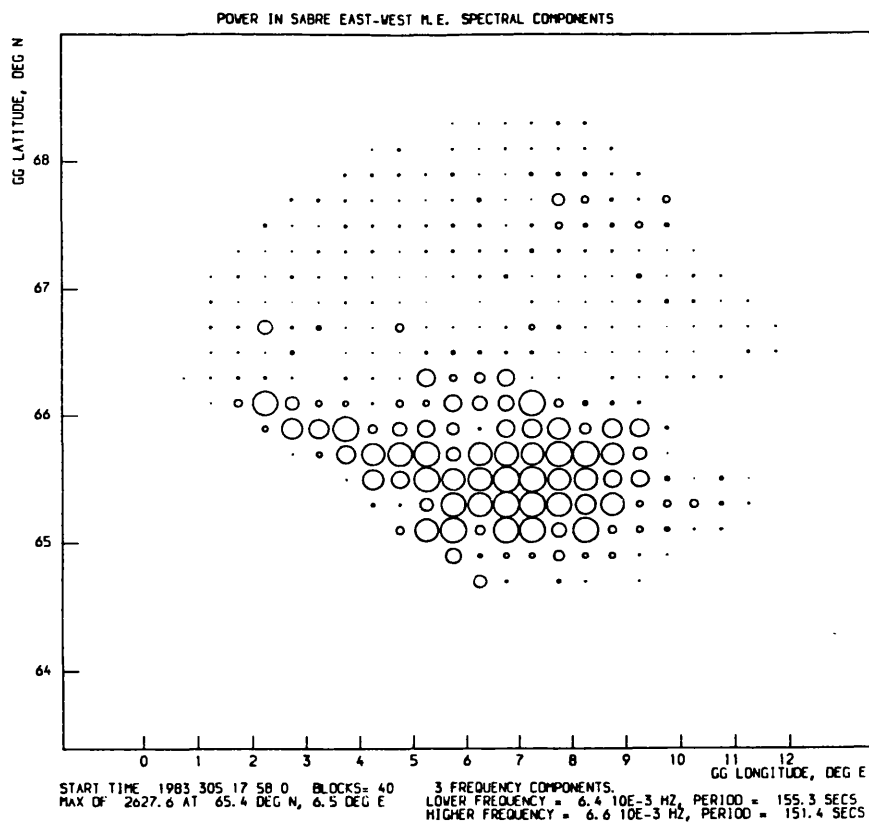


**Figure 5.16**

The latitudinal and longitudinal variation across the SABRE viewing area of the wave spectral power at the dominant Pi2 pulsation period for an event occurring during an interval of low magnetic activity. In this case a broad band of strong power is observed encompassing many cells in the viewing area.

spectral power is equally likely to move west or east. This is not dependent on magnetic activity or background flow direction. It is dependent on the position of the SABRE viewing area relative to the substorm current wedge (see later). There is no dependence of the physical extent of the change in position of the cell on magnetic activity (Figure 5.17) nor on the time interval between the onsets of the two Pi2 pulsations involved (Figure 5.18).

Only 5 of 22 intervals of Pi2 pulsation activity give inconsistent results for the change in position of the SABRE viewing area relative to the substorm current wedge (as derived from the bay perturbations in magnetic records) and the direction of the longitudinal change in the position of the cell exhibiting the peak wave spectral power in the SABRE Pi2 pulsation data. If the substorm current wedge apparently moves westward over the viewing area for example, the position of the cell exhibiting peak spectral power in the SABRE viewing area also moves to the west. The lack of consistent polarisation azimuths over the two pulsations often makes it difficult to assign a quantifiable relationship between the two. It is therefore usually only possible to state qualitatively (utilising the H and D ground magnetic bay perturbations) that the SABRE viewing area has remained in a similar position relative to the wedge, inside the wedge to the west of centre for example, or that it has moved across the centre or either of the edges of the wedge during the course of the two Pi2 pulsations.

The results that were obtained from 15 of the 22 intervals are presented in Figure 5.19 where the above mentioned relationship is apparent, especially when the wedge has moved to the west, although there is a large scatter present in the data. There are however a number of events for which the relationship does not hold (top left

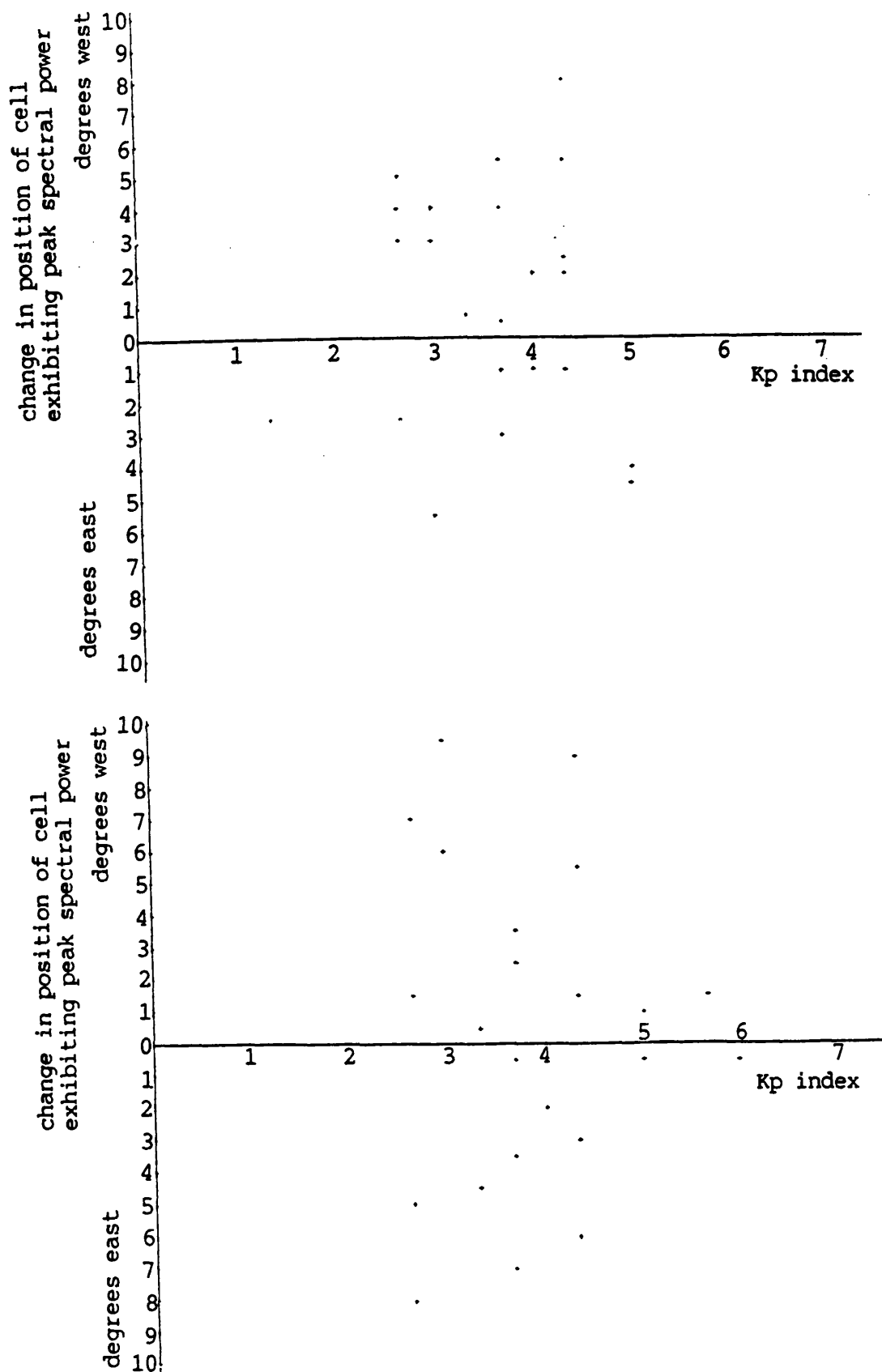


Figure 5.17

The relationship between the magnitude and direction of the change in position of the cell in the SABRE viewing area exhibiting peak wave spectral power at the dominant Pi2 pulsation period and magnetic activity. East-west velocity component data are presented above north-south velocity component data. The analysis was restricted to the change over the first two Pi2 pulsations in a train.

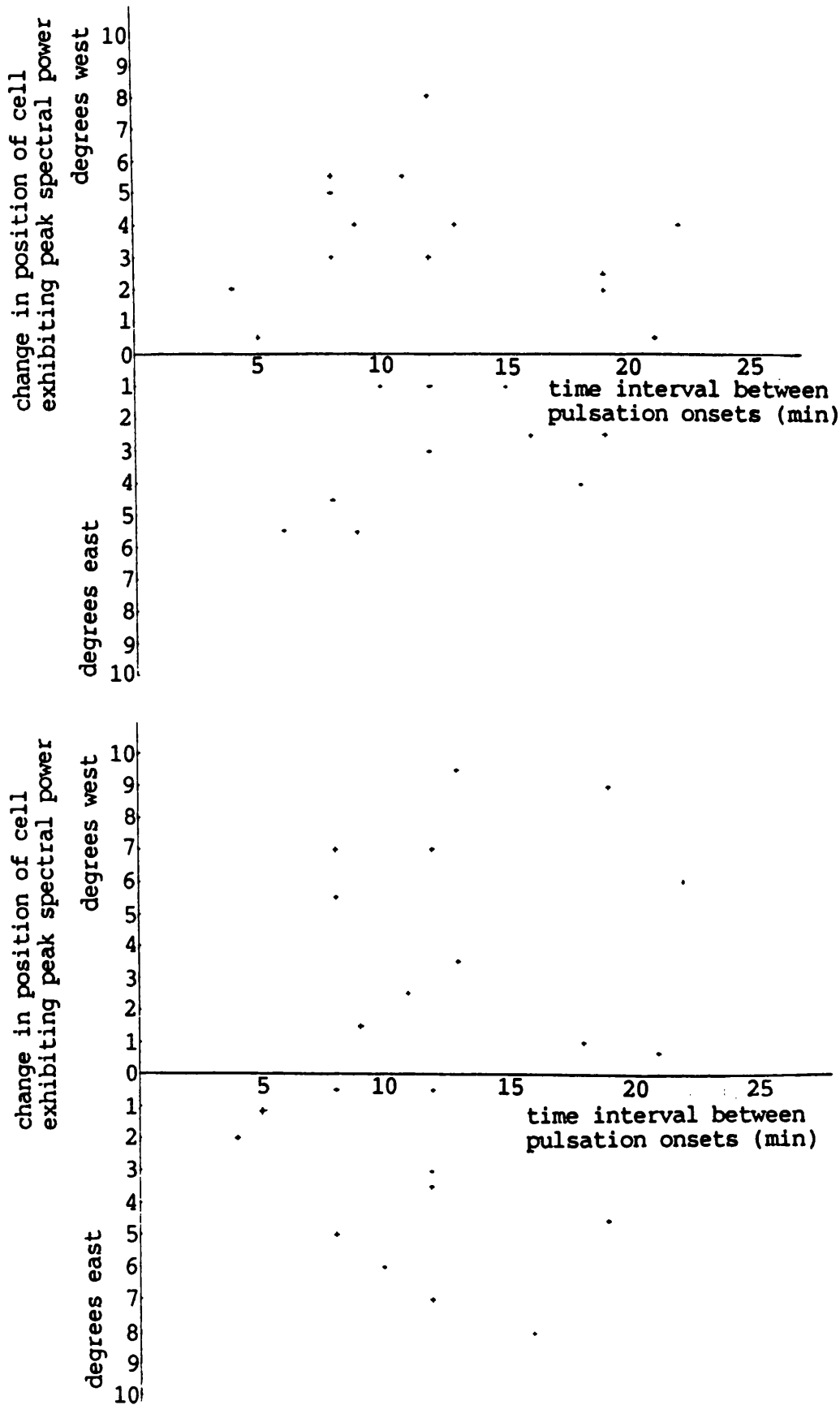


Figure 5.18

The relationship between the magnitude and direction of the change in position of the cell in the SABRE viewing area exhibiting peak wave spectral power at the dominant Pi2 pulsation period and the time interval between the onsets of the two Pi2 pulsations. East-west velocity component data are presented above north-south velocity component data.

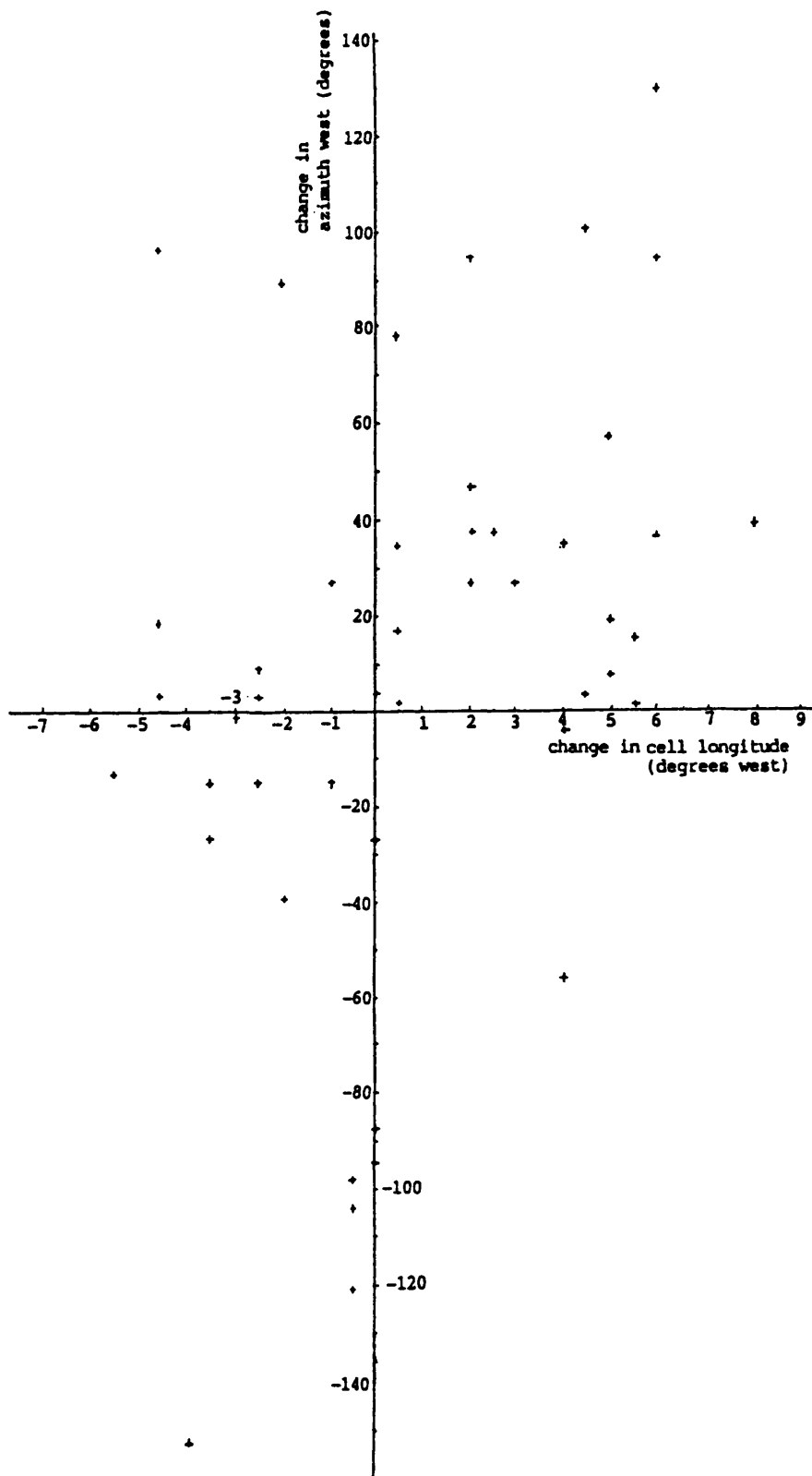


Figure 5.19

The relationship between the change in position of the SABRE viewing area as determined from ground magnetic Pi2 pulsation polarisation azimuths and the westward movement across the viewing area of the position of the cell exhibiting peak wave spectral power at the dominant Pi2 pulsation period.

and bottom right quadrants). There are also a significant number of events for which the change in cell longitude is less than one degree implying that the wedge does not always move. No allowance has been made for the time interval between successive pulsations or for the level of magnetic activity at the time. These factors were found previously to have no effect on the magnitude of the change in position of the cell. Polarisation azimuth changes derived from magnetic records from all three magnetometer stations have been included in this one plot to increase the number of data points available.

In a study of the longitudinal evolution of eleven multiple onset substorms Gelpi et al. (1985a) determined that the centre of the substorm current wedge, as determined from the azimuth pattern of the Pi2 polarization ellipse, moved west on five events, east on two events and remained at roughly the same longitude on four events.

It is also interesting to relate the SABRE derived results to those of Rostoker et al. (1987b) who examined VIKING auroral image data at the time of evening sector intensifications. They observed an expansion both to the west and to the east of the region of substorm onset, the expansion being symmetrical about the point of the initial intensification. It was stated that the sense of movement of the intensification on the ground, would depend on the observer's position relative to the initial intensification. If it were to the west the expansion would appear westward and similarly if it were to the east the expansion would appear eastward. The same should also be true for the SABRE observations, and this is indeed what is observed. It was also observed that the change in position of the intensification to the west was episodic in nature, similar to the longitudinal change in

position of the SABRE cell exhibiting peak wave spectral power.

Although this study centred on the changes involved over the first two pulsations in a train, in subsequent pulsations the position of the cell exhibiting peak wave spectral power oscillated longitudinally in over half the events while it kept a consistent direction or had the two regimes mixed in the remaining events. These observations should be treated carefully as the presence of pre-existing current systems may influence the results for later pulsations. In the study of Gelpi et al. (1985a), the individual pulsations from the eleven multiple onsets were examined and similar results obtained. There was no set direction for the movement of the substorm current wedge centre with the following pulsation of a train. The centre moved westward eight times, eastward six times and remained at the same longitude eight times. In addition, the wedge centre could move westward then eastward or vice-versa in subsequent pulsations from the same train. This is of interest in view of the oscillating and westward moving current system envisaged by Samson (1985) for the generation and subsequent development of Pi2 pulsations.

The final study in this section was an examination of the background flow patterns in the SABRE viewing area in relation to the change in position of the cell exhibiting peak wave spectral power over a series of Pi2 pulsations. Of the 22 intervals investigated only one involves the longitudinal movement westward of a region of southward flow at the time of the pair of pulsations. Even then, the peak power cells are located equatorward of the region of southward flow, in the region of background westward flow that is present throughout the pulsations. The majority of events (9) occur at times when the viewing area is full of backscatter and the pulsations are only represented by changes

in the magnitude and/or direction of the velocity. Almost equally probable (8 intervals) is that the flows in the viewing area are highly structured with the presence of vortices or shears in the flow. These features are not directly related to the cells exhibiting the peak wave spectral power derived from the pulsation time series. The remaining four intervals occur at times when only small patches are present in the viewing area and they tend to die-out towards the end of the pulsations involved. There is no particular position for the SABRE viewing area relative to the substorm current wedge for any of these categories.

#### 5.4 Summary

The spatial features observed in the SABRE flow patterns associated with the Pi2 pulsations generally depict a north-south perturbation in the direction of the changing amplitude background east-west directed flow, although vortex-like structures are often observed at the lower edge of the backscatter returns present. Oppositely rotating vortical flows were observed during two intervals containing six pulsations and although the sense of rotation remained the same for each vortex during the series of pulsations, it was observed that these flows appeared coincidentally with the onset of the particular pulsation involved. The onset of regions of southward directed flow often correspond to the start of the Pi2 pulsations and these regions also frequently move longitudinally through the SABRE viewing area as the pulsation progresses. As magnetic activity increases and the auroral zone system of field-aligned and ionospheric currents move equatorward towards the SABRE viewing area, so the spatial flow patterns observed become more complicated with many regions of different strength and direction of flow being present. The gaps between these regions and the shears in flow observed seem to be the signature of conductivity

structure in the ionosphere or of the presence of the field-aligned currents mentioned above. In the opposite extreme, at times of lowest magnetic activity, a switching on and off of a small region of backscatter is frequently observed coincident with the pulsation in the magnetic records. The SABRE viewing area is then thought to be located equatorward of the auroral zone, the patch of backscatter possibly appearing and disappearing with the electric field of a standing Alfvén wave as it arrives at the northern hemisphere.

The wave spectral power in the SABRE Pi2 pulsation is quite localised, the maximum power for the dominant period is normally observed in only a few cells in the viewing area. There is no correlation between this dominant period and the position in the viewing area at which the maximum power is observed. The position of the cell exhibiting peak wave spectral power changes in a way consistent with the change in position of the SABRE viewing area relative to the substorm current wedge. If the wedge moves westward over the viewing area, the position of the cell moves west with the second pulsation in a train and similarly moves east if the substorm current wedge moves to the east. With subsequent pulsations in a series the position of this cell either oscillates longitudinally, continues in the one direction or has a mixture of the two. There is no consistent magnitude or rate of change involved in these changes, a result similar to that obtained earlier when examining the position of the SABRE viewing area relative to the substorm current wedge.

It is thought possible to relate not only the westward movement of the region of southward flow in the SABRE data with the observed westward motion of the WTS, but also the change in position of the cell exhibiting peak wave spectral power in the SABRE viewing area with the

westward and eastward expansion and movement of the region of auroral intensification at substorm onset. This latter signature is dependent on the initial position of the SABRE viewing area, to the west or east of the centre of the substorm current wedge, at the time of the first of the pair of pulsations.

Having presented the general characteristics of the Pi2 pulsations observed by SABRE, the following chapter will concentrate on specific events in greater detail to investigate some of these features more closely.

## CHAPTER 6

### CASE STUDIES

#### 6.1 Introduction

In this chapter, four of the 49 intervals during which SABRE observed Pi2 pulsations are studied in greater detail. The examples were chosen to highlight a particular feature of the SABRE observations which could be related to theory or previous observations of Pi2 pulsations. In addition, the events chosen occur at different levels of magnetic activity, at different local times and at different positions relative to the substorm current wedge and the Pi2 pulsation generation region.

#### 6.2 Case study 1 : eastward electrojet Pi2 pulsations

##### 6.2.1 SABRE and magnetometer pulsation signatures

The interval of interest on day 54, 1983 consists of two Pi2 pulsations, from 17:38 U.T. to 17:42 U.T. and from 17:48 U.T. to 17:55 U.T.. Although no data are available from the BGS auroral zone station at Tromso for this time, a standard magnetogram from this location exhibits the classical evening-sector sharp negative perturbation in the north-south (H) component at the time of substorm onset. In the EISCAT magnetometer cross data, the H-component perturbation changes from being slightly positive or zero at all stations for the first pulsation to being negative at all stations for the second. These data imply that the EISCAT cross was initially in the eastward electrojet

or near the Harang discontinuity during the first pulsation but that the substorm onset region has moved across the stations by the time of the second. The cross is now in the westward electrojet. A change from positive to negative D-component perturbations between the two pulsations indicates the movement of a field-aligned current across the longitude of the cross. In contrast, the H-component perturbations at Nordli and Faroes are positive for both pulsations, placing these stations, and therefore the SABRE viewing area, in the eastward electrojet at the time of the two pulsations. The predominantly westward flow observed by SABRE throughout this interval (see below) is consistent with this interpretation of the magnetometer data. The D-component perturbations at Faroes and Nordli are positive for the first pulsation but slightly negative at Nordli for the second. This suggests that the field-aligned current associated with the onset region is starting to have an effect at Nordli. This apparent westward motion of the substorm region is discussed further later in the investigation.

Figure 6.1a(6.1b) illustrates the unfiltered magnetometer H(D) components from three BGS stations with the corresponding east-west (north-south) SABRE drift velocity component presented below. The SABRE data were obtained by averaging data over a small region in the viewing area (64.6-64.8 degrees north, 6-8 degrees east).

A comparison of the waveforms in Figures 6.1a and 6.1b indicates that the east-west velocity component (north-south electric field) is the stronger with the second Pi2 pulsation superimposed on a bay-like, background structure. The north-south velocity oscillates around a constant value of southerly velocity. The 'bay' in the SABRE east-west component commences with the start of the first pulsation then returns

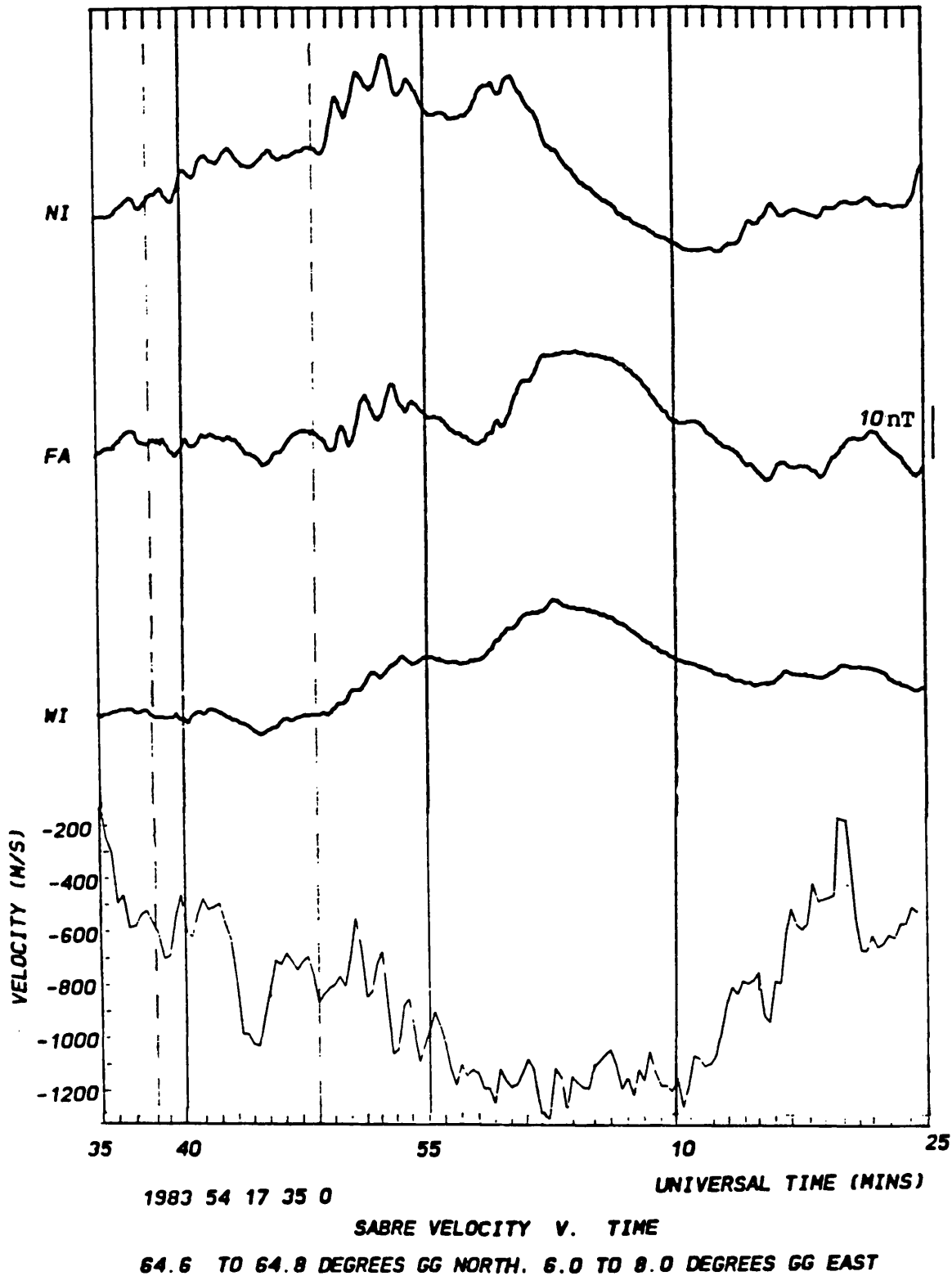
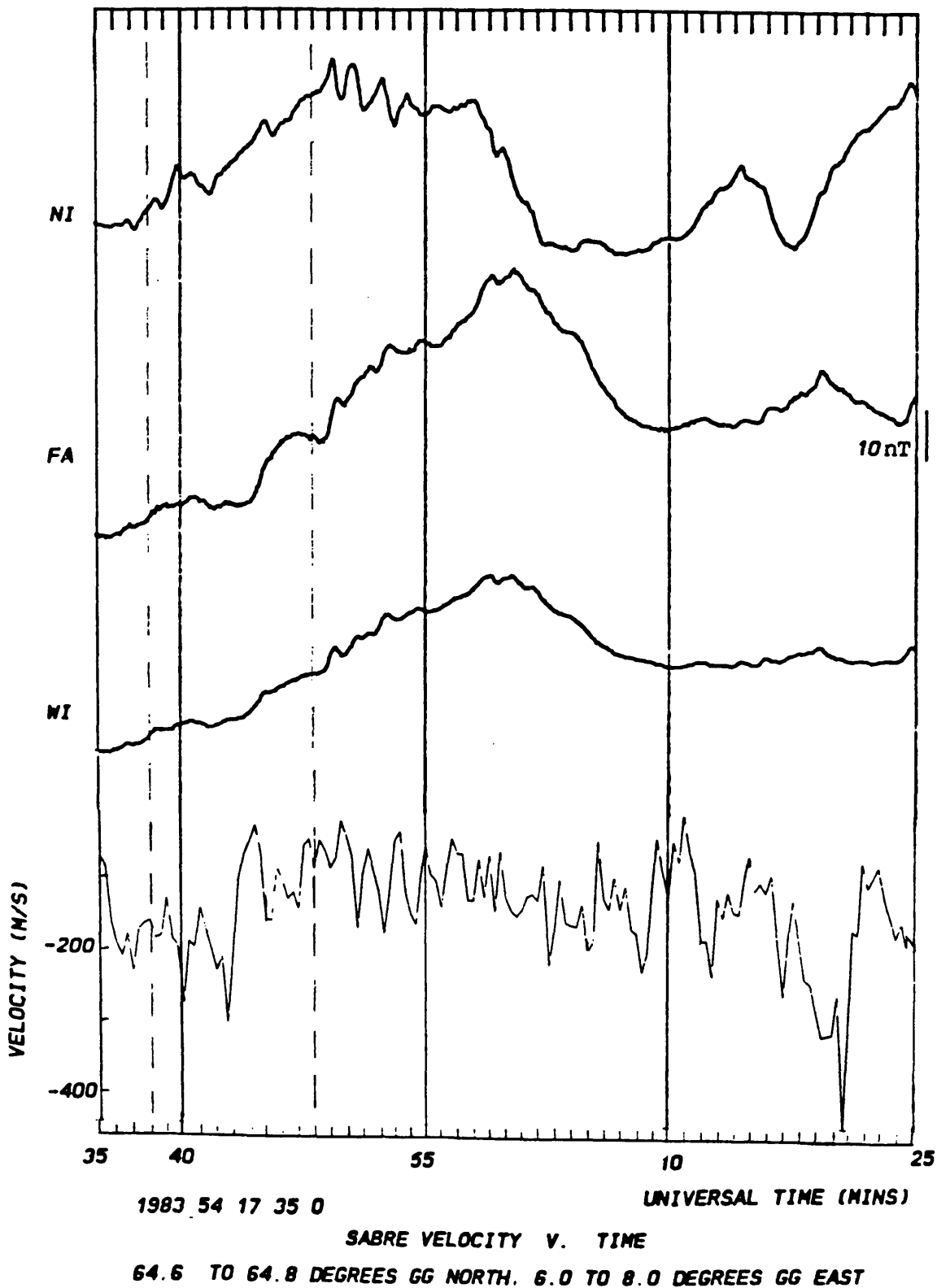


Figure 6.1a  
 Unfiltered ground magnetometer H-component data from Nordli, Faroes and Wick compared with SABRE east-west velocity component data averaged over a small region of the viewing area. Dotted lines delineate the onset times of the two Pi2 pulsations at 17:38 U.T. and 17:49 U.T.



**Figure 6.1b**  
 The same time series data as Figure 6.1a but for the ground magnetometer D-compared compared with SABRE north-south velocity component data.

to pre-event levels some time after the second. This is equivalent to an enhancement of the southward component of the ionospheric electric field at the onset of the first event followed by a decrease of this component after the second Pi2 pulsation. Latitudinal and longitudinal profiles of the time series data indicate no relative time delay in the onset time of either Pi2 pulsation across the viewing area.

### 6.2.2 Spectral Analysis

Results obtained from the FFT and ME spectral analysis of the two pulsations under investigation are presented in Table 6.1.

Table 6.1

Pi2 Pulsation: 17:38 - 17:42 U.T.

<u>Magnetometer</u>	<u>Period (s)</u>			
		<u>FFT</u>		<u>ME</u>
	H	D	H	D
Faroer (FA)	90.9	no peak	111.1	no peak
Nordli (NI)	90.9	125.0	111.1	111.1
Wick (WI)	no peak	no peak	no peak	no peak
SABRE	no spectrum			107.5

Pi2 Pulsation: 17:48 - 17:55 U.T.

<u>Magnetometer</u>	<u>Period (s)</u>			
		<u>FFT</u>		<u>ME</u>
	H	D	H	D
Faroer (FA)	no peak	90.9	90.9	90.9
Nordli (NI)	90.9	90.9	90.9	100.0
Wick (WI)	no peak	125.0	100.0	100.0
SABRE	no spectrum			95.2

The dominant periods determined from the analysis (Section 3.3.2) concurred well between the dominant SABRE east-west velocity component and the magnetometer records although in some cases there were no peaks observed. An FFT spectral analysis of the SABRE data was attempted, however, the 20s resolution of the SABRE data resulted in

there being too few spectral estimates (7 and 13 respectively for the two events) to produce a well-resolved spectrum for such short lived pulsations.

The ME spectral peaks in the SABRE data and the variation of the wave spectral power over the entire SABRE viewing area were examined in the manner described in Section 3.3.2. The latitudinal and longitudinal variation of the wave spectral power in the dominant pulsation period of the first pulsation is presented in Figure 6.2a for the two separate velocity components. The wave power is strongly localised in what appears to be an elliptical region in the lower half of the viewing area for the east-west component, while the north-south component is of lesser strength and exhibits a double structure in the power.

During the second Pi2 pulsation, the area of peak power in the east-west component has expanded and moved westward (Figure 6.2b). In the north-south component there are now two main areas of power, both of which are equatorward and to the west of that in the first. Although the dominant period under investigation decreases, from 107.5s to 95.2s over the two events, this was found in the previous chapter to have no effect on the position of the cell in the SABRE viewing area which exhibits peak wave spectral power.

### 6.2.3 Spatial velocity studies

The spatial structure in the SABRE irregularity drift velocity data throughout the sequence of Pi2 pulsations is now presented. The background ionospheric flow during the interval is mostly uniform and westward (Figure 6.3) as is expected for the background eastward electrojet at this time. This was the case throughout the first

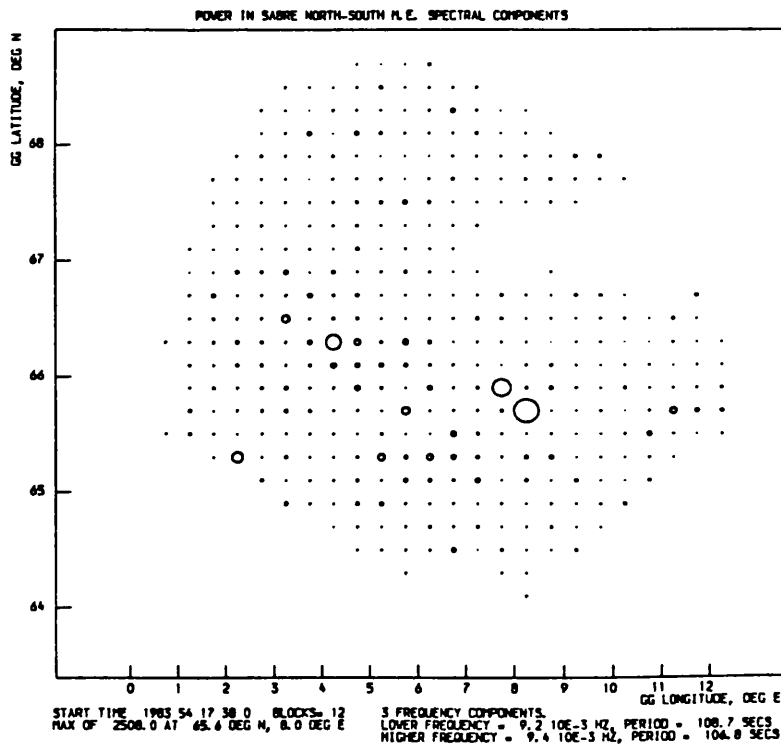
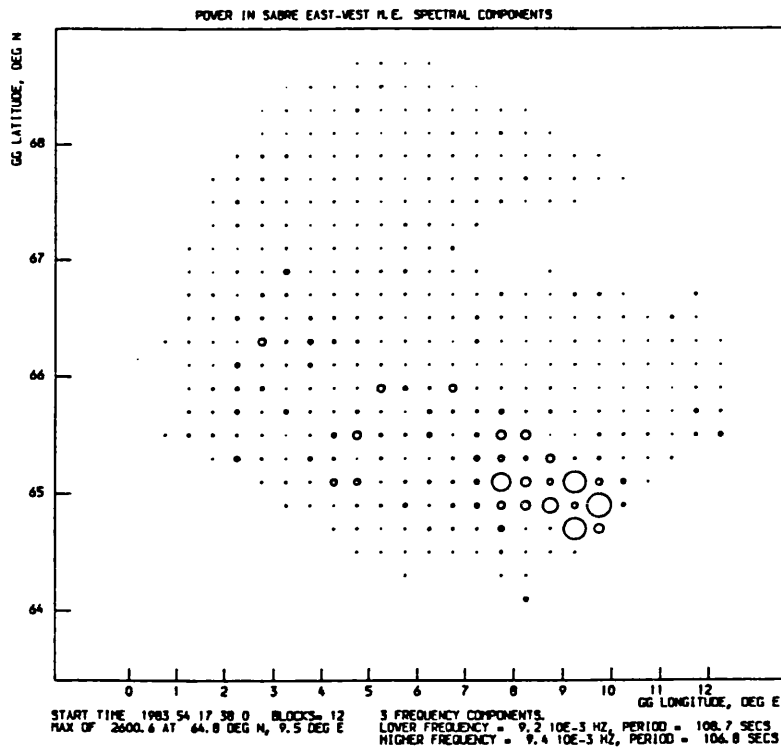


Figure 6.2a

The latitudinal and longitudinal variation across the SABRE viewing area of the wave spectral power at the dominant Pi2 pulsation period for the pulsation starting at 17:38 U.T.. East-west velocity component data are presented above the north-south velocity component data.

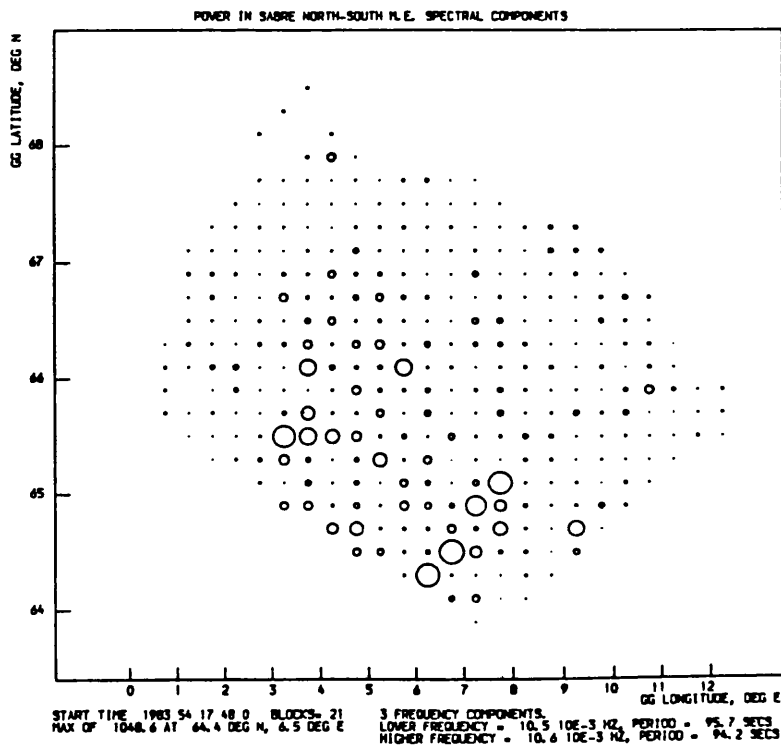
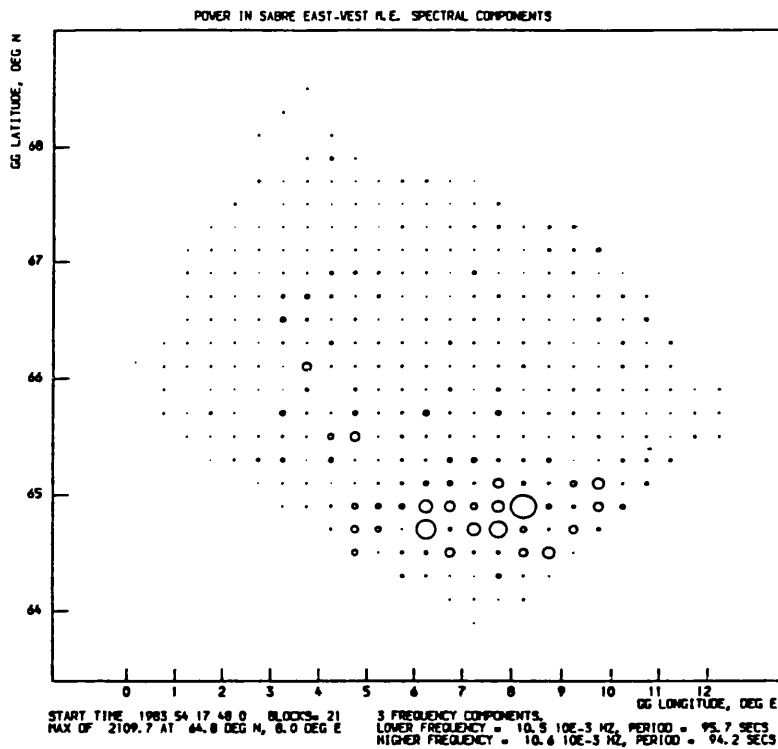


Figure 6.2b

The latitudinal and longitudinal variation across the SABRE viewing area of the wave spectral power at the (different) dominant Pi2 pulsation period for the pulsation starting at 17:49 U.T.. East-west velocity component data are presented above the north-south velocity component data.

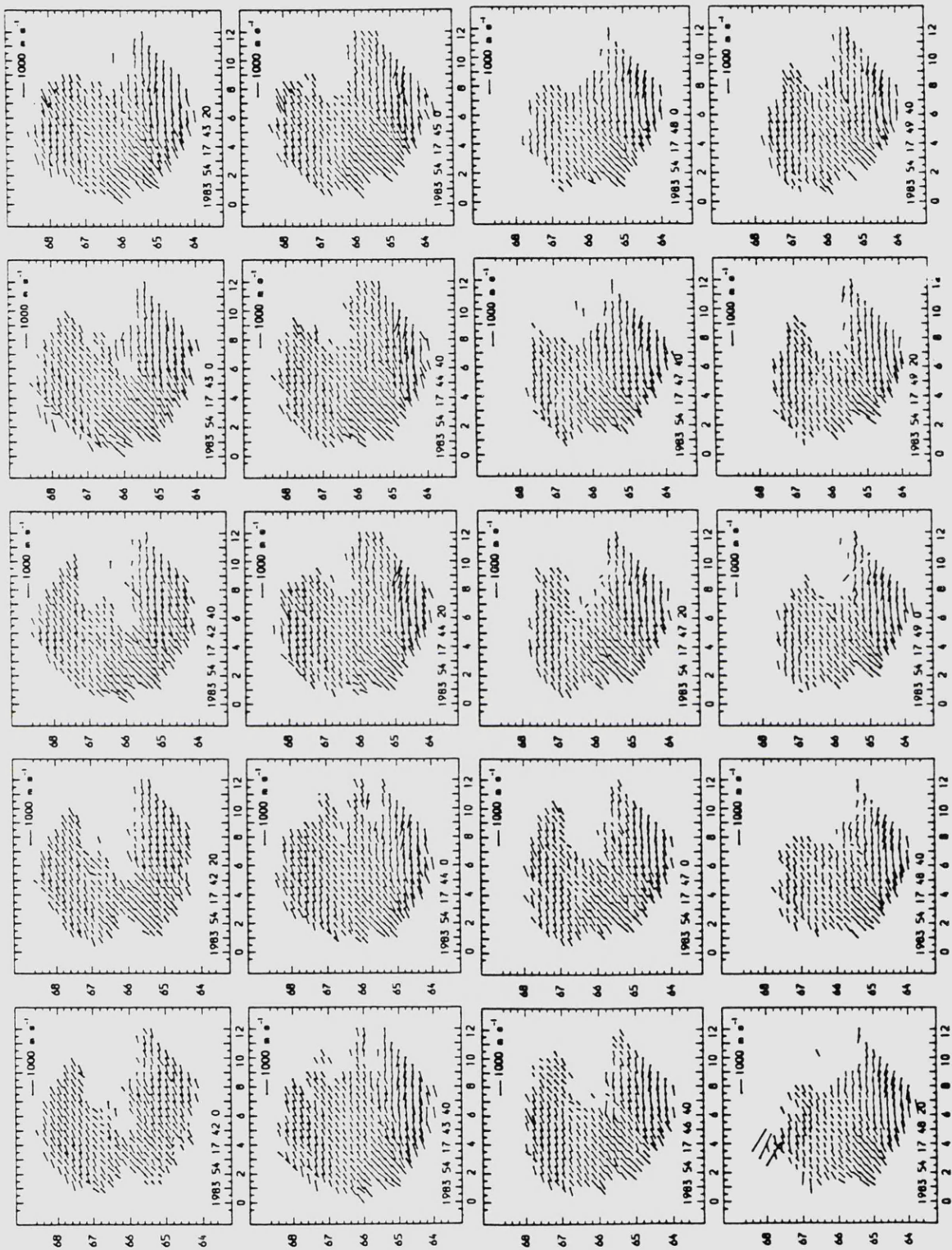


Figure 6.3

A sequence of SABRE spatial velocity plots starting just at the end of the first pulsation (17:42), between the two pulsations, at the onset (17:48) and during the second Pi2 pulsation of the pair. The vortex-like feature in the flow appears about 17:43 toward the equatorward edge of the viewing area and remains until after the end of the second pulsation. (Not all SABRE plots are presented from this interval, those from 17:45:20 to 17:46:20 are omitted).

pulsation which ends at 17:42 U.T.. Just after the end of this event, at 17:43 U.T., a different feature first appears in the lower part of the viewing area in the region where the peak wave spectral power for the second event is observed. The flow exhibits a clear southward component to the west and a weaker northward component to the east, and is reminiscent of the upper half of a vortex structure. This feature remains in the flow from 17:43 U.T., past the onset of the second pulsation at 17:48 U.T., and throughout the interval of the second pulsation. It finally dies away at about 18:15 U.T., well after the end of the second pulsation and around the time that the 'bay' in the east-west velocity component returns to pre-event levels.

Closer examination of the magnitude of the velocity in this area indicates the presence of stronger flows than those in the northern part of the viewing area, suggesting a boundary of some description between the two regions of differing flow.

#### 6.2.4 Polarisation analysis

Polarisation hodograms were constructed from the raw east-west, north-south SABRE velocity components for the two events (Figures 6.4a,b) for regions where the wave spectral power was high. The events under consideration are two of the few for which a determination of the polarisation sense was possible from the unfiltered velocity components. For the majority of events examined, the presence of background bays normally results in no 'ellipses' being produced when the analysis is attempted.

For the first pulsation, two regions of differing polarisation are found, counter-clockwise in the west and clockwise in the east. In addition to this longitudinal separation, there is also a latitudinal

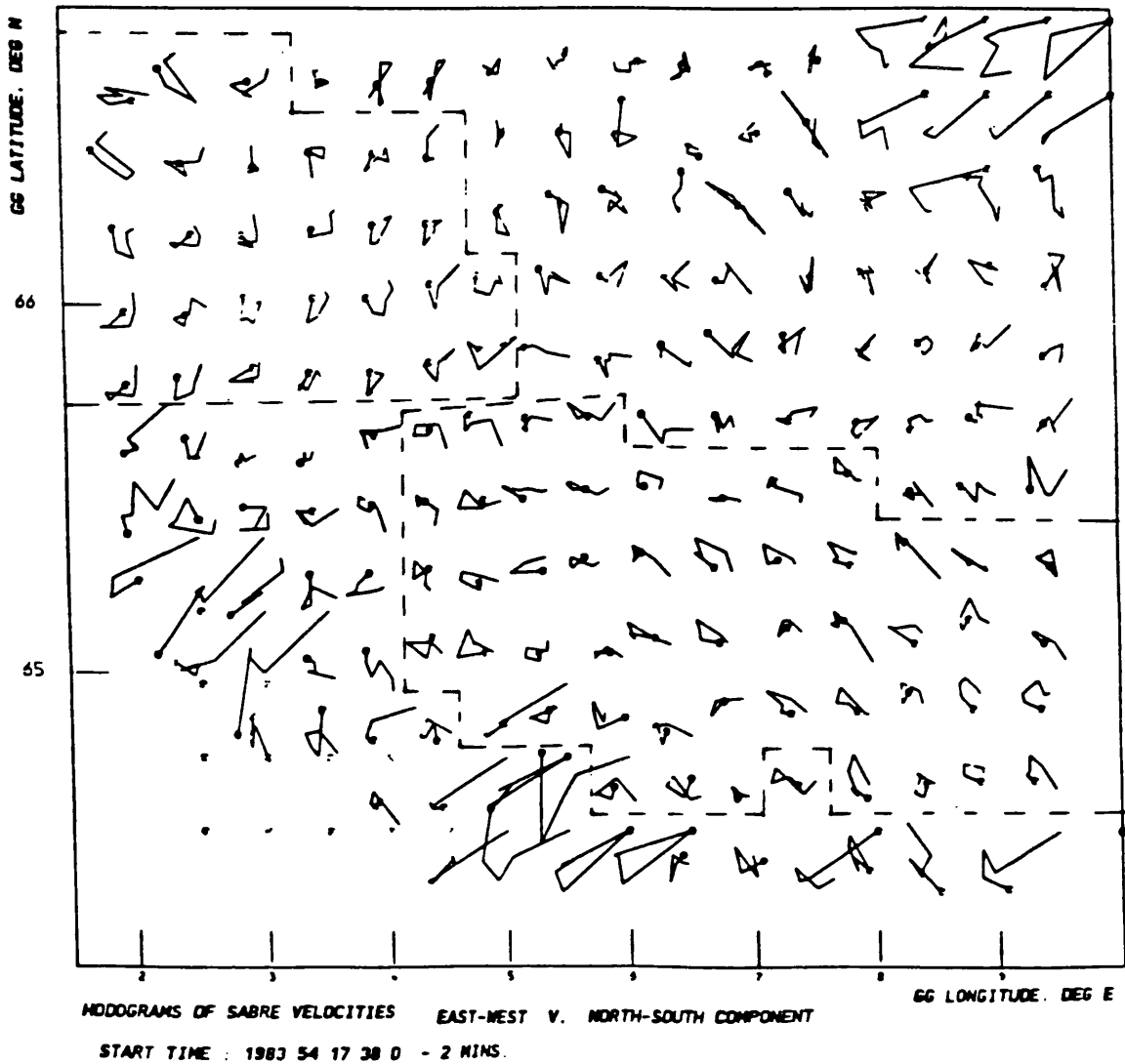
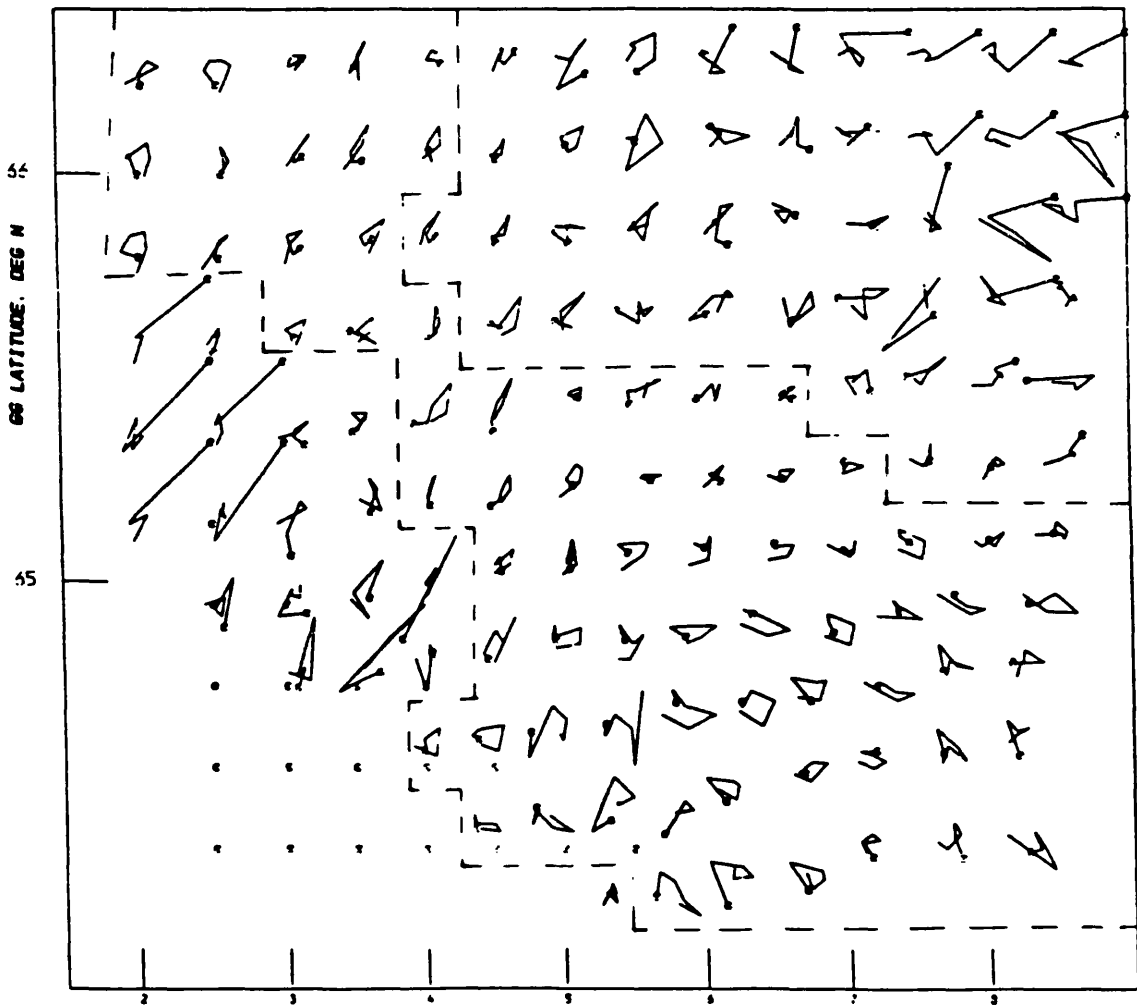


Figure 6.4a

Polarisation hodograms constructed from SABRE east-west and north-south velocity components in regions where the wave spectral power was found to be high displayed as a function of latitude and longitude in the SABRE viewing area. These data are for the Pi2 pulsation starting at 17:38 U.T.. The dashed lines delineate regions of differing polarisation in the viewing area, counter-clockwise to the north-west and clockwise to the south-east.



HODOGRAMS OF SABRE VELOCITIES      EAST-WEST V. NORTH-SOUTH COMPONENT      GG LONGITUDE. DEG E  
 START TIME : 1983 54 17 49 20 - 2 MINS.

Figure 6.4b  
 SABRE polarisation data presented in the same format as Figure 6.4a  
 but for the Pi2 pulsation starting at 17:49 U.T. in this case.

demarcation between the two regions at around 65 degrees north (Figure 6.4a). The polarisation changes sense between the two regions of different flow. The polarisation sense is everywhere clockwise for high wave spectral power during the second pulsation (Figure 6.4b).

#### 6.2.5 Summary of case study 1

Vortex-like structures have been observed previously in the equivalent ground currents of magnetometer array data at the time of Pi2 pulsations (Pashin et al., 1982; Lester et al., 1985; Glassmeier et al. 1988). Of particular relevance to this case study is the observation by Lester et al. (1985) of a pair of Pi2 pulsations in the eastward electrojet far from the generation region of the pulsations. The vortices these authors observed changed their sense of rotation with half the pulsation period. The observed results could be re-produced assuming a field-line resonance theory for the generation of the pulsations.

Field line resonance theory also predicts an amplitude maximum and a latitudinal change in polarisation sense about the latitude of the resonance region and such a reversal has been observed before (Bjornsson et al. 1971; Fukunishi 1975). The appearance of an enhancement in velocity magnitude with the spatial vortex structure may indicate an amplitude peak in the SABRE viewing area during this interval. However, it is only present during and after the second pulsation. Similarly, although a latitudinal change in polarisation is observed in this study, it is only present in the data from the first pulsation. The lack of FFT-derived amplitude and phase measurements means that it is not possible to state definitively that either or both of the pulsations arise from a field line resonance mechanism.

The additional SABRE observational feature of a latitudinal change which is also off-set in longitude has also been observed previously (Pashin et al. 1982; Samson and Harrold, 1983; Samson and Rostoker, 1983). These authors arranged their results in substorm centred coordinates and predict a four quadrant and multi region polarisation pattern respectively. The change from CCW to CW polarisation sense when going from higher to lower latitudes suggests that the SABRE viewing area is situated at the western edge of the substorm onset region for the first event. The CW polarisation for the second pulsation suggests that the SABRE viewing area is now even closer to the onset region implying a westward movement of this region. The model of Pashin et al. (1982) predicts an enlargement and westward movement of this region of enhanced current. It is interesting that the region of peak wave spectral power observed by SABRE also moves to the west and enlarges in area over the two pulsations. The complete polarisation pattern is not observed in this study perhaps because the regions of peak wave spectral power were relatively small or because the width of the viewing area (12 degrees) is too small to observe the total current system, typically 40 degrees of longitude (Samson and Harrold, 1983).

In the model of Samson and Rostoker (1983), the two regions of differing polarisation in the unfiltered data arise from the interaction and movement of the pair of field-aligned current sheets and the ionospheric currents associated with them. The current system moves westward to produce the oscillatory pulsation signature observed on the ground. The vortex delineating two regions of SABRE flow may be the signature of one of the field-aligned current sheets.

The interaction of field-aligned and ionospheric currents may be

equivalent to a theory of Pi2 pulsation generation suggested by Southwood and Hughes (1985). They illustrate how two circularly polarised waves of equal wavelength but different amplitude could, if travelling in opposite directions and being of opposite polarisations, combine to reproduce the substorm current wedge pattern of polarisation azimuths deduced by Lester et al. (1983). The two waves being surface waves excited at a boundary where the ionospheric conductivity has changed abruptly (Ellis and Southwood (1983), Glassmeier (1984), Yarker and Southwood (1986)). The directions of the Pi2 pulsation polarisation azimuths could be predicted by this model, the observed changing value of ellipticities could not. Recent work by Yarker and Southwood (1986) has made a start on a time dependent solution to the problem which may make it possible for the ellipticities to be included. This theory may not be applicable to the west of the substorm onset region as is the case in the interval under discussion.

It seems that the pulsations in this event may best be described by the modelled currents of Samson and Harrold (1983) with the SABRE viewing area situated to the west of the region of onset initially but becoming closer for the second pulsation. However, the possibility remains that they are generated by the field line resonance mechanism but the lack of SABRE FFT spectral analysis means it is not possible to prove this conclusively.

### 6.3 Case Study 2: flow pattern features

#### 6.3.1 SABRE and magnetometer pulsation signatures

The second event identified for a case study occurred between 23:30 U.T. on day 355 1982 and 00:20 U.T. on day 356 1982. During this period magnetometer records are only available from the low latitude

BGS station at Wick, although the normal magnetogram from Tromso indicates that a substorm onset occurred with the first Pi2 pulsation observed at Wick. The interval contains four Pi2 pulsations all of which are well resolved by SABRE, particularly in the filtered velocity components (Figure 6.5).

### 6.3.2 Spectral analysis

The results of a comparative ME spectral analysis of the Wick magnetometer and SABRE data are given in Table 6.2. The majority of the wave spectral power is found in the east-west velocity component of the SABRE data.

Table 6.2

<u>event</u>	<u>Wick magnetometer</u>		<u>SABRE</u>
	<u>H-component period(s)</u>	<u>D-component period(s)</u>	<u>east-west velocity component period(s)</u>
Pi2 23:40-23:44	76.9	76.9	93.4
Pi2 23:48-23:52	52.6	62.5	87.3
Pi2 23:54-23:59	90.9	100.0	127.2
Pi2 00:14-00:19	66.7	66.7	137.5(61.6)

There is a clear discrepancy between the dominant period identified by Wick and SABRE for all events, except perhaps for the last event for which a second period (61.6s) exhibited only slightly less spectral power than the dominant period. In all cases the SABRE dominant period is higher than that observed at Wick. This is due to the complex system of field-aligned and ionospheric currents present at the time of the pulsation (see below) which suggest that SABRE is located close to the generation region of the pulsations whereas Wick is equatorward and observes the single resonant pulsation period which is normally seen at lower latitudes.

WICK MAGNETOMETER Day 355/356 1982

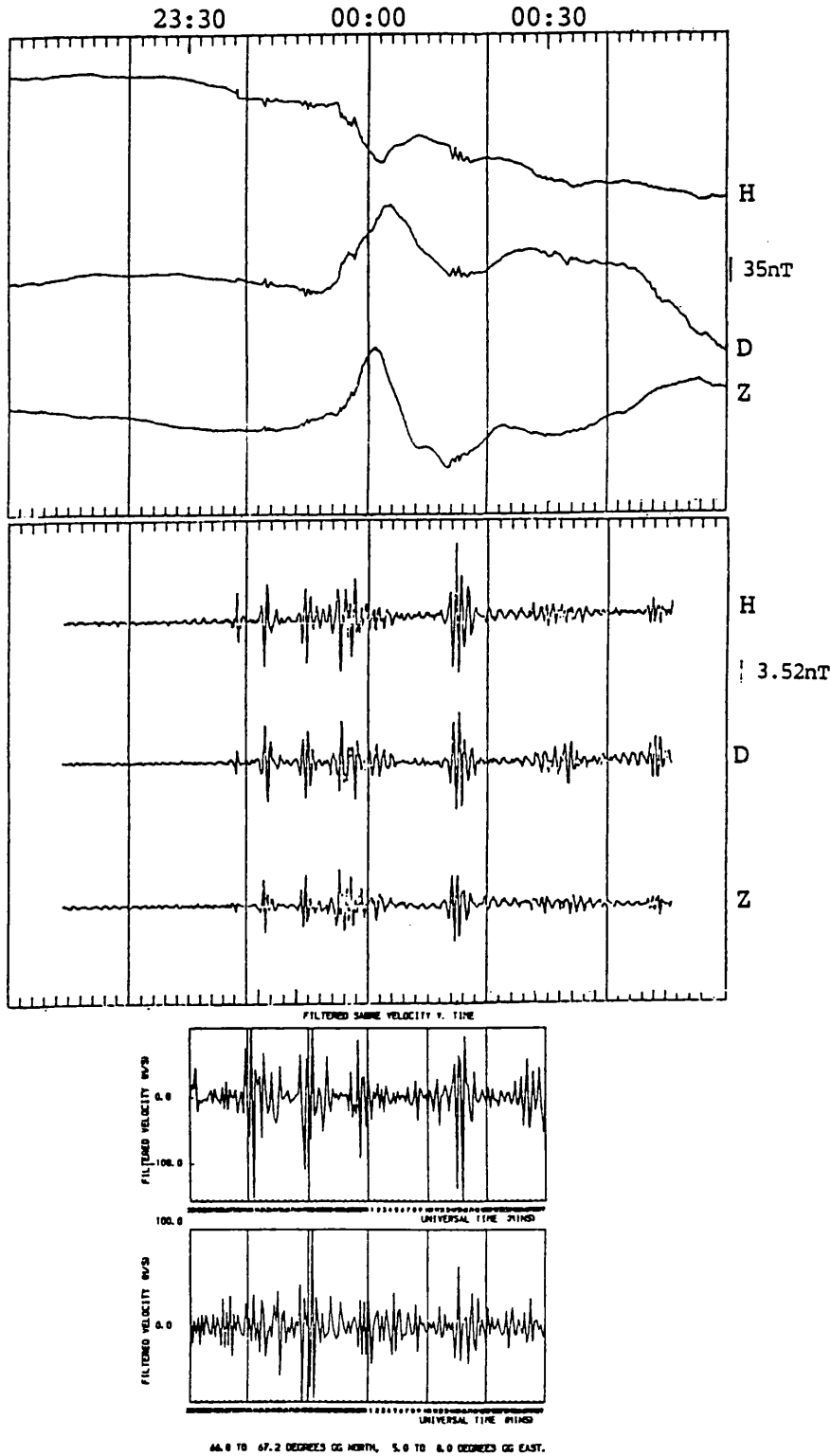


Figure 6.5

Time series data for the event on day 355/356 1982. From top to bottom of the figure, unfiltered and filtered ground magnetometer data from the only operational station at this time (Wick) are presented together with filtered SABRE east-west and north-south velocity component data.

### 6.3.3 SABRE flow patterns

The most interesting feature of this event is the way in which the observed spatial characteristics of the irregularity drift velocity flow patterns vary as the sequence of Pi2 pulsations progresses (Figure 6.6). At the time of onset of the first Pi2 pulsation, at 23:40 U.T., a region of south-eastward flow appears in the north-east of the viewing area and moves equatorward through the SABRE viewing area replacing all the backscatter that was previously present. Coincident with the onset of the second Pi2 pulsation at 23:49 U.T. the velocity flow turns sharply southward and is accompanied by a sudden drop in the backscatter present. This situation lasts only for 40 seconds after which the flow returns to a south-east direction and the entire region of south-east directed flow moves to the south. This is accompanied by the appearance of a separate region of eastward flow in the poleward half of the viewing area. A disruption of this uniformity, into many regions of highly structured flow (including the appearance of a vortex-like flow in the lower half of the viewing area) is then observed at the time of the third Pi2 pulsation (23:54 U.T.). The gaps between the different flow regions and the presence of a shear in the ionospheric flow suggest the presence of field-aligned current sheets.

It is apparent from the data that the auroral oval has moved equatorward over the SABRE viewing area during the first three pulsations, bringing with it the highly complex system of ionospheric and field-aligned currents associated with substorm onset and development in the auroral zone. The EISCAT magnetometer cross Z-component data indicate that all available stations are situated to the north of centre of the westward electrojet during the three

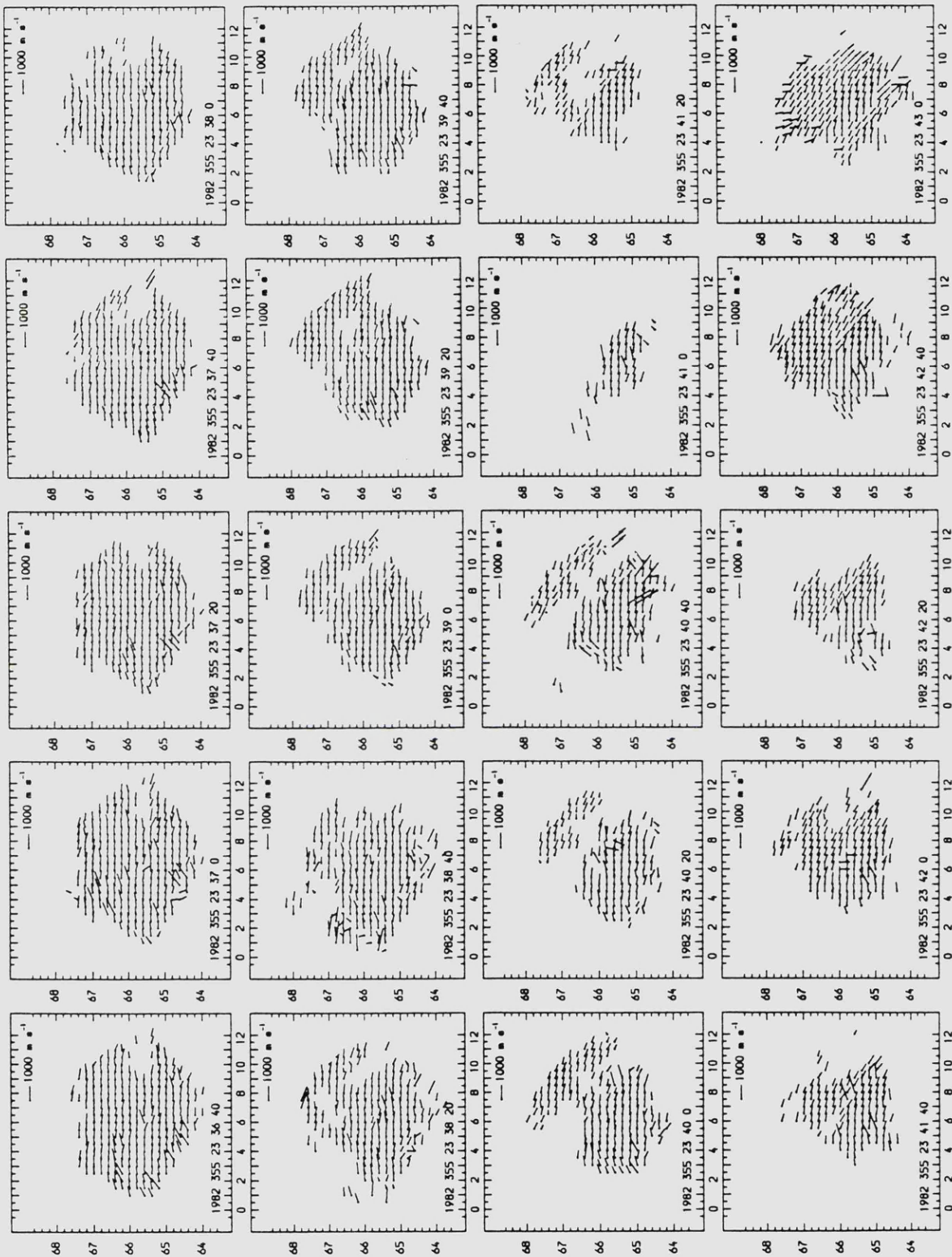


**Figure 6.6**

A sequence of SABRE spatial velocity plots indicating the complex flow patterns obtained throughout the duration of the Pi2 pulsations on day 355/356 1982.

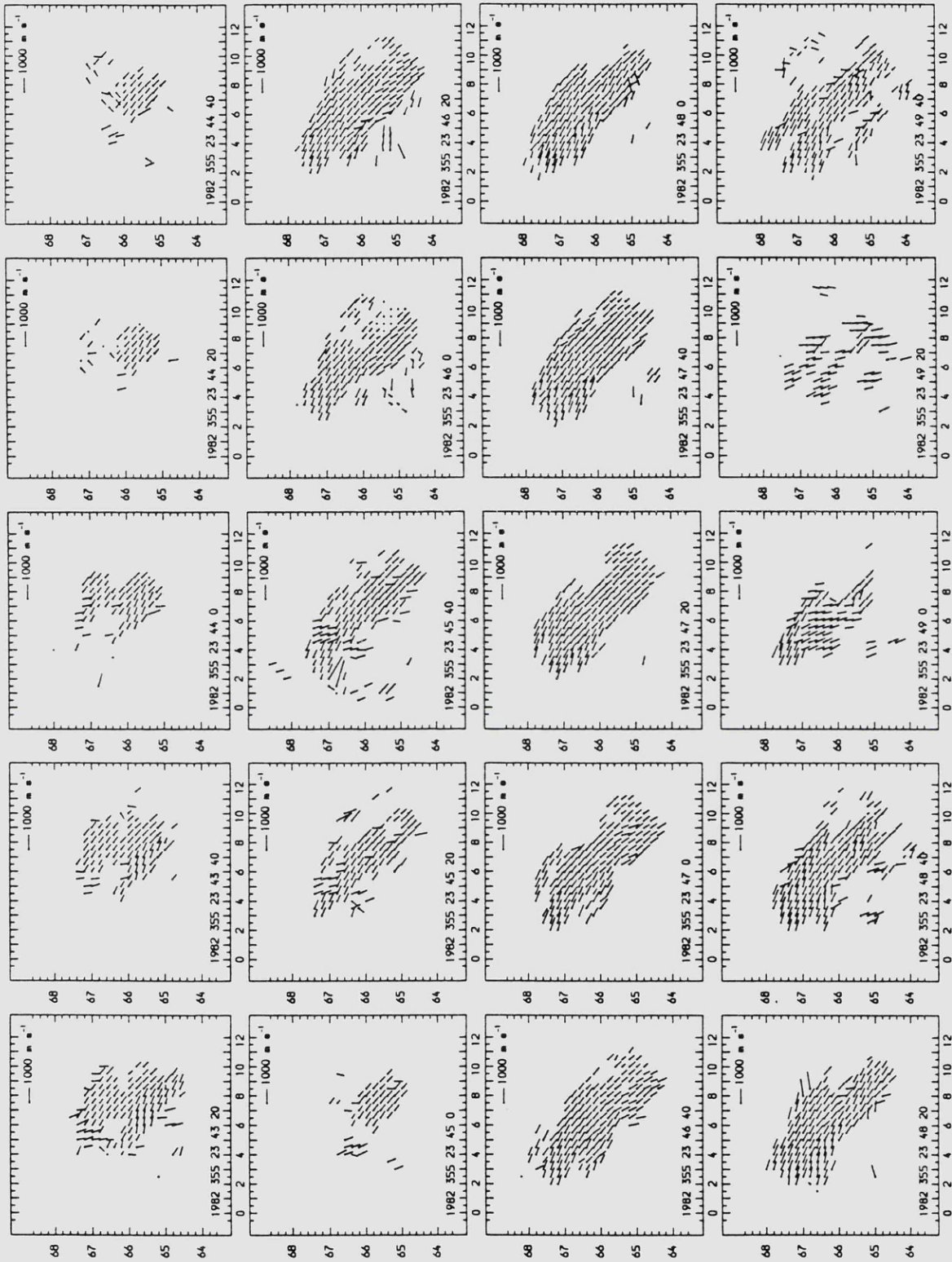


Figure 6.6 continued

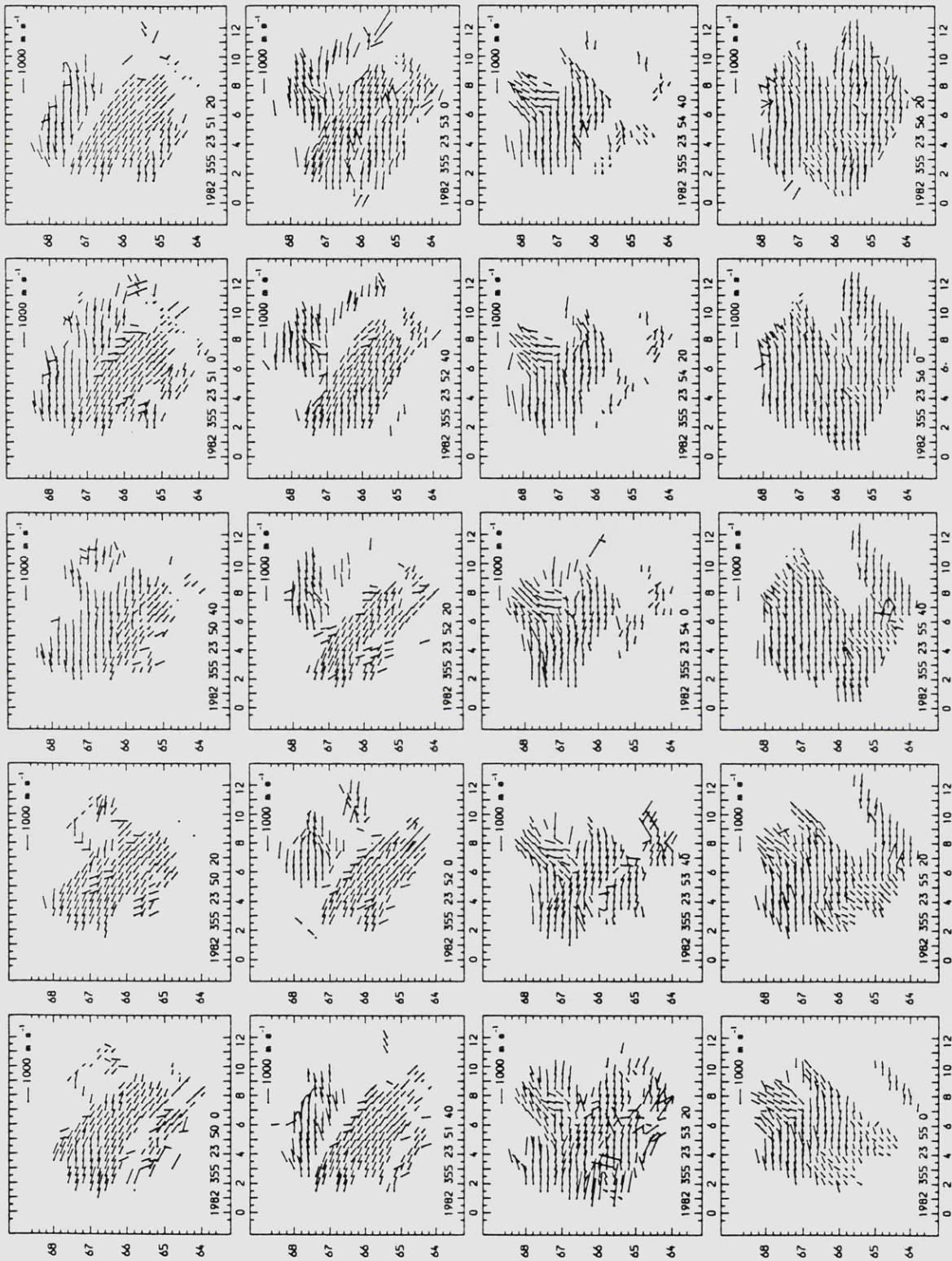


Figure 6.6 continued

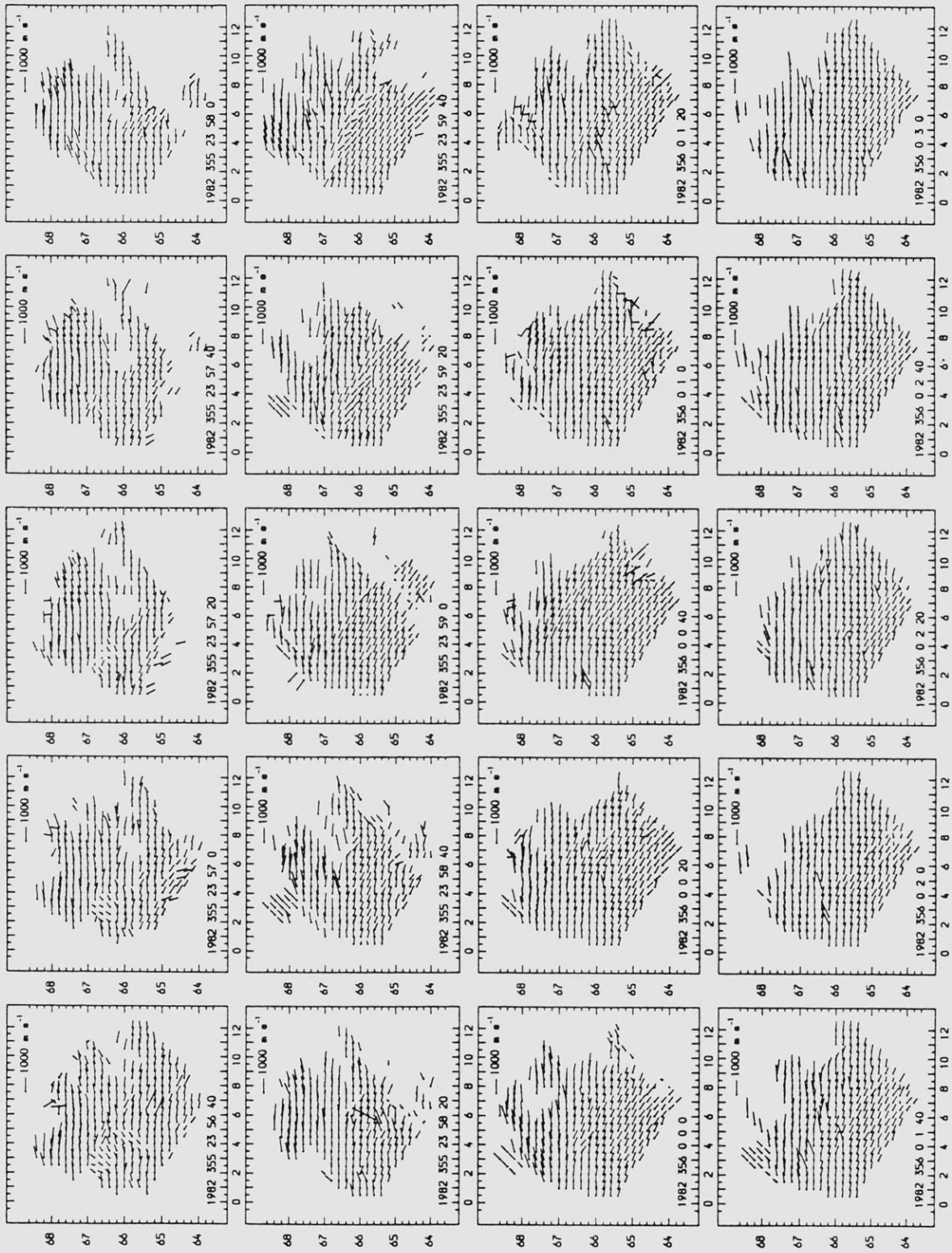


Figure 6.6 continued

pulsations. As the lowest latitude station is SOD at 67.4 degrees geographic north, the SABRE viewing area is equatorward of the magnetometer cross and nearer the westward electrojet. The unfiltered magnetogram from Wick at the time of the three pulsations displays features which are similar to those caused by the passage overhead or slightly poleward of a WTS (Kisabeth and Rostoker, 1973). There is a sharp decrease in the negative H-component, a pronounced positive onset in the D-component and a transition from positive to negative Z-component.

At the onset of the final Pi2 pulsation in the train, 00:14 U.T., a region of northward directed flow is observed in the north-west of the SABRE viewing area, accompanied by the disappearance of a large area of backscatter from the east of the viewing area. This situation lasts until the end of the pulsation at 00:19 U.T.. The flow pattern returns subsequently to the normal steady eastward flow typical of the westward electrojet, suggesting that the substorm current systems have now retreated polewards once more. This suggestion is supported by the fact that the final Pi2 pulsation is by far the clearest and is observed over a wide range of longitude and latitude within the SABRE viewing area (Figure 6.7). It is also the only pulsation of the four for which the dominant period is similar from the two observation systems. The EISCAT cross Z-component magnetograms confirm this conclusion. For this final pulsation all available stations except SOD at the lowest latitude were positioned to the north of centre of the westward electrojet, SOD being to the south of centre. This implies that the centre of the electrojet is flowing between 67.4 and 68 degrees north, and that SABRE is now equatorward of the auroral zone generation region of the Pi2 pulsation.

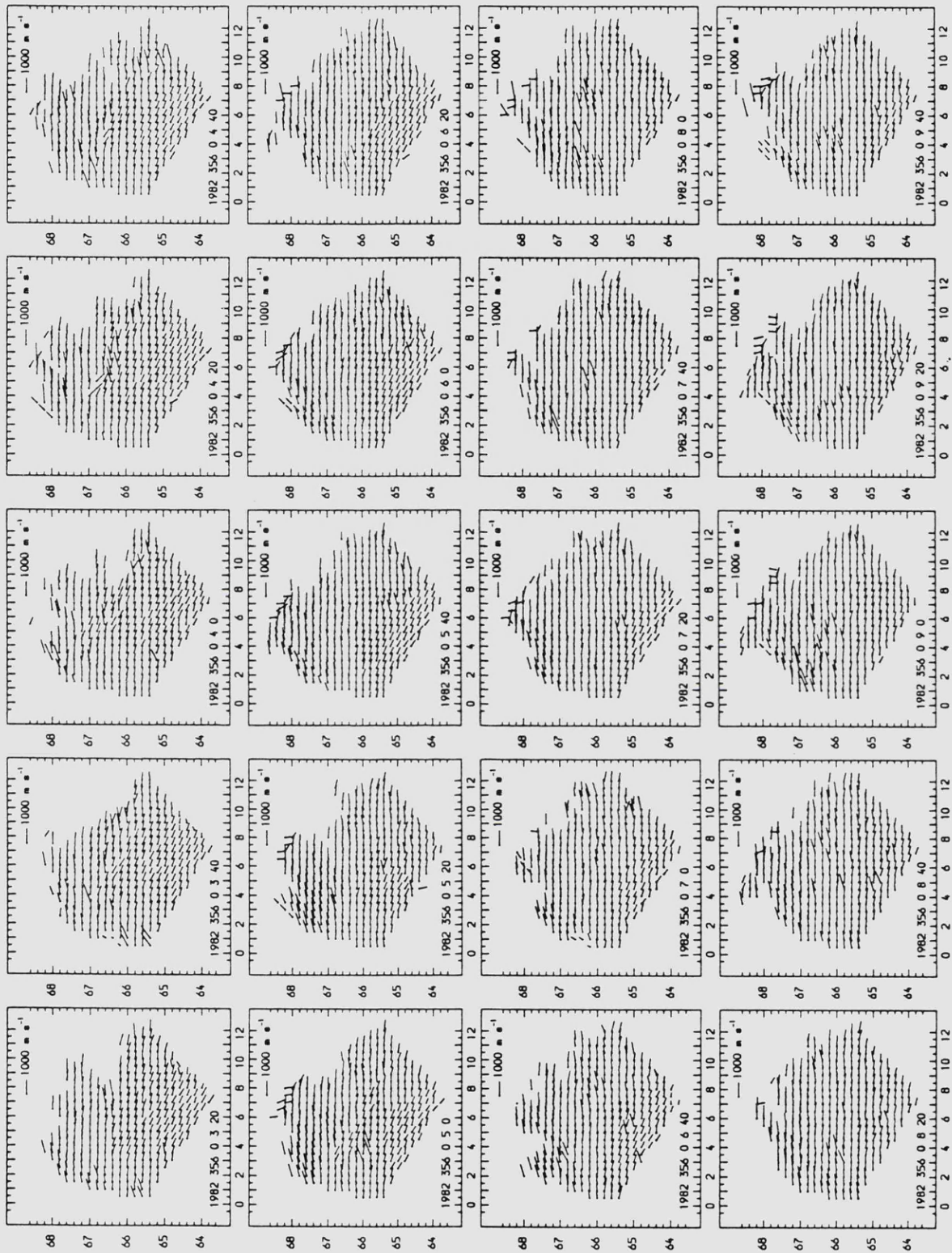


Figure 6.6 continued

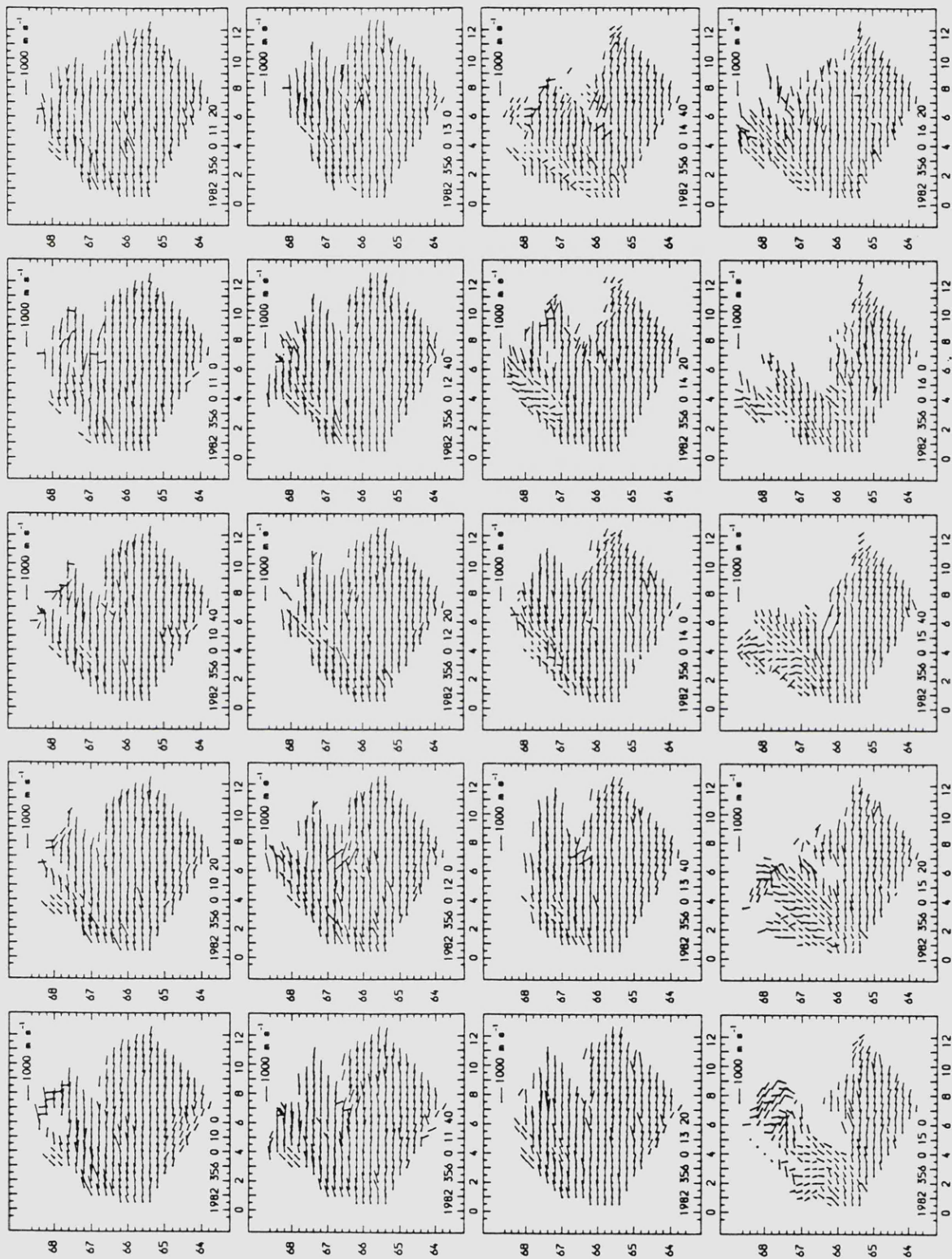


Figure 6.6 continued

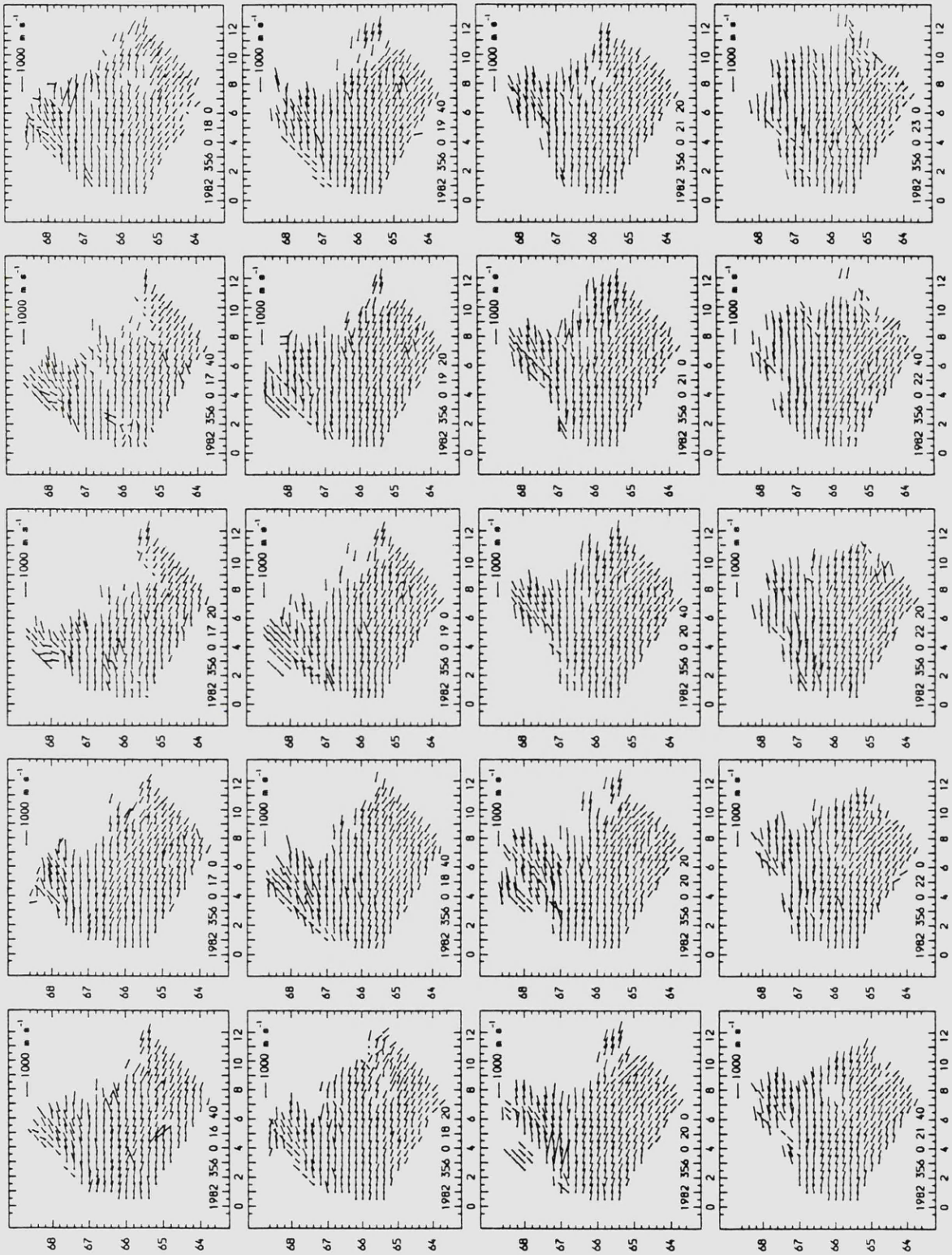
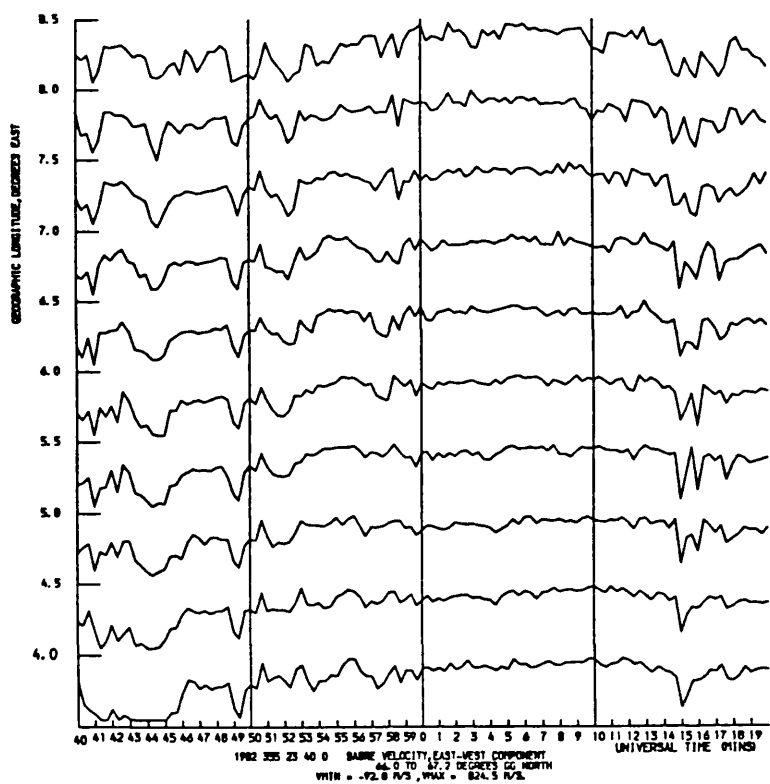
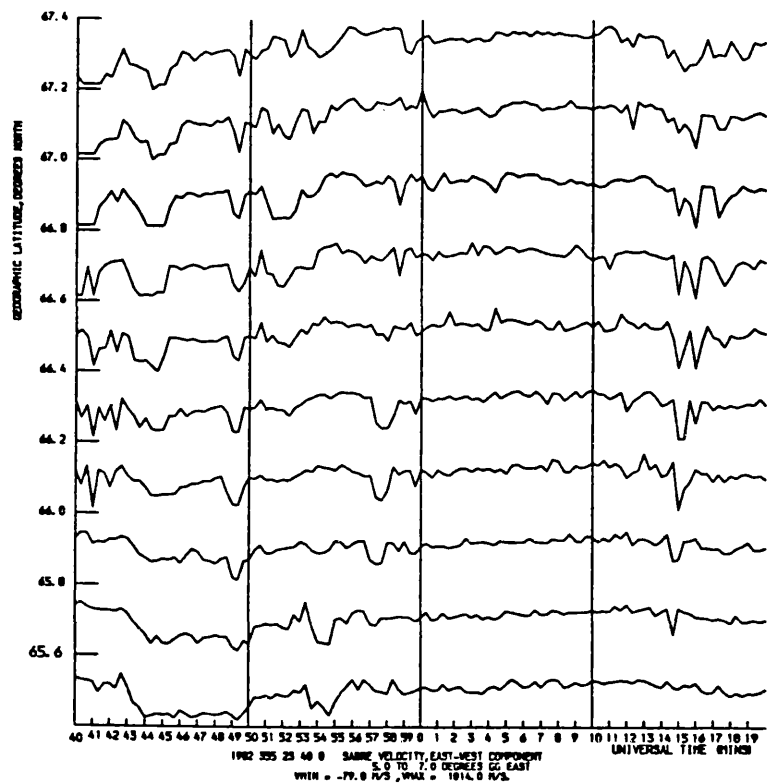


Figure 6.6 continued



**Figure 6.7**

Stacked plots of SABRE east-west velocity component data indicating that the final Pi2 pulsation of the train (commencing 00:14 U.T.) was observed over a large region of the SABRE viewing area. At the top is a latitudinal scan averaged over 2 degrees of longitude while below is a longitudinal scan averaged over 1.2 degrees of latitude.

A further consideration is that Southwood and Hughes (1985) suggest that the earthward surge of plasma in the magnetotail at substorm onset should manifest itself as a southward surge of flow in the ionosphere at the same time. This is observed at the time of the first and second pulsations. The region of northward flow observed at the beginning of the final pulsation is hard to explain therefore unless it is related to some sort of return flow from the ionosphere to the magnetosphere.

#### 6.4 case study 3: repetition time between Pi2 pulsations and changing position of peak power cell correlates with movement of wedge

##### 6.4.1 SABRE, magnetometer Pi2 pulsation data and spectral analysis

The case study concerns the investigation of four Pi2 pulsations observed between 21:30 U.T. and 23:00 U.T. on day 103, 1983 by both SABRE and the BGS magnetometers at Faroes and Nordli. Each pulsation is accompanied, in the Tromso auroral zone magnetogram, by a negative onset in the H-component, the classic signature of a substorm onset in the night-time sector (Figure 6.8). From the EISCAT cross data the westward electrojet moved equatorwards from between 67.4 and 68 degrees north for the first Pi2 pulsation, to around 67.4 for the second and third, to below the lowest latitude station of the EISCAT magnetometer cross at 66.9 degrees north for the final pulsation. This seems reasonable as the level of magnetic activity implied by the change in the H-component of the Tromso normal magnetogram increases during this interval. The final pulsation is associated with the largest H-component change. There appears to be a common repetition time of around twenty minutes between the four pulsations, a fact noted in previous observations of Pi2 pulsations by Stuart (1972b). McClay and Radoski (1967) explained such a period as the expected travel time of an Alfvén wave disturbance there and back along part of

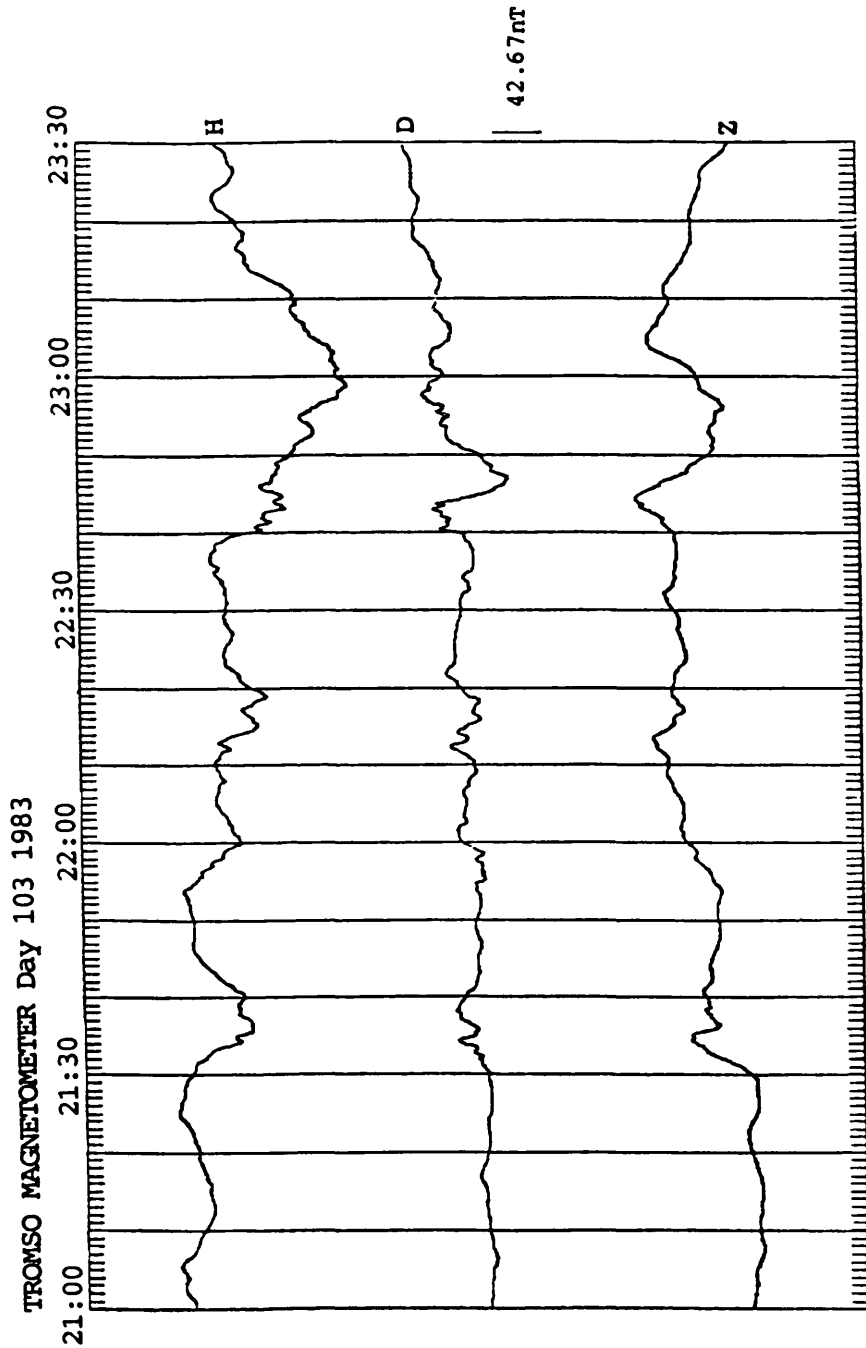


**Figure 6.8**

Time series data from the BGS auroral zone station at Tromso on day 103 1983 depicting a series of four substorm onsets or intensifications at 21:29, 21:50, 22:11 and 22:38 U.T.

the length of the magnetotail.

The flow patterns observed in the SABRE radar data are rather patchy and variable. There is a tendency for the backscatter returns to be strong with changeable direction of flow at the start of the pulsations, but to weaken and disappear totally towards the end.

The ME spectra obtained from the Pi2 pulsations observed by both SABRE and the magnetometers (Table 6.3) are broadband with dominant spectral peaks observed at periods ranging from 120s down to around 50s, close to the 40s limiting period of the SABRE observations. In Table 6.3 the dominant peak observed at each magnetometer station and in the SABRE east-west velocity component is quoted first with the remainder listed in order of relative strength. There is only one peak period observed at Faroes for the first two pulsations whereas Nordli observes multiple peaks for all four pulsations. This suggests that Faroes is initially some way from the interaction region where the pulsations are generated. It is also possible that the periods observed are harmonically related to each other within the 1mHz resolution of the magnetometer spectral analysis.

A stacked latitudinal profile of SABRE time series data (Figure 6.9a) indicates that the onset of the first Pi2 pulsation occurs earlier at lower latitudes and appears to propagate northwards. This feature is also apparent in the RTV data presented in Figure 6.9b. These data suggest a pulse of energy hitting the plasmasphere at lower latitudes first then moving to higher latitudes. This may result from the propagation earthward from a new neutral line of a fast mode compressional wave (Singer et al. 1983). If this were so there should

Table 6.3

<u>magnetometer station</u>	<u>H-component period(s)</u>	<u>D-component period(s)</u>
<u>Pi2 21:29-21:35</u>		
Faroes	91.0	58.8
Nordli	111.1,66.7,45.5	125.0,71.4,47.6
SABRE (east-west)	96.5,56.2	
<u>Pi2 21:50-22:00</u>		
Faroes	83.3	76.9
Nordli	91.0,52.6	100.0,71.4,58.8
SABRE (east-west)	96.5,135.9,58.9	
<u>Pi2 22:11-22:20</u>		
Faroes	125.0,62.5	83.3,47.6
Nordli	91.0,62.5,47.6	125.0,66.7,40.0
SABRE (east-west)	105.8,65.4	
<u>Pi2 22:38-22:48</u>		
Faroes	125.0,91.0,66.7,45.5	111.1,66.7
Nordli	125.0,55.6	71.4,100.0,50.0
SABRE (east-west)	98.0,115.0,66.4,48.4	

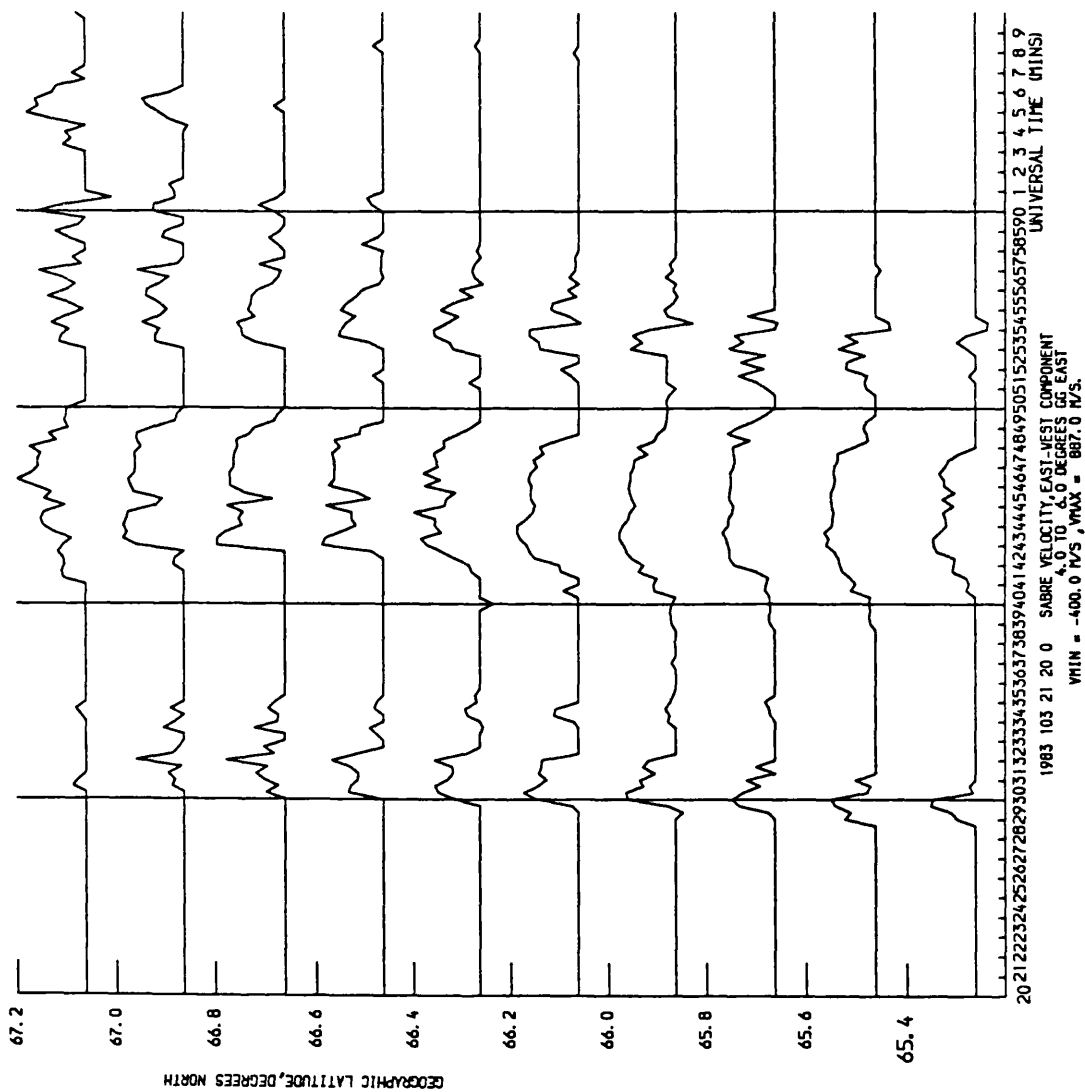


**Figure 6.9a**

A latitudinal stackplot of SABRE east-west velocity component time series data averaged over two degrees of longitude in the centre of the SABRE viewing area. The onset time of the first Pi2 pulsation (21:29 U.T.) becomes progressively later at higher latitudes.

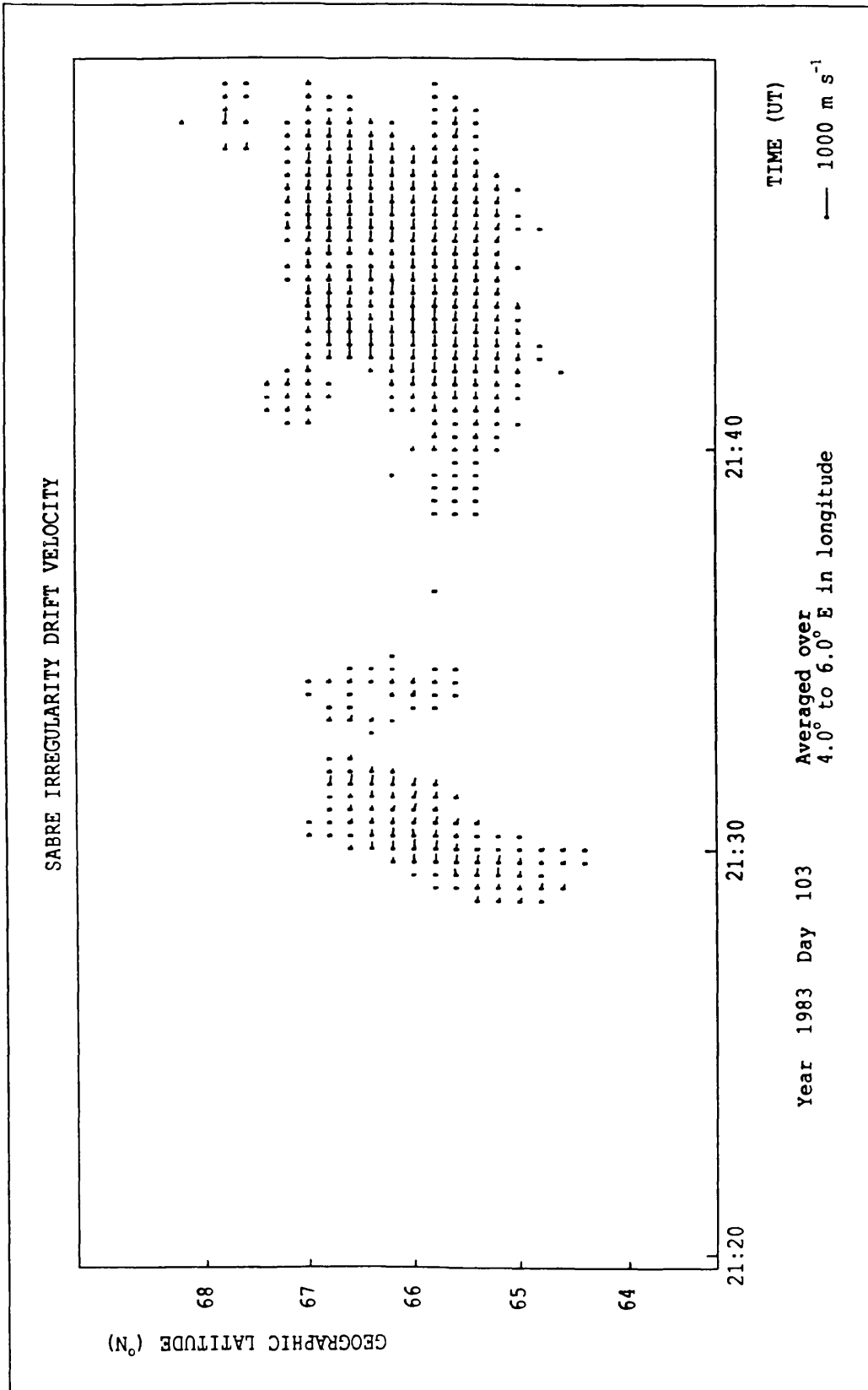


**Figure 6.9b**

A SABRE RTV plot illustrating that the onset of backscatter at the time of the first pulsation (21:29U.T.) on day 103, 1983 is progressively later at higher latitudes.

be a time of flight delay between the wave arriving at lower and higher latitudes. As there is no way of knowing the plasma density and magnetic field strength and orientation at the time (from which the Alfvén velocity and time of flight may have been calculated) no comment can be made on this substorm scenario. Singer et al. (1983) suggest that this fast-mode wave couples via a surface wave resonance at the plasmapause from where it propagates azimuthally to a large range of longitudes. This may be the signal at a single period observed at Faroes for the first two pulsations.

As a result of the broadband nature of the wave source, the Pi2 pulsations are represented by somewhat irregular and rapidly varying traces in the SABRE time series data for both of the irregularity drift velocity components (Figure 6.10). The main periods derived from SABRE and magnetometer records are, however, in reasonable agreement and so the study concentrates on the strongest pulsation period of around 100s in the SABRE data.

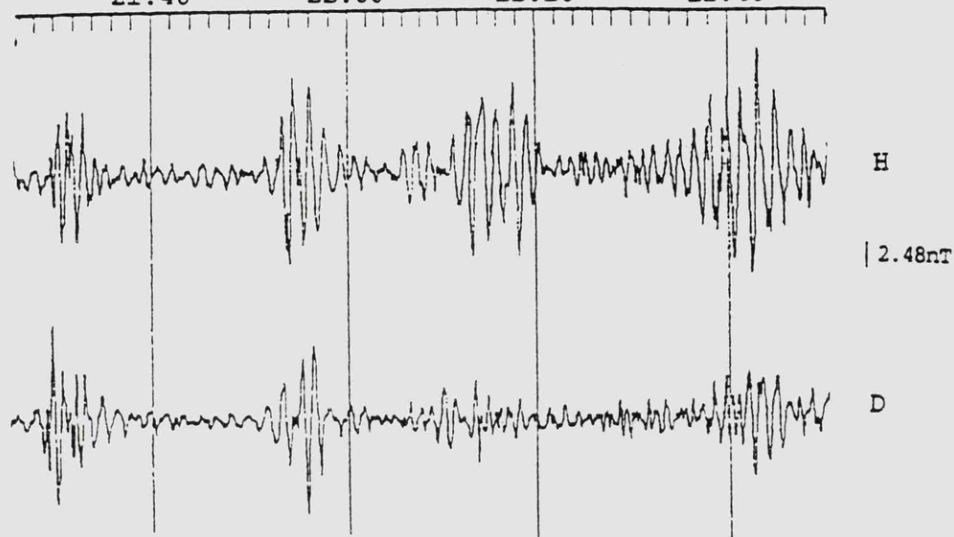
#### 6.4.2 Substorm current wedge movement from SABRE ME spectral analysis

The study of the sequence of all four Pi2 pulsations enabled a quantifiable analysis of the change in position of the cell in the SABRE viewing area exhibiting peak wave spectral power at the dominant Pi2 period with the spatial and temporal change in position of the entire viewing area relative to the substorm current wedge. The latter are determined by the horizontal (H-D) polarisation azimuths derived from the Faroes and Nordli magnetometer records. These are recorded in Table 6.4.

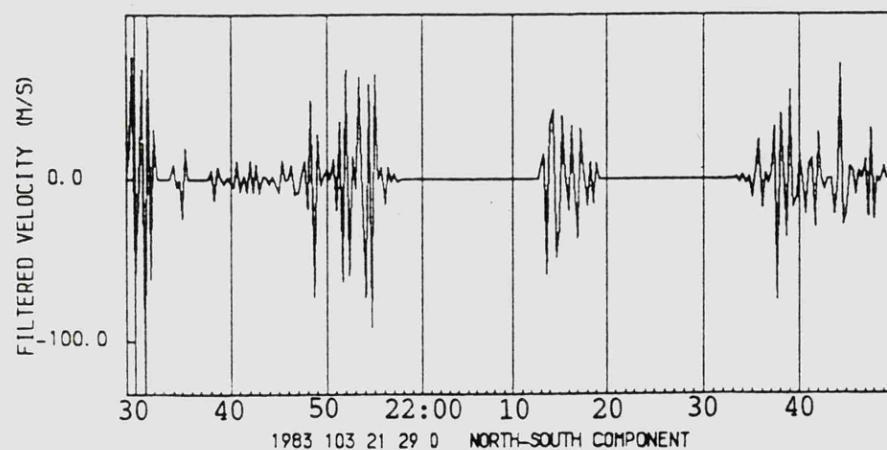
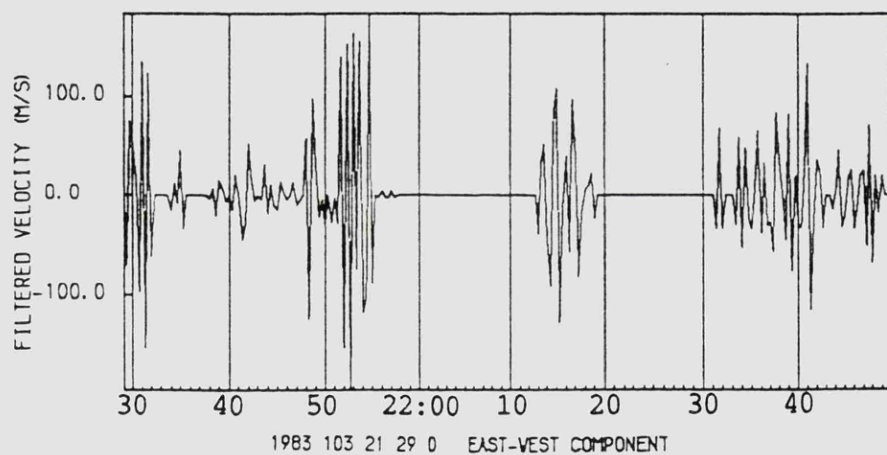
In discussing this event, it is assumed that the onset of the four individual pulsations is coincident with the generation of a series of

NORDLI MAGNETOMETER Day 103, 1983

21:40 22:00 22:20 22:40



FILTERED SABRE VELOCITY V. TIME



65.6 TO 65.8 DEGREES GG NORTH, 4.0 TO 6.0 DEGREES GG EAST.

Figure 6.10

Time series data for the four Pi2 pulsations on day 103 1983. From top to bottom of the figure, filtered ground magnetometer data from Nordli (H and D components) are presented together with filtered SABRE east-west and north-south velocity component data.

Table 6.4

<u>magnetometer</u> <u>station</u>	<u>azimuth</u> <u>orientation</u> (degrees E of N)	<u>position relative</u> <u>to substorm wedge</u>	<u>longitude of</u> <u>SABRE cell</u>
<u>Pi2 21:29-21:35</u> Faroes Nordli	4.0 -53.9	centre in east	10.0 E
<u>Pi2 21:50-22:00</u> Faroes Nordli	11.5 21.0	in west in west	5.0 E
<u>Pi2 22:11-22:20</u> Faroes Nordli	-89.5 4.5	FAC west centre	5.5 E
<u>Pi2 22:38-22:48</u> Faroes Nordli	27.2 -10.7	in west in east	8.5 E

four separate substorm current wedges as opposed to the spatial and temporal development of a single system of substorm currents. The twenty minute delay between pulsation onsets and the observation of backscatter by SABRE between pulsations (Figure 6.9a,b) suggest that this should be the case. The azimuths from Faroes and Nordli indicate that these stations have changed position relative to the centre of the substorm current wedges during the first two pulsations. The changes imply that the second wedge was generated to the west of the first. For the third pulsation, the new wedge is generated in roughly the same longitudinal sector as for the second pulsation. In this case however the wedge also appears to be narrower, almost half the wedge width, as determined by the polarisation azimuths, is contained in the longitudinal separation between Faroes and Nordli. The difference in azimuths obtained from the two stations for the four Pi2 pulsations (57.9, 9.5, 85.0 and 37.9) suggests that the width of successive substorm current wedges is very variable. The generation of the final wedge at the time of the final pulsation occurred further to the east relative to the third wedge. Over the interval of the event a similar situation is observed in the change in longitudinal position of the SABRE cell under consideration, although there is little change between the second and third pulsations. Although a qualitative analysis of this kind can lead to errors in the interpretation of the later pulsations because current systems established by the first two might affect the subsequent behaviour, the substorm electrojet was always situated poleward of the latitude of the magnetometers at Faroes and Nordli, albeit not by more than two or three degrees for the final pulsation (Section 6.4.1).

The patterns observed are similar for the other main pulsation period of around 60s with a large change in the same direction associated

with the first two pulsations and lesser changes, if any, associated with the final two. The latitude of the cells in the SABRE viewing area involved in these studies decreases with decreasing dominant period by about a degree over the range of periods observed.

#### 6.4.3 Summary of case study 3

The suggestion that these Pi2 pulsations arise from the coupling of a compressional source of energy originating in the tail might indicate that each pulse of energy sets-up a separate field aligned and ionospheric substorm current system rather than continually developing a single wedge. Each system is then generated further westward relative to the first apart from the final event. The twenty minute repetition time between the pulsations may be related somehow to the geometry of the tail, perhaps through the formation of multiple neutral lines at successively larger downtail distances. (The time difference between the onsets of the final two pulsations is larger than before). It may be that successive open field lines are being re-connected in the tail, an earthward pulse of energy being associated with each re-connection until the last open field line re-connects and the main phase of the substorm commences. (The energy previously stored in the tail is now unloaded). The final pulsation of the four had the largest negative change associated with it in the Tromso magnetometer H-component data.

The observations of Rostoker et al. (1987b) are also interesting in trying to understand this event. They examined VIKING auroral image data and observed that within the expanded region of auroral intensity, separate intensifications can occur at more westerly longitudes and that these regions of enhancement do not move once they have intensified. It was also possible for a subsequent

intensification to occur at a more easterly longitude than before. The addition of an eastward expansion and movement of the substorm system of field-aligned and ionospheric currents (Webster et al., 1989) to the westward movement of the substorm currents in the model for Pi2 pulsation generation of Samson and Rostoker (1983) may also be relevant to this event.

The pulsations might also be the result of cavity resonances between the x-type neutral line in the tail and the plasmopause near the earth. The period of the wave should increase if the impulse results from the successive re-connection of open field lines located further down the tail. If the period remains the same, the production of multiple substorm current wedges at varying longitudinal positions across the width of the tail is implied, with the downtail distance of the neutral line remaining roughly constant. This might explain the changes observed in the location of the cell exhibiting peak wave spectral power in the SABRE viewing area. It is not clear if the SABRE spectral analysis is sufficiently refined to pick-out any differences in period present between successive pulsations. The presence of spectral peaks at lower periods may represent similar cavity mode waves at higher harmonics of the fundamental cavity mode period. The same comment about the resolution of the SABRE spectral analysis probably applies.

## 6.5 case study 4: low magnetic activity

### 6.5.1 Introduction

The final case study examines an event occurring around 21:00 U.T. on day 101, 1983 which consisted of two Pi2 pulsations separated by seven minutes in the ground magnetic records. Magnetic activity was very low at this time ( $K_p=2-$ ,  $Lerwick-K=1$ ) but a negative change in the

H-component in the normal magnetogram from Tromso indicates that a substorm onset had occurred. Additionally, the EISCAT cross magnetometer data position the westward electrojet between stations ALT and KAU at around 69.5 degrees north, so that the SABRE viewing area is located equatorward of the auroral zone generation region for the two Pi2 pulsations during this interval.

#### 6.5.2 Occurrence of SABRE backscatter

Backscatter returns are first observed by SABRE at the onset of the first pulsation and die-out at the end of the second indicating that the backscatter appears to have been produced by the onset of the first pulsation. There is very little backscatter observed in the SABRE viewing area during this event. The small region of backscatter which is present moves equatorward from about 68 to 66 degrees north during the interval (Figure 6.11). In addition a small region of backscatter, located equatorward of the main region, appears and disappears during the event.

#### 6.5.3 SABRE and magnetometer pulsation signatures

The SABRE time series data of the two irregularity drift velocity components are different to those observed on the ground (Figure 6.12). Although the onset of backscatter returns observed by SABRE is coincident with the onset of the first pulsation on the ground, SABRE does not observe this pulsation well. The first clear oscillations in the SABRE data appear before the onset of the second event on the ground and continue after the nominal end of the second event. It may be that the ground pulsation is heavily damped however as there is some indication in the unfiltered magnetometer data that the event continues after 21:00 U.T. at Nordli. There are more cycles observed by SABRE for the second pulsation. It appears that SABRE observes only

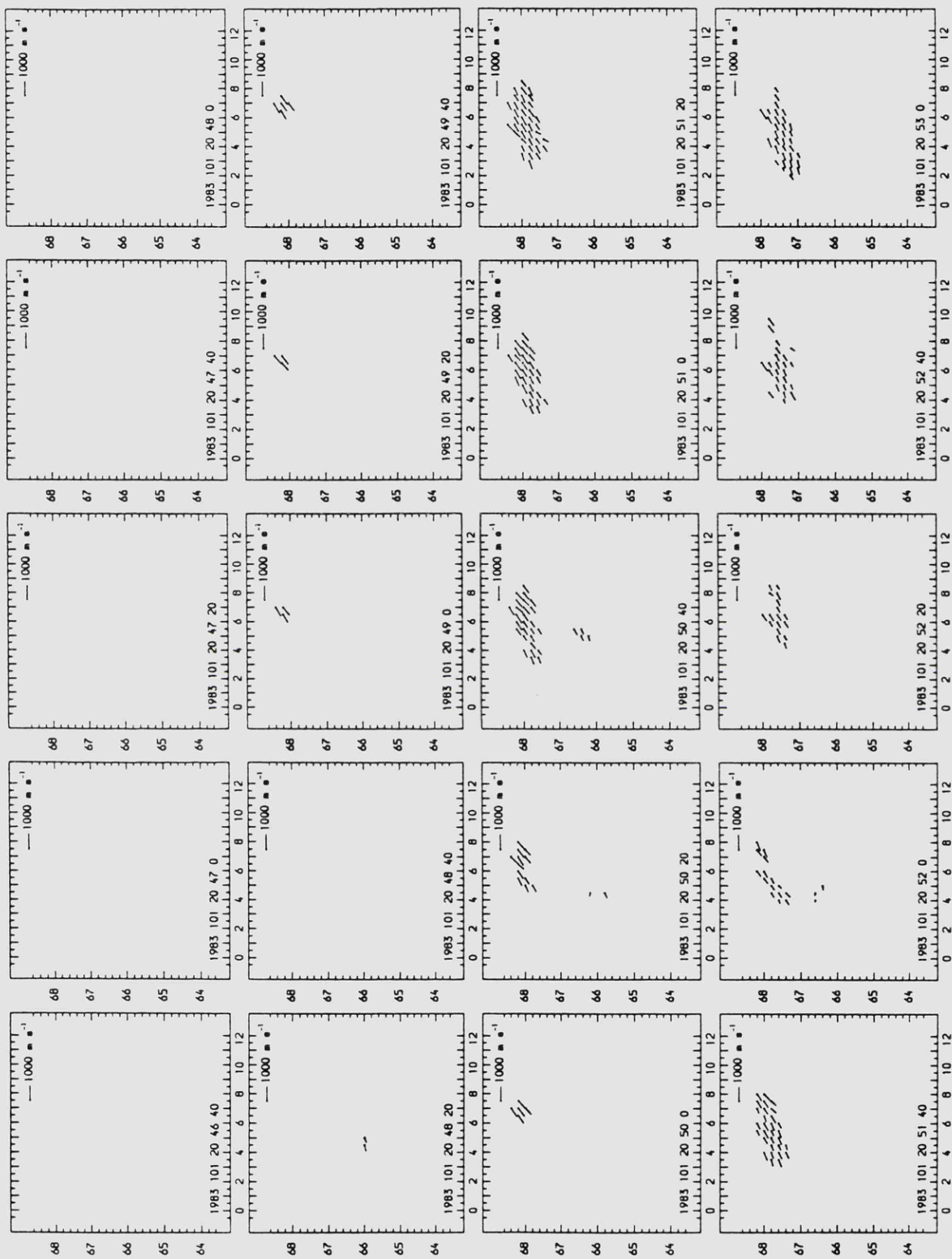


Figure 6.11

A sequence of SABRE spatial velocity plots obtained during the event on day 101 1983. There is little backscatter observed and the small region present moves equatorward through the viewing area during the event accompanied by the on-off switching of a smaller patch below it.

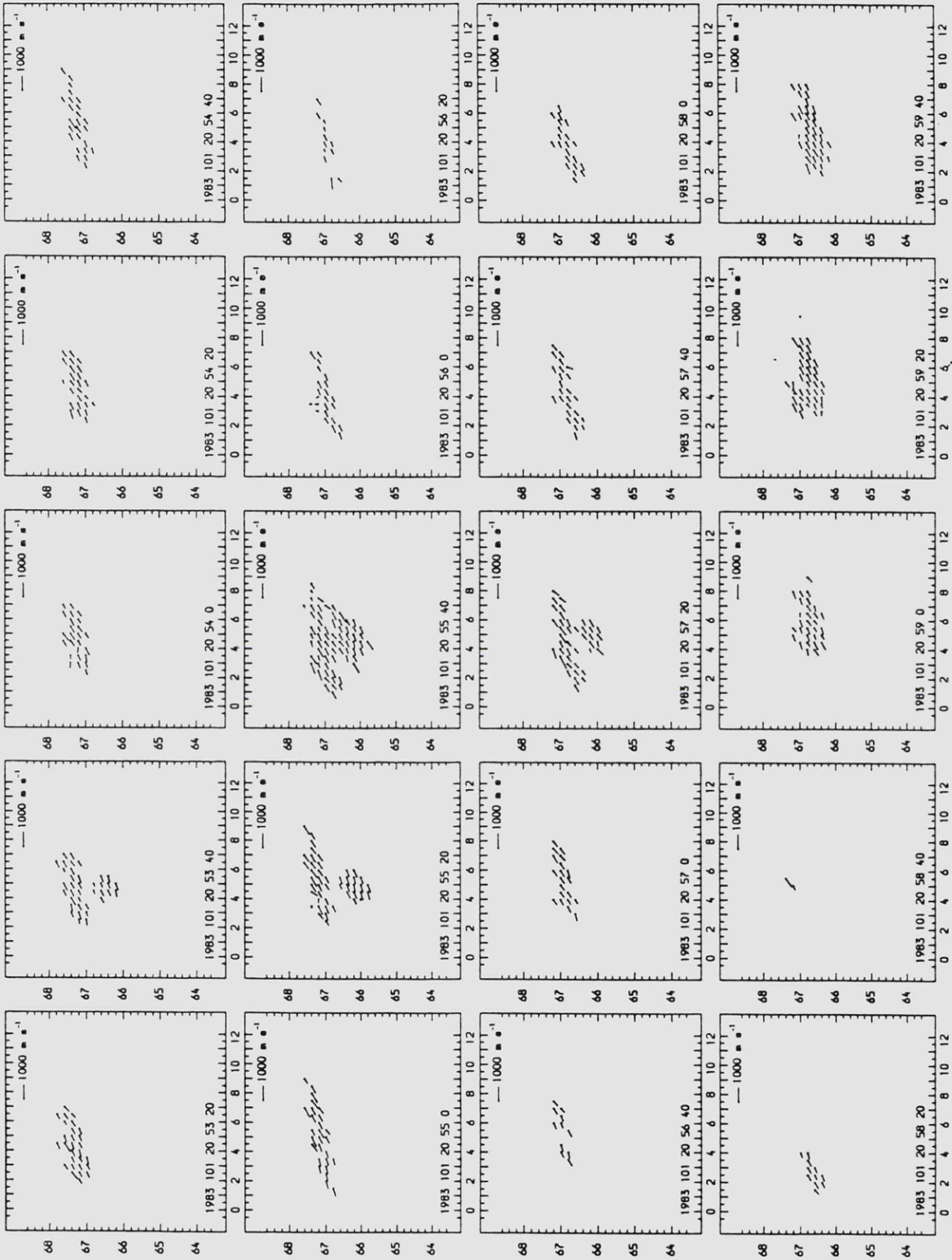


Figure 6.11 continued

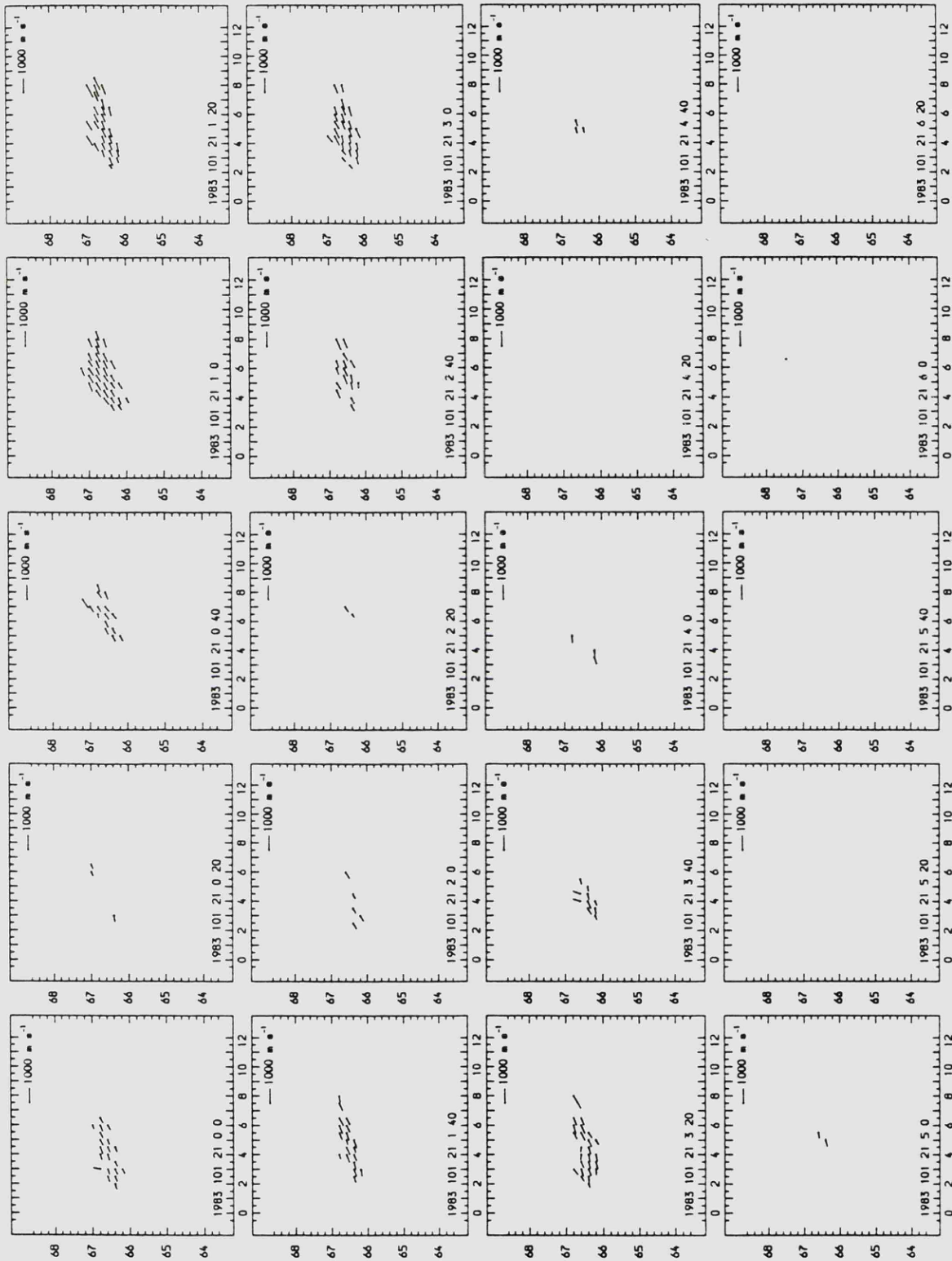
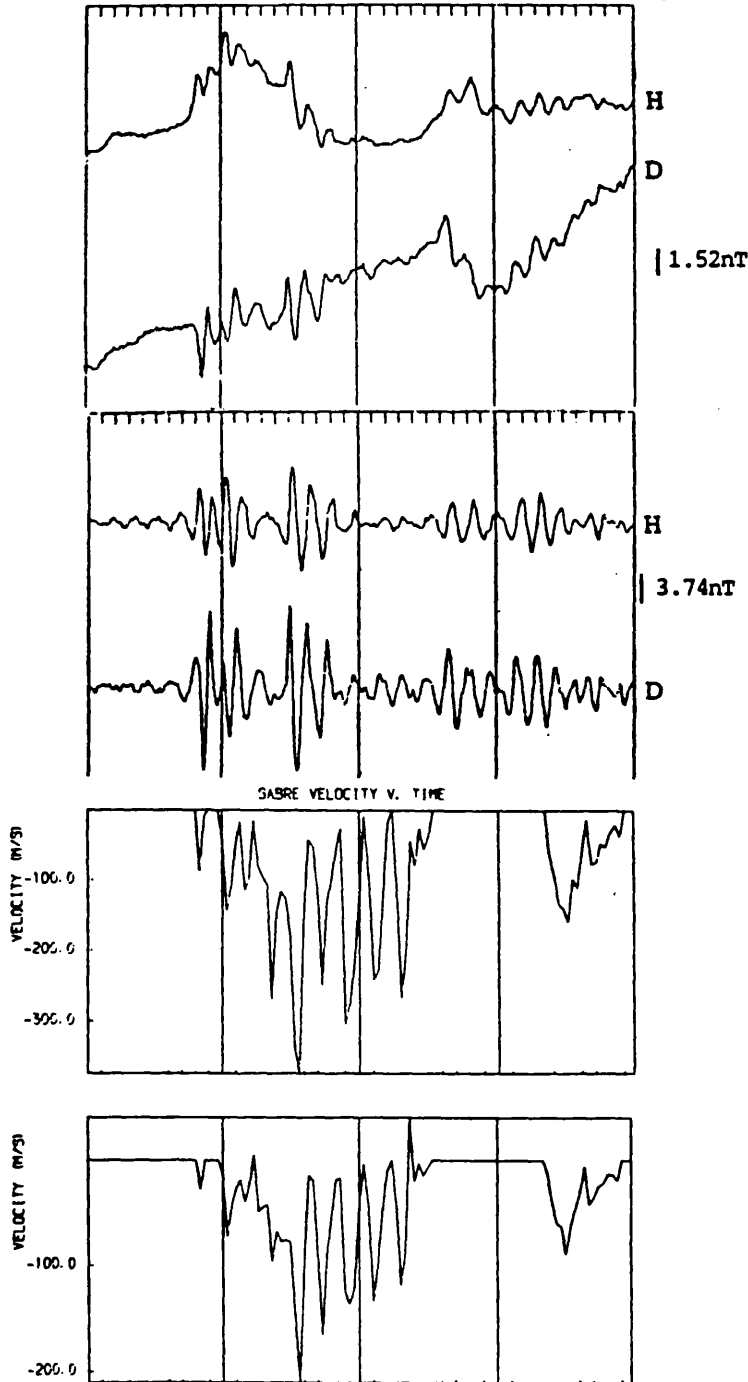


Figure 6.11 continued

NORDLI MAGNETOMETER Day 101 1983  
 20:40 20:50 21:00 21:10 21:20



64.0 TO 67.6 DEGREES GG NORTH, 4.0 TO 6.0 DEGREES GG EAST.

1953 101 20 40 0 EAST-WEST COMPONENT  
 1953 101 20 40 5 NORTH-SOUTH COMPONENT

Figure 6.12

Time series data for the Pi2 pulsations on day 101 1983. From top to bottom of the figure, unfiltered and filtered ground magnetometer data from Nordli are presented together with SABRE east-west and north-south velocity component data. The SABRE data were averaged over the small region of back scatter present during the event.

one pulsation of longer duration than the two observed on the ground. The SABRE pulsation is very much an on-off affair, characterised by the appearance and disappearance of the small region of backscatter below that which is continually present. This is well illustrated in the RTV type plot presented earlier (Figure 5.11). However, the construction of a time series by averaging over the whole region of backscatter observed during the pulsation, indicates that the poleward region produces a bay-like signature on top of which the equatorward on-off backscatter returns superimpose the oscillatory signature of the pulsation in the SABRE data (Figure 6.13). The polarisation sense (counter-clockwise) at the magnetometer stations places the SABRE viewing area equatorward of the auroral zone currents therefore reinforcing the idea that SABRE is observing the wave itself without contamination from the substorm currents in this case.

#### 6.5.4 Spectral analysis and possible pulsation generation mechanisms

It is apparent, even by visual inspection of the respective waveforms, that the pulsation periods observed on the ground and in the ionosphere are somewhat different. On the ground, the dominant ME period for the first pulsation is about 60s and this increases to around 90s for the second. The dominant ME period for the five cycles of the SABRE pulsation starting just before 20:54 U.T. is 117s. The differences between the SABRE and ground signatures and dominant periods suggest that the pulsation signature is being altered and possibly shielded in some way in travelling from the ionosphere to the ground magnetometer. The ground signature lasts as long as the SABRE signature but seems to be damped out, dividing what is a single pulsation in the ionosphere into two separate pulsations on the ground. The fact that the SABRE pulsation is an on-off affair implies that when the Alfvén wave, bouncing between conjugate ionospheres,

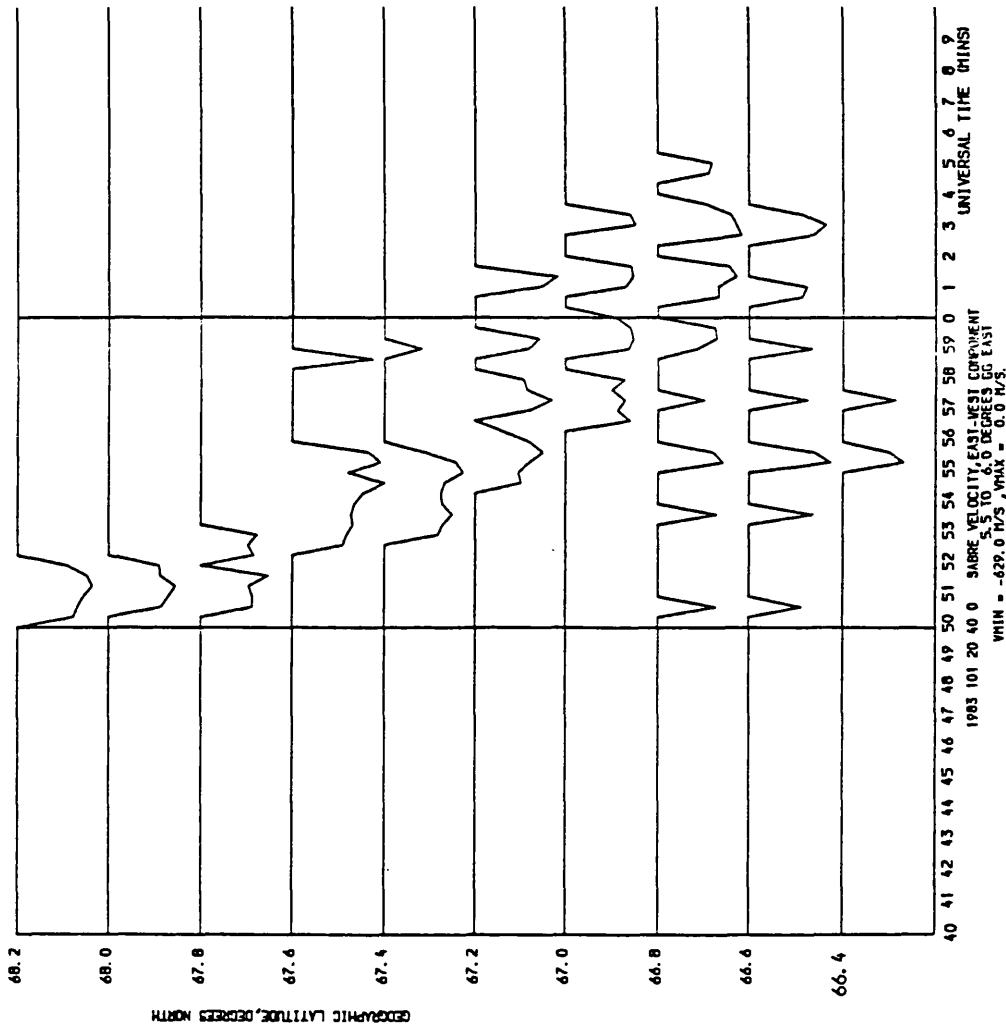


Figure 6.13

A latitudinal stackplot of SABRE east-west velocity component time series data averaged over a single cell in the viewing area. The SABRE Pi2 signature (Figure 6.12) is the combination of a poleward background bay and an equatorward oscillatory on-off switching.

returns to the northern auroral zone the electric field associated with the wave raises the ionospheric electric field above the threshold value for the generation of the irregularities observed by SABRE. The wave-like signature in the SABRE time series data is thus produced. However, there appeared to be no damping associated with the SABRE signature, so the damped ground signature still remains to be explained.

The spatial extent of the region of the SABRE viewing area which has peak wave spectral power at the dominant pulsation period (117s) is larger than usual (Figure 6.14). The data were averaged over fourteen frequency components in this case as the Pi2 pulsation signature was obtained over a large region of the viewing area and the ME spectral peak obtained was broader than usual. As the SABRE viewing area is located equatorward of the auroral zone generation region, SABRE is observing a different Pi2 pulsation signature in the small area of the ionosphere observed. The wave signature alone is being observed, there is no contribution from the substorm current systems.

This event is the only SABRE Pi2 pulsation for which it was possible to undertake FFT spectral analysis in addition to the ME analysis already mentioned. The dominant spectral period occurred at 113s, in agreement with the ME analysis within the resolution of the SABRE FFT spectrum. The amplitude and phase characteristics of the SABRE east-west velocity component at this dominant period (Figure 6.15) are similar to those expected theoretically if a field line resonance is present. There is an amplitude maximum within the SABRE viewing area across which the phase of the wave changes by 180 degrees. However, the theory of Walker (1980) has the phase decreasing from lower to higher latitudes. Orr (1984) states that an increase in phase with



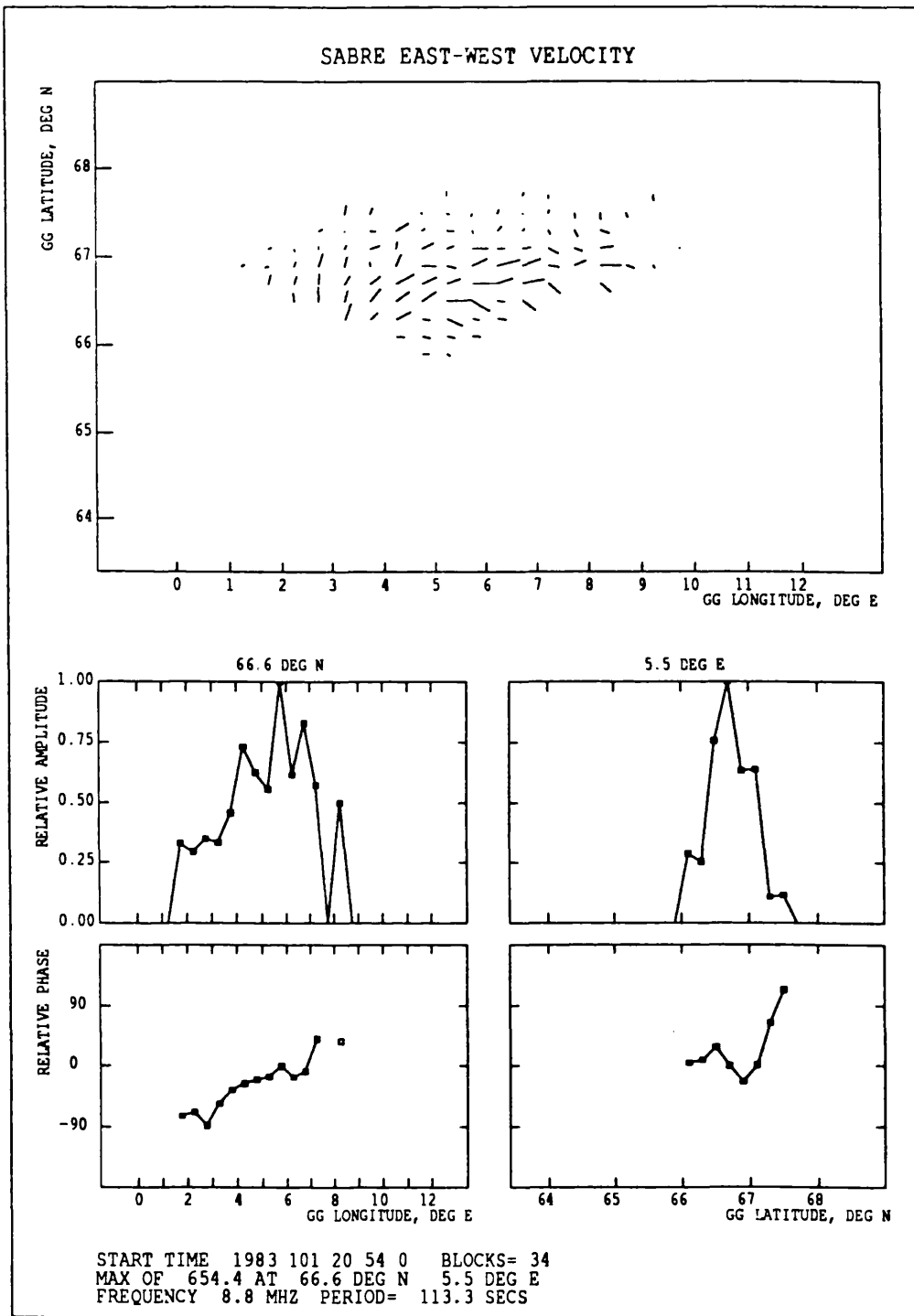


**Figure 6.15**  
 Amplitude and phase characteristics determined from FFT spectral analysis of the SABRE east-west velocity component data on day 101, 1983. The amplitude and phase as a function of latitude are similar to those predicted theoretically when a field line resonance is responsible for the generation of the pulsation.

latitude as observed in this case implies a resonance at the plasmopause (i.e. Waldock et al., 1983), the opposite phase change occurring with a resonance at the plasmasphere and plasmatrough. This is a very narrow resonance region from about 66.8 to 67.6 degrees north and it delimits the change in the SABRE Pi2 pulsation signature from the background bay-like response poleward of the resonance from the on-off switching of the wave itself at, and equatorward of, the resonance region. The SABRE polarisation derived from the FFT and hodogram analysis both produce linear polarisation at the resonance and CCW polarisation equatorward of it in agreement with the CCW polarisation observed on the ground equatorward of the resonance. The derived azimuths of about 66 degrees are also in agreement with the ground azimuths of around 80 degrees.

#### 6.6 Summary and conclusions

From the case studies of SABRE Pi2 pulsations presented in this chapter it is apparent that, although the pulsations are all well observed, there is no single signature in the SABRE data, whether in the time series or spatial flow patterns, that is indicative of the presence of a Pi2 pulsation. In general, the signature changes with changing magnetic activity and also with the position of the SABRE viewing area relative to the substorm current wedge and/or the Pi2 pulsation generation region.

Different Pi2 pulsation generation mechanisms are suggested by the polarisation and spectral analysis undertaken during different events. Possibilities include the coupling of a compressional source of energy from the magnetosphere to the ionosphere, the coupling of wave energy through a field line resonance or the interaction and movement of field-aligned and ionospheric currents generated at an ionospheric

boundary produced by changes in ionospheric conductivity.

The presence of vortices in the flow and changing polarisation sense across the viewing area while SABRE is located in the eastward electrojet far from the pulsation generation region is consistent with the signature expected to the west of onset in the modelled field-aligned and ionospheric currents of Samson and Rostoker (1983). This current system moves to the west and a possible signature of this was also observed by SABRE.

The level of magnetic activity must also be considered, as with the second and final studies, when suggesting possible generation mechanisms for the Pi2 pulsations. When magnetic activity is low, the SABRE viewing area is located equatorward of the pulsation generation region. The on-off signature in the SABRE time series suggests the presence of an Alfvén wave propagating between the conjugate ionospheres changing the ionospheric conductivities and currents and therefore switching on and off the electric field observed by SABRE. In this case, the wave itself is observed by SABRE without contamination from the substorm current systems in the generation region to the north. The results of SABRE FFT spectral analysis suggest that this signature results from a field line resonance being set-up with the narrow resonance region observed in the poleward half of the SABRE viewing area. At times of higher magnetic activity when the SABRE viewing area is located within the substorm current systems, the ionospheric signature of the earthward flow of plasma at substorm onset is often observed at the onset time, and in association with, the Pi2 pulsation. Shears in the flow indicate the presence of ionospheric conductivity gradients or sheets of field aligned current associated with the waves.

Finally there is the possibility of the coupling of a compressional source of energy in the magnetotail to the ionosphere exciting some sort of resonance at the plasmasphere. The repetition time between the pulsations observed may result from geometrical considerations in the tail, possibly from the successive re-connection of open field lines each sending a pulse of energy earthward to generate a pulsation when this Alfvén impulse impinges on the auroral ionosphere. The SABRE data suggest that each surge sets-up a new substorm current wedge at the onset of each individual pulsation. The apparent width and east/west longitudinal movement of the position of wedge generation was variable during the train of pulsations. Therefore the azimuthal width and location of the region of substorm onset in space is variable throughout the train even if the relative change in downtail position is more uncertain.

The present studies confirm the wide range and complexity of the possible coupling processes which can occur between the magnetosphere and ionosphere during Pi2 pulsation activity. The availability of both direct ionospheric current measurement (from SABRE) in addition to the conventional magnetometer data has greatly enhanced the ability to identify some of these pulsation generation mechanisms.

## CHAPTER 7

### CONCLUSIONS

#### 7.1 Introduction

The Pi2 pulsations that are associated with substorm onset have been investigated experimentally by means of a coherent radar, SABRE, and a network of ground magnetometers. The radar has enabled these pulsations to be examined for the first time with high spatial resolution and, in addition, has provided direct measurements of the pulsations in the ionosphere itself thus avoiding the spatial integration present in the magnetometer results. This has enabled new light to be shed on the generation and propagation mechanisms of this class of pulsation.

#### 7.2 Principal results of the study

The radar observations of the substorm associated Pi2 pulsations indicate that the oscillatory, impulsive signal appears in time series data from both irregularity drift velocity and backscatter intensity. The velocity measurements however have been mainly employed for this study. The pulsations occurred both as individual events during quieter magnetic intervals and in trains during more active times. The amplitudes of the pulsations were not well correlated with the corresponding ground magnetometer based measurements. The observed dominant periods were found to be in best agreement (within the resolution of the spectral analysis employed) when the period was

constant at all the available magnetometer sites and the SABRE viewing area was inside the substorm current wedge. The SABRE Pi2 pulsation signature from this position occurred on the back of a dc bay-like perturbation in the background velocity. This could be accounted for in terms of the position of the viewing area relative to the substorm enhanced electrojet. Data from the east-west velocity component indicate that the magnitude of this 'bay' was linearly related to the amplitude of the accompanying Pi2 pulsation.

A second type of SABRE Pi2 pulsation signature exhibited an on-off switching of the irregularity drift velocity which is related to the re-configuration of the ionospheric conductivity and electric field produced by an Alfvén wave impinging on the auroral ionosphere. The re-configuration has the effect of sending the ionospheric electric field alternately above and below the threshold for generation of the ionospheric irregularities which are necessary to produce the radar backscatter.

Studies of the polarisation of the Pi2 pulsations observed by SABRE were difficult due to the 20s integration time of the radar. A definite sense of polarisation could however be determined for many of the events. Changes in the polarisation sense during a single Pi2 pulsation were also observed. When the polarisation was linear or nearly so, a value for the azimuth of the polarisation ellipse could be obtained. This linear polarisation also rotated in azimuth during many of the pulsation events recorded. On comparing the ground based polarisation azimuth with that derived from SABRE data, there is some evidence that a 90 degree rotation of the azimuth occurs in travelling from the ionosphere to the ground. This only appeared to be the case for the data from the two higher latitude magnetometer stations. The

presence or otherwise of a rotation is important in establishing the mode of wave present at the time since only the Alfvén wave ellipse should be rotated on travelling through the ionosphere.

The enhanced spatial resolution of the SABRE system enabled the flow patterns in the ionospheric currents at the time of a Pi2 pulsation to be observed in much greater detail than previously possible. The patterns observed depend on the level of magnetic activity and the position of the SABRE viewing area relative to the substorm enhanced region. If the activity was moderate or high, SABRE observed very complicated flows which include vortices, pairs of vortices and shears in the flow which are related to the complicated current systems present at substorm onset and to sheets of field-aligned current. The observation of sudden southward turnings of the flow at the onset time of Pi2 pulsations may be related to the earthward surge of plasma at substorm onset or, as these regions of flow often subsequently move westward across the viewing area, to the WTS or a similar region of enhanced ionospheric substorm current. When activity is low the viewing area is equatorward of the substorm current systems and few backscatter returns are normally observed. During the recovery phase of a substorm, the backscatter returns present had a tendency to be L-shell aligned.

The wave spectral power at the dominant Pi2 pulsation period was normally localised to only a few cells in the SABRE viewing area (an area of some  $40 \times 40 \text{ km}^2$ ). The only exception being at times of lowest magnetic activity when many cells over a wide longitudinal area exhibited high spectral power. A study of this power distribution over the course of a train of Pi2 pulsations indicates that the magnitude and direction of the longitudinal change in cell position is directly

related to the apparent change in the position of the substorm current wedge. If the wedge appears to expand and move to the west, the cell exhibiting peak wave spectral power also moves to the west. A similar eastward motion was also observed on occasions. This 'expansion' was also observed from the changing polarisation azimuths in the Nordli and Faoes magnetometer data when attempting to position the SABRE viewing area relative to the substorm current wedge during a train of pulsations. It should be noted that the SABRE data cannot distinguish between multiple substorm current wedge generation as opposed to the development of a single wedge during the above analysis.

The four special case study intervals studied suggest that the following mechanisms can produce the observed SABRE signatures

- a) the interaction of a pair of field-aligned current sheets
- b) the field line resonance
- c) highly structured field-aligned currents associated with WTS
- d) the magnetotail geometry associated with a plasmaspheric resonance

The results indicate that the Pi2 pulsation signature observed depends on the position of the SABRE viewing area relative to the substorm generation region. This is of key importance in the interpretation of the data in terms of theoretical and observational models of Pi2 pulsation generation.

### 7.3 Indications of future work

The study of Pi2 pulsations with the SABRE or a similar system could be greatly enhanced by an increase in the time resolution of the radar. Although the pulsation signatures are clear enough in the present observations, improved time resolution would enable FFT spectral analysis of many more of the Pi2 pulsations. This would determine the amplitude and phase variation across the viewing area

and would enable a definite comment to be made more often on the possible generation mechanisms of the wave itself. A greater time resolution would also enable the azimuth of the SABRE polarisation ellipse to be calculated more frequently and so improve the poor statistics that exist in certain local time sectors and in certain regions relative to the current wedge when comparing ground magnetometer and SABRE azimuths. The question of whether a rotation of the wave polarisation ellipse occurs on travelling through the ionosphere could thus be better resolved.

Another major suggestion for future work would be a detailed analysis of the Pi2 pulsation signatures observed in the backscatter intensity data obtained from the two individual radars of the SABRE system. Time series data in this thesis have already indicated that the pulsations are observed in the backscatter intensity data but the spectral and polarisation characteristics of these pulsations has not been investigated here.

The siting of the BGS network of magnetometers on either side of the viewing area was constrained by geographical considerations but it was possible to determine the position of the viewing area relative to the substorm current wedge when the level of magnetic activity was low. At times of higher activity the results become more inconsistent. The installation of magnetometers at the same latitude but further to the east and west would help in establishing the position of the viewing area relative to the current wedge during more active periods.

The comparison of SABRE data with satellite measurements in the magnetotail during substorms may also be an area of worthwhile future investigation. In particular, the forthcoming Cluster mission,

consisting of four spacecraft, will obtain measurements with high spatial and temporal resolution in the tail. How these data relate to the flows and signatures observed by SABRE and ground magnetometer networks during substorm onset and Pi2 pulsations should lead to a great increase in the understanding of the physical processes involved.

## Appendix A: Maximum Entropy Spectral Analysis

### A.1 Introduction

The technique of power spectrum analysis is employed to identify the dominant periods present in time series data. The power spectral density function of a time series provides a frequency domain description of the data, any dominant periods appear as sharp peaks above the background noise level in the spectral data. Lines with high signal to noise ratios are likely to represent physically meaningful events. A technique often employed in spectral analysis studies is that of the Fourier transform. However, this technique is limited in frequency resolution by the length of the data set under investigation and so could not be employed routinely in the present study of SABRE Pi2 pulsations. For a data set T seconds long containing N samples, the frequency resolution is  $1/T$  cycles/second. The data sampling rate ( $dT$ ) is then  $T/N$  and the maximum frequency which may be investigated is  $1/2dT$  (the Nyquist frequency). Fourier analysis was however employed in the analysis of the ground magnetometer data where the sampling rate is generally sufficient for a well-defined spectrum to be produced. In practice, a Fast Fourier Transform routine from the NAG library was utilised in calculating the power spectrum. The FFT algorithm calculates discrete Fourier coefficients far more quickly by eliminating repetition in parts of the calculation and so reducing the number of operations from  $N*N$  to  $N\log_2N$ .

### A.2 Maximum Entropy Spectral Analysis

With only a limited set of data available, a different technique, that of maximum entropy (ME) is usually considered superior to Fourier

analysis for the identification of spectral lines. The ME method has a frequency resolution which is independent of the length of the data set. For this reason ME spectral analysis was routinely employed throughout the SABRE investigations of the short lived Pi2 pulsations where relatively few data points are available due to the 20s time resolution of the SABRE data. A detailed account of the technique and the theory behind it is presented by Ulrych and Bishop (1975). The original computer programme was derived from the work of Ulrych and Bishop by W.C. Bain.

The ME spectral analysis technique consists of two independent steps. The first of these is the Burg technique from which a prediction error filter (PEF) of length, or order,  $m$  is computed. When this filter is run in both directions over the  $M$  data points of the process under investigation, the mean square prediction error of the system is minimised. It is the length of this PEF ( $m$ ) that is critical in achieving the enhanced spectral resolution theoretically possible with the ME technique. Since the data are being used to predict later (or earlier) values of the data, the method is also called auto-regressive. The second step employs the  $m$  prediction error coefficients in an expression to estimate the power spectral density by maximising the entropy or information content of the available data. The entropy of a system is the average information per time interval where the total information content ( $I_{\text{total}}$ ) is related to the sum of the individual pieces of information ( $I$ ) determined by the probabilities ( $p_i$ ) of occurrence of each individual event. The information and probability are related by

$$I = k \ln(1/p_i) \quad k = \text{constant}$$

where the logarithm is employed as information is normally considered an additive quantity. If the system is observed over a long time interval (T), then the total information content is given by

$$I_{\text{total}} = k(p_1 \ln(1/p_1) + p_2 \ln(1/p_2) + \dots)$$

and  $\text{Entropy} = I_{\text{total}}/T$

The relationship between information and probability implies that the entropy is a measure of the uncertainty described by a set of probabilities. If, in a system, all the probabilities are zero except one which is unity, then the entropy is zero as no uncertainty exists. Otherwise the entropy is always positive.

The expression for the entropy is then maximised subject to the constraints that the total probability is unity and that the sum of the individual pieces of information multiplied by their probabilities equals the total information content of the system. The technique produces smooth spectra of very high resolution from which an accurate determination of the dominant period of a variation may be obtained. There are however several difficulties associated with the ME spectral analysis technique. In particular, the smoothness and stability of the spectrum is very sensitive to the choice of the ratio  $m/M$ . This is equivalent to the choice of the length or order (m) of the PEF. Too short a PEF results in a spectrum which is highly smoothed thereby nullifying the main resolution advantages of the ME technique, while too long a PEF introduces spurious detail into the spectrum. This ratio was normally set at around 1/3 as suggested on a theoretical basis by Ulrych and Bishop (1975) and as employed previously by various authors (e.g. Sutcliffe, 1975; Stuart et al., 1979).

It should be noted that although the actual amplitude of the spectral lines produced by the ME technique are very sensitive to the position in the spectrum that they occur, the area under the spectral line which is proportional to the total spectral power is much less so. The variance of the integrated power spectrum is much smaller than the variance of the power spectrum estimate. This integrated ME power spectrum has been employed in astronomical studies in the past (Jensen and Ulrych, 1973).

## References

- Akasofu, S.-I., 1964, Planet. Space Sci. 12, 273.
- Akasofu, S.-I., 1968, Polar and Magnetospheric Substorms, D.Reidel, Dordrecht, Netherlands.
- Akasofu, S.-I., 1977, Physics of Magnetospheric Substorms, D.Reidel, Dordrecht, Netherlands.
- Akasofu, S.-I., (Ed), 1979, 'What is a Magnetospheric Substorm?' in Dynamics of the Magnetosphere, p.447, D.Reidel, Dordrecht, Netherlands.
- Akasofu, S.-I., 1981, Space Sci. Rev. 28, 121.
- Akasofu, S.-I., Chapman, S. and Meng, C.-I., 1965, J. Atmos. Terr. Phys. 27, 1275.
- Axford, W.I. and Hines, C.O., 1961, Can. J. Phys. 39, 1433.
- Baker, D.N., Fritz, T.A., McPherron, R.L., Fairfield, D.H., Kamide, Y. and Baumjohann, W., 1985, J. Geophys. Res. 90, 1205.
- Baranskiy, L.N., Troitskaya, V.A., Sterlikova, I.V., Gokhberg, M.B., Ivanov, N.A., Khortchenko, I.P., Munch, J.W. and Wilhelm, K., 1980, J. Geophys. 48, 1.
- Baumjohann, W., 1983, Adv. Space Res. 2, 55.
- Baumjohann, W. and Glassmeier, K.-H., 1984, Planet. Space Sci. 32, 1361.
- Baumjohann, W., Pellinen, R.J., Opgenoorth, H.J. and Nielsen, E., 1981, Planet. Space Sci. 29, 431.
- Behrens, J. and Glassmeier, K.-H., 1986, J. Geophys. 59, 195.
- Bjornsson, A., Hillebrand, O. and Voelker, H., 1971, Z. Geophys. 37, 1031.
- Cahill, L.J., Jr., Greenwald, R.A. and Nielsen, E., 1978, Geophys. Res. Lett. 5, 687.

- Carpenter, D.L., 1963, J. Geophys. Res. 68, 1675.
- Chen, L. and Hasegawa, A., 1974a, J. Geophys. Res. 79, 1024.
- Chen, L. and Hasegawa, A., 1974b, J. Geophys. Res. 79, 1033.
- Clauer, C.R. and McPherron, R.L., 1974, J. Geophys. Res. 79, 2811.
- Craven, J.D. and Frank, L.A., 1985, Geophys. Res. Lett. 12, 465.
- Craven, J.D. and Frank, L.A., 1987, J. Geophys. Res. 92, 4565.
- Doobov, A.L. and Mainstone, J.S., 1973, Planet. Space Sci. 21, 731.
- Dungey, J.W., 1961, Phys. Rev. Lett. 6, 47.
- Ellis, P. and Southwood, D.J., 1983, Planet. Space Sci. 31, 107.
- Feldstein, Y.I., 1963, Geomagn. Aeron. 3, 183.
- Fukinishi, H., 1975, J. Geophys. Res. 80, 98.
- Gelpi, G.C. and Bering, E.A., 1984, J. Geophys. Res. 89, 10847.
- Gelpi, C., Hughes, W.J., Singer, H.J. and Lester, M., 1985a, J. Geophys. Res. 90, 6451.
- Gelpi, C., Hughes, W.J. and Singer, H.J., 1985b, J. Geophys. Res. 90, 9905.
- Gelpi, C., Singer, H.J. and Hughes, W.J., 1987, J. Geophys. Res. 92, 2447.
- Glassmeier, K.-H., 1984, J. Geophys. 54, 125.
- Glassmeier, K.-H., 1988, Planet. Space Sci. 36, 801.
- Glassmeier, K.-H., Baumjohann, W., Korth, A. and Gough, P., 1988, Ann. Geophys. 6, 287.
- Gough, H. and Orr, D., 1984, Planet. Space Sci. 32, 619.
- Green, C.A., 1976, Planet. Space Sci. 24, 79.
- Hargreaves, J.K., Chivers, H.J.A. and Nielsen, E., 1979, J. Geophys. Res. 84, 4245.
- Hones, E.W., Jr., 1979a, Space Sci. Rev., 23, 393.
- Hones, E.W., Jr., 1979b, 'Plasma Flow in the Magnetotail and its Implications for Substorm Theories' in Dynamics of the Magnetosphere (edited by Akasofu, S.-I.) p545, D. Reidel, Dordrecht, Netherlands.

- Hughes, W.J., 1974, Planet. Space Sci. 22, 1157.
- Hughes, W.J., 1982, Rev. Geophys. Space Phys. 20, 641.
- Hughes, W.J. and Southwood, D.J., 1976a, J. Geophys. Res. 81, 3234.
- Hughes, W.J. and Southwood, D.J., 1976b, J. Geophys. Res. 81, 3241.
- Hughes, W.J. and Singer, H.J., 1985, J. Geophys. Res. 90, 1297.
- Hultqvist, B., 1987, Geophys. Res. Lett. 14, 379.
- Iijima, T. and Potemra, T.A., 1976a, J. Geophys. Res. 81, 2165.
- Iijima, T. and Potemra, T.A., 1976b, J. Geophys. Res. 81, 5971.
- Inhester, B., Baumjohann, W., Greenwald, R.A. and Nielsen, E., 1983, J. Geophys. Res. 88, 155.
- Inoue, Y., 1973, J. Geophys. Res. 78, 2959.
- Jacobs, J.A. and Sinno, K., 1960, Geophys. J. 3, 333.
- Jacobs, J.A., Kato, Y., Matsushita, S. and Troitskaya, V.A., 1964, J. Geophys. Res. 69, 180.
- Jensen, O.G. and Ulrych, T.J., 1973, Astron. J. 78, 1104.
- Kan, J.R., Longenecker, D.U. and Olson, J.V., 1982, J. Geophys. Res. 87, 7483.
- Kisabeth, J.L. and Rostoker, G., 1973, J. Geophys. Res. 78, 5573.
- Kuwashima, M. and Saito, T., 1981, J. Geophys. Res. 86, 4686.
- Lester, M. and Orr, D., 1981, J. Atmos. Terr. Phys. 43, 947.
- Lester, M. and Orr, D., 1983, Planet. Space Sci. 31, 143.
- Lester, M., Hughes, W.J. and Singer, H.J., 1983, J. Geophys. Res. 88, 7958.
- Lester, M., Hughes, W.J. and Singer, H.J., 1984, J. Geophys. Res. 89, 5489.
- Lester, M., Glassmeier, K.-H. and Behrens, J., 1985, Planet. Space Sci. 33, 351.
- Lin, C.C. and Cahill, L.J., Jr., 1975, Planet. Space Sci. 23, 693.
- Luhr, H., Thurey, S. and Klocker, N., 1984a, Geophys. Surveys 6, 305.
- Luhr, H., Klocker, N. and Thurey, S., 1984b, J. Geophys. Res. 89, 41.

- Mallinckrodt, A.J. and Carlson, C.W., 1978, *J. Geophys. Res.* **83**, 1426.
- Maltsev, Yu.P., Leontyev, S.V. and Lyatsky, W.B., 1974, *Planet. Space Sci.* **22**, 1519.
- McClay, J.F. and Radoski, H.R., 1967, *J. Geophys. Res.* **72**, 4525.
- McPherron, R.L., 1979, *Rev. Geophys. Space Phys.* **17**, 657.
- McPherron, R.L., Russell, C.T. and Aubry, M.P., 1973, *J. Geophys. Res.* **78**, 3131.
- Mier-Jedrzejowicz, W.A.C. and Southwood, D.J., 1979, *Planet. Space Sci.* **27**, 617.
- Mier-Jedrzejowicz, W.A.C. and Southwood, D.J., 1981, *J. Atmos. Terr. Phys.* **43**, 911.
- Murphree, J.S., Cogger, L.L., Anger, C.D., Wallis, D.D. and Shepherd, G.G., 1987, *Geophys. Res. Lett.* **14**, 407.
- Nagai, T., 1987, *J. Geophys. Res.* **92**, 2432.
- Nagai, T., Singer, H.J., Ledley, B.G. and Olsen, R.C., 1987, *J. Geophys. Res.* **92**, 2425.
- Nielsen, E. and Schlegel, K., 1983, *J. Geophys. Res.* **88**, 5745.
- Nielsen, E. and Schlegel, K., 1984, *J. Geophys. Res.* **89**, 3498.
- Nishida, A., 1979, *J. Geophys. Res.* **84**, 3409.
- Nishida, A., Bame, S.J., Baker, D.N., Gloeckler, G., Scholer, M., Smith, E.J., Terasawa, T. and Tsurutani, B., 1988, *J. Geophys. Res.* **93**, 5579.
- Olson, J.V. and Rostoker, G., 1975, *Planet. Space Sci.* **23**, 1129.
- Opgenoorth, H.J., Pellinen, R.J., Baumjohann, W., Nielsen, E., Marklund, G. and Eliasson, L., 1983, *J. Geophys. Res.* **88**, 3138.
- Orr, D., 1975, *Ann. Geophys.* **31**, 77.
- Orr, D., 1984, *J. Geophys.* **55**, 76.
- Orr, D. and Hanson, H.W., 1981, *J. Atmos. Terr. Phys.* **43**, 899.
- Pashin, A.B., Glassmeier, K.-H., Baumjohann, W., Raspopov, O.M., Yahnin, A.G., Opgenoorth, H.J. and Pellinen, R.J., 1982, *J. Geophys.*

51, 223.

Potemra, T.A., Iijima, T. and Saflekos, N.A., 1980, 'Large-scale characteristics of Birkeland Currents' in Dynamics of the Magnetosphere (edited by Akasofu, S.-I.) p.165, D. Reidel, Dordrecht, Netherlands.

Pytte, T. and Trefall, H., 1972, J. Atmos. Terr. Phys. 34, 315.

Pytte, T., McPherron, R.L. and Kokubun, S., 1976, Planet. Space Sci. 24, 1115.

Reiff, P.H., 1983, 'The use and misuse of statistical analyses' in Solar-Terrestrial Physics (edited by Carovillano, R.L. and Forbes, J.M.) p.493, D. Reidel, Dordrecht, Netherlands.

Rijnbeek, R.P., Cowley, S.W.H., Southwood, D.J. and Russell, C.T., 1984, J. Geophys. Res. 89, 786.

Robinson, T.R., 1986, J. Atmos. Terr. Phys. 48, 417.

Rostoker, G., 1967, Can. J. Phys. 45, 1319.

Rostoker, G. and Samson, J.C., 1981, Planet. Space Sci. 29, 225.

Rostoker, G. and Eastman, T.E., 1987, J. Geophys. Res. 92, 12187.

Rostoker, G., Akasofu, S.-I., Foster, J., Greenwald, R.A., Kamide, Y., Kawasaki, K., Lui, A.T.Y., McPherron, R.L. and Russell, C.T., 1980, J. Geophys. Res. 85, 1663.

Rostoker, G., Akasofu, S.-I., Baumjohann, W., Kamide, Y. and McPherron, R.L., 1987a, Space Sci. Rev. 46, 93.

Rostoker, G., Vallance Jones, A., Gattinger, R.L., Anger, C.D. and Murphree, J.S., 1987b, Geophys. Res. Lett. 14, 399.

Rostoker, G., Savoie, D. and Phan, T.D., 1988, J. Geophys. Res. 93, 8633.

Rothwell, P.L., Silevitch, M.B. and Block, L.P., 1986, J. Geophys. Res. 91, 6921.

Rothwell, P.L., Silevitch, M.B., Block, L.P. and Tanskanen, P., 1988, J. Geophys. Res. 93, 8613.

- Saito, T., Yumoto, K. and Koyama, Y., 1976, Planet. Space Sci. 24, 1025.
- Sakurai, T. and McPherron, R.L., 1983, J. Geophys. Res. 88, 7015.
- Samson, J.C., 1982, Planet. Space Sci. 30, 1239.
- Samson, J.C., 1985, J. Geophys. 56, 133.
- Samson, J.C. and Rostoker, G., 1983, Planet. Space Sci. 31, 435.
- Samson, J.C. and Harrold, B.G., 1983, J. Geophys. Res. 88, 5736.
- Samson, J.C. and Harrold, B.G., 1985, J. Geophys. Res. 90, 12173.
- Samson, J.C., Harrold, B.G. and Yeung, K.L., 1985, J. Geophys. Res. 90, 3448.
- Shepherd, G.G., Anger, C.D., Murphree, J.S. and Vallance Jones, A., 1987, Geophys. Res. Lett. 14, 395.
- Sherwood, V.E., Macintosh, S.M. and Stuart, W.F., 1973, J. Atmos. Terr. Phys. 35, 1407.
- Singer, H.J., Hughes, W.J., Fougere, P.F. and Knecht, D.J., 1983, J. Geophys. Res. 88, 7029.
- Singer, H.J., Hughes, W.J., Gelpi, C. and Ledley, B.G., 1985, J. Geophys. Res. 90, 9583.
- Smits, D.P., Hughes, W.J., Cattell, C.A. and Russell, C.T., 1986, J. Geophys. Res. 91, 121.
- Southwood, D.J., 1974, Planet. Space Sci. 22, 483.
- Southwood, D.J. and Hughes, W.J., 1983, Space Sci. Rev. 35, 301.
- Southwood, D.J. and Hughes, W.J., 1985, J. Geophys. Res. 90, 386.
- Southwood, D.J. and Stuart, W.F., 1980, 'Pulsations at the substorm onset' in Dynamics of the Magnetosphere (edited by Akasofu, S.-I.), p341, D. Reidel, Dordrecht, Netherlands.
- Stuart, W.F., 1972a, J. Atmos. Terr. Phys. 34, 829.
- Stuart, W.F., 1972b, J. Atmos. Terr. Phys. 34, 817.
- Stuart, W.F., 1974, J. Atmos. Terr. Phys. 36, 851.
- Stuart, W.F. and Booth, D.C., 1974, J. Atmos. Terr. Phys. 36, 835.

- Stuart, W.F. and Macintosh, S.M., 1974, *J. Atmos. Terr. Phys.* **36**, 425.
- Stuart, W.F., Green, C.A. and Harris, T.J., 1977, *J. Atmos. Terr. Phys.* **39**, 631.
- Stuart, W.F., Brett, P.M. and Harris, T.J., 1979, *J. Atmos. Terr. Phys.* **41**, 65.
- Sun, W. and Kan, J.R., 1985, *J. Geophys. Res.* **90**, 4395.
- Sutcliffe, P.R., 1975, *Planet. Space Sci.* **23**, 1581.
- Thompson, W.B., 1983, *J. Geophys. Res.* **88**, 4805.
- Troitskaya, V.A., 1967, in *Solar-Terrestrial Physics*, p.213, London-New York Academic Press.
- Troitskaya, V.A. and Gul'elmi, A.V., 1967, *Space Sci. Rev.* **7**, 689.
- Ulrych, T.J. and Bishop, T.N., 1975, *Rev. Geophys. Space Phys.* **13**, 183.
- Villante, U., 1975, *Planet. Space Sci.* **23**, 723.
- Waldock, J.A., Jones, T.B., Nielsen, E. and Southwood, D.J., 1983, *Planet. Space Sci.* **31**, 573.
- Waldock, J.A., Jones, T.B. and Nielsen, E., 1985, *Radio Sci.* **20**, 709.
- Waldock, J.A., Southwood, D.J., Freeman, M.P. and Lester, M., 1988, *J. Geophys. Res.* **93**, 12883.
- Walker, A.D.M., 1980, *Planet. Space Sci.* **28**, 213.
- Walker, A.D.M., Greenwald, R.A., Stuart, W.F. and Green, C.A., 1979, *J. Geophys. Res.* **84**, 3373.
- Webster, D.J., Samson, J.C. and Rostoker, G., 1989, *J. Geophys. Res.* **94**, 3619.
- Wiens, R.G. and Rostoker, G., 1975, *J. Geophys. Res.* **80**, 2109.
- Wilkinson, P.J., Nielsen, E. and Luhr, H., 1986, *J. Geophys. Res.* **91**, 5839.
- Yarker, J.M. and Southwood, D.J., 1986, *Planet. Space Sci.* **34**, 1213.

Reference is also made to the following unpublished material.

Stuart, W.F. and Green, C.A., 1981, IGS Geomagnetism Unit Report No. 28.

Lester, M., Singer, H.J., Smits, D.P. and Hughes, W.J., 1989, accepted for publication in J. Geophys. Res.

SABRE AND MAGNETOMETER STUDIES OF  
SUBSTORM ASSOCIATED PULSATIONS

ERIC GEORGE BRADSHAW

ABSTRACT

This thesis describes an experimental investigation of the geomagnetic pulsations (Pi2) associated with the onset of magnetospheric substorms undertaken with the Sweden And Britain Radar aurora Experiment (SABRE) in conjunction with a network of ground-based magnetometers. The signatures observed on the two measuring systems are compared and have been interpreted in terms of the substorm current wedge and the substorm enhanced electrojet regions. The polarisation of the SABRE Pi2 pulsations is also investigated.

The excellent spatial resolution of the SABRE radar has enabled the complex system of field-aligned and ionospheric currents associated with substorm onset and Pi2 pulsations to be examined in great detail. A southward turning of the flow often observed at substorm onset may be related to the earthward surge of plasma at onset. The subsequent westward movement of these regions may be related to the westward travelling surge. This movement, and a less frequent eastward movement, is also observed in studies of the SABRE wave spectral power.

Four intervals of Pi2 activity have been selected for detailed study and the observed features related to different theoretical and observational models for the generation of these waves. The SABRE signature depends on the position of the viewing area relative to the substorm enhanced electrojet. The results are consistent with a field line resonance in one interval and the interaction of a pair of field-aligned currents in another. The highly complex structure of the substorm current systems in the magnetotail is apparent in the ionospheric radar data from the remaining two intervals.

The high spatial resolution attained in the present observations far exceeds that achieved with other techniques. Moreover, the radar monitors the actual ionospheric currents directly allowing an enhanced understanding of the underlying production mechanisms for the Pi2 pulsation events.